ATLAS OF

VOLCANIC LANDFORMS ON MARS

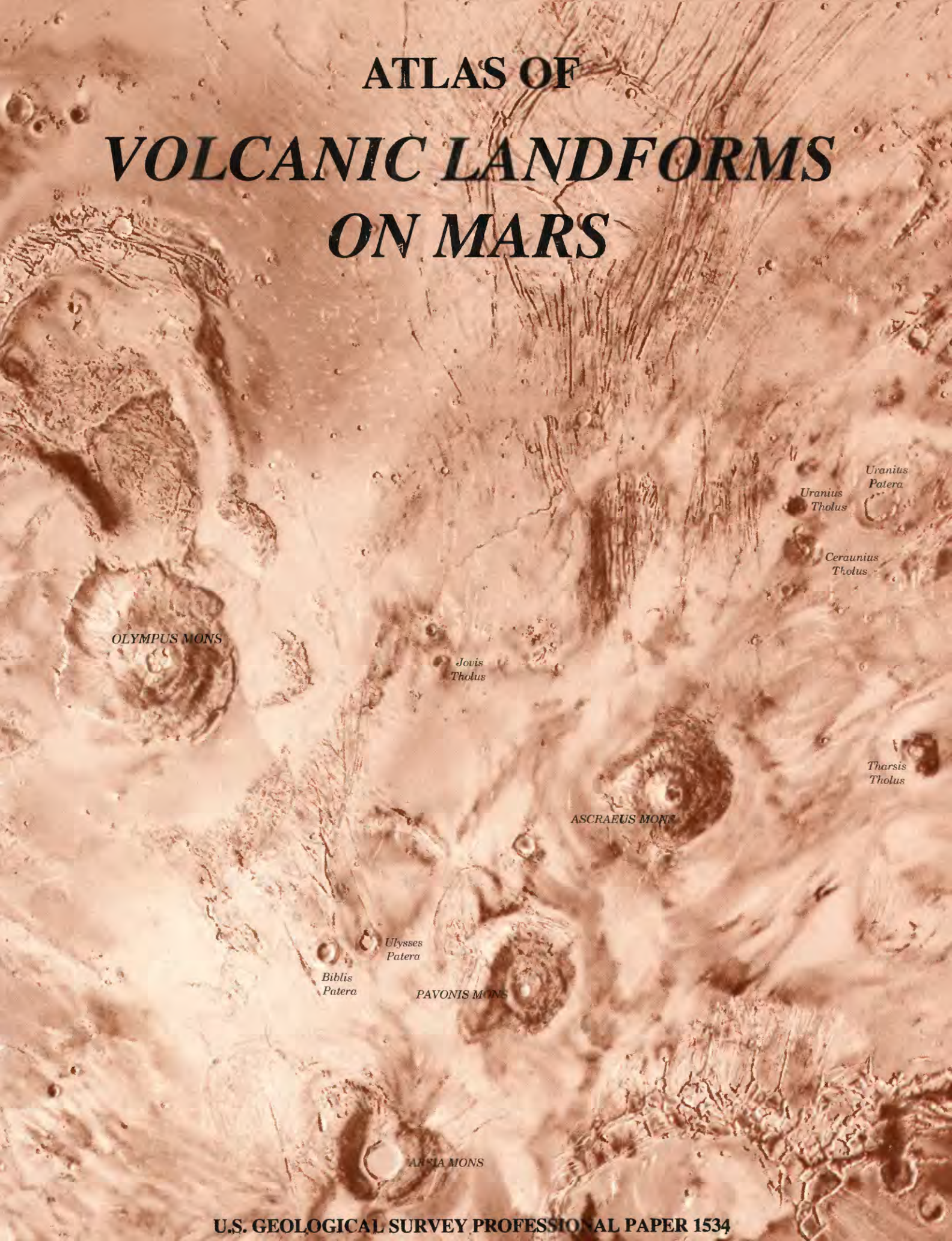

U.S. GEOLOGICAL SURVEY PROFESSIONAL PAPER 1534

ATLAS OF
VOLCANIC LANDFORMS ON MARS

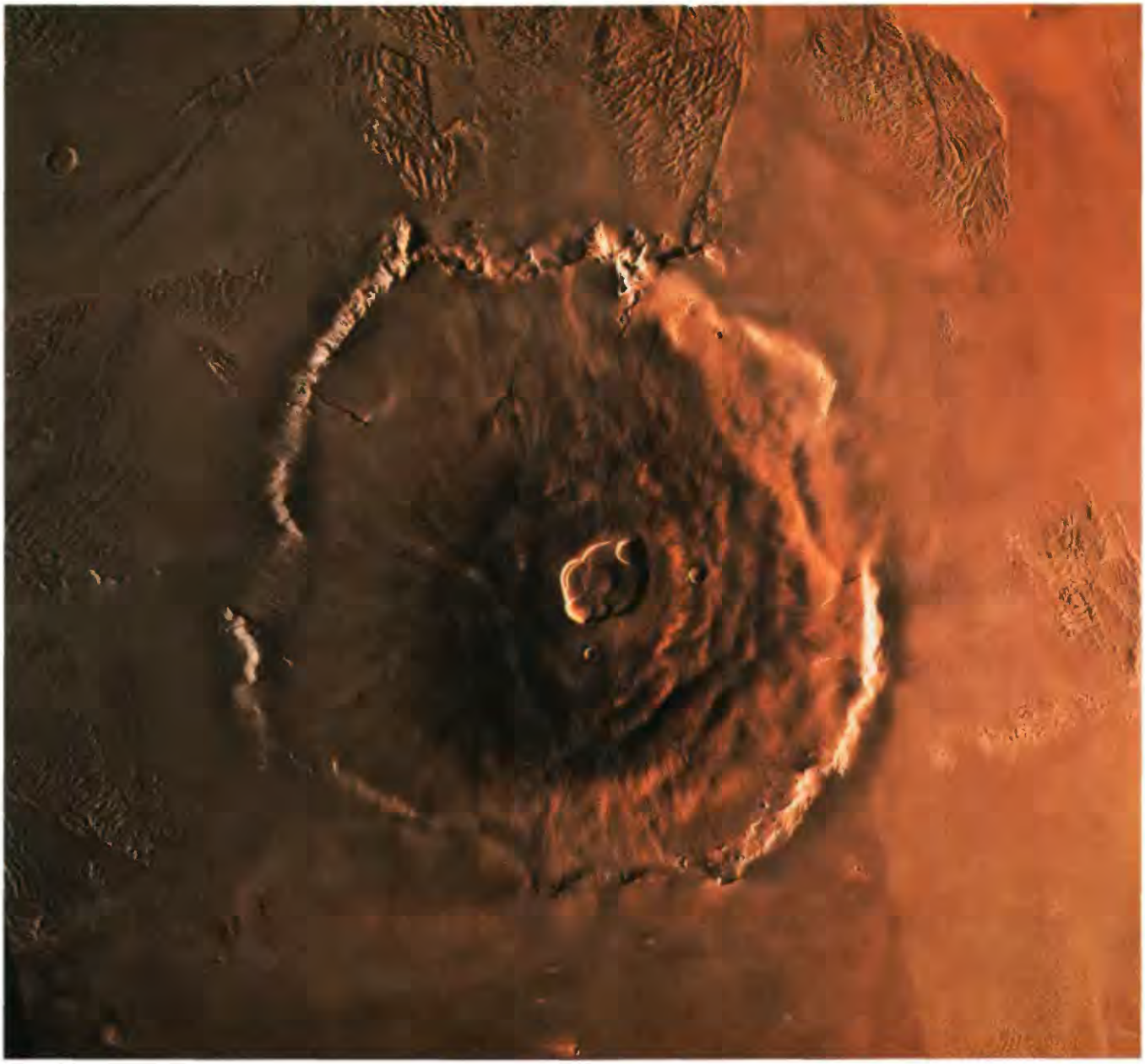

Olympus Mons, largest known volcano in the Solar System, is about 26 km high, more than 600 km across at base, and surrounded by a well-defined scarp as much as 6 km high. Lava flows drape over the scarp in places and cover much of surrounding plains. Ridged and grooved aureole materials are conspicuous around base of volcano. Summit caldera is almost 3 km deep and 65 by 85 km across. Image produced by merging medium-resolution digital-image model of Mars with low-resolution color observations; image processing by Alfred McEwen and Annie Allison, U.S. Geological Survey, Flagstaff, Ariz.

Atlas of Volcanic Landforms on Mars

By Carroll Ann Hodges *and* Henry J. Moore

U.S. GEOLOGICAL SURVEY PROFESSIONAL PAPER 1534

UNITED STATES GOVERNMENT PRINTING OFFICE, WASHINGTON : 1994

U.S. DEPARTMENT OF THE INTERIOR

BRUCE BABBITT, *Secretary*

U.S. GEOLOGICAL SURVEY

ROBERT M. HIRSCH, *ActingDirector*

For sale by
U.S. Geological Survey, Map Distribution
Box 25286, MS 306, Federal Center
Denver, CO 80225

Library of Congress Cataloging in Publication Data

Hodges, Caroll Ann.
Atlas of volcanic landforms on Mars / by Carroll Ann Hodges and Henry J. Moore.
p. cm. — (U.S. Geological Survey professional paper ; 1534)
1. Mars (Planet)—Surface—Atlases. 2. Volcanoes—Atlases. 1. Moore, H.J. (Henry J.), 1928– . II. Title. III. Series: Geological Survey professional paper ; 1534.
QB641.H64 1992 92–43717
559.9'23—dc20 CIP

CONTENTS

PLATE

[Plate is in pocket]

TABLE

Atlas of Volcanic Landforms on Mars

By Carroll Ann Hodges *and* Henry J. Moore

INTRODUCTION

Spacecraft exploration of the Solar System during the last decades of the 20th century has provided an incomparable opportunity for research on the geologic evolution of planets and satellites. Volcanology is particularly appropriate for comparative studies because of the insights gained regarding planetary composition and thermal history. Spacecraft imagery of the several planets and satellites with rocky surfaces has revealed volcanic landforms that resulted from diverse styles of eruption, permitting inferences to be drawn about magmatic components and petrology. Indeed, we have discovered that our Solar System hosts an astonishing array of volcanic phenomena that disclose much information about the respective geologic histories of our planetary neighbors.

The huge shield volcanoes on Mars were a striking revelation of the Mariner 9 mission in 1971 and, together with the enormous channels and canyons, presented a quite-unexpected planetary landscape (Masursky and others, 1972; McCauley and others, 1972; Carr, 1973, 1976b). The Viking mission in 1976, with two landers and two orbiting spacecraft, greatly augmented our perception of the martian surface and our understanding of the geologic processes that have shaped it. Morphologic analyses indicate that martian shield volcanoes and the vast lava plains surrounding them are chiefly basaltic in composition, analogous to terrestrial oceanic shield volcanoes and smaller features within continental basaltic fields.

Spacecraft images of other planetary bodies show contrasting volcanic landforms. Large constructs similar to those on Mars do not occur on the Moon, for example. Aside from several small cinder cones and lava domes, lunar volcanism consisted mainly of vast outpourings of basalt that formed the maria, or "seas," flooding lunar impact basins; radiometric dating of samples returned to Earth established the antiquity of these volcanic episodes at about 3.5 Ga. Elsewhere in the Solar System, however, volcanism is active—and different from that on Earth. Scientific excitement rose dramatically when large, energetic eruption plumes as tall as 300 km were discovered on the Jovian satellite Io during the Voyager encounters in 1979. This chance observation provided the first evidence that volcanic processes are actively occurring beyond Earth. Io, a tidally stressed, dynamic body (Peale and others, 1979), is apparently undergoing continuous resurfacing; in addition to plume fallout, broad lava flows emanate from calderas with low relief (1–3 km high) that are associated with conspicuous thermal anomalies (Carr, 1986b; Gaskell and others, 1988; Schaber and others, 1989). Although Io is thought to be a highly differentiated silicate body, sulfur and sulfur compounds appear to be important constituents of its present surface materials, giving the satellite its unusual yellow and red colors (Gradie and Veverka, 1984; Nash and others, 1986). Triton, the largest satellite of Neptune, also is evidently a differentiated body that exhibits a rigid crust of probable water ice overlain by nitrogen frost. Two geyserlike plumes that were observed on Voyager 2 images have been interpreted as solar-driven nitrogen-gas geysers (Smith and others, 1989). The Magellan spacecraft has only recently (1990) begun to return images of Venus, which, despite its similarities to Earth in size and density, displays a distinctive landscape with its own characteristic styles of volcanism (Head and others, 1991) and tectonism (Saunders and others, 1991). Volcanism is apparently widespread throughout the Solar System, and analyses of martian volcanoes will necessarily evoke comparisons with those of other planetary bodies, particularly Earth and Venus.

Shield volcanoes on Mars were first recognized and are especially numerous in the Tharsis region, mainly in the northwest quadrant of the accompanying planetary map (pl. 1). The four most prominent are Ascraeus, Pavonis, and Arsia Montes, aligned northeast-southwest along the Tharsis ridge, and the grandest of all, Olympus Mons (see Frontispiece), northwest of the ridge (fig. I–1). Summit elevations of Olympus and Ascraeus Montes exceed 25 km, and Arsia and Pavonis Montes are 20 and 18 km high, respectively; relief ranges from about 25 km at Olympus to 11 km at Pavonis (U.S. Geological Survey, 1989). Each of these massive shields is several times larger than any volcano on Earth; the summit of Mauna Loa, Hawaii, stands only 9 km above the ocean floor. Seven additional shields, similar to, but much smaller than, the four Mars volcanoes just named, have dimensions (relief ranging from less than 1 to 5–6 km) more nearly comparable to those

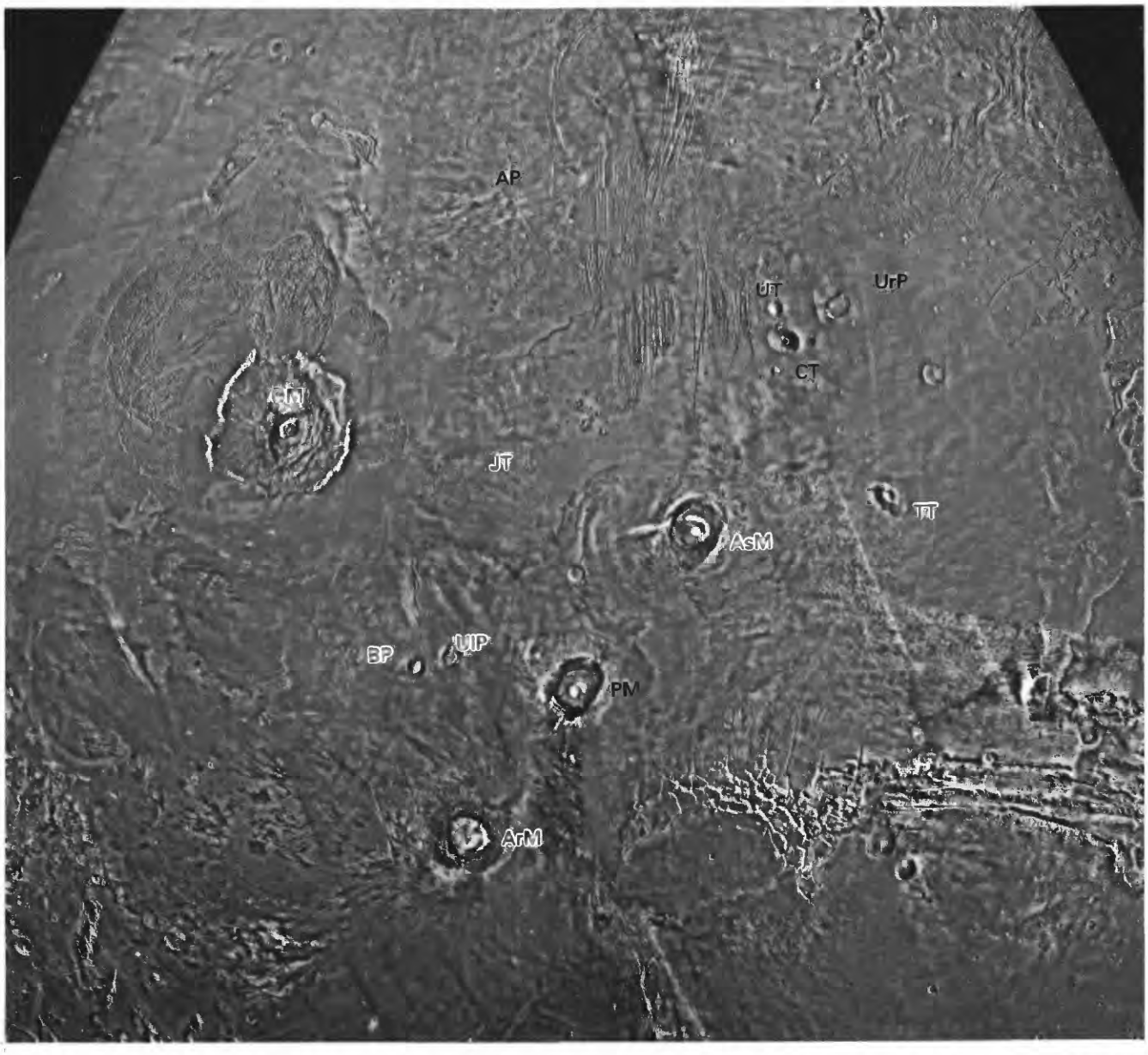

Figure I–1. Tharsis region of Mars, showing locations of principal volcanic provinces and shield volcanoes: Olympus Mons (OM) at left center; Ascraeus Mons (AsM), Pavonis Mons (PM), and Arsia Mons (ArM), from northeast (right center) to southwest (lower center) along Tharsis ridge; and broad, low shield of Alba Patera (AP) at upper center. Minor shields: Biblis Patera (BP), Ulysses Patera (UlP), Jovis Tholis (JT), Tharsis Tholus (TT), Uranius Patera (UrP), Uranius Tholus (UT), and Ceraunius Tholus (CT). Area approximately the same as in figure I–2. Center-to-center distance from Ascraeus Mons to Arsia Mons is approximately 1,500 km. Digital-image mosaic compiled by U.S. Geological Survey's Image Processing Facility, Flagstaff, Ariz.

of such terrestrial volcanic provinces as the Hawaiian and Galápagos Islands. Identification of these features as volcanic leaves little doubt because of the close morphologic similarities to terrestrial counterparts (Carr and Greeley, 1980). Large volcanic edifices also occur in the Elysium region (pl. 1), about 4,500 km west of Olympus Mons; the shapes of these structures, however, appeared in Mariner images to differ from those of the Tharsis shield volcanoes, provoking speculations about possible contrasts in structure, composition, and eruptive style.

The extensive lava flows associated with both the Tharsis and Elysium shields suggested that numerous smaller volcanic landforms of various types should also exist; a systematic search for them led to compilation of this atlas. Among the lesser features that

have been identified as conclusively or probably volcanic are (1) small shield volcanoes (less than 10 km across), commonly associated with fracture systems; (2) fields of densely clustered cratered cones or domes; and (3) arcuate chains of symmetrical cones. Other features of more ambiguous origin include low, circular domes with shallow summit depressions, extensive collapse pits, cratered and uncratered mesas and buttes that resemble Icelandic tablemountains, and dikelike structures.

Our intent here is to portray all martian constructional landforms that can be interpreted unequivocally as volcanic and to present examples of the more enigmatic features for which a volcanic interpretation currently seems as plausible as any other. Interpretations of extraterrestrial landforms are necessarily based on comparison with, and extrapolation from, terrestrial landforms whose morphologic and dimensional attributes are similar. For some volcanic features on Mars, such as the low shield volcanoes of the Tempe-Mareotis province, exact analogs exist on Earth; however, most martian landforms differ greatly in scale, context, or some other aspect, and photogeologic interpretation must rely heavily on a combination of several diagnostic features and criteria (Greeley and Spudis, 1981). An objective of this atlas is to facilitate further studies in comparative volcanology by providing a compendium of information on the morphology and variety of martian volcanoes and attendant landforms. The atlas should also be useful in planning future spacecraft missions to Mars.

DIMENSIONS OF FEATURES

The average dimensions of the large volcanic edifices as listed here are primarily from Pike and Clow (1981b). Some uncertainty exists in these values, arising from interpretations of base configurations as well as from the somewhat limited and varied sources of topographic information. If we noted obvious disparities with the most recent 1:15,000,000-scale topographic maps (U.S. Geological Survey, 1989, 1991), we modified the dimensions accordingly. Elevations are from these maps, with a contour interval of 1.0 km; probable error in these contours is ±1.0 km between 30° N. and 30° S., and ±1.5 km elsewhere. Overall heights and base diameters of some volcanoes are uncertain because they are partly buried by younger flows, and true configurations are obscured by an unknown thickness of lava. Profiles of some small volcanic edifices and tube-fed flows were obtained by using photoclinometry (for example, Davis and Soderblom, 1984); errors in the relief of these small features may be as great as 30 percent.

NOMENCLATURE

Geographic names on Mars derive from Latin words (the planet itself is named for the Roman god of war), and it may be helpful to clarify some of the most common terms applied to volcanic and related features, as defined by Strobell and Masursky (1990). The largest martian volcanic edifices are called *montes* (singular, *mons*, "mountain"), and the smaller ones *tholi* (singluar, *tholus*, "small domical mountain or hill"). Other volcanoes of low relief are identified by the names of their summit depressions, called *paterae* (singular, *patera,* "shallow crater with scalloped or complex edge"), but not all paterae on the planet are atop volcanoes. Northern plains units are *planitiae* (singular, *planitia*, "low plain"), and highlands plains are *plana* (singular, *planum*, "plateau or high plain"). Clusters of fractures and grabens are *fossae* (singular, *fossa*, "long, narrow, shallow depression"). The term "low shield" designates small volcanoes with dimensions (2–10 km across) similar to those of low shield volcanoes on Earth (Greeley, 1977b, 1982).

DISTRIBUTION OF VOLCANIC LANDFORMS

Two major terrain types characterize the martian surface: a vast, low-lying northern plains unit, and the cratered highlands, primarily in the Southern Hemisphere. The boundary between these two terrains is commonly an escarpment, 1 to 3 km high (U.S. Geological Survey, 1976, 1989). As is readily apparent on the accompanying map (pl. 1), all of the great shield volcanoes and most of the lesser volcanic landforms on Mars are localized in the northern plains province. The densely cratered highlands have few demonstrably volcanic landforms, and those that can be identified confidently, specifically Tyrrhena and Hadriaca Paterae, have little relief. A few features in the highlands morphologically resemble those of terrestrial continental calderas, resurgent domes, and composite volcanoes, but these features are rare and questionable. The confinement of most large martian shield volcanoes to the plains is somewhat analogous to the localization of the largest basaltic shield volcanoes on Earth within the ocean basins; the martian volcanoes are, however, as much as three times higher and five times broader than their terrestrial counterparts.

The so-called Tharsis bulge, encompassing much of the Tharsis volcanic region, is topographically the highest part of the planet; it rises 8 to 9 km above datum (U.S. Geological Survey, 1989, 1991) and is surmounted by the large shield volcanoes Ascraeus,

Pavonis, and Arsia Montes. A conspicuous and extensive system of radial fractures (Carr, 1984) surrounds the Tharsis bulge. Lava flows emanating from these volcanoes totally cover the adjacent plains (figs. I–1, I–2), which meet the nearest highlands province, Syria Planum to the southeast, along an escarpment more than 1 km high.

The Tharsis region, as defined here, includes those volcanoes aligned along the northeast-trending axis of the Tharsis bulge, all adjacent shields, and localized areas of minor volcanic features in the Ceraunius Fossae and Tempe-Mareotis provinces (pl. 1); the entire region covers about a quarter of the planet's surface. In addition to the specific provinces outlined and described within the Tharsis region, the plains surrounding the volcanoes are characterized by conspicuous lava flows, fissure vents, and small, barely discernible low-shield vents, but these features are not sufficiently distinctive to include here. General relations between lava flows, small volcanoes, vents, and the large Tharsis volcanoes are shown in figure I–2 (see Mouginis-Mark and others, 1982b). For a discussion of the extensive and conspicuous lava plains units of Tharsis, the reader is referred to the series of 13 maps by D.H. Scott and coworkers (Scott, 1981; Scott and Tanaka, 1981a–e; Scott and others, 1981a–e, g). Theilig and Greeley (1986) described some of the small-scale surface features that characterize the Tharsis lava flows.

The Elysium region includes Elysium Mons, Albor Tholus, Hecates Tholus, Apollinaris Patera, and some lesser provinces (fig. I–3). Elysium Mons surmounts a structural and topographic high somewhat similar to the Tharsis bulge, but only about 2 to 3 km above datum.

The major volcanoes of the highlands province are Hadriaca and Tyrrhena Paterae, respectively on the northeast rim and flank of the large Hellas impact basin. These shield calderas have low relief (1–2 km), but each is surrounded by a radial pattern of channels. Two large, partly foundered calderas near the north boundary of the highlands erupted conspicuous lava flows that formed the volcanic plains within Syrtis Major (fig. I–4). Several candidates for silicic caldera domes, one possible composite cone, two probably volcanic paterae, and several small enigmatic features also occur in the highlands, but the array of volcanic landforms does not compare to that of the northern plains. Lucchitta (1987, 1990) presented evidence for relatively young mafic volcanism in the Valles Marineris equatorial canyon system, but these dark-gray patches, interpreted as vents, do not exhibit significant positive relief, and they are not discussed further here.

TECTONICS, ERUPTIVE STYLE, AND PETROLOGY

In contrast to Earth, Mars does not have belts of composite cones (stratovolcanoes) like those of the Cascades, Andes, and other ranges of the American Cordillera, or the island arcs of the Aleutians and the western Pacific rim. These edifices, built of both effusive and pyroclastic layers, with typically concave slopes ranging from about 10° to 35° (Macdonald, 1972), have resulted from magma generation and eruption along the subduction zones between oceanic plates and the overlying, more silicic continental plates. Composite volcanoes also characterize continental rift zones, as in East Africa. Such volcanoes may attain great heights, 3 to 5 km above sea level, but their volumes are trivial in comparison with those of oceanic shield volcanoes: Mauna Loa is 300 times larger volumetrically than Fujiyama, one of Earth's largest composite cones (Williams and McBirney, 1979). Composite volcanoes vary in composition, although they are predominantly andesitic, and their eruptions are more commonly explosive than effusive, producing vast pyroclastic deposits. Oceanic shield volcanoes, in contrast, are characterized by effusive eruptions of low-viscosity basaltic lavas, normally convex profiles, and slopes averaging about 2°–12° (Macdonald, 1972).

According to Carr (1973, 1984), the differences in size, type, and distribution between the volcanoes on Mars and those on Earth "* * * appear to result largely from the absence of plate tectonics on Mars." Although extensional faulting may have occurred

► **Figure I–2.** Sketch map of Tharsis region of Mars, showing geographic relations between volcanoes and lava flows. Area approximately the same as in figure I–1. Montes: OM, Olympus; AsM, Ascraeus; PM, Pavonis; ArM, Arsia. Tholi: CT, Ceraunius; TT, Tharsis; UT, Uranius; JT, Jovis Tholus. Patera shields: AP, Alba; BP, Biblis; UlP, Ulysses; UrP, Uranius. Collapse structure: HF, Halex Fossae. Volcanic fields with small edifices: CF, Ceraunius Fossae; SP, Syria Planum; TM, Tempe-Mareotis; TV, Tempe Volcano; UPn, Uranius Patera north. Volcano subunits: AsMf, Ascraeus Mons lava fans; Pa, Pavonis Mons east lava apron; ArMf, Arsia Mons lava fans. Aureole materials: OMa, Olympus Mons; AsMa, Ascraeus Mons; PMa, Pavonis Mons; ArMa, Arsia Mons. Outlines denote lava-flow fields of various volcanic centers; arrows within outlines indicate paleoflow directions of lavas. Dashes, lava fans of Ascraeus, Pavonis, and Arsia Montes; dashes near Tempe Volcano, lava-tube ridges; dots, small volcanic edifices with low relief; irregular line with small dots, fissures; hachures, calderas. Mercator projection.

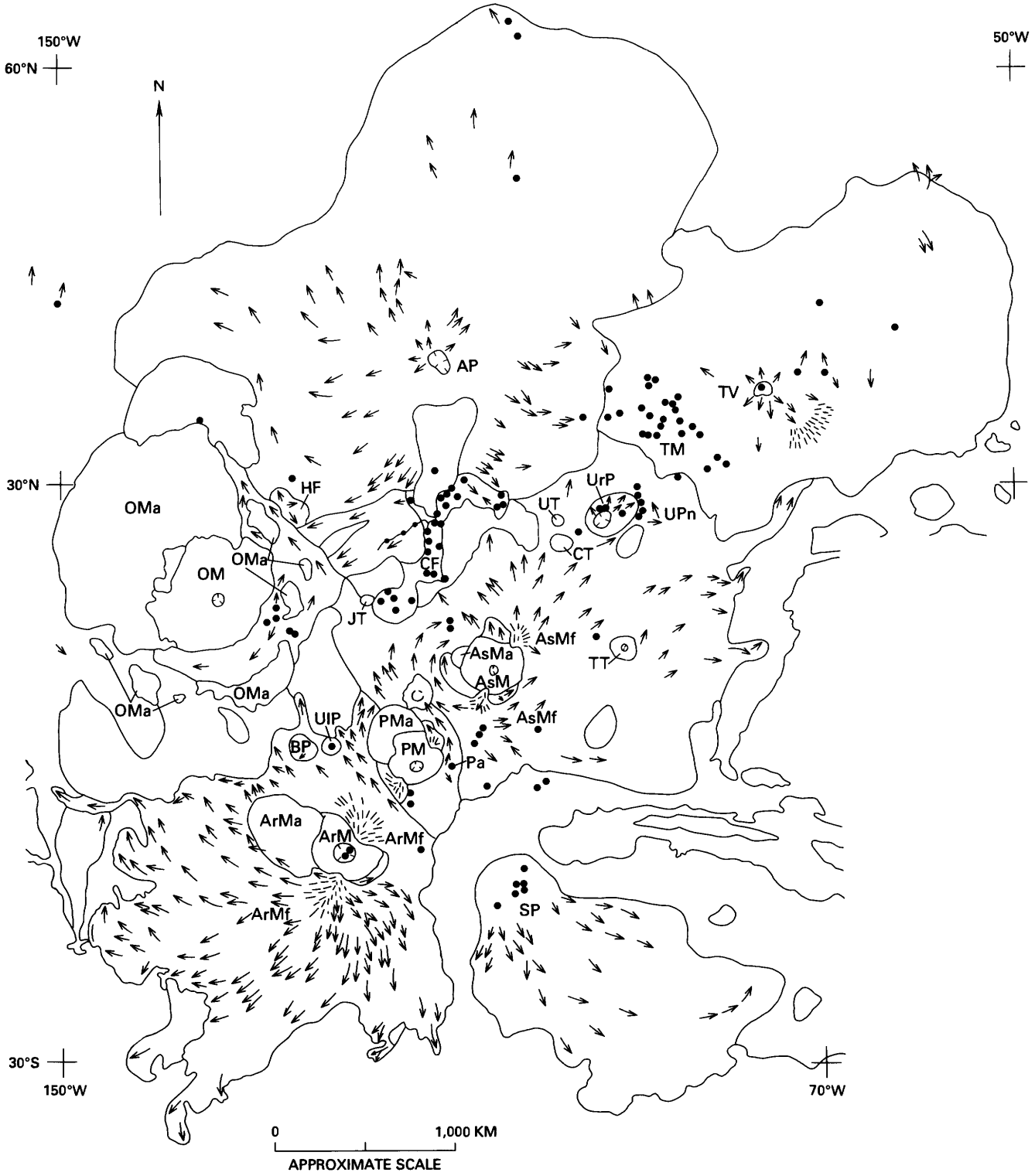
150°W
60°N
N
50°W
30°N
30°S
150°W
70°W
AP
TV
TM
HF
OMa
OM
UrP
UT
UPn
CT
CF
JT
AsMf
AsMa
AsM
TT
UIP
PMa
BP
PM
Pa
ArMa
ArM
ArMf
SP
0
1,000 KM
APPROXIMATE SCALE

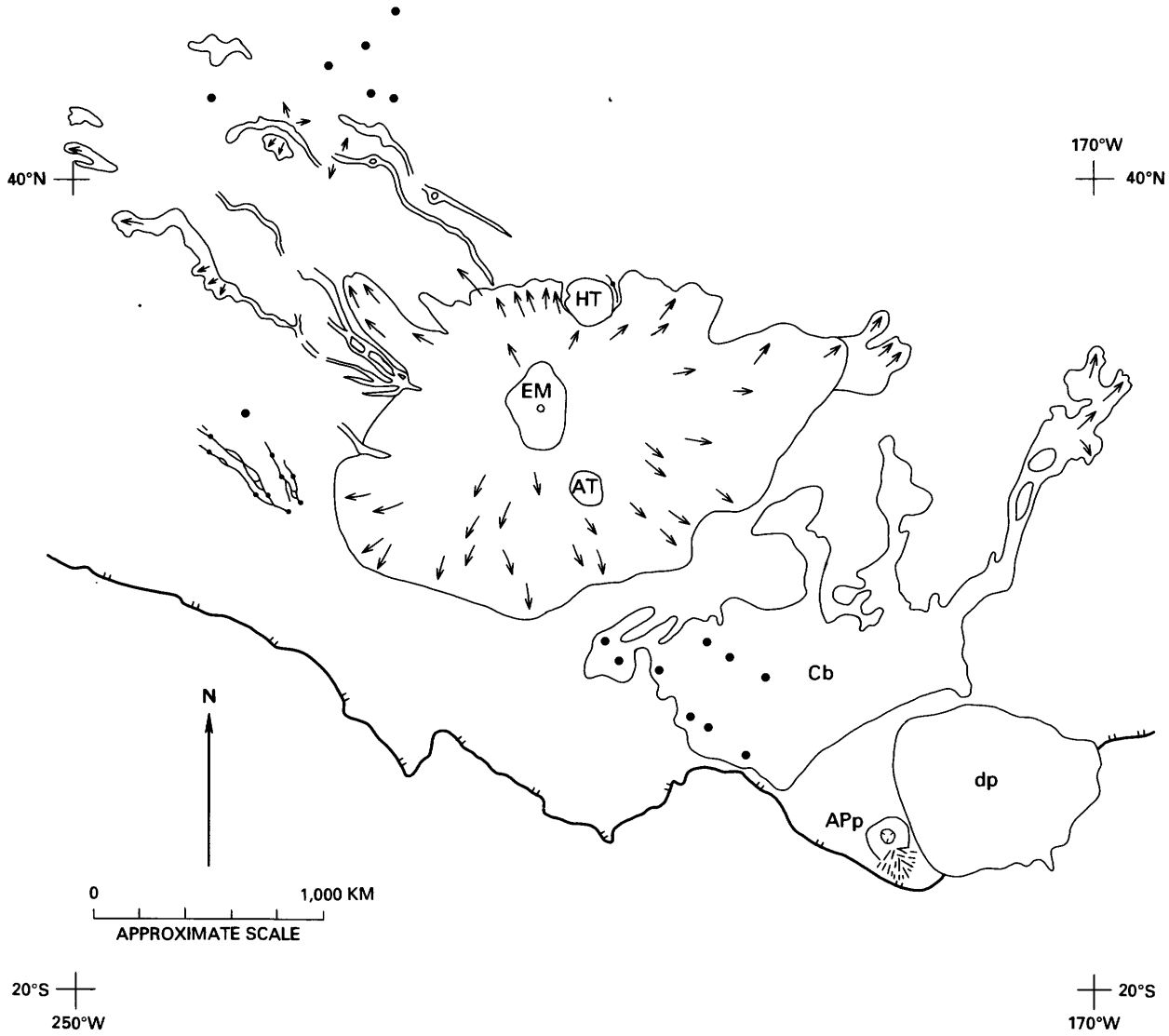

Figure I–3. Sketch map of Elysium region of Mars, showing relations between volcanoes, lava flows, and channels. EM, Elysium Mons, AT, Albor Tholus; HT, Hecates Tholus; ApP, Apollinaris Patera shield; Cb, Cerberus Planitia lava field; dp, thick deposits of possible pyroclastic debris. Outlines denote lava-flow fields of various volcanic centers; arrows within outlines indicate paleoflow directions of lavas. Long, narrow features are discrete flows or channels. Outline with paired hachures, boundary scarp between highlands and northern plains; dashes, apron of Apollinaris Patera; dots, small volcanic edifices with low relief; irregular line with small dots, fissures; hachures, calderas. Mercator projection.

along the great canyon system of Valles Marineris, which spans more than 3,000 km along the equatorial belt of the planet, there is no evidence of the rifting and accompanying extension required by plate tectonics; no discrete plate segments are definable, and no indication of spreading, migration, or subduction is apparent. Mars is a one-plate planet, and thus development of composite cones as we know them on Earth may have been precluded.

The great volcanoes of the Tharsis ridge achieved their immensity at least in part because they were stationary over their respective hotspots (Carr, 1973, 1976b). In contrast, terrestrial shield volcanoes are small "because the Earth's mobile plates move growing shields away" from their deep magma sources (Wood, 1984a). As pointed out by Carr (1980), however, a volcano can grow only as high as a column of magma can be forced to rise; that height is governed in part by the pressure head that results from differences in density between the magma and the surrounding rocks. Carr (1974, 1976a, 1980) estimated that the depth to magma generation at the Tharsis volcanoes must have been about 200 km to attain the pressure difference necessary for magma to rise to

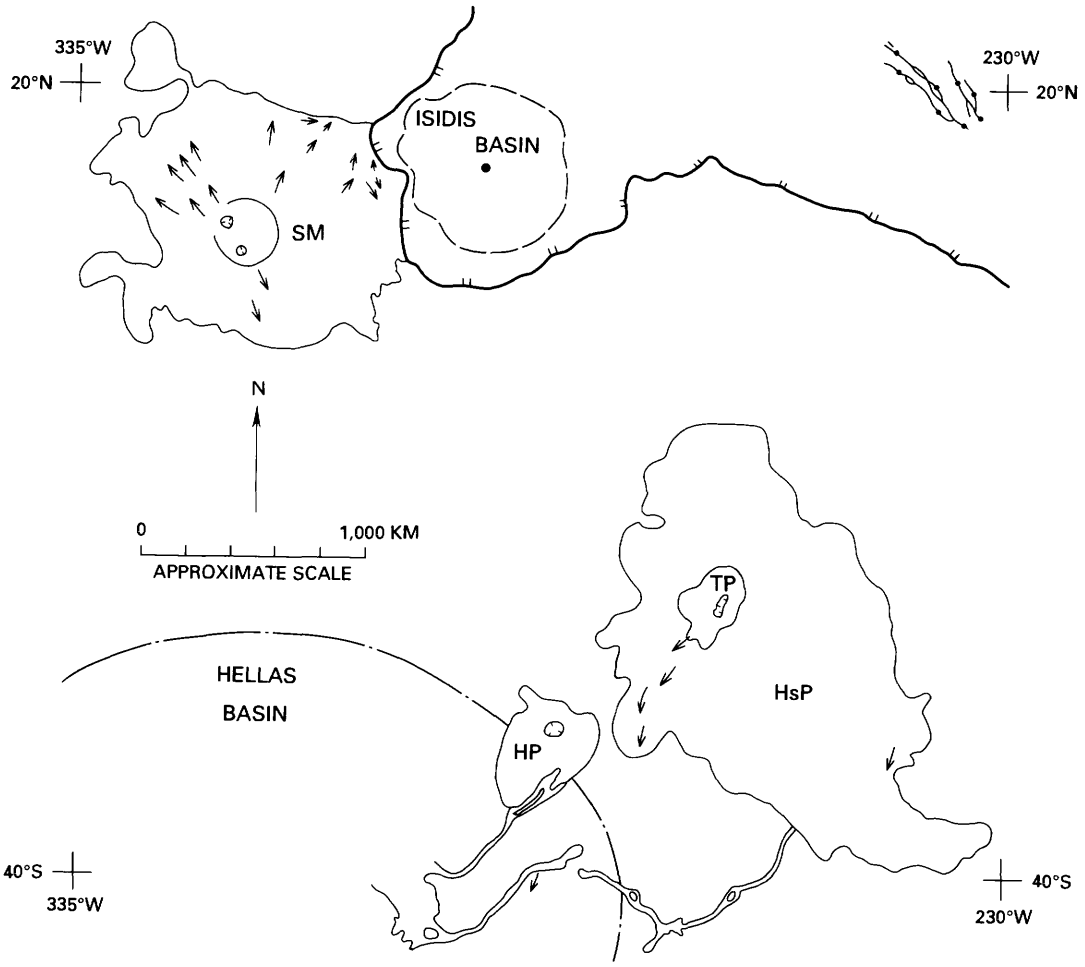

Figure I–4. Sketch map of Syrtis Major and part of Hellas Basin regions, showing relations between calderas, volcanoes, lava flows, and channels. HP, Hadriaca Patera; TP, Tyrrhena Patera; HsP, Hesperia Planum; SM, Syrtis Major. Outlines denote lava-flow fields of various volcanic centers; arrows within outlines indicate paleoflow directions of lavas. Dot-dashed arc marks most conspicuous ring of Hellas impact basin; short dashes, Isidis impact basin; line with paired hachures, boundary scarp between highlands and northern plains; dot, chains of small cratered cones; irregular line with small dots, fissures; hachures, calderas. Mercator projection.

elevations above 25 km. In contrast, generation of magma by partial melting of the mantle beneath Hawaiian shield volcanoes is thought to occur at about 60-km depth (Eaton and Murata, 1960). On Earth, lithospheric plates are only a few kilometers thick at the midoceanic ridges, whereas beneath the topographically highest parts of the continents, plates may be as thick as 100 km; on Mars, the apparently stationary, globally continuous, elastic lithosphere has been estimated at 100 to 200 km thick (Solomon and Head, 1990). According to Plescia and Saunders (1982), the extensive systems of normal faults and fractures so conspicuous in the Tharsis region resulted from several discrete episodes of tectonism that began in the southern part of the plains province (Thaumasia area) and migrated first to the northern Syria Planum area and later to the central Tharsis region near Pavonis Mons; volcanic eruptions predominated between periods of tectonism and culminated in the development of the huge Tharsis shield volcanoes. The topographic prominence of the Tharsis region may be attributable to the combined effects of volcanic construction and "compositional buoyant uplift" (Phillips and others, 1981).

Several investigators have speculated that pyroclastic activity played a significant role in shaping the martian landscape (Malin, 1977; Saunders and others, 1980; Mouginis-Mark and others, 1982a; Scott and Tanaka, 1982; Greeley and Crown, 1990; Crown and Greeley, 1990a, b). On Earth, extensive pyroclastic materials are commonly more silicic than basalt, so that positive identification of such materials on Mars

has important implications for composition, as well as eruptive style. Scott and Tanaka (1982) proposed that a substantial part of the plains west and southwest of Olympus Mons in the Amazonis Planitia area, and the fluted deposits around Apollinaris Patera are composed of welded and nonwelded ignimbrites. Francis and Wood (1982) noted, however, that the physical appearance of these deposits is equally characteristic of many fine-grained, bedded sedimentary deposits; and the absence of an identifiable source caldera for such widespread (more than 1 million km^2) ash deposits virtually precludes an analogy with terrestrial ignimbrites. Thick pyroclastic deposits likely of basaltic composition may exist around the large highlands calderas Tyrrhena Patera (Greeley and Crown, 1990) and Hadriaca Patera (Crown and Greeley, 1990a, b). Several highlands structures a few kilometers across have been compared to the resurgent domes of terrestrial continental calderas, such as Valles Caldera in New Mexico or Cerro Galán in Argentina, which commonly erupt enormous volumes of pyroclastic ejecta; although the evidence is not compelling, these rugged highlands features are illustrated and discussed in the following text. By far the best candidate for a composite volcano is the symmetrical structure south of Apollinaris Patera in the Aeolis quadrangle. Conical in shape, it is about 30 km across at the base and 2 km high, with deeply dissected flanks and a summit caldera. Another landform of possible silicic composition lies northwest of Olympus Mons, where a cluster of features reminiscent of terrestrial rhyolitic and dacitic domes is associated with crenulated-ridge deposits that resemble viscous, silicic lava flows (Fink, 1980; Hodges, 1980b).

Wilson and Head (1983) noted that the probable abundance of CO_2 and H_2O in the uppermost crustal deposits of Mars could engender explosive eruptions, regardless of magma composition. Instead of the silicic pyroclastic volcanism common on Earth, massive tephra deposits in the martian highlands could have been produced by the explosive comminution of basaltic lava as it interacted with subsurface ice or ground water (Reimers and Komar, 1979; Crown and Greeley, 1990b). The strong geomorphic evidence for a high volatile content in the martian crust, together with the high water content of shergottite, nakhlite, and chassignite (SNC) meteorites, thought to be of martian origin (Johnson and others, 1990), supports the interpretation that basaltic pyroclastic deposits occur. Crown and Greeley (1990b) believed that the "morphologies and the energetics of explosive eruptions are consistent with both magmatic and hydromagmatic origins" for the large highland shields of Tyrrhena and Hadriaca Paterae, but they concluded that the regional setting was more favorable for hydromagmatic (phreatomagmatic) processes.

Francis and Wood (1982), however, pointed out that phreatomagmatic activity is unlikely to have produced such large volcanoes as the highlands paterae, inasmuch as initial water-charged eruptions would probably evolve to less explosive activity as the conduit became coated with lava, reducing water/magma interaction. They speculated that paterae might, instead, be formed by volatile-rich kimberlitic eruptions during a stage of vigorous degassing early in the planet's history. Wood (1984a) concluded from a survey of the calderas thus far identified in the Solar System that the highland paterae constitute a class of calderas unique to Mars.

Based on terrestrial comparisons, the inescapable conclusion is that most volcanoes on Mars formed largely by effusive eruptions of basaltic lavas. Hulme (1976) and Zimbelman (1985) suggested that the most recent flows on the flanks of Olympus and Ascraeus Montes may be basaltic andesite or andesite, with higher silica contents than Hawaiian basalts, and that the steeper, uppermost slopes of Elysium Mons may be surfaced by more differentiated flows or pyroclastic deposits (Scott and Allingham, 1976; Malin, 1977; Blasius and Cutts, 1981), as occurs at Hawaiian shield volcanoes. Evidence for major silicic or felsic volcanism is equivocal at best, however, implying that martian crustal history with respect to mineralogic differentiation and fractionation may differ greatly from that of Earth (Francis and Wood, 1982). The confinement of most postulated felsic volcanic features to the highlands suggests that, if differentiation did occur, a compositional distinction could have developed between the martian crust of the northern lava plains and that of the southern cratered highlands. Such a compositional difference might be similar to the general mafic/felsic dichotomy between the ocean basins and continents on Earth, but data are unavailable to test this inference.

ATMOSPHERIC INFLUENCE

Volcano/ice interactions have been invoked to explain numerous enigmatic features on Mars, particularly in the northern plains. Justification for such interpretations ultimately requires a knowledge of atmospheric history, detailed analysis of which is beyond the scope of this atlas, but brief comments on the planet's volatile budget are pertinent.

The history of the martian atmosphere, a topic of extensive investigation and debate (for example, Fanale, 1976; Fanale and Cannon, 1979; Toon and others, 1980; Hunten and others, 1989; Pepin, 1985;

Pollack and others, 1987; Dreibus and Wänke, 1987; Kasting and Toon, 1989), is related intrinsically to the volcanic record. The composition of the present atmosphere, derived mainly from volcanic outgassing, is largely CO_2 (95.3 volume percent), with 2.7 percent N_2, 1.6 percent Ar, and only 0.13 percent O_2 (Owen and others, 1977). Water vapor is near saturation for night-time temperatures, ranging from 1 to 100 precipitable micrometers (pr μm, the depth of water that would result if all the vapor in the atmosphere were precipitated evenly over the entire planetary surface) and averaging about 12 pr μm (Farmer and Doms, 1979). Atmospheric pressure on Mars currently averages only about 7 mbars (Pollack and others, 1987), less than 1/100 that on Earth; it varies by about a factor of 10 from the summit of Olympus Mons, at 26 km above datum, to the floor of the Hellas Basin, at −4 km (Carr, 1984). Liquid water is everywhere unstable at the surface, and ice is stable throughout the year only at the poles. Surface temperatures range from 150 K at the winter pole to 220 K at low latitudes (Carr, 1987), so that, depending on time of day, location, and season, water will evaporate, sublimate, or freeze (Carr, 1984). (The mean martian temperature is 218 K; Earth's present mean temperature is 288 K.) Most of the outgassed volatile materials retained by the planet are trapped within the martian megaregolith and polar icecaps rather than in the atmosphere (Carr, 1984). Mars today is a polar desert, but it may not always have been so.

Numerous channels and valley networks that appear to have formed or been modified by fluvial and (or) glacial erosion (Carr and Clow, 1981; Lucchitta, 1981; Baker, 1982; Gulick and Baker, 1990a, b) suggest that the atmosphere was once considerably denser than it is now (Carr, 1981; Pollack and others, 1987); the more temperate climate thus created could have permitted ice and (or) water to exist at the surface in the equatorial regions of the planet. Baker and others (1990) postulated that Mars underwent cyclical epochs during which atmospheric pressure was well above its current level, permitting intense fluvial, glacial, and related processes to occur in conjunction with formation of a northern-hemispheric ocean. Mouginis-Mark (1990) observed that channels near the southeast base of Olympus Mons indicate recent release of water in the Tharsis region. Parker and others (1989) cited evidence for standing bodies of water in the northern plains. Schaefer (1990) concluded that an ocean 1,000 to 2,800 m deep could have inundated the lowland terrain, enabling deposition of extensive carbonate beds several hundred or more meters thick.

To raise the surface temperature above the freezing point of water, "atmospheres containing several bars of CO_2" would be required (Pollack and others, 1987). According to Dreibus and Wänke (1987), most of the water incorporated in the planet during accretion would have been reduced by metallic Fe to yield H_2, which would escape; thus, the occurrence of H_2O at the surface largely depended on volcanic outgassing. The escape velocity of Mars, 5 km/s, is less than half that of Earth (11.5 km/s) but is sufficiently high to have retained outgassed H_2O and CO_2 for billions of years. The controlling mechanism seems to have been the efficiency of outgassing, which Pollack and Black (1979) estimated at 1/20 to 1/5 that of Earth.

Carr (1986a, 1987) summarized geologic and geomorphic evidence that suggests an important role for water as an erosional agent, as well as the presence of ground ice at latitudes above 30°. Further support for an early volatile-rich planet is found in SNC meteorites, which are widely assumed to be of martian origin (Wood and Ashwal, 1981; McSween, 1985; Carr, 1987; Dreibus and Wänke, 1987). These stony meteorites not only are volatile-rich but also have distinctive differentiated compositions and show remarkably young crystallization ages of 1.3 Ga—3 b.y. younger than any other known meteorites (Wood and Ashwal, 1981; Dreibus and Wänke, 1987).

The issue of present and past martian water endowment has been continuously debated since the Viking mission; theoretical analyses, largely driven by geologic observation and interpretation, have yielded progressively increasing estimates of the total water budget on the planet. In the late 1970's, immediately after the Viking Lander mission, Anders and Owen (1977), using argon-isotopic data, estimated that Mars hosted only enough water to cover the planet to a depth of 9 m. On the basis of nitrogen-isotopic data, McElroy and others (1977) estimated that about 120 m of water had outgassed. Subsequent reassessments of nitrogen sinks led Yung and McElroy (1979) to increase the water estimate to as much as 500 m. Greeley (1987) concluded that water released in association with surface volcanism amounted only to 46 m planetwide. On the basis of analyses of halogens in SNC meteorites and assumptions regarding the amount of H_2O left in the mantle of Mars after accretion and oxidation of metallic Fe, Dreibus and Wänke (1987) concluded that 36 ppm H_2O remained in the martian mantle, corresponding to a planetwide envelope 130 m thick. Carr (1986a, 1987) suggested that the equivalent of 500 to 1,000 m of water planetwide could have outgassed. Inasmuch as the planet's original inventory is now thought to reside largely within the northern icecap and within the regolith, this retained water, when

encountered by magma both before and after eruption, would have influenced martian landscape development. Aside from features of apparent hydromagmatic origin, escarpments and impact craters also show morphologic modifications, such as terrain "softening" and fluidized ejecta blankets, that may indicate the presence of ground ice in the escarpment and target materials. The interaction of magma with both water and ice, in the subsurface as well as at the surface, is likely to have occurred, and geomorphic analyses may provide evidence of where and when either state of H_2O has existed.

For example, large debris aprons termed "aureoles" occur on the northwest sides of each of the main shield volcanoes atop the Tharsis ridge; these lobate deposits have a surface texture and morphology different from those of the more conspicuous aureoles that surround Olympus Mons but strongly resembling those of the relatively small debris lobes at the northwest base of the Olympus Mons escarpment. All of these deposits have been interpreted as products of glacial processes (Williams, 1978; Hodges and Moore, 1979; Lucchitta, 1981). Inasmuch as they show a conspicuous decrease in size from the oldest volcano, Arsia Mons, to the youngest, Olympus Mons, an ice-related hypothesis of origin for these materials has implications for the interpretation of climatic history and, if valid, suggests that intense glaciation was occurring during or after formation of Arsia Mons, decreasing over time to a much less extensive stage by the end of Olympus Mons development. Alternatively, the relative sizes of the aureoles could reflect the decreasing ages of the volcanoes under essentially static glacial conditions. Demise of the last glacial ice could have provided the water inferred by Mouginis-Mark (1990) to have carved recent channels at the southeast base of Olympus Mons.

GRAVITATIONAL INFLUENCE

Acceleration of gravity at the surface of Mars is about 3.7 m/s^2, approximately 3/8 that of Earth (9.8 m/s^2), and the difference should be reflected in the shapes and sizes of volcanic landforms. Low surface gravity, in combination with low atmospheric pressure, dictates that explosive eruptions on Mars should produce such fine-grained and widely dispersed ejecta that a positive construct around a vent would be lower and wider than on Earth or might not form at all (Wilson and Head, 1983). Such an effect may be manifest at the highlands calderas Tyrrhena and Hadriaca Paterae, which have very low relief. Low gravity also may augment the construction of massive shield volcanoes. All other variables being equal, lower surface gravity causes lava flows to be thicker on Mars than on Earth (for example, Moore and others, 1978).

STRATIGRAPHY AND RELATIVE AGES OF VOLCANIC LANDFORMS

Estimates of the relative ages of martian volcanic edifices and eruptive centers rely on the interpretation of superposition and intersection relations and the number of superimposed impact craters obtained from crater counts. (Interpretation of the impact origin of craters is based on the overall morphology of their flanks and ejecta blankets, as well as on their inner configuration and relation to surrounding grade.) Superposition and intersection criteria have priority over crater counts if the evidence is conflicting. For the purposes of this atlas, stratigraphic ages were obtained from the three latest geologic maps of the planet, at 1:15,000,000 scale (Scott and Tanaka, 1986; Greeley and Guest, 1987; Tanaka and Scott, 1987), and are designated by system and rock unit. The time-stratigraphic systems established for Mars are, from oldest to youngest, Noachian, Hesperian, and Amazonian (Scott and Carr, 1978). Volcanic processes have been active throughout the history of the planet, but the major shield-building eruptions appear to have occurred during the Late Hesperian (Tanaka, 1986) and Early Amazonian (Greeley and Spudis, 1981) epochs. The age relations between the principal shield volcanoes and small eruptive centers, based on crater counts, are plotted in figure I–5. The flanks, lava fans, and calderas of large shield volcanoes are dated separately where crater-count data permit. The flanks and calderas of the Tharsis shields were resurfaced by lavas through late Amazonian time, and small edifices also erupted through the late Amazonian (fig. I–5).

In the procedure for estimating relative ages from the number of superposed impact craters, a frequency distribution of craters as a function of size is established. The relative ages of landforms are expressed as the cumulative number of craters per square kilometer that are larger than a given diameter (generally 1.0 km), with an uncertainty related to the number of craters counted (U.S. National Aeronautics and Space Administration, 1978). Landforms and surfaces with a smaller number of superposed craters per unit area are presumed to be younger than those with a larger number of superposed craters per unit area. In the following descriptions of volcanic provinces, relative ages are reported as the cumulative number of craters larger than 1.0 km in diameter per square

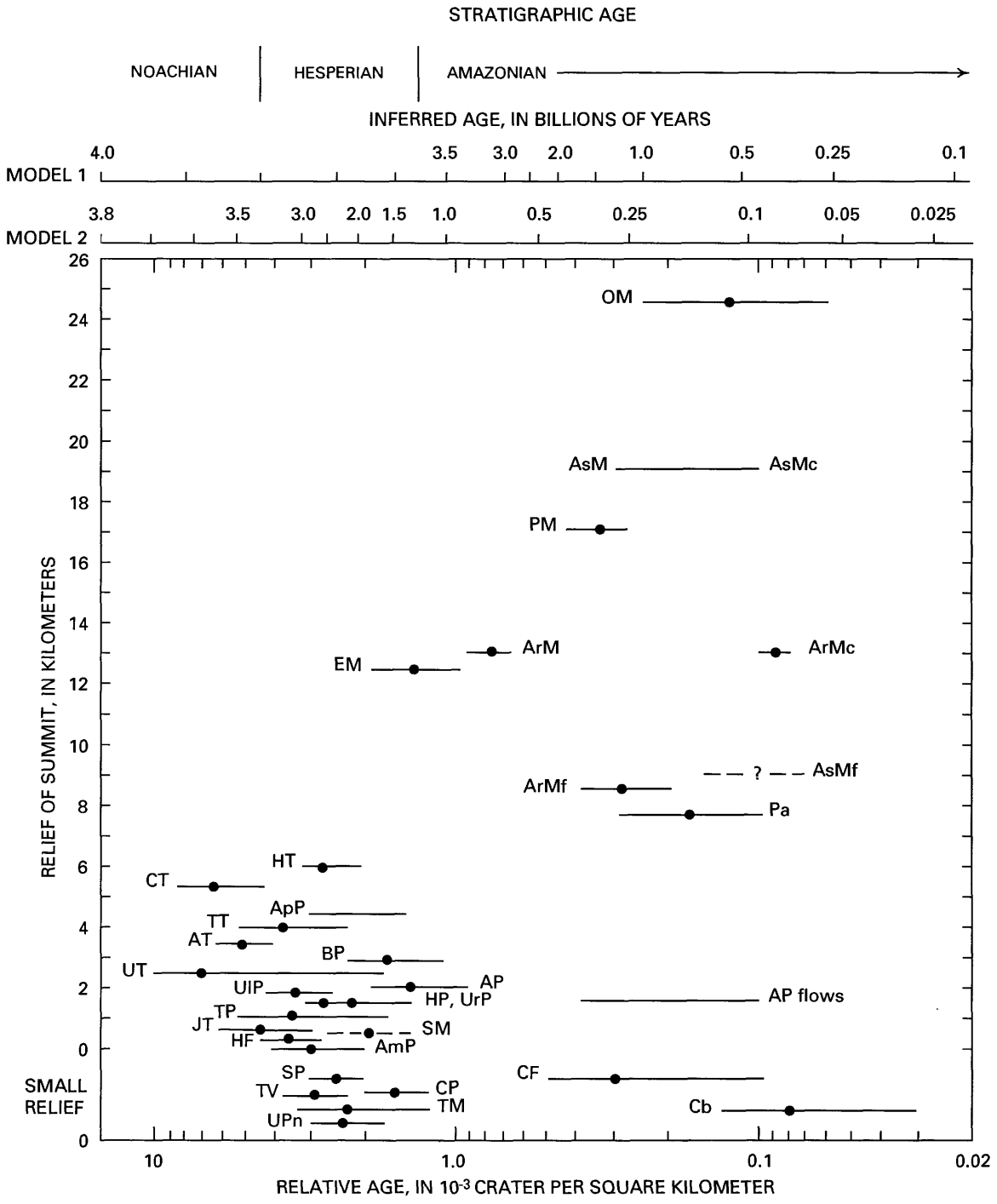

Figure I–5. Summit relief versus relative age of volcanoes and related subunits on Mars. Lines with dots represent best estimates of ages (dots) and error ranges in ages (ends of lines); lines without dots represent estimated age ranges (ends of lines) (AsM is older than its caldera, AsMc, and is so indicated); dashed line with question mark (AsMf) is based on superposition and geologic interpretation; dashed line with dot represents best estimate of relative age (dot) and geologic interpretation for error range (SM). Montes: OM, Olympus; AsM, Ascraeus; PM, Pavonis; ArM, Arsia; EM, Elysium. Tholi: HT, Hecates; CT, Ceraunius; TT, Tharsis; AT, Albor; UT, Uranius; JT, Jovis. Patera shields: AP, Alba; UrP, Uranius; BP, Biblis; UlP, Ulysses; ApP, Apollinaris; AmP, Amphitrites; TP, Tyrrhena; HP, Hadriaca; SM, Syrtis Major. Collapse structure: HF, Halex Fossae. Volcanic fields with small edifices: SP, Syria Planum; TV, Tempe Volcano; TM, Tempe-Mareotis; UPn, Uranius Patera North; CP, Chryse Planitia; CF, Ceraunius Fossae; Cb, Cerberus. Volcanic sub-units: ArMf, Arsia lava fans; ArMc, Arsia caldera; AsMf, Ascraeus lava fans; AsMc, Ascraeus caldera; Pa, Pavonis east lava apron. Model ages at top from (1) Neukum and Hiller (1981) and (2) Soderblom (1977); estimated stratigraphic ages from Tanaka (1986) and geologic maps by Scott and Tanaka (1986) and Greeley and Guest (1987).

kilometer. Sources for these data are, chiefly, Neukum and Hiller (1981), Plescia and Saunders (1979), and H.J. Moore (unpub. data, 1990). If the province description does not include a relative age, the area is too small to obtain reliable crater-count data.

Ages (in years) estimated from relative ages are model dependent, and those reported here have been inferred from two models: model 1, largely promoted by Gerhard Neukum (Neukum and Wise, 1976; Neukum and others, 1978; Neukum and Hiller, 1981); and model 2, developed by L.A. Soderblom (Soderblom and others, 1974; Soderblom, 1977). Inferred ages according to these two models may differ by a factor of nearly 5. For example, for a relative age of 1×10^{-3} craters/km^2, the inferred age is 3.4 Ga in model 1 and 0.9 Ga in model 2. No attempt is made here to evaluate the relative merits or accuracy of these two models; however, we note that if SNC meteorites do derive from Mars, as is widely assumed, the case for the older ages in model 1 is greatly weakened. Ages estimated from superposed impact craters larger than 4 km in diameter, and reckoning of cratering rates for Mars from various sources (Hartmann and others, 1981), yield ages and uncertainties similar to those in the model 1–2 range reported here. For example, the age range of the Chryse Planitia area is here given as 3.6 to 1.1 Ga, reasonably close to that (3.8–1.2 Ga) reported by Hartmann and others (1981). Differences in the reported ages are partly related to the fact that materials of a volcano are not everywhere of the same age.

Relative age, stratigraphic age, and the two models for inferred age versus the relief of volcanic features are plotted in figure I–5. Several observations are illustrated by this plot. (1) Volcanic processes have been active throughout the history of Mars, but the major shield-building eruptions apparently occurred during the Hesperian (Tanaka, 1986) and Amazonian (Greeley and Spudis, 1981) periods. Volcanism began on Mars before about 3.9–3.6 Ga and persisted to about 0.1–0.02 Ga. Indeed, Soderblom and others (1974) speculated that volcanism could be active on the planet even today. (2) The volcanic edifices fall into three fairly distinct groups: (a) shield volcanoes with huge relief that are mainly Amazonian in age, except Elysium Mons, which may be late Hesperian or early Amazonian; (b) large shield volcanoes with moderate relief that are primarily Hesperian and Noachian in age, except Alba Patera, which may be late Hesperian or early Amazonian; and (c) small volcanoes with low relief that are Hesperian and Amazonian. (3) Regardless of model, many volcanic landforms on Mars that appear to be relatively pristine are as old as 3.5 to 1 Ga, in contrast to those on Earth, where coeval rocks have long since been deformed, metamorphosed, and eroded. (4) The largest shield volcanoes, many of which have datable subunits, were active for long periods of time (Neukum and Hiller, 1981)—possibly as long as 0.2 to 2.0 Ga, depending on the model; in contrast, large shield volcanoes on Earth have lifetimes of only a few million years (Wood, 1984a). The smaller martian shield volcanoes with low to moderate relief were active concurrently with the large shields during Hesperian and Amazonian time. The general sequence described here is mostly consistent with the relative chronology of martian volcanoes derived by Landheim and Barlow (1991) on the basis of crater-size/frequency-distribution curves, using craters in the 1.5- to 8-km-diameter range.

ATLAS ORGANIZATION AND ILLUSTRATIONS

This atlas includes an index map, at 1:25,000,000 scale (pl. 1). All provinces dominated by volcanic or possibly volcanic features are outlined schematically on this map, and characteristic landforms are indicated for each; base outlines of the major shield volcanoes are drawn as accurately as possible. Representative photographs (most greatly reduced in scale) portray the dominant landform(s) in each province. Numbers correspond to the 1:5,000,000-scale Mars Chart (MC) of Batson and others (1979) that includes the volcanic province, and letters distinguish separate features or provinces within the chart area; if there is overlap, a second number refers to the adjacent chart. The provinces are summarized in table 1.

For each named province or feature discussed and illustrated in the text, the following information is included: (1) number of the best Viking 211-series mosaic(s) (Evans, 1982; mosaic numbers higher than 5869, undocumented); (2) MC number and identifying letter; (3) center or boundary coordinates, as appropriate, to the nearest degree; (4) approximate dimensions; (5) estimated relative age; (6) inferred age; (7) stratigraphic age; (8) an outline of especially distinctive characteristics; (9) a detailed description and applicable interpretations; (10) a concise list of references, and (11) representative illustrations. Where appropriate, photographs of possible terrestrial analogs are included for comparison. Each province description was intended essentially to stand alone, to enhance the use of this atlas as a reference volume; therefore, although redundancies in the descriptions of similar features in different provinces are numerous, we decided against consolidation (except for minor shield volcanoes of the Tharsis region).

Reference is sometimes made to controlled mosaics in the Miscellaneous Investigations Series Maps of MC subquadrangles prepared by the U.S. Geological Survey at 1:2,000,000 scale (Batson, 1990), in addition to the 211-series mosaics; these mosaics cover the entire planet and include the Viking Orbiter frame numbers used to prepare them. All of the relevant MC subquadrangles are listed in table 1. For some volcanic features and areas, Miscellaneous Investigation Series controlled mosaics were prepared by the U.S. Geological Survey at 1:500,000 scale on transverse Mercator projections; these Mars Transverse Mercator (MTM) controlled mosaics, which are used for special geologic studies, include high-resolution Viking Orbiter images and the frame numbers used to prepare them. Available MTM controlled mosaics include parts or all of Olympus, Arsia, Ascraeus, and Elysium Montes, Alba, Tyrrhena, and Hadriaca Paterae, and Tempe-Mareotis Fossae.

Organization of the text is as follows: The numerous provinces of the Tharsis region, where volcanism was especially widespread and intense, are described and illustrated first, from large, unambiguous structures to small, enigmatic features. After Tharsis, the Elysium region and adjacent provinces are reviewed, followed by the minor provinces of the northern plains. The large calderas of Syrtis Major and the several large shield volcanoes in the cratered highlands are next addressed, succeeded by small volcanic features within the highlands. Finally, the small, isolated landforms of the north polar province at the margin of the icecap are discussed.

A few words about Viking photographic coverage are in order. The entire planet was photographed at a resolution of 200 m (Carr, 1984) by Orbiters A and B (identified by revolution/frame number), and some areas are covered at much higher resolutions (extended-mission S-frames) down to 10 m—a superb and remarkable technological achievement. Nonetheless, the collection has some limitations for purposes of interpretation and comparison with terrestrial landforms. Many features normally diagnostic of volcanic provinces on Earth (for example, dikes, necks, or lava-flow textures) could be well below the limits of resolution of Viking Orbiter images of a specific area. Thus, we may have overlooked some small volcanic features in the northern plains (north of 50° N.), simply because image resolution is insufficient to identify them.

In each of the photographs that follow, north is generally at the top unless otherwise indicated; north arrows, where shown, are approximate. Viking Orbiter images are orthographic (rectified; scale constant) except for a few rectilinear (oblique; scale variable) frames, as noted. Digital-image mosaics are sinusoidal-equal-area projections. Photographs of possible terrestrial analogs are interspersed throughout the atlas with their presumed martian counterparts. Topographic profiles of martian features are included where available.

The bibliography is not exhaustive; references are limited to those cited, but they represent a selection of principal observations and ideas from the large body of literature related to volcanism on Mars. Detailed reviews of the planet's geologic history and interpretations of its landscape are provided in the splendid books by Mutch and others (1976), Baker (1982), and Carr (1981, 1984).

In this atlas, comparative characteristics are discussed and tentative interpretations proposed, but the primary emphasis is on the identification, description, and classification of volcanic constructs, based on morphologic characteristics as described by Pike (1978) and Pike and Clow (1981a, b). For some features, more complete analyses can be found in the references. This compilation developed over a period of many years, during which our own thinking and that of our colleagues evolved and changed; any inconsistencies that remain are probably attributable in part to the long period of gestation. Although we endeavored to make a thorough and comprehensive survey of the planet's surface, we may have failed to identify some volcanic landforms, and our interpretations may differ from those of other investigators who have found or will find additional features of volcanic origin; we welcome amendments to our inventory.

Table 1. Volcanic provinces of Mars, listed sequentially by Mars Chart number, with documentation data and brief interpretive description

[Selected Viking frames listed are representative but may not include every image available. Additional frame numbers are listed in the mosaic indices (Evans, 1982). Mars Chart subquadrangles from Batson and others (1979); selected Viking 211-series mosaics through number 5869 from Evans (1982); mosaic numbers higher than 5869 are undocumented]

Mars Chart (MC) province identification	Volcanic province	Mars Chart (MC) subquadrangle	Location (lat., long. W.)	Viking 211-series mosaic	Viking revolution/ frame	Interpretative description
1A	Borealis	1B, 1D	77°–81° N., 60°–75°	5562, 5869	70B/09, 70B/27, 70B/29, 560B/42	Four cratered cones, all of different shape; two flat-topped mesas without craters—probable cinder cones and maars; possible tablemountains.
2A	Arcadia Planitia	2 SC	42°–50° N., 140°–162°	5558	115A/11–28	Several low convex domes with summit depressions atop series of arcuate parallel ridges; associated with linear trough containing median ridge—possible silicic eruptive center.
2B	Olympus Mons Aureole North.	2 SC	33°–35° N., 133°–137°	5327	49B/04, 49B/06	Small cluster of cones with summit craters amid disintegrating margin of aureole materials—possibly cinder cones or pseudocraters.
3A–2	Alba Patera	2 SE, 2 NE, 3 NW, 3 SW, 3 SE	40° N., 110°	5065, 5068, 5071, 5728	7B/01–94, 252S/01–34, 516A/03–07, 857A/01–24	Major shield volcano, probably basaltic, with central caldera; broad, flat summit area outlined by numerous curvilinear grabens; low relief of about 2 to 5 km; flows, lava tubes, channels, and associated features on flanks of shield.
3B	Tempe-Mareotis	3 SE	31°–40° N., 79°–91°	5813	627A/01–58	Small, low shields of various shapes; excellent examples, 2 to 7 km across, with surrounding flow aprons, localized by fractures; numerous collapse pits and leveed fissures—features characteristic of basaltic volcanism.
3C–9	Ceraunius Fossae	3 SW, 9 NE	16°–40° N., 92°–117°	5391	224A/01–70, 516A/08–32	Small, low shields with conspicuous lava flows superposed on densely fractured terrain; numerous collapse pits aligned along fractures and grabens.
3D	Tempe Volcano	3 SE	38° N., 76°	5866	519A/15, 704B/52	Isolated volcano with irregular peak and radial pattern of narrow lava flows; lava tubes and tube ridges to southeast.
3E–4	Tempe Patera	3 SE, 4 SW	44° N., 62°	5866	704B/30–39	Central depression that resembles caldera, with radial pattern of broad channels but no obvious edifice; also, filled lava ring and possible silicic dome.
4A	Acidalia Planitia	4 SE	34°–48° N., 3°–31°	5025, 5036, 5557	26A/21–40, 35A/61–82, 38A/11–32, 70A/01–12, 72A/01–25	Small cones with summit craters, resembling cinder cones or pseudocraters, amid remnants of highlands plateau; also, cratered ridges that could be tablemountains of subglacial origin.
6A	Utopia Planitia Northwest.	6 NW	47°–51° N., 284°–291°	5078	11B/01–05	Narrow, arcuate, parallel ridges similar to those in Isidis Planitia (13B–14) that consist partly of conical, cratered elements—pattern possibly caused by fracture-controlled chains of cinder cones.
6B–7	Utopia Planitia	6 NE, 6 SE, 7 NW, 7 SW, 7 SC	40°–50° N., 223°–273°	5072, 5080	9B/01–60, 10B/10–69	Small cratered buttes and mesas designated as "type" tablemountains, possibly formed by subglacial eruptions; terrain flooded by lava that embays impact craters.

Table 1. Volcanic provinces of Mars, listed sequentially by Mars Chart number, with documentation data and brief interpretive description—Continued

Mars Chart (MC) province identification	Volcanic province	Mars Chart (MC) subquadrangle	Location (lat., long. W.)	Viking 211-series mosaic	Viking revolution/ frame	Interpretative description
6C–14	Utopia Planitia South---	6 SE, 6 SW, 14 NW	24°–36° N., 254°–277°	5781, 5884	572A/03–08, 572A/27–36, 608A/03–09, 645A/01–48, 838A/25–27	Narrow arcuate ridges and knobs, possibly formed by coalescent volcanic cones; furrows with central ridges; ridges and chains of cratered cones; some cones atop small plateaus with marginal cracks, resembling terrestrial pressure plateaus or, possibly, tablemountains.
7A	Phlegra Montes----------	7 NE, 7 SE	43°–55° N., 178°–210°	5579, 5993	76B/84–90, 279S/04–50, 776A/27–34, 810A/29	Narrow curvilinear ridges, similar to those with more obvious cone elements; irregular rilles or troughs forming distinctively patterned ground that may have formed by volcano/ice interaction.
7B–15	Elysium Mons, Albor Tholus, Hecates Tholus.	7 SW, 7 SC, 15 NW	14°–39° N., 202°–233°	5601, 5643, 5787, 5906	86A/31–46, 106A/81–88, 541A/01–46, 651A/01–24, 729A/01–03, 732A/13, 846A/13–22, 881A/06, 881A/08, 881A/10	One major and two minor shield volcanoes, numerous flows, channels, collapse pits, and extensive irregular terrain; many possible examples of lahars and hyaloclastite ridges; apparent pyroclastic deposits at summits of all three shields.
8A–9	Olympus Mons----------	8 NE, 8 SE, 9 NW	18° N., 133°	5275, 5276, 5323, 5360, 5722	512A/23–71, 852A/5–12, 890A/32–50, 890A/61–71	Largest shield volcano on Mars, with conspicuous caldera and distinctive basal escarpment, lava flows and tubes; related aureole lobes of uncertain and controversial origin.
8B–9	Olympus Mons South --	8 SE, 9 SW	0°–11° N., 120°–150°	5512, 5513, 5944	44B/11–49, 355S/01–20, 469S/01–36, 470S/01–36, 471S/01–36, 888A/03–16	Eroded deposit resembling Icelandic moberg—may be pyroclastic debris; few cratered cones and tablemountain features, lava domes, and lava tubes.
8C	Amazonis Planitia-------	8 NW	16° N., 171°	5845	691A/43–44	Two symmetrical cones with summit craters—possibly cinder cones; debris lobe at base of one, resembling lava flow.
9A–17	Pavonis Mons ----------	9 SW, 9 SE, 17 NW, 17 NE	0.5° N., 112.5°	5514	49B/33–41, 49B/73–80, 49B/89–94, 90B/29–36, 388B/01–20, 643A/23–30, 643A/52–54	Major shield volcano, with lava flows, channels, tubes, and collapse pits; large lava fans on northeast and southwest flanks, and younger lava apron on east flank; conspicuous lobe of textured aureole materials beyond northwest flank, with marginal parallel (concentric) ridges resembling a sequence of recessional moraines; origin of aureole uncertain.
9B	Ascraeus Mons----------	9 SE, 9 NE	11° N., 104°	5373, 5725	223A/03–16, 224A/81–96, 401B/14–24, 516A/44–54, 892A/07–16, 892A/29–36	Major shield volcano; large fans of distinct lava flows to northeast and southwest; flows, channels, and pits on flanks; small crescentic aureole of textured material at northwest base; origin of aureole uncertain.
9C	Uranius Patera, Uranius Tholus, Ceraunius Tholus, Tharsis Tholus.	9 NE, 9 SE	12°–27° N., 90°–100°	5373, 5639, 5863, 5904	225A/11–16, 516A/21–24, 662A/02–12, 699A/09–16, 857A/43–48, 858A/20–26	Four minor shield volcanoes, each with conspicuous summit caldera. Shield of Uranius Patera is asymmetric and has cratered cones and lava flows on flanks; Uranius Tholus is nearly conical, with filled caldera; Ceraunius Tholus has conspicuous channels on flanks; Tharsis Tholus is conspicuously faulted.
9D	Jovis Tholus----------	9 NW	18° N., 118°	5430, 5639	41B/19, 516A/36, 890A/05	Minor shield volcano; unusually low relief; flanks buried by surrounding lava flows.

Table 1. Volcanic provinces of Mars, listed sequentially by Mars Chart number, with documentation data and brief interpretive description—Continued

Mars Chart (MC) province identification	Volcanic province	Mars Chart (MC) subquadrangle	Location (lat., long. W.)	Viking 211-series mosaic	Viking revolution/ frame	Interpretative description
9E	Biblis Patera, Ulysses Patera.	9 SW	1°–3° N., 120°–126°	5513	44B/50, 49B/85, 641A/79, 641A/82	Two minor shield volcanoes; Biblis shield has asymmetric flanks; Ulysses shield is scarred by large impact craters.
9F–10	Uranius Patera North---	9 NE, 10 NW	27°–30° N., 87°–97°	5787	626A/61–70	Low shields and domes, associated with flows, fissures, grabens, cone chains, and collapse pits.
9G	Halex Fossae ----------	9 NW	25°–31° N., 123°–130°	5330, 5537, 5771	43B/18–30, 623A/01–59, 853A/10, 890A/32	Volcanotectonic structure with ring fractures, partly buried by flows from Olympus Mons, Alba Patera, and elsewhere; prominent buttes with radial flow patterns.
11A	Chryse Planitia ----------	11 NW	18°–25° N., 34°–44°	4989, 4990, 4992, 4994, 5051	3A/01–02, 4A/33–37, 6A/16–21, 6A/33–42, 8A/33–37	Broad, low, pancake-shaped shields with small craters; long, narrow linear, dikelike ridges, cratered and uncratered cones, and buttes and knobs resembling volcanic necks.
13A	Syrtis Major—Nili and Meroe Paterae.	13 SE, 13 SW	7°–9° N., 292°–293°	5853, 5862, 6059	341S/47, 375S/13, 375S/32, 716A/06–20, 716A/46–53	Two calderas, one circular, one partly foundered—probable sources of surrounding flood lavas.
13B–14	Isidis Planitia ----------	13 SE, 13 NE, 14 SW, 14 NW	5°–25° N., 262°–282°	5579, 6041, 6051, 6054, 6070, 6077	67B/55–63, 142S/01–14, 142S/21–30, 143S/01–14, 143S/21–30, 144S/01–15, 145S/01–24, 146S/01–24, 147S/01–24, 148S/01–24, 149S/01–24, 150S/01–24, 499A/55–60	Curvilinear ridges and cratered cones occurring singly or in doublets, triplets, and long chains; detailed morphology visible on high-resolution extended-mission (S) images.
14A	Hephaestus Fossae -----	14 NE	21°–25° N., 234°–239°	—	647A/42–47	Isolated cratered domes or cones.
15A	Cerberus ----------	15 SE	0°–8° N., 194°–208°	6075	385S/42–48, 596A/10, 596A/12, 596A/14, 596A/16, 635A/54, 672A/61–64, 672A/66–68	Very low volcanic shields, 50 to 100 km in diameter, with circular to linear vents surrounded by radial textures and long lava flows; extensive volcanic plains.
17A	Arsia Mons ----------	17 NW	9° S., 120.5°	5228, 5248, 5302, 5317, 5324, 5820	42B/11–20, 42B/31–46, 52A/07–08, 56A/01–52, 62A/41–48, 90A/01–12, 641A/57–64, 641A/83, 641A/85, 890A/51–52	Major shield volcano, with lava flows, channels, tubes, and collapse pits; low shields in caldera; enormous lava fans on northeast and southwest flanks; associated aureole deposits at base of northwest flank, with conspicuous parallel (concentric) ridges in finely striated pattern resembling recessional moraines; origin of aureole uncertain.
17B–18	Syria Planum ----------	17 NE, 17 SE, 18 SW	8°–30° S., 82°–109°	5780	643A/33–43, 643A/57–70, 643A/81–94	Eruptive center, with flows, fissures, low shields, collapse pits, and curious protuberances.
18A	Coprates Chasma South.	18 SE	19° S., 59°	5750	610A/24, 610A/26	Two large, radially dissected knobs, one with summit crater and one without, somewhat resembling silicic composite cones or caldera domes.
22A	Tyrrhena Patera ---------	22 SW	22° S., 253.5°	5213, 5730, 6034, 6092	87A/10–17, 365S/33–45, 365S/62–74, 445A/41–56	Highlands volcanic shield with unusual dumbell-shaped caldera surrounded by broad, deep channels; flanks possibly composed of pyroclastic debris.

Table 1. Volcanic provinces of Mars, listed sequentially by Mars Chart number, with documentation data and brief interpretive description—Continued

Mars Chart (MC) province identification	Volcanic province	Mars Chart (MC) subquadrangle	Location (lat., long. W.)	Viking 211-series mosaic	Viking revolution/ frame	Interpretative description
23A	Apollinaris Patera -------	23 NE	8.5° S., 186°	5213, 5852, 6083	88A/48–51, 372S/56–58, 603A/41–42, 635A/57	Broad shield volcano with large caldera, highly dissected flanks, basal escarpment, and large lava fan, surrounded by extensive deposits of poorly consolidated, possibly pyroclastic material, apparently wind sculptured.
23B	Aeolis----------	23 SE	19° S., 188°	5760, 5945	430S/23, 596A/53	Conspicuous symmetrical cone with nearly filled summit crater and radially dissected flanks; distinctive morphology among highlands features—good candidate for composite volcano.
23C	Elysium South----------	23 NW	2°S–0.5° N., 209°–218°	5813	724A/01–24	Small area at margin of fluted deposits on boundary between Elysium plains and highlands plateau; long, narrow, curvilinear ridges, associated with at least two cratered cones—possibly volcanic.
25A–D	Thaumasia ----------	25 NE, 25 NW	37°–42° S., 88°–111°	5471	56A/66, 57A/02, 57A/05, 57A/07, 63A/08, 63A/13, 567A/73, 567A/76	Four isolated, rugged highlands peaks, radially dissected, somewhat resembling resurgent caldera domes—possibly volcanic.
27A–28	Amphitrites and Peneus Paterae.	27 SE, 28 SW	52°–65° S., 292°–333°	5335, 5524, 5976	94A/65–76, 361S/01–17, 539B/49	Two flooded, low-rimmed, circular depressions on southwest flank of Hellas Basin; several mesas with rimless craters resembling table-mountains—possible calderas may be source of flows forming Mare Australis.
28A	Hadriaca Patera----------	28 NE	31° S., 267°	5211, 5213, 5977	87A/01–04, 97A/39–42, 408S/01–08, 408S/67–69, 410S/01–08	Highlands volcanic shield with caldera; prominent V-shaped valleys on flanks; flanks possibly composed primarily of pyroclastic debris; large collapse depressions at southeast base of shield.
29A	Arrhenius ----------	29 NW	40°–45° S., 235°–240°	5870	586B/31–41, 518A/48, 518A/50	Field of clustered, dark buttes and knobs, many cratered; lobate ground pattern suggestive of lava plains—possibly volcanic.

ACKNOWLEDGMENTS

Numerous people contributed to the genesis, development, and production of this volume, most notably our many colleagues in the community of planetary geologists with whom discussion and debate over the years has been lively indeed. We are particularly indebted to Charles A. Wood and Ronald Greeley, both of whom reviewed the manuscript and made numerous suggestions that considerably improved both its content and effectiveness. Robert I. Tilling offered invaluable commentary on several drafts of the introduction that ensured conformity with the parlance of terrestrial volcanology. Richard J. Pike also reviewed the introduction, provided copies of his topographic profiles of volcanoes, and offered encouragement and suggestions throughout the development of this project. Joan D. Swann and Kathlene M. Hoyt, curators of the U.S. Geological Survey's Image Processing Facility in Flagstaff, Ariz., were indispensible in providing us with all the necessary Viking Orbiter images, mosaics, and digital-image mosaics. The superb color rendition of Olympus Mons (frontispiece) was prepared by Alfred McEwen and Annie Allison of that facility. Philip A. Davis, introduced us to his photoclinometry computer program and facilitated acquisition of many images when the authors' funds had run out. Dale M. Schneeberger and David C. Pieri kindly furnished us with their original mosaic of Alba Patera, which was skillfully reproduced by Hal E. McCord and pieced together by Lori Moore. Photographs of terrestrial features, contributed by Donald L. Baars, Ronald Greeley, James B. Moore, Shanaka L. de Silva, Tom Simkin, Richard S. Williams, Edward W. Wolfe, and Charles A. Wood, have added an important dimension to this atlas and are greatly appreciated. Lowell Kohnitz reproduced countless photographs with meticulous care and good humor. George A. Havach was singularly helpful in preparing this work for publication, and we are particularly indebted to Susan García for her essential skills in computer command and control. Finally, we are grateful to our many U.S. Geological Survey colleagues, both in and out of the Branch of Astrogeology, with whom ideas were generated and tested. Much of this work was performed under National Aeronautics and Space Administration (NASA) contract W–15,814 and the Mars: Evolution of Volcanism, Tectonism, and Volatiles (MEVTV) Program, and we deeply appreciate the continued support of Joseph M. Boyce, NASA Planetary Science Program Manager.

MAJOR PLAINS PROVINCES

THARSIS REGION

MAJOR SHIELD VOLCANOES

OLYMPUS MONS

(Mosaic: 211–5360; MC: 8A–9; Coordinates: 18° N., 133° W.)

Approximate dimensions (km):	
Base diameter (avg)	800
Summit elevation	26
Relief	24–26
Caldera diameter	65 by 85
Caldera depth	2.5
Height/base ratio	0.03
Estimated relative age (100^{-3} craters/km^2):	
Scott and Tanaka (1980)	0.2±0.05
	0.12±0.06
Inferred age (Ga):	
Model 1	0.25–1.0
Model 2	0.06–0.24
Stratigraphic age:	
Amazonian; Olympus Mons Formation	

DISTINCTIVE CHARACTERISTICS

(1) Morphologically analogous to terrestrial oceanic shield volcano, with broad convex flanks (fig. 1*A*).
(2) Summit caldera with nested collapse craters and rim terraces (fig. 1*B*).
(3) Encircling basal scarp, 2 to 10 km high (fig. 1*A*).
(4) Lava-tube ridges and long, narrow lava flows with lobes, levees, and channels on lower flanks, draped over scarp in places (figs. 1*A*, 1*D*).
(5) Aureole deposits—lobes of rough, ridged, and fractured material forming broad, generally accordant, distinctively textured surfaces, nearly surrounding base of volcano, especially conspicuous and massive to the north-northwest (fig. 1*A*). Obvious differences in states of degradation and burial among separately identifiable units suggest sequential development. Formation of aureole materials preceded final eruptions of volcano.
(6) Lobate, overlapping debris aprons at west-northwest base of scarp, each with conspicuous series of long, curvilinear ridges parallel to (concentric with) exterior margin of deposits (fig. 1*F*).
(7) Strong positive gravity anomaly (344 mGal at a spacecraft altitude of 275 km) coincident with volcano and extending northwestward over major aureole lobes (Sjogren, 1979).

DISCUSSION

The immensity of Olympus Mons is without known counterpart in the Solar System (see frontispiece). Earth's largest volcano, Mauna Loa in Hawaii, stands only 9 km above the ocean floor, has a summit caldera 2.7 by 6 km (fig. 1*C*), and is approximately 120 km across at its base. (Accurate dimensions are difficult to define, inasmuch as Mauna Loa is built on the foundations of older volcanoes, notably Mauna Kea.) The aspect (height to base diameter) ratio of Olympus Mons, however, compares closely to that typical of terrestrial oceanic shield volcanoes, as exemplified by the Hawaiian Islands. The flanks of the martian shield have an average slope of about 4° (Blasius and Cutts, 1981) but locally may be as steep as 10° near the summit (Scott, 1982); flanks of terrestrial shield volcanoes generally slope from 2° to 10°, rarely as high as 15° (Macdonald, 1972). Most of the subaerial slopes of Mauna Loa, for example, average about 3°–6°; the steepest average slope is 8° at 3.3-km elevation (Mark and Moore, 1987).

The height of Olympus Mons indicates long-term crustal stability (Carr, 1973), whereas growth of the Hawaiian shield volcanoes is eventually terminated by severance from the magmatic conduit as the Pacific Plate drifts northward (Clague and Dalrymple, 1987). On the basis of terrestrial magma and mantle densities, Carr (1976a, b, 1980) estimated that a lithospheric thickness of about 200 km would have been required for basaltic magma to rise to the summit of Olympus Mons. In contrast, similar calculations and seismic evidence in Hawaii indicate a depth to the magma source region at Mauna Loa of about 60 km (Eaton and Murata, 1960). Wilson and others (1991) noted, however, that the relation between volcano height and depth to magma source is considerably more complex than commonly assumed in such calculations. On the basis of stress analyses of ridges

► **Figure 1.** Olympus Mons. *A*, Olympus Mons and aureole deposits, with representative profile (at scale larger than image). Numbers 1 through 8 indicate apparent sequence of aureole materials, from oldest to youngest; arrows denote nested caldera (a), basal scarp (b), lava flows draped over scarp (c), and debris aprons at northwest base of scarp (d; see fig. 1*F*). Sun illumination mainly from right, except at left center and lower right corner, where it is from left. Digital-image mosaic. North-south profile across approximate center of volcano drawn from topographic map M1M 19/134 T (U.S. Geological Survey, 1981c; Wu and others, 1984).

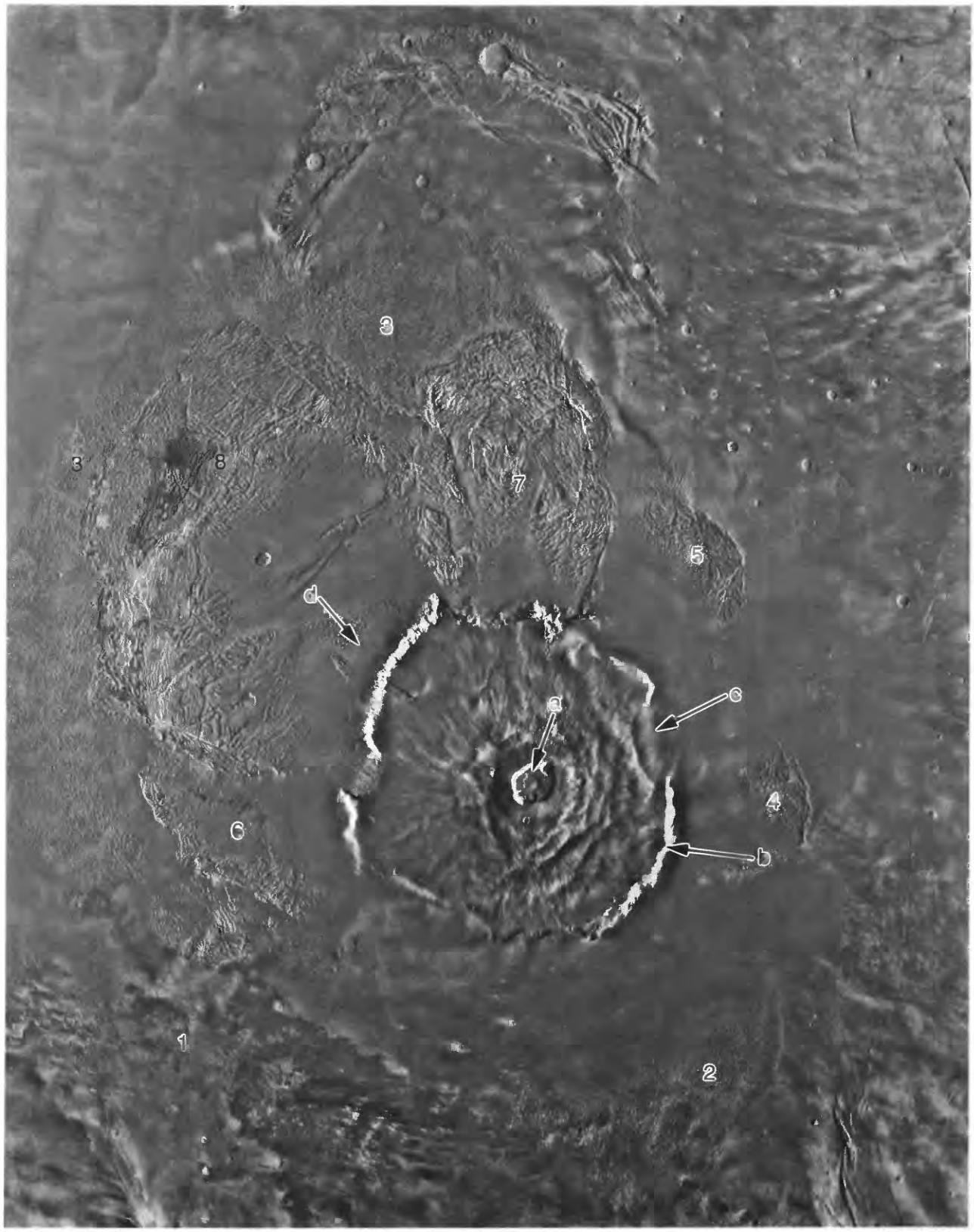

0 100 200 KILOMETERS

S N

0 100

SCALE IN KILOMETERS

15°N 25°N

and grabens within the present Olympus Mons caldera, Zuber and Mouginis-Mark (1990) concluded that the magma-storage chamber, from which magma withdrawal caused subsidence of the summit caldera floor, was situated within the shield at a depth of about 15 km—a position comparable, after appropriate scaling, to the depth (1.5–6.5 km) of the summit storage reservoir at Kilauea, as determined from earthquake and ground-deformation data (Tilling and others, 1987).

The flanks of Olympus Mons are draped by long, narrow, ribbonlike flows, most of which appear to emanate from vents on the terraced upper flanks (Carr and others, 1977) or from the central caldera (Greeley, 1973). Flows with leveed channels and collapsed lava-tube ridges are common, similar to those of terrestrial basaltic shield volcanoes. Both photogeologic and quantitative analyses of lava flows on and near the flank of Olympus Mons suggest that the rheologic properties of the lavas are consistent with a basalt or basaltic-andesite composition (Greeley, 1973; Zimbelman and Fink, 1989). The Olympus Mons caldera (fig. 1*B*) evolved through a series of collapse events that produced six distinct craters and accompanying features in a relatively short period of time, as indicated by similar crater-size/frequency curves for all parts of the caldera (Mouginis-Mark and others, 1990). The morphology of the volcano indicates its formation by effusive, Hawaiian-style (Macdonald, 1972) eruptions.

The conspicuous escarpment encircling the base of Olympus Mons, with slopes as steep as 35° (fig. 1*A*),

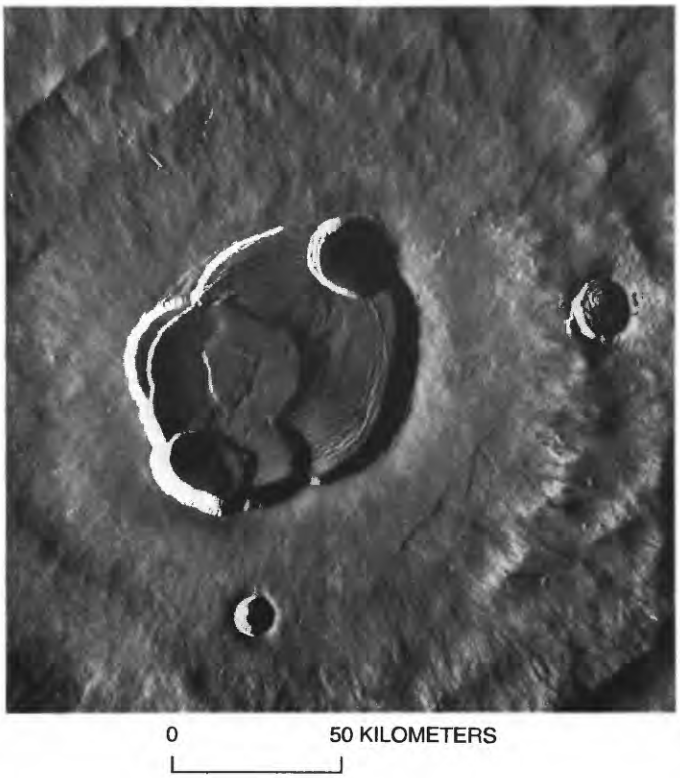

B, Summit caldera of Olympus Mons, showing multiple collapse depressions, with conspicuous lava flows and channels radial to rim. Craters to south and east are of impact origin. Sun illumination from right. Viking Orbiter frame 890A68.

C, Summit caldera of Mauna Loa Volcano, Hawaii, showing configuration of intersecting collapse pits much like caldera of Olympus Mons. Elongation of summit caldera is due to its localization along a major rift. Sun illumination from right. NASA-Ames *U–2* high-altitude photograph taken in 1974 (from Carr and Greeley, 1980), courtesy of Ronald Greeley.

is perplexing, particularly inasmuch as none of the other Tharsis volcanoes has such a feature; only Apollinaris Patera, in the Elysium region, has a similar (though much less conspicuous) basal escarpment. Materials exposed in the scarp appear to be layered (Borgia and others, 1990; Morris and Tanaka, in press). Numerous explanations for this scarp have been proposed, including normal faulting (Morris and Dwornik, 1978); thrust faulting (Harris, 1977; Morris, 1981, 1982; Borgia and others, 1990); erosional removal of underlying cratered terrain, except where protected by the volcano (Head and others, 1976); eolian erosion of nonresistant basal material, such as ash-flow tuff (King and Riehle, 1974); the modified edge of a deposit, possibly the last aureole, emplaced before the main shield began to develop (Tanaka, 1981); gravity sliding of the lower flanks away from the volcano (Carr, 1975; Lopes and others, 1980, 1982; Hiller and others, 1982; Francis and Wadge, 1983); and gravity sliding along a basal detachment zone lubricated by ice in the martian regolith (Tanaka, 1985). In yet another explanation, Hodges and Moore (1979, 1980) noted a similarity of the scarp to the subaqueous flanks of oceanic shield volcanoes and, more specifically, to their subglacial counterparts, Icelandic tablemountains; they suggested that the Olympus Mons escarpment could have resulted from a subglacial eruptive episode. On Earth, oceanic shields display breaks in slope at sea level; the average subaerial slope from the shoreline of Mauna Loa and Kilauea up to about 2-km elevation is 4°, whereas at 500 m below sea level the average slope steepens abruptly to 13°, ranging from about 8° to as high as 25° in areas where landslides have occurred (Mark and Moore, 1987). This slope discontinuity on Hawaiian shield volcanoes was interpreted by Moore and Fiske (1969) as comparable to that of Icelandic tablemountains, which are small shield volcanoes (approx 1–6 km across) atop steep-sided pedestals formed by subglacial eruptions (fig. 1*E*).

D, Lower east flank of Olympus Mons, showing lava flows (arrows f) and lava-tube ridges (arrows t). Northeast-trending flows cascaded over modified scarp of shield pedestal and subsequently were embayed by north-trending flows (arrows n) from south. Sun illumination from right. Viking Orbiter frame 890A36.

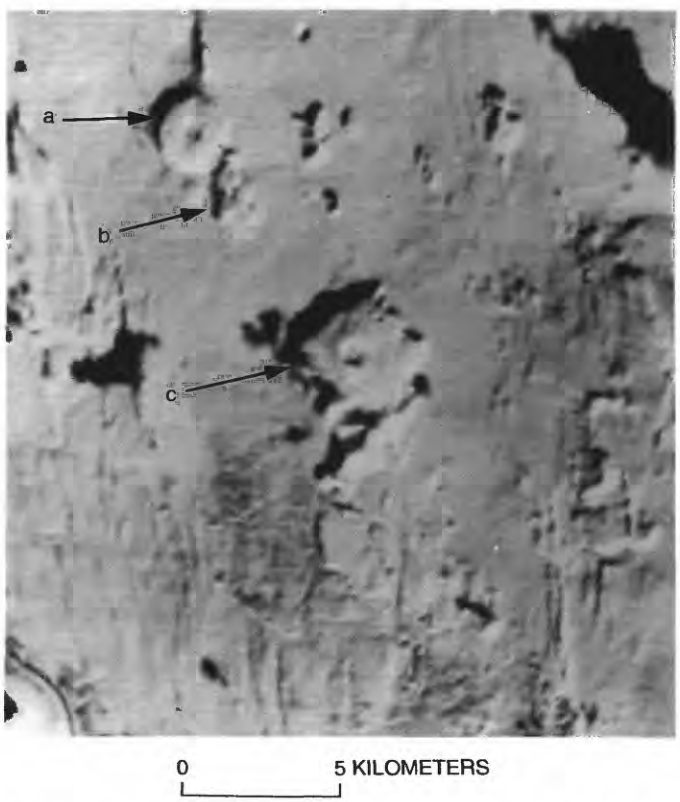

E, Three tablemountains in northern Iceland: Bæjarfjall (arrow a), Kvíhólafjöll (arrow b), and Gæsafjöll (arrow c). Gæsafjöll has cap of subaerial lava; other two tablemountains apparently consist entirely of moberg (hyaloclastite). All three have summit craters. Sun illumination from right. Landsat image, courtesy of R.S. Williams.

The topographic configuration of tablemountains was governed by confinement of the eruption by an ice-cap (Kjartansson, 1960; Jones, 1966, 1969, 1970; Einarsson, 1968) rather than an ocean, and subaerial erosion has enhanced the steepness of the slope; but in either case the transition between subglacial or subaqueous and subaerial eruption accounts for the break in slope, with thin basaltic lava flows superposed on a base of pillow basalts and hyaloclastites.

Extrapolating across orders of magnitude, Hodges and Moore (1979, 1980) invoked an analogous, subglacial eruptive process to explain the perimeter scarp around Olympus Mons. A possible factor in localizing ice in the Tharsis region was suggested by Schultz (1985), who cited evidence for polar wander on Mars and proposed that Olympus Mons was "very close to the north pole during its initial development." As for the total water/ice budget of the planet, current proposals include amounts as high as 1,000 m planetwide (Carr, 1986a, 1987); if localized in the Tharsis region, this volume could account for the few kilometers of ice required to form a subglacial pedestal for this gigantic shield.

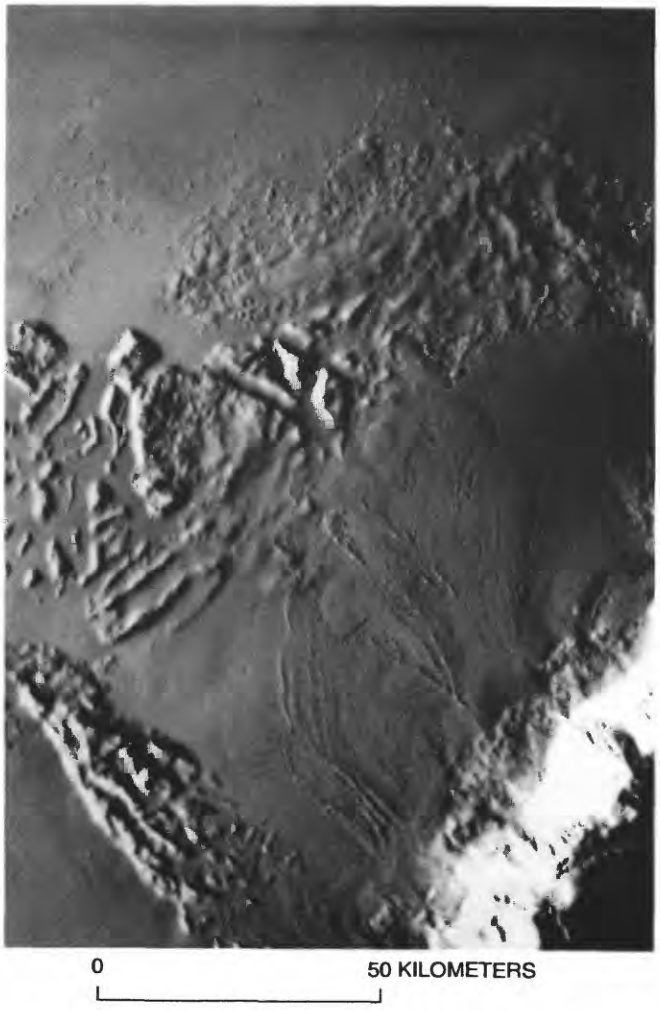

F, Debris aprons at base of northwest scarp of Olympus Mons (arrow d, fig. 1*A*). Superposition of marginal ridges (lower left center) on blocks of aureole materials suggests possible deposition by ice as glacier or rock-glacier debris rather than by landslide (Lucchitta, 1981). These deposits are morphologically similar to much larger aureole deposits at northwest bases of Arsia, Pavonis, and Ascraeus Montes. Sun illumination from left. Viking Orbiter frame 512A44.

Gravity-controlled deposition evidently occurred at the west-northwest base of the scarp, where overlapping debris aprons are conspicuous (arrow d, fig. 1*A*; fig. 1*F*). These have been interpreted as landslides (Blasius, 1976), but the finely striated pattern of the ridges concentric with the margins of the lobes more closely resembles the morphology of terrestrial glaciers or rock glaciers. Lucchitta (1981) compared these Olympus Mons debris aprons to the tongue-shaped center and marginal ridges of Alaskan glaciers and rock glaciers. The analogy seems especially apt because the martian ridges are superposed on older blocks and ridges of aureole deposits, which might have deflected landslide debris moving at the ground surface. If ice were the transporting medium, however, ridges of morainal material could have been deposited over preexisting relief upon sublimation or melting of the ice (Lucchitta, 1981). These deposits are morphologically similar to the broad and much larger aureole lobes at the northwest bases of Arsia, Pavonis, and Ascraeus Montes.

The Olympus Mons aureole deposits (fig. 1*A*) are controversial in origin and generally are considered to be somehow related to the basal scarp. They have been interpreted as landslide deposits, produced by failure of the outermost flanks of the volcano (Lopes and others, 1980, 1981, 1982; Hiller and others, 1982; Francis and Wadge, 1983; Tanaka, 1985); as ash-flow tuffs erupted from separate vents (Morris, 1982); as eroded lava flows (McCauley and others, 1972; Carr, 1975); as shallow, high-density, lopolithic intrusive bodies (Shoemaker and Blasius, 1974); as low-angle gravity thrust-deformation structures, resulting from loading by the volcano (Harris, 1977); and as moberglike materials derived from subglacial eruptions at as many as eight different vents (Hodges and Moore, 1979). Each of these hypotheses poses some difficulty, but the strong positive gravity anomaly observed over the most extensive aureole deposits northwest of the volcano (Phillips and Bills, 1979; Sjogren, 1979) supports the presence of magmatic rocks at depth and would seem to negate hypotheses

of surficial origin. Hiller and others (1982), however, maintained that this anomaly can be accounted for by the observed mass of the volcano and its aureole deposits and thus is consistent with a surficial source.

Although Olympus Mons is among the youngest volcanoes on Mars (Neukum and Hiller, 1981), its age relations to other young volcanoes are less clear because of its isolation. Lavas from Olympus Mons are superposed on the surrounding aureole deposits and adjacent plains, but below the scarp on the east and south they are covered by still-younger lava flows (fig. I–2). Because of the volcano's isolation, heavy reliance must be placed on the number of superposed impact craters to establish a relative age. By all analyses, Olympus Mons is the youngest martian shield volcano (Neukum and Hiller, 1981; Tanaka, 1986; Landheim and Barlow, 1991), although subunits of Ascraeus, Pavonis, and Arsia Montes may be comparable (fig. I–5). Nonetheless, despite its pristine appearance, Olympus Mons is vastly older (1,000–60 Ma) than any of its terrestrial analogs.

REFERENCES

Blasius (1976)
Blasius and Cutts (1981)
Borgia and others (1990)
Carr (1973, 1975, 1976a, b, 1980, 1986a, 1987)
Carr and Greeley (1980)
Carr and others (1977)
Clague and Dalrymple (1987)
Eaton and Murata (1960)
Einarsson (1968)
Francis and Wadge (1983)
Greeley (1973)
Harris (1977)
Head and others (1976)
Hiller and others (1982)
Hodges and Moore (1979, 1980)
Jones (1966, 1969, 1970)
King and Riehle (1974)
Kjartansson (1960)
Landheim and Barlow (1991)
Lopes and others (1980, 1981, 1982)
Lucchitta (1981)
Macdonald (1972)
McCauley and others (1972)
Mark and Moore (1987)
Moore and Fiske (1969)
Morris (1981, 1982)
Morris and Dwornik (1978)
Morris and Tanaka (in press)
Mouginis-Mark and others (1990)
Neukum and Hiller (1981)
Phillips and Bills (1979)
Schultz (1985)
Scott and Tanaka (1980)
Shoemaker and Blasius (1974)
Sjogren (1979)
Solomon and Head (1990)
Tanaka (1981,1985, 1986)
Tilling and others (1987)
U.S. Geological Survey (1981a)
Williams and McBirney (1979)
Wilson and others (1991)
Wu and others (1984)
Zimbelman and Fink (1989)
Zuber and Mouginis-Mark (1990)

ARSIA MONS

Mosaics: 211–5317, 17NW MC: 17A Coordinates: 9° S., 120.5° W.

Approximate dimensions (km):	
Base diameter	700
Summit elevation	20
Relief	13
Caldera diameter	132
Caldera depth	0.6
Height/base ratio	0.02
Estimated relative age (10^{-3} craters/km^2):	
Central shield (Plescia and Saunders, 1979)	0.8±0.1
Lava fan	0.3±0.1
Caldera fill	0.09±0.1
Inferred age (Ga):	
Central shield:	
Model 1	2.6–3.4
Model 2	0.6–0.9
Lava fan:	
Model 1	0.9–1.7
Model 2	0.2–0.4
Caldera fill:	
Model 1	0.4–0.5
Model 2	0.08–0.1
Stratigraphic age:	
Amazonian; Tharsis Montes Formation	

DISTINCTIVE CHARACTERISTICS

(1) Typical central-shield morphology with convex flanks (figs. 2*A*, 2*B*).
(2) Large lava fans emanating from vents high on northeast and south-southwest flanks (fig. I–2), aligned parallel to trend of Tharsis ridge (arrows 2, fig. 2*A*).
(3) Lava flows, channels, and lava-tube ridges on flanks, fans, and summit.
(4) Near-circular caldera surrounded by circumferential fractures and grabens (fig. 2*A*).
(5) Aureole deposits at northwest base, forming a distinctive, broad lobe of rugged materials (approx 400 by 500 km across). Outer margin is distinguished by narrow ridges forming a conspicuous striated pattern parallel to outer edge of deposits (arrows 3–5, fig. 2*A*; fig. 2*C*); a similar but less conspicuous, concentric pattern is also discernible in rugged, highly textured deposits central to this lobe.
(6) Numerous collapse pits associated with lava tubes and grabens.
(7) Low shields on lava plains filling caldera (arrow 6, fig. 2*A*).

DISCUSSION

Although none is as enormous as Olympus Mons, each of the three shield volcanoes aligned along the Tharsis ridge (fig. I–1) has, at 13 to 19 km, substantially more relief than the largest terrestrial shield, Mauna Loa in Hawaii (9 km). The profile of Arsia Mons (figs. 2*A*, *B*) suggests that it most resembles the inverted-soupbowl shape of the Galápagos shield volcanoes (fig. 2*D*), which also are characterized by concentric faults and grabens around a summit caldera (Simkin and Howard, 1970). Carr and others (1977) noted a line of low hills across the caldera floor (arrow 5, fig. 2*A*) between the northeast-southwest-trending vent areas and interpreted them as secondary shield volcanoes. Long, narrow flows emanate from the summit area, but the latest, most profuse activity appears to have been related to parasitic cones (Roth and others, 1980) or lava fans with their apices localized high on the northeast and southwest flanks (Crumpler and Aubele, 1978; Mouginis-Mark and others, 1982b), conspicuously aligned with the trend of the Tharsis ridge (fig. I–2; arrows 2, fig. 2*A*). Flows from these lava fans are typically 2 to 4 km wide and 11 to 20 m thick (Moore and others, 1978). Flows from Arsia Mons can be traced for more than 1,000 km to the south and southwest, probably indicating low viscosities and high eruption rates (approx 5×10^3–5×10^4 m^3/s) from a huge magma chamber, if analogous to terrestrial eruption conditions (Walker, 1973; Wood, 1984b). Deep radial valleys and high radial ridges dominate the northwest flank of the volcano; some of these ridges, as much as 6 to 10 km wide and 400 m high, may represent flows, possibly rock glaciers, landslides, mudflows, or silicic lavas (Moore, 1979).

The aureole, with its marginal belt of finely striated terrane (arrow 3, fig. 2*A*; fig. 2*C*), constitutes one of the most perplexing aspects of Arsia Mons. The striations are particularly enigmatic because they traverse a clearly young impact crater (arrow 4, fig. 2*A*; fig. 2*C*) without deviation or deformation and are superposed on lava flows of the southwestern lava fan. Attempts to interpret this terrane have provoked controversy, but a widely accepted explanation has thus far eluded investigators. Among the hypotheses proposed are (1) that the aureole deposits behind the striated ridges constitute a large landslide detached from the flanks of the volcano, and that the concentric ridges are folds or reverse faults in underlying terrain at the frontal margin caused by drag of the slide (Carr and others, 1977); or (2) that the aureole deposits represent recessional moraines deposited by a retreating icecap (Williams, 1978; Lucchitta, 1981), the water for which could have been generated

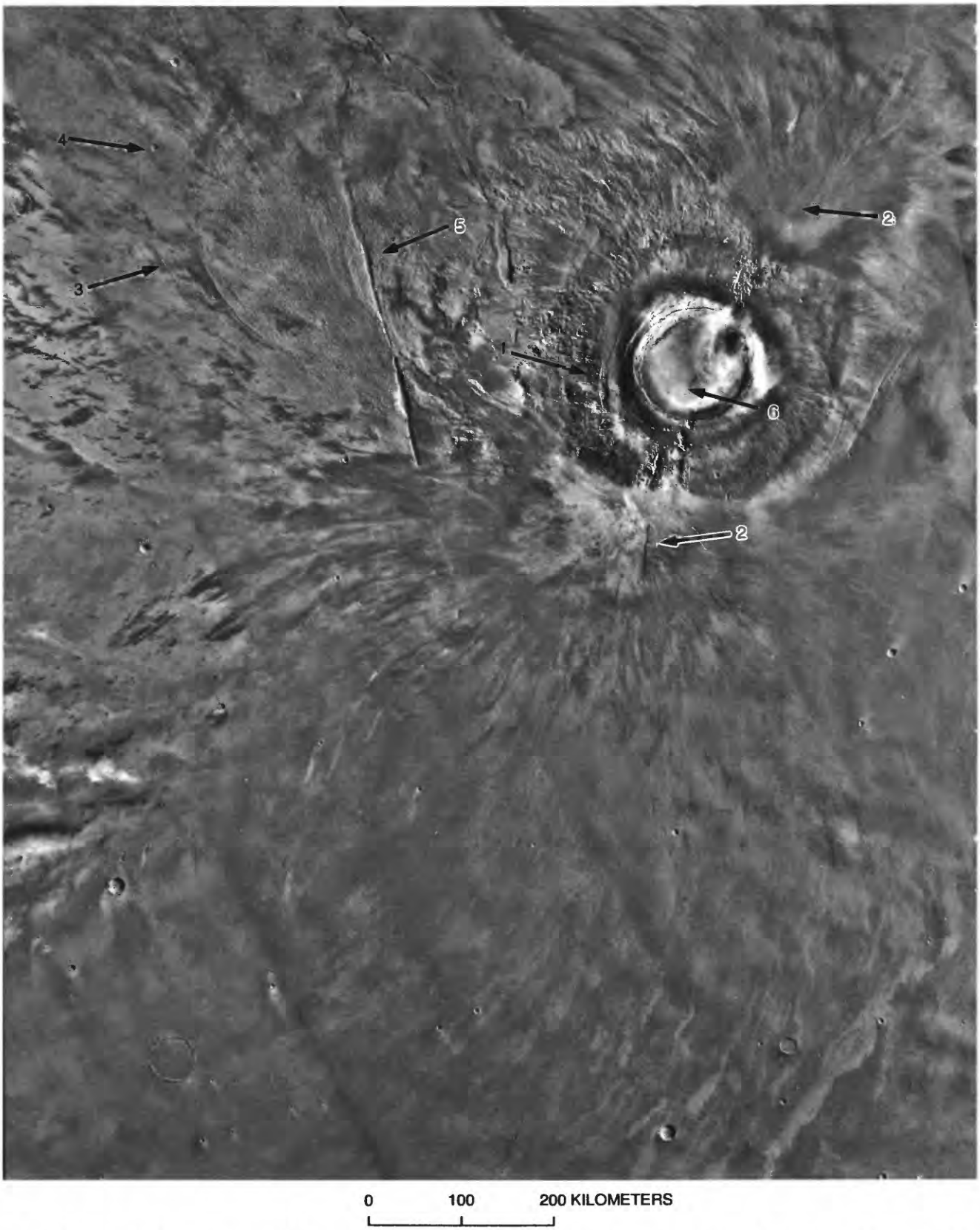

Figure 2. Arsia Mons. *A*, Arsia Mons and aureole deposits. Numbered arrows indicate features described in text: (1) central shield, (2) lava fans, (3) aureole deposits with marginal striations, (4) young impact crater traversed by aureole striations (see fig. 2*C*), (5) aureole interior deposits, (6) row of hummocks trending northeast-southwest across caldera floor. Sun illumination from right. Digital-image mosaic

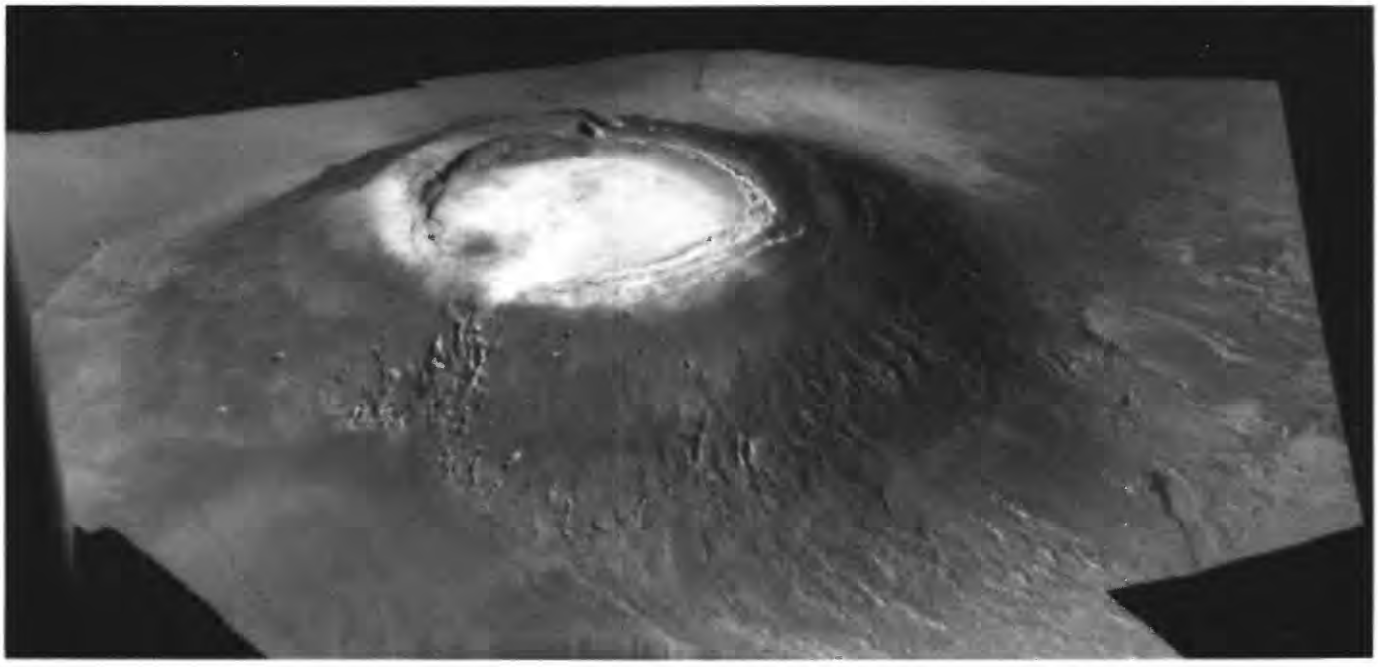

B, Computer-processed image of Arsia Mons, showing pronounced domical shape. Caldera is about 130 km across. View southward, about 25° above horizon. Illustration from U.S. Geological Survey's Image Processing Facility, Flagstaff, Ariz.

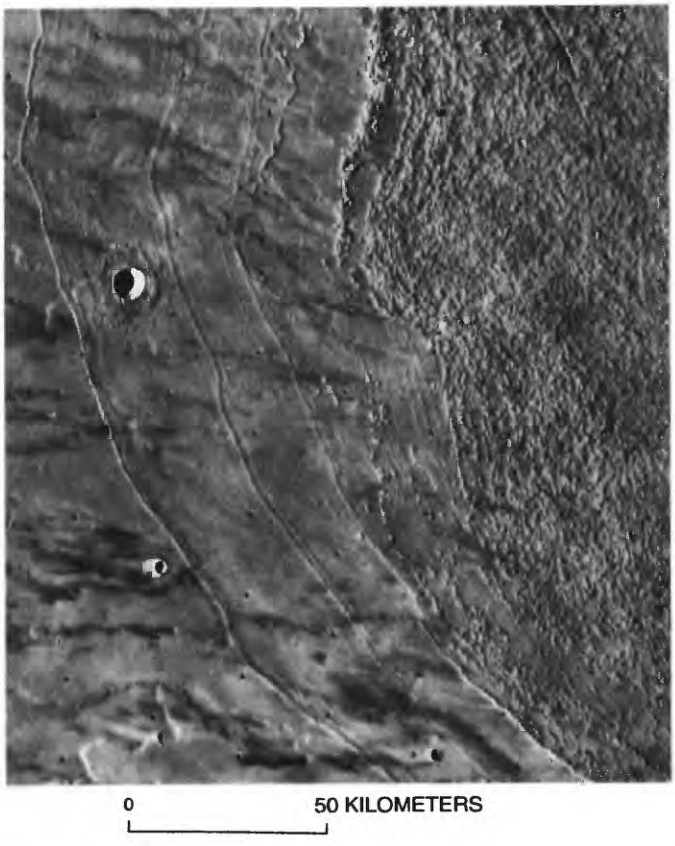

► *C*, Striated margin of Arsia Mons aureole deposits. Striations cross impact crater with no deformation of underlying terrain. Pattern of parallel curvilinear ridges is somewhat similar to that of glacial recessional moraines shown in figure 2*E*. Sun illumination from left. Viking Orbiter frame 042B35.

by exhalation from the volcano (Hodges and Moore, 1979). The regularity of spacing and the continuity of the ridges are remarkable and seem more compatible with a passive, depositional origin as moraines (fig. 2*E*) than with an active, deformational origin. No scarp is apparent from which so large an amount of landslide material could have derived, and the highly regular pattern of ridges does not resemble the distorted terminal pressure ridges characteristic of landslides. Williams (1978) documented glacial retreat without deformation of underlying topographic features in Iceland and drew an analogy with the undeformed crater within the striated terrain. According to this hypothesis, the interior of the aureole lobe (for example, arrow 5, fig. 2*A*) would be largely ground-moraine or, possibly, rock-glacier debris. We favor this interpretation here, but it requires earlier climatic conditions markedly different from those of today. The nearly identical characteristics of the aureole deposits at Pavonis and Ascraeus Montes suggest that any genetic interpretation applicable to one must be applicable to all such deposits, and thus a landslide origin seems less likely than a climate-related cause.

Superposition relations show that surface flows of the Arsia central shield are older than the most recent caldera fill and the two lava fans. Additionally, the

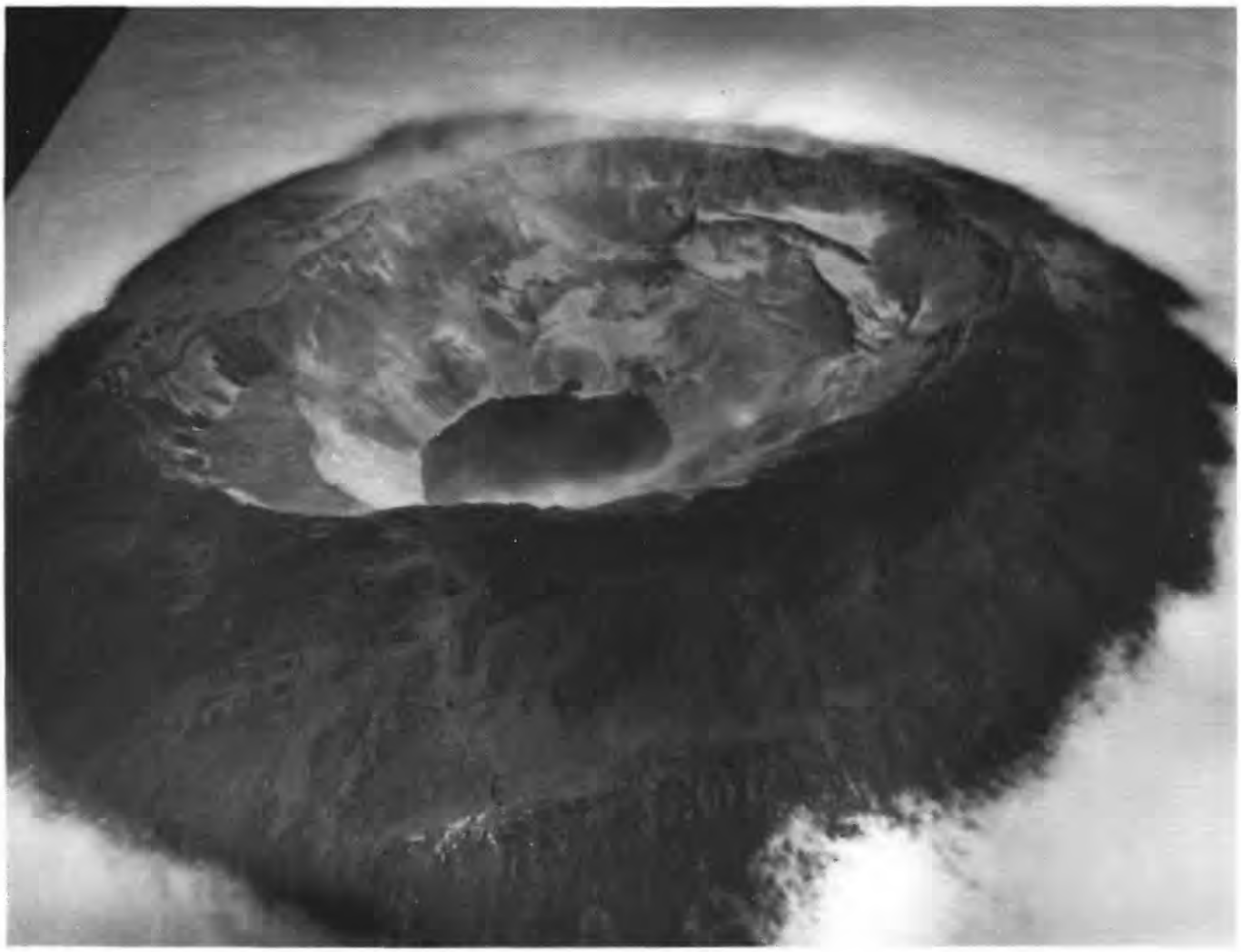

D, Fernandina Island in the Galápagos Islands, showing shield volcano and summit caldera. Caldera is about 7 km in longest dimension. Arcuate fractures and cinder/spatter-cone chains circumferential to caldera resemble tectonic features surrounding caldera of Arsia Mons (fig. 2*A*). In contrast to Hawaiian shield volcanoes, Galápagos shields have upper flanks that are unusually steep (max 34°) toward summit (Simkin and Howard, 1970); Tharsis volcanoes are similar. Summit lava flows are numerous on both Fernandina Island and Arsia Mons. Photograph courtesy of Tom Simkin.

E, Recessional "washboard" moraines deposited by retreating glacier (left) in Iceland. Dark color of glacier is due to rocky carapace. Distance between outermost ridge and glacier margin is about 700 m. Continuity and regularity of spacing of moraines are reminiscent of ridged pattern at outer margin of Arsia Mons aureole deposits (figs. 2*A*, 2*C*). Sun illumination from left. Photograph courtesy of R.S. Williams.

aureole deposits are superposed on flows of the southwestern lava fan; the northeastern lava fan appears to be younger than Pavonis Mons. Relative ages of the Arsia Mons units are difficult to establish because of the areal extent and youth of these units. Judging from independent crater counts, the caldera fill is about the same age as Olympus Mons, whereas the lava fans are older and Arsia Mons still older (fig. I–5). Inferred ages imply that Arsia Mons could have been volcanically active for as long as 2 to 3 b.y. (model 1) or at least several hundred million years (model 2)—much longer, in either case, than single terrestrial volcanoes are presumed to remain active.

REFERENCES

Carr and others (1977)
Crumpler and Aubele (1978)
Hodges and Moore (1979)
Lucchitta (1981)
Moore (1979)
Moore and others (1978)
Mouginis-Mark and others (1982b)
Neukum and Hiller (1981)
Plescia and Saunders (1979)
Roth and others (1980)
Simpkin and Howard (1970)
Walker (1973)
Williams (1978)
Wood (1984b)

PAVONIS MONS

Mosaic: 211–5514 MC: 9A–17 Coordinates: 0.5° N., 112.5° W.

Approximate dimensions (km):	
Base diameter	460
Summit elevation	18
Relief	11
Caldera diameter	48
Caldera depth	3
Height/base ratio	0.02
Estimated relative age (10^{-3} craters/km^2):	
Central shield (Plescia and Saunders, 1979)	0.35±0.08
Lava apron, east flank	0.2±0.1
Inferred age (Ga):	
Central shield:	
Model 1	1.1–1.9
Model 2	0.25–0.4
Lava apron:	
Model 1	0.4–1.3
Model 2	0.1–0.3
Stratigraphic age:	
Amazonian; Tharsis Montes Formation	

DISTINCTIVE CHARACTERISTICS

(1) Summit ringed plain (probably earliest caldera), about 110 km in diameter and relatively flat, surrounding present caldera (fig. 3*A*).
(2) Caldera small relative to magnitude of shield.
(3) Large lava fans emanating from vents high on northeast and south-southwest flanks (fig. I–2), similar in orientation to lava fans at Arsia Mons (fig. 2*A*).
(4) Lava apron low on east flank; lava flows, channels, and lava-tube ridges on northeastern lava fan and eastern apron (fig. 3*C*).
(5) Concentric grabens and fractures around flanks and base of volcano (fig. I–1; arrows 1, fig. 3*B*).
(6) Aureole deposits at northwest base, about 400 by 400 km across, forming a distinctive, well-defined lobe of blocky material marked by a striated pattern of ridges parallel to outer margin (arrow 2, fig. 3*B*), similar to striated margin of aureole at Arsia Mons (figs. 2*A*, 2*C*) but somewhat smaller in areal extent. Two widely spaced radial ridges in central part of aureole (arrow 3, fig. 3*B*) appear to be levees at margins of a broad flow channel within these materials.

DISCUSSION

Among the three large central shields aligned atop the Tharsis ridge (fig. I–1), Pavonis Mons is distinguished by its relatively small but deep, circular summit caldera, a surrounding summit plain that likely represents an earlier, filled caldera (fig. 3*A*), and its broad aureole lobe at the northwest base (fig. 3*B*). As at Arsia Mons, large lava fans occur on the northeast and southwest flanks. Lavas from a separate vent on the east flank of Pavonis Mons form the eastern lava apron, which is superposed on, and thus younger than, the northeastern lava fan (fig. 3*C*).

The resemblance between the aureole deposits of Pavonis (fig. 3*B*) and Arsia (figs. 2*A*, 2*C*) Montes is striking. The outer margin is demarcated by a prominent continuous ridge, interior to which are less distinctive, but clearly defined, concentric ridges amid subdued blocky materials. As at Arsia Mons, a persuasive terrestrial analogy for this extremely regular ridge pattern is the series of recessional moraines deposited by a retreating glacier (Williams, 1978), or the surface morphology of rock glaciers (Lucchitta, 1981). No scarp is apparent from which so large an amount of landslide materials could have derived, nor is the regular pattern of ridges consistent with a landslide interpretation. An icecap localized on the volcano during past climatic regimes could have been enhanced on the northwest-facing flank by orographic effects on wind circulation (Hodges and Moore, 1979). The radial levees may be attributable to a secondary meltwater stream or mudflow, or to lateral moraines of a glacial tongue. Although surface ice does not now exist on Mars except at the poles, permafrost and ground ice are commonly thought to occur across much of the planet (Carr and Schaber, 1977; Lucchitta, 1985), and previous climatic regimes may have included substantial amounts of surface ice and water (Carr, 1986a, 1987; Baker and others, 1990, 1991).

Relative ages of components of Pavonis Mons parallel those of Arsia Mons. Crater counts suggest that the central shield of Pavonis Mons is younger than that of Arsia Mons, but the northeastern lava fan of Arsia is superposed on the southwestern lava fan of Pavonis Mons. Crater counts indicate comparable ages for the eastern lava apron of Pavonis Mons, the lava fans of Arsia Mons, and Olympus Mons (fig. I–5). Thus, a complex history of overlapping volcanic events over a long period of time characterizes the Tharsis volcanoes.

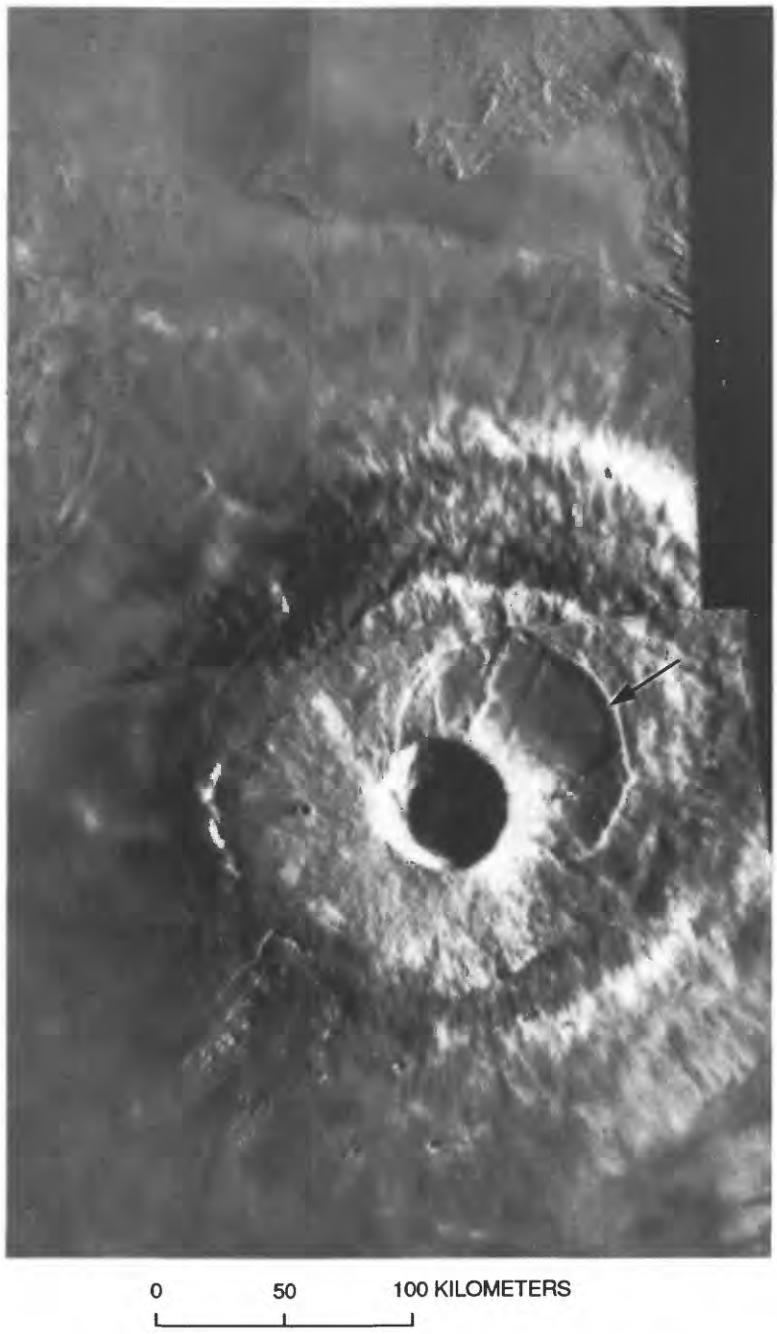

Figure 3. Pavonis Mons. *A*, Pavonis Mons, showing details of summit ringed plain surrounding caldera. Outer scarp on northeast flank (arrow) likely represents earlier caldera rim, subsequently flooded by lava flows with mare-type ridges. Sun illumination from right. Viking Orbiter frames 643A25 and 643A27.

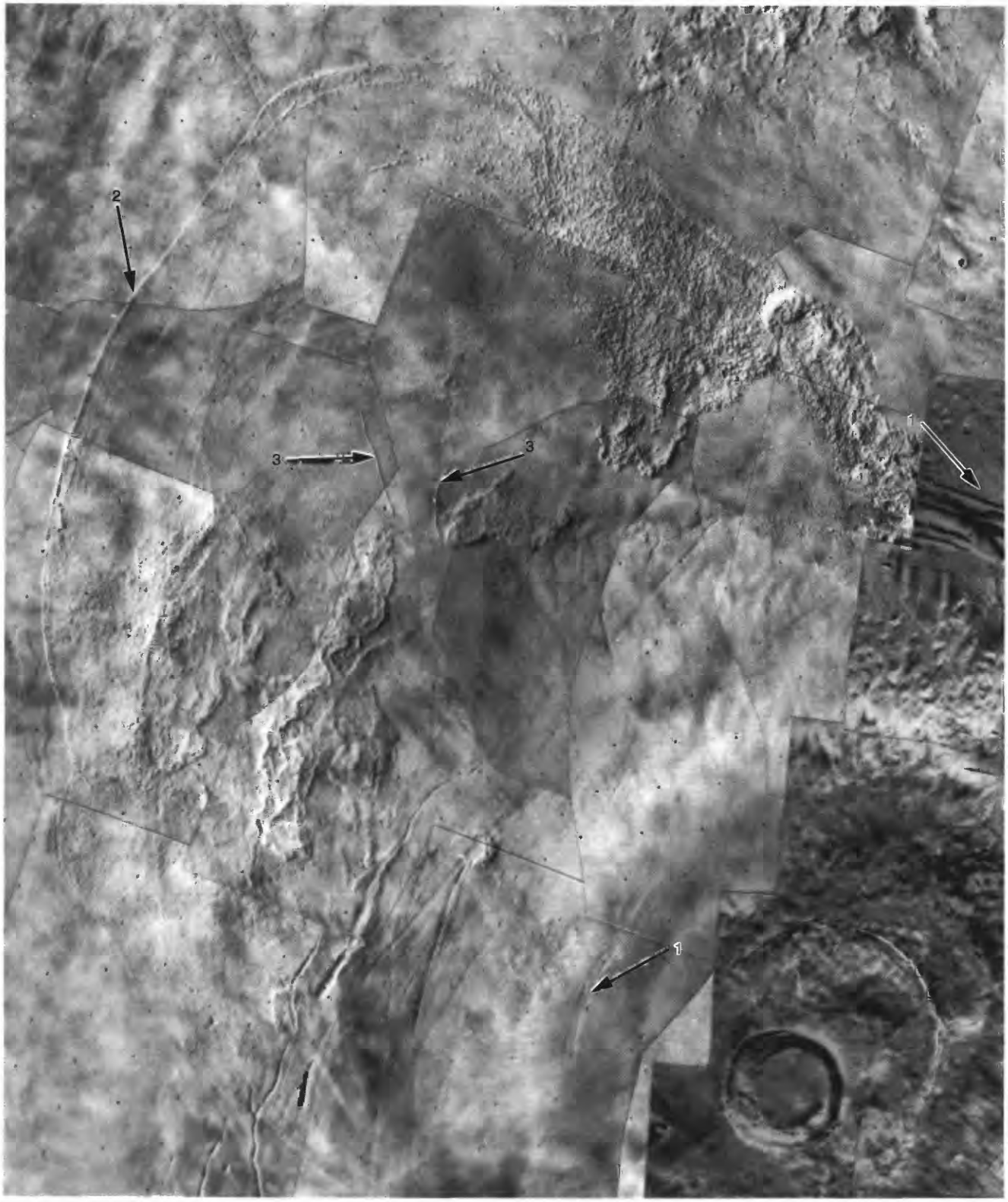

B, Pavonis Mons aureole deposits. Numbers in arrows correspond to distinctive characteristics: (1) concentric grabens and fractures on flanks and around base of shield; (2) outer margin of aureole deposits, marked by striated pattern of parallel ridges; (3) ridges radial to shield in central part of aureole deposits. Aureole deposits, which are morphologically similar to those of Arsia Mons (figs. 2*A*, 2*C*) and Ascraeus Mons (fig. 4*A*), probably are of similar origin; they also are morphologically similar to debris aprons at northwest base of Olympus Mons (fig. 1*F*). Sun illumination from right in lower-right quadrant, from left elsewhere. Part of Viking Orbiter mosaic 211–5514.

C, Flows of lava apron on east flank of Pavonis Mons. Sun illumination from left. Viking Orbiter frame 388B07.

REFERENCES

Baker and others (1990, 1991)
Carr (1986a, 1987)
Carr and Schaber (1977)
Hodges and Moore (1979)
Lucchitta (1981, 1985)
Plescia and Saunders (1979)
Williams (1978)

ASCRAEUS MONS

Mosaic: 211–5373 MC: 9B Coordinates: 11° N., 104° W.

Approximate dimensions (km):	
Base diameter	435
Summit elevation	26
Relief	21
Central caldera diameter	avg 55
Caldera depth	2.5
Height/base ratio	0.05
Estimated relative age (10^{-3} craters/km^2):	
Central shield (Neukum and Hiller, 1981)	0.3
Caldera fill (Neukum and Hiller, 1981)	0.1–0.3
Inferred age (Ga):	
Central shield:	
Model 1	1.3
Model 2	0.26
Caldera fill:	
Model 1	0.5–1.3
Model 2	0.1–0.25
Stratigraphic age:	
Amazonian; Tharsis Montes Formation	

DISTINCTIVE CHARACTERISTICS

(1) Typical shield morphology, with terraced, convex flanks (fig. 4*A*).

(2) Complex caldera showing a series of successive collapse episodes (fig. 4*B*).

(3) Lava fans on northeast and south-southwest flanks paralleling trend of Tharsis ridge, similar in orientation to lava fans on Pavonis and Arsia Montes (fig. I–2).

(4) Numerous lava flows, channels, lava-tube ridges, rilles, and collapse pits (arrow 3, fig. 4*A*; fig. 4*C*) on flanks of volcano and surrounding lava fans.

(5) Aureole deposits at base of west flank (arrow 4, fig. 4*A*) considerably smaller in areal extent (90 by 190 km) than those at Arsia and Pavonis Montes but clearly composed of similar materials, with an identical striated pattern of ridges parallel to a well-defined outer margin.

(6) Low shield volcanoes south of south-southwest lava fan (fig. I–2; arrows 5, fig. 4*A*).

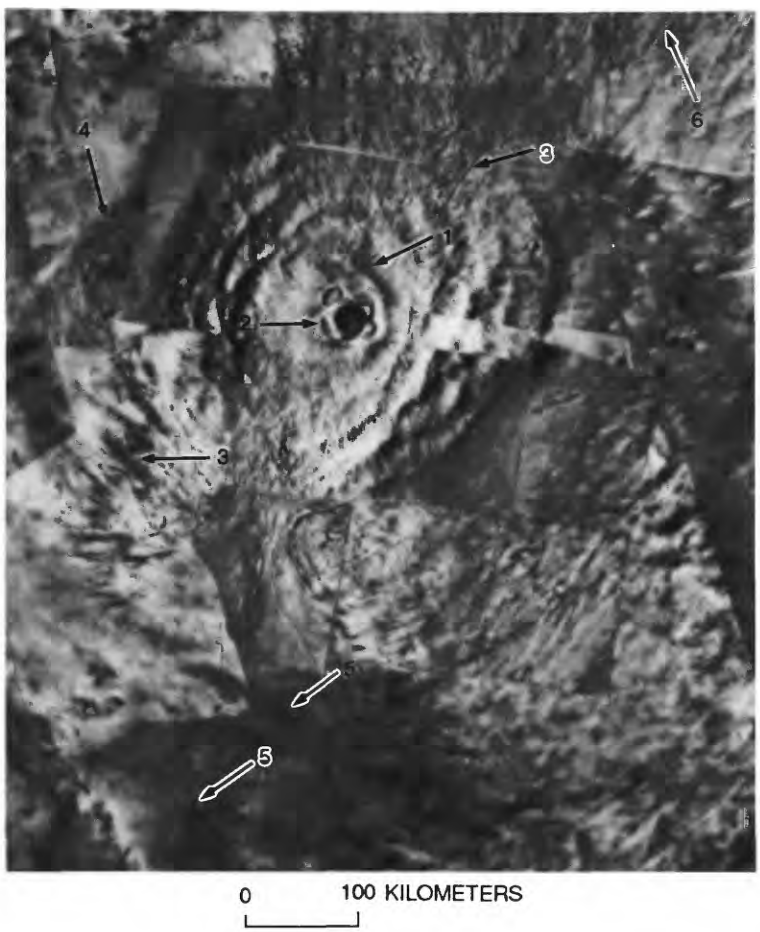

◀ **Figure 4.** Ascraeus Mons. *A.*, Ascraeus Mons. Distinctive characteristics (arrows) include (1) typical shield morphology with terraced, convex flanks; (2) complex caldera, showing succession of collapse episodes; (3) numerous channels, lava tubes, rilles, and collapse pits on flanks; (4) aureole deposit similar to those of Arsia and Pavonis Montes; (5) several low shields on lava plains to south-southwest; and (6) thick lava flows. Sun illumination from right. Parts of Viking Orbiter photomosaic subquadrangles MC–9SE and MC–9NE (U.S. Geological Survey, 1980a, b).

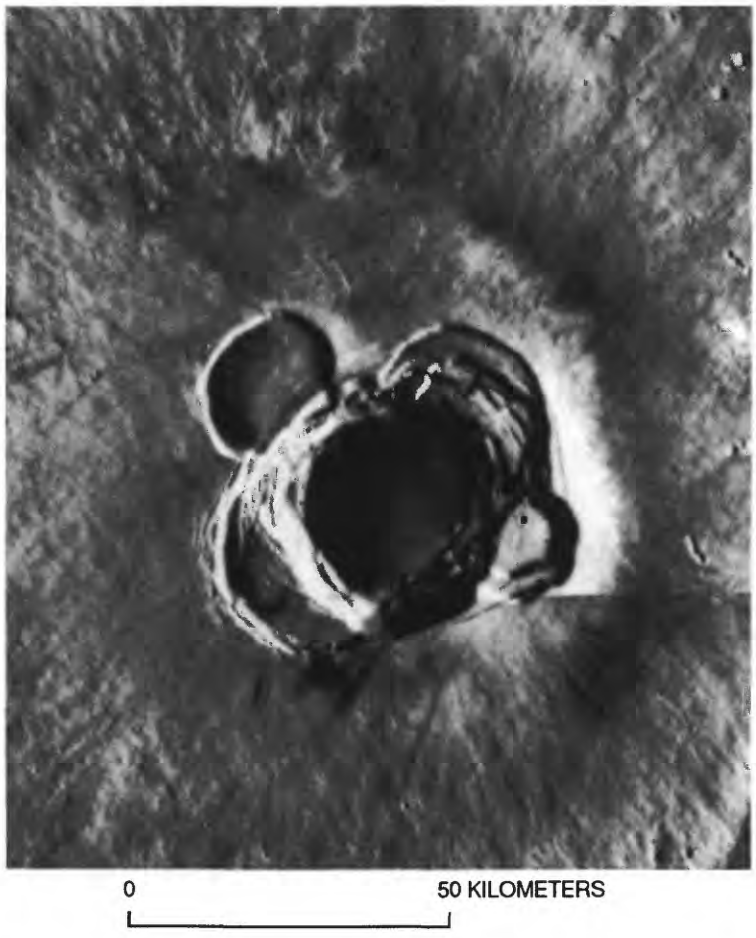

B, Summit caldera of Ascraeus Mons, showing complex sequence of collapse structures. Sun illumination from right. Parts of Viking Orbiter frames 892A11 and 892A32.

DISCUSSION

Ascraeus Mons is similar in many respects to Arsia, Pavonis, and Olympus Montes (fig. I–1). At least eight successive collapse episodes have been delineated within the complex caldera (Zimbelman and McAllister, 1985). As at Arsia Mons, two large lava fans are superposed on an older central shield volcano. The fan on the south-southwest flank has an apex near 15-km elevation and can be traced 200 km southward from this apex. The fan on the northeast flank has an apex near 12-km elevation and extends some 300 km or more northeastward. An unusually large number of concentric rilles and pit-crater chains are visible at the north and south base. Numerous small shield volcanoes occur on a subtle ridge to the south-southwest (fig. I–2, arrows 5, fig. 4*A*). Rheologic properties inferred for the lava flows near the summit suggest that these flows are of basalt or basaltic andesite (Zimbelman, 1985; Moore and Ackerman, 1989a, b). Zimbelman and McAllister (1985) inferred that long individual flows are aa, whereas planar areas consist of pahoehoe.

Although the aureole materials at Ascraeus Mons are much less extensive and less conspicuous than at Arsia and Pavonis Montes, they show the same distinctive striations concentric with the outermost margin of the lobe. As at the other two volcanoes, these deposits are confined to the base of the northwest flank, on the downslope side of the Tharsis ridge (fig. 4*A*). A ragged escarpment occurs upslope from the aureole, and a large block of apparent bedrock is isolated between the scarp and the terminal ridges. As at Arsia and Pavonis Montes, the morphology and context of this aureole most persuasively resemble those of the moraines of a retreating glacier, and that hypothesis is reiterated here to explain the origin of the aureoles at all three Tharsis volcanoes. The possible existence of surface ice on each volcano has been discussed elsewhere (Williams, 1978; Hodges and Moore, 1979; Lucchitta, 1981).

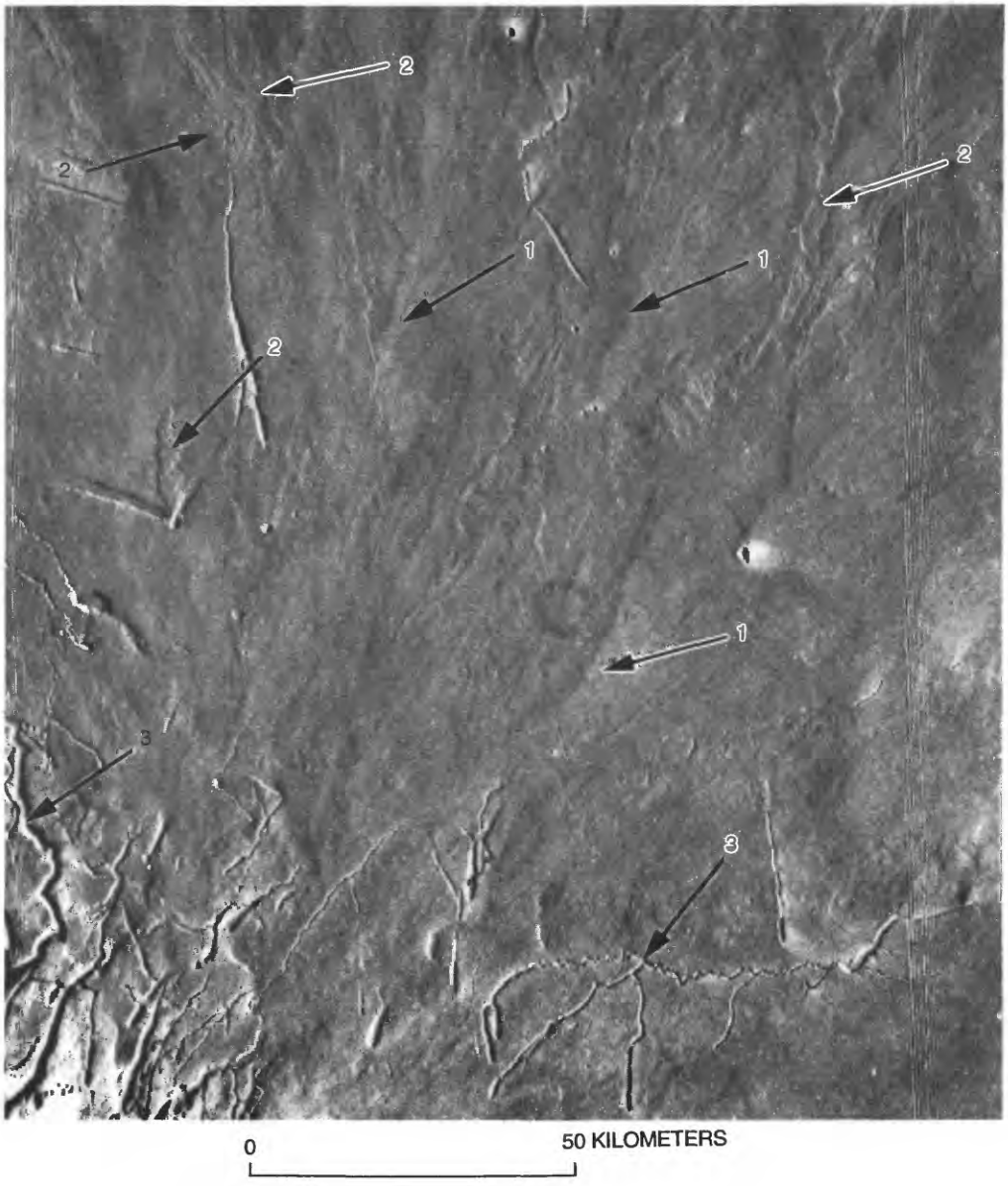

C, Lava fan on northeast flank of Ascraeus Mons. Numbered arrows denote (1) lava ridges (probable lava tubes), (2) lava flows with and without marginal levees, and (3) collapsed lava tubes or channels. Shadow ring near center and vertical bands along sides of image are artifacts. Sun illumination from right. Viking Orbiter frame 892A14.

The aureole deposits at the Tharsis ridge volcanoes differ decidedly from the large aureoles around Olympus Mons but strongly resemble the small debris lobes at the base of the shield's escarpment (fig. 1*F*). The deposits decrease in areal extent from the oldest shield volcano, Arsia Mons, to the youngest, Ascraeus Mons, and the small lobes at Olympus Mons complete this sequence; all of these deposits occur on the northwest side of the volcanoes, and all have been interpreted as products of glacial or related processes (Williams, 1978; Lucchitta, 1981), localized on the northwest flanks by the orographic effects of wind circulation (Hodges and Moore, 1979). If these hypotheses are valid, the progression in size of the deposits from oldest (Arsia Mons) to youngest (Olympus Mons) may simply reflect the decreasing ages of the shields under relatively static glacial conditions; alternatively, the decreasing areal extent of the ridged deposit lobes could indicate a progressive change in climatic regime from intense glaciation to the conditions of limited ice today.

Crater counts (Neukum and Hiller, 1981) on Ascraeus Mons suggest an age comparable to that of Olympus Mons (fig. I–5), a result consistent with the striking morphologic similarities of these two shield volcanoes; additionally, of the three Tharsis volcanoes, relief and summit elevation of Ascraeus Mons most nearly approach those of Olympus Mons, suggesting progressive thickening of the lithosphere. Lavas of the southern fan of Ascraeus merge with those from the eastern apron of Pavonis Mons and appear to be the same age. Relative ages of the four giant Tharsis volcanoes suggest eruptions and lava effusions that overlap in time, but the temporal sequence of their surfaces, from oldest to youngest, is (1) Arsia Mons, (2) Pavonis Mons, (3) Ascraeus Mons, and (4) Olympus Mons (fig. I–5), the same sequence as deduced by Wood (1976) on the basis of caldera complexity and morphology. The total duration of volcanism appears to have been approximately 1.0 to 3.5 b.y.

REFERENCES

Hodges and Moore (1979)
Lucchitta (1981)
Moore and Ackerman (1989a, b)
Neukum and Hiller (1981)
Williams (1978)
Wood (1976)
Zimbelman (1985)
Zimbelman and McAllister (1985)

ALBA PATERA

Mosaics: 211–5065, 211–5068, 211–5071 MC: 3A–2 Coordinates: 40° N., 110° W.

Approximate dimensions (km):	
Base diameter	1,200
Summit elevation	6–7
Relief	2–5
Caldera diameter (scalloped)	120
Youngest caldera	40 by 60
Caldera depth	Shallow
Height/base ratio	0.003
Estimated relative age (10^{-3} craters/km^2):	
Shield:	
Neukum and Hiller (1981)	1.4±0.5
Plescia and Saunders (1979)	1.8±0.1
	1.5±0.4
Young flows, west flank:	
Neukum and Hiller (1981)	0.1 to 0.4
Inferred age (Ga):	
Model 1:	
Shield	3.3–3.6
	3.6
	3.5–3.6
Flows	0.4–1.7
Model 2:	
Shield	0.9–1.8
	1.7–1.8
	1.0–1.8
Flows	0.1–0.4
Stratigraphic age:	
Amazonian-Hesperian; Alba Patera Formation	

DISTINCTIVE CHARACTERISTICS

(1) Concentric-fracture system, about 500 km in diameter (arrow 1, fig. 5*A*), marking break in slope between relatively flat summit and gentle flanks. General northward trend of fractures and grabens south of caldera interrupted by shield, resulting in somewhat arcuate, concentric pattern around volcano, and northeastward trend northeast of shield.

(2) Height-to-base ratio about a tenth those of other major shield volcanoes; diameter twice as large as that of base of Olympus Mons, but relief little more than a tenth as great.

(3) Flanks characterized by well-defined, digitate, lobate lava flows as long as hundreds of kilometers, lava-tube ridges, and channels (fig. 5*B*).

(4) Conspicuous dendritic channel networks on or within lava flows (figs. 5*B*, 5*H*).

(5) Numerous collapse pits along grabens (fig. 5*C*); several small cratered domes (fig. 5*D*) that may be cinder cones.

DISCUSSION

Alba Patera is areally the largest and, in some respects, the most perplexing of the major shield volcanoes. Its low relief in comparison with that of Olympus Mons and the Tharsis volcanoes (fig. I–1) is striking and may reflect its greater age and the extent of crustal compensation thus presumed to have occurred (Carr and others, 1977). Its distinctive concentric pattern of fractures and grabens is apparently due to the deviation imposed by the volcano on a densely spaced network of fractures trending north into the structure, encircling it, and diverging to the northeast on the north side of the shield. At its summit is a caldera complex showing a sequential development of collapse structures (arrows 4, 5, fig. 5*A*). Cattermole and Reid (1984) inferred that the complexity of this summit structure indicates a lengthy period of effusive activity, interspersed with periods of caldera subsidence; an extensive duration of effusion, consistent with the inferred ages, was also determined by Carr and others (1977) and Greeley and Spudis (1981) on the basis of flow characteristics.

The flanks are characterized by vast lava sheetflows (fig. I–2) that apparently originated near the ring fractures; long, digitate flows (fig. 5*B*); narrow ridges that appear to be lava-tube-fed flows, with axial channels or chains of collapse pits; pit craters along grabens; and numerous small cratered domes that resemble spatter or cinder cones (Greeley and Spudis, 1981). Tanaka and others (1988) identified volcanic units related to Alba Patera over an area of about 3×10^6 km^2. Analyses suggest that the rheologic properties of the lavas are consistent with basaltic compositions and that effusion rates ranged from 10^3 to 10^6 m^3/s (Cattermole, 1986a, 1987, 1990). Except for their vastly larger size, the lava channels strongly resemble those common in Hawaii (figs. 5*E*, 5*F*) and on the Snake River Plain, Idaho (fig. 5*G*). On the west flank, particularly, are localized areas of fine-textured dendritic channels that resemble terrestrial fluvial systems (fig. 5*H*), although they are not oriented properly with respect to slope (Greeley and Spudis, 1981). Carr and others (1977) attributed this pattern to distributary (second order) lava tubes formed by budding of multiple flows through upstream (first order) lava tubes. Lava flows on the west flank extend about 1,500 km from the summit caldera. The entire area resembles the complex of features exhibited along the southwest rift zone of Mauna Loa in Hawaii (fig. 5*F*). Cattermole (1986a, b) concluded that this enormous, low shield volcano was built up by massive effusions of highly fluid sheetflows, followed gradually by massive but less rapidly extruded tube-fed and channel flows erupted from vents and fissures.

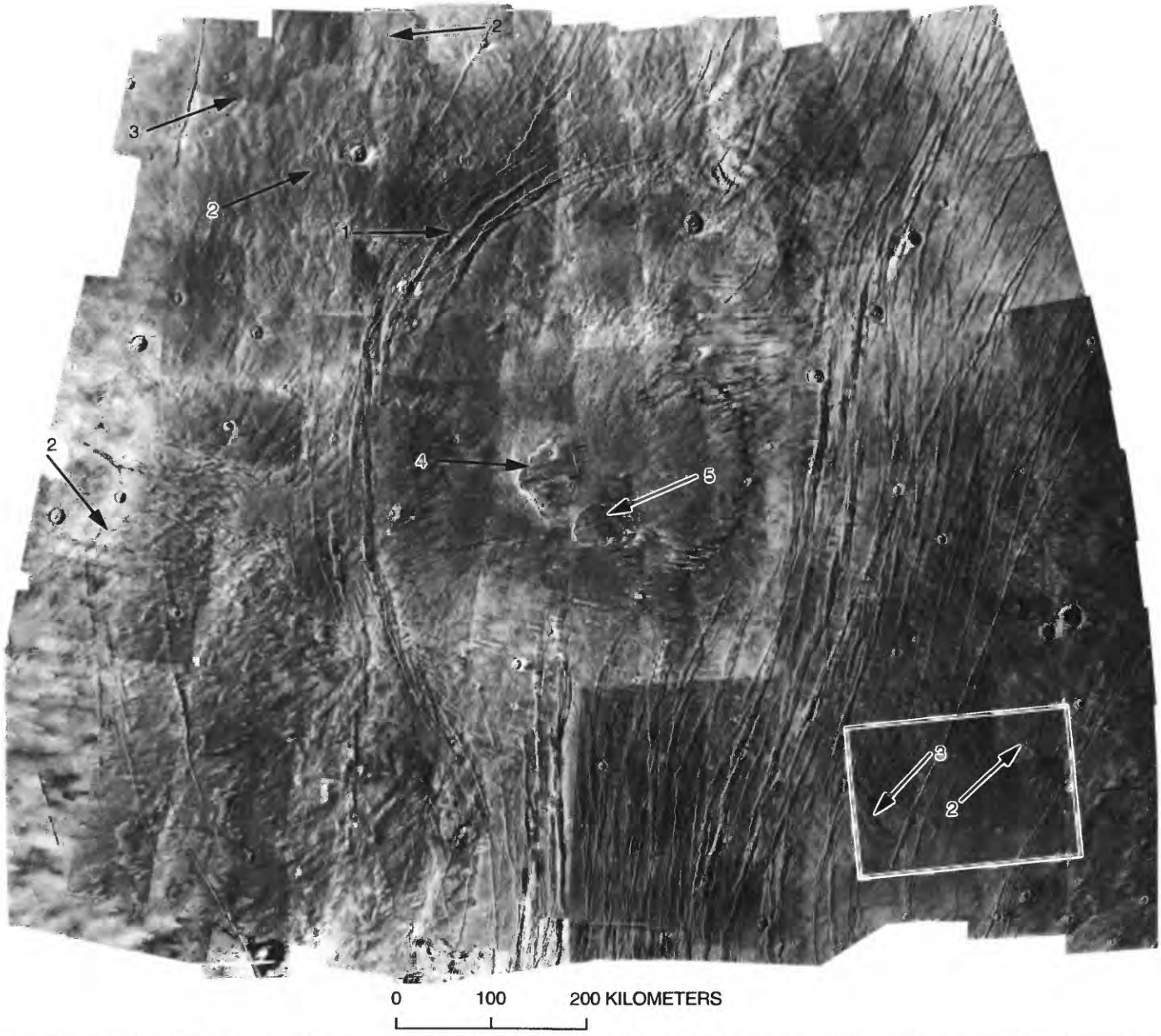

Figure 5. Alba Patera. *A*, Alba Patera and surrounding shield. Numbered arrows correspond to distinctive features: (1) summit ring fractures, (2) lava flows, (3) lava tubes, (4) summit caldera, (5) latest collapse depression within caldera. Box at lower right outlines area of figure 5*C*. Sun illumination from right. Viking Orbiter mosaic from Schneeberger and Pieri (1991).

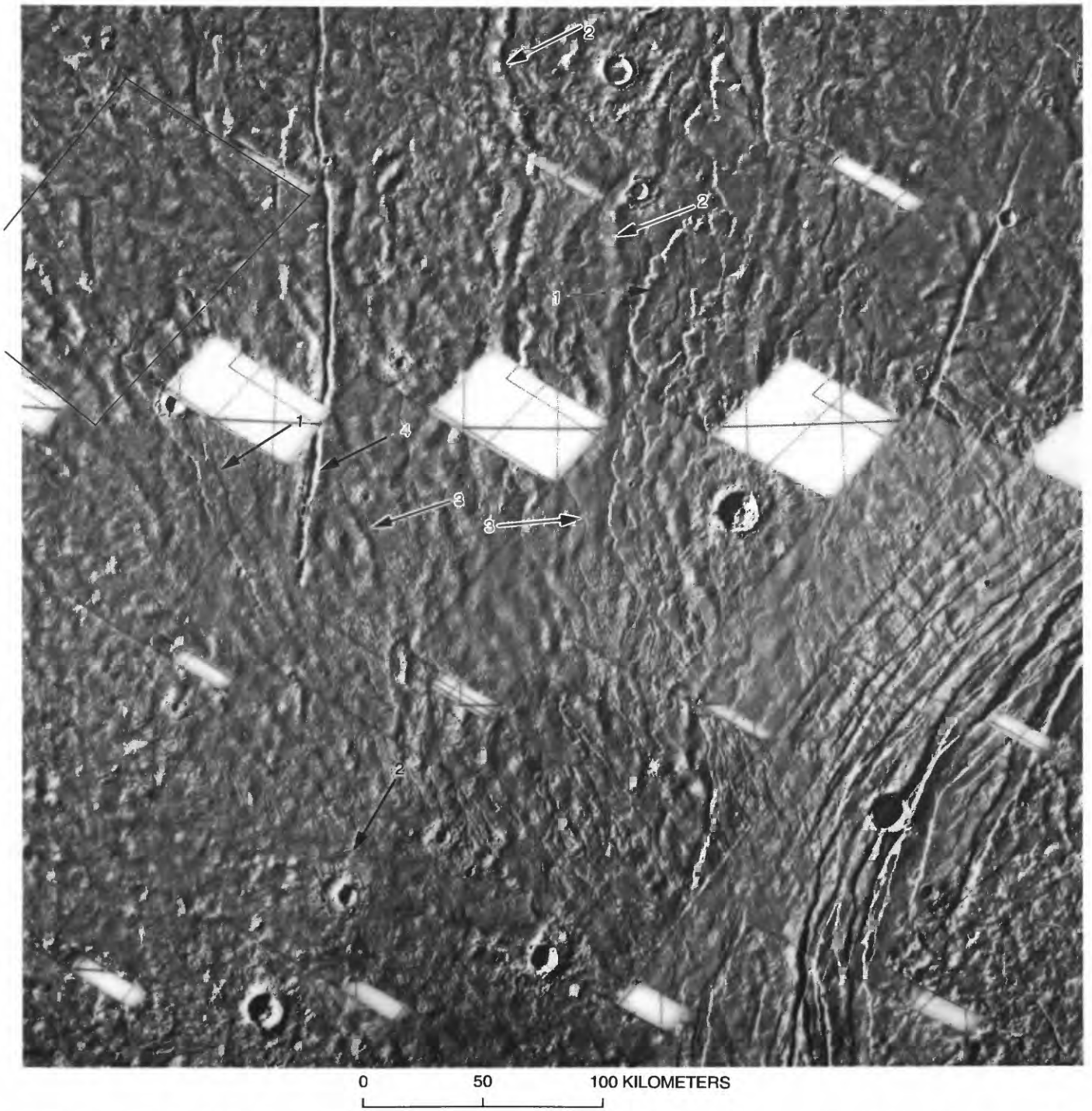

B, Northwest flank of Alba Patera. Numbered arrows denote (1) lava flows, (2) ridges that are probably lava tubes, (3) lava channels, and (4) fissures. Lava tubes are especially numerous and commonly can be identified by chains of collapse pits along ridge axes. Conspicuous fissures may have been vents for flows. Box at upper left outlines area of figure 5*D*. Sun illumination from left. Part of Viking Orbiter mosaic 211–5071.

Mouginis-Mark and others (1988) concluded that pyroclastic activity occurred early in the volcano's history, and suggested a five-stage model for the evolution of Alba Patera: (1) explosive eruptions emplaced a volatile-rich ash layer; (2) lava flows erupted from the summit covered the ash; (3) water released from the heated ash layers carved the dendritic channels; (4) late effusive eruptions emplaced long lava flows on the shield's flanks, and additional meltwater was released from the ash; and (5) the summit collapsed, with attendant faulting. Wilson and Mouginis-Mark (1987) assessed the contribution of volatile materials from Alba Patera to the atmosphere. Gulick and Baker (1990a, b) proposed that the latest period of fluvial-valley development on the planet occurred on the north flank of Alba Patera during the last major episode of ocean formation in middle to late Amazonian time; the valleys were carved by atmospheric precipitation in easily eroded materials of low permeability. Schneeberger and Pieri (1991) conducted an extensive morphologic and geologic analysis of the shield and concluded that its history could be summarized in four main phases: (1) eruption of floodlike flows from fissures; (2) possible emplacement of pyroclastic deposits; (3) eruption of voluminous tabular, crested, and undifferentiated flows from a central vent; and (4) effusion of leveelike flows, collapse of the summit caldera, and final graben formation.

Geologic mapping (Scott and Tanaka, 1986) and crater counts (Neukum and Hiller, 1981) suggest a long history for Alba Patera, and this large, low shield is generally included in the older volcano group (fig. I–5). The conclusion that Alba Patera is older than the other four major Tharsis volcanoes is also attained by applying Wood's (1976) method of deducing age relations on the basis of shield morphology and complexity.

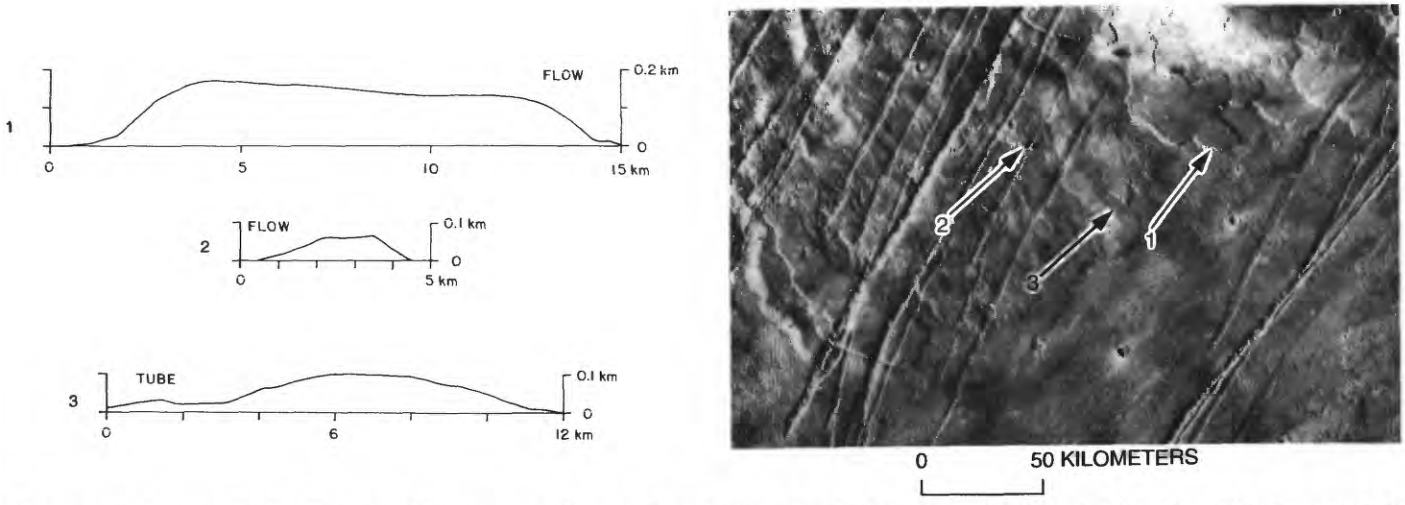

C, Area southwest of Alba Patera, with representative profiles. Arrows denote lava flows (1, 2) and tube ridge (3) transected by grabens and collapse craters. Sun illumination from left. Viking Orbiter frame 516A05. Vertical exaggeration in profiles, 10×.

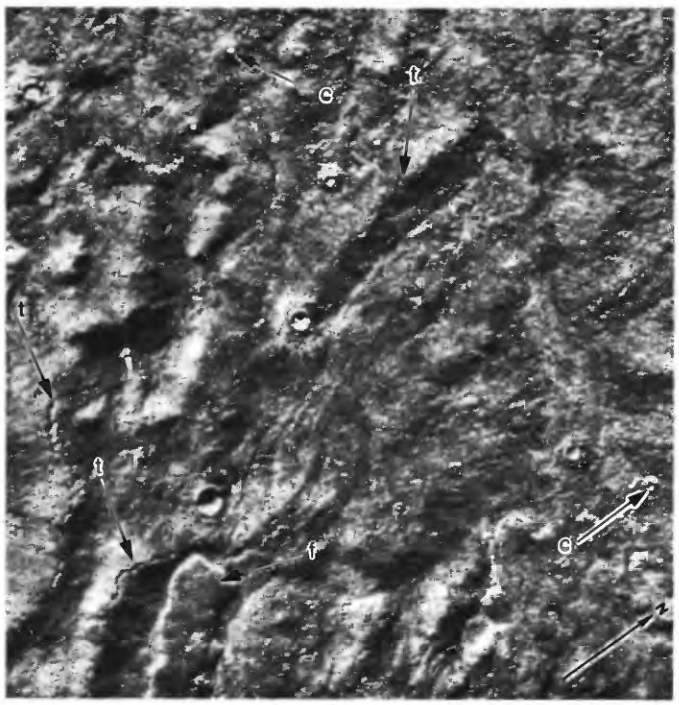

◄ *D*, Area at west edge of figure 5*B*. Distal end of long digitate flow (f, bottom left) to southeast is marked by prominent scarp. Ridges with axial troughs and collapse pits are lava-tube-fed flows (t). Several small cratered domes may be cinder cones (c). Sun illumination from upper left. Viking Orbiter frame 7B20.

► *E*, Mauna Ulu, Hawaii, showing lava channel developed in pahoehoe flows. Lava levees form a broad arch along axis of channel, similar to configuration of channels on flanks of Alba Patera. Sun illumination from right. From Greeley (1974); photograph courtesy of Ronald Greeley.

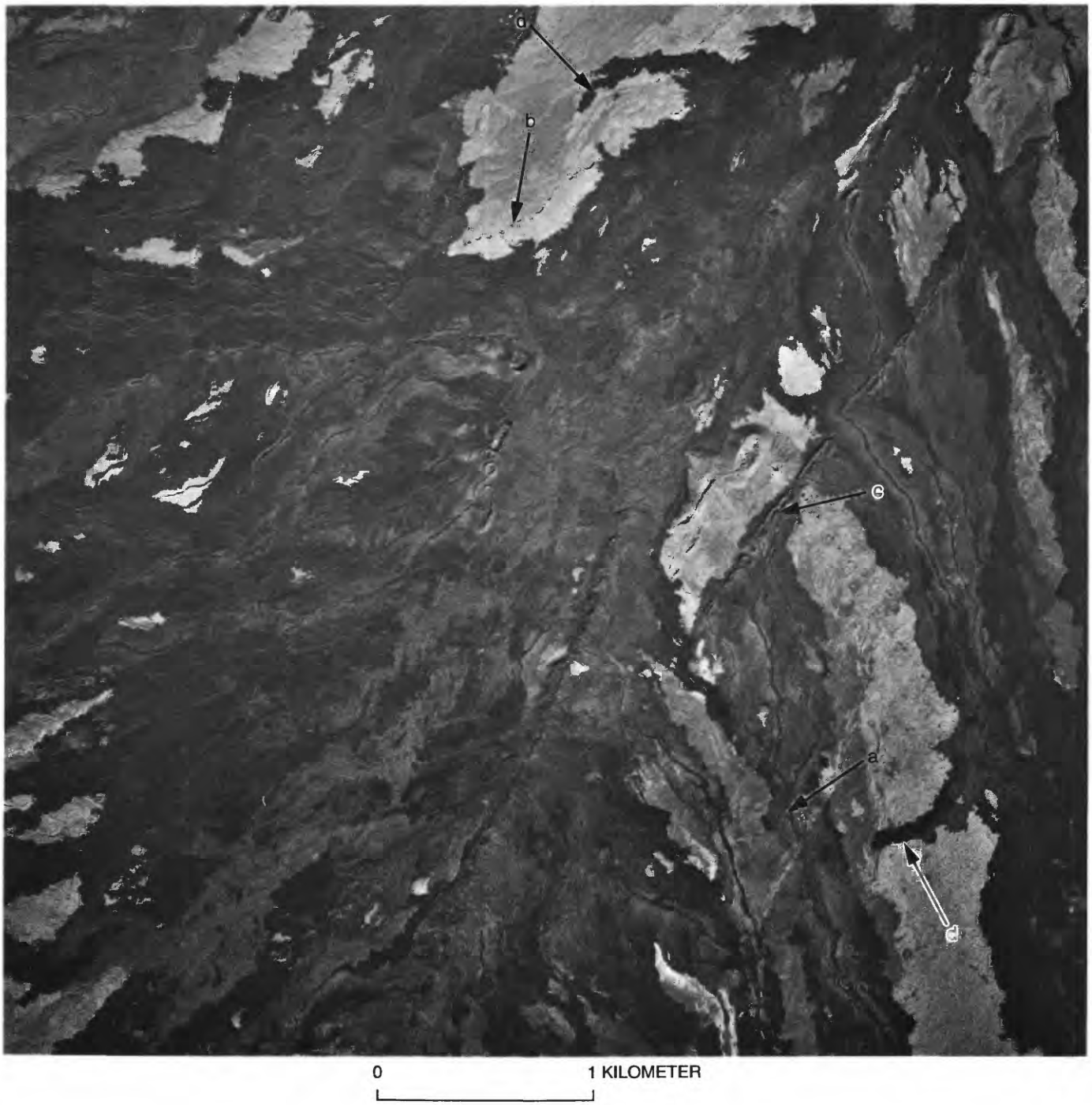

F, Southwest rift zone of Mauna Loa, Hawaii. Arrows denote lava channel (a), lava tube (b), aligned spatter cones (c), and aa flows (d). Entire complex of features resembles that on flanks of Alba Patera (fig. 5*A*). Sun illumination from lower right. U.S. Department of Agriculture photograph EKL–2CC–189, taken December 23, 1964.

◀ *G*, Snake River Plain, Idaho, showing pit crater and lava tube/channel, with numerous cut-off branches and parallel lava tubes along main structure (Greeley, 1977a). Older lava tubes, lava channels, and craters (arrows) are visible throughout area. Sun illumination from right. U.S. Department of Agriculture photographs CXR–8AA–106 and CXR–8AA–108, taken June 28, 1960.

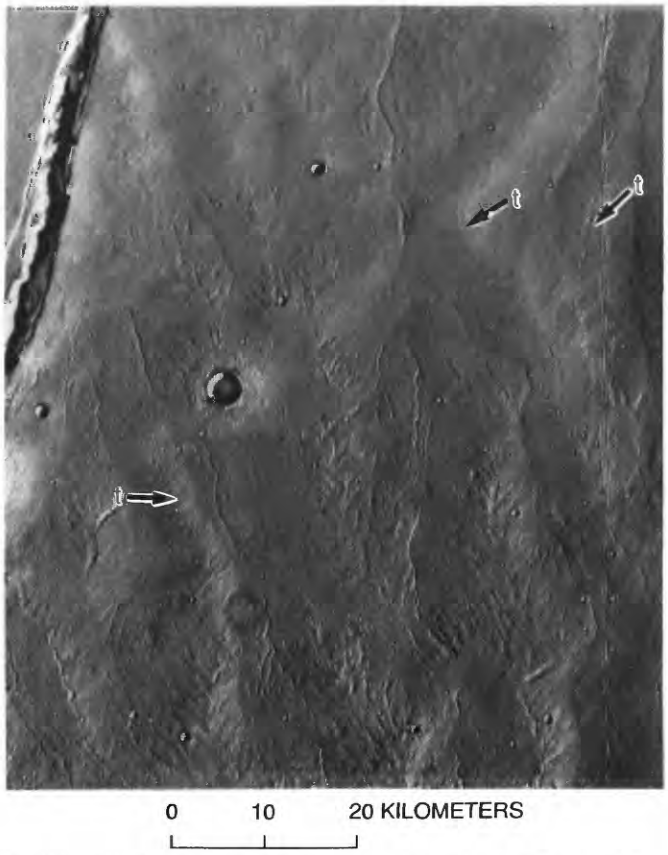

H, West flank of Alba Patera, showing dendritic pattern of lava channels and collapse pits. Intermittent appearance of channels and orientation with respect to slope suggest that they are lava tubes (arrows t) and distributary channels unrelated to fluvial activity. Conspicuous trench formed by coalescent pit craters probably marks fissure-vent system. Vertical band on right side of photograph is an artifact. Sun illumination from right. Viking Orbiter frame 252S04.

REFERENCES

Carr and others (1977)
Cattermole (1986a, b,1987, 1990)
Cattermole and Reid (1984)
Greeley (1974, 1977a)
Greeley and Spudis (1981)
Gulick and Baker (1990a, b)
Mouginis-Mark and others (1988)
Neukum and Hiller (1981)
Plescia and Saunders (1979)
Schneeberger and Pieri (1991)
Scott and Tanaka (1986)
Tanaka and others (1988)
Wilson and Mouginis-Mark (1987)
Wood (1976)

MAJOR PLAINS PROVINCES

THARSIS REGION

MINOR SHIELD VOLCANOES

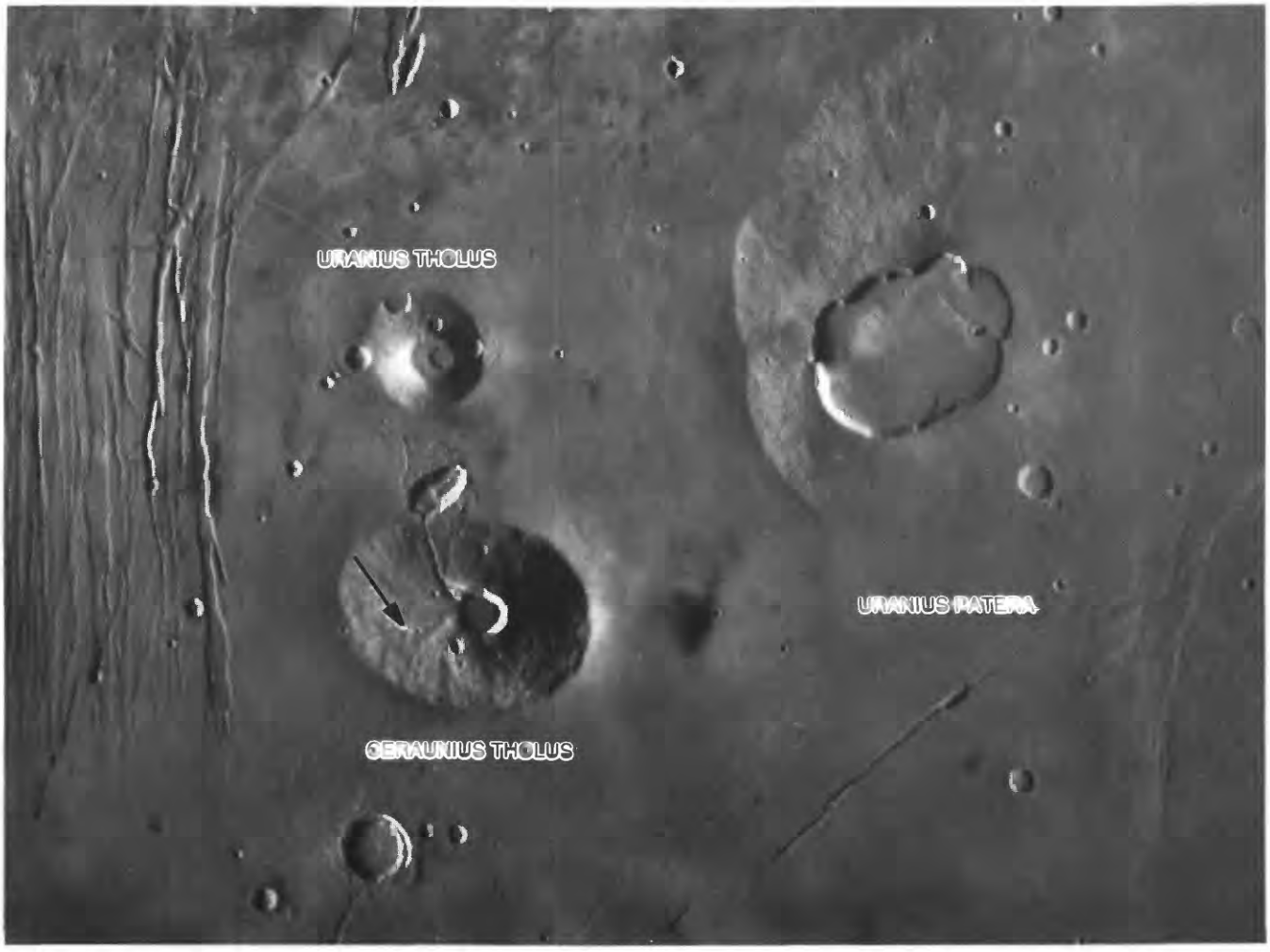

URANIUS PATERA

Mosaic: 211–5904 *MC: 9C* *Coordinates: 26° N., 93° W.*

Approximate dimensions (km):	
Base diameter	230 by 275
Summit elevation	5–6
Relief	1.6
Caldera diameter	110 by 90
Caldera depth	0.9
Height/base ratio	0.007
Estimated relative age (10^{-3} craters/km^2)	2.2±0.8
Inferred age (Ga):	
Model 1	3.6–3.7
Model 2	1.3–2.8
Stratigraphic age:	
Undesignated	

DISTINCTIVE CHARACTERISTICS

(1) Caldera with scalloped walls; caldera diameter large relative to base diameter (figs. 6*A*, 6*B*).
(2) Low height-to-base ratio.
(3) Caldera located asymmetrically with respect to flanks.
(4) Small satellitic cones or low shield volcanoes on flanks, probably subsidiary vents (fig. 6*B*).
(5) Long, digitate flows extending downflank from caldera (fig. 6*B*).
(6) Shield elongate northeast-southwestward.

◄ **Figure 6.** Uranius Patera, Uranius Tholus, and Ceraunius Tholus. *A*, Uranius Patera and Uranius and Ceraunius Tholi, with representative profiles. Lava flows and low shield volcanoes are conspicuous on flanks of Uranius Patera. Ridges and valleys, probably volcanic flows and channels, characterize flanks of Uranius and Ceraunius Tholi. All three minor shield volcanoes, clustered at northeast end of Tharsis ridge, are embayed by younger lava flows that obscure their true bases so that original relief is unknown. Arrow denotes chain of collapse craters on flank of Ceraunius Tholus. Sun illumination from left except on east and south sides of Uranius Patera, where it is from right. Digital-image mosaic. Vertical exaggeration in profiles: Uranius Patera, 4×; Uranius and Ceraunius Tholi, none.

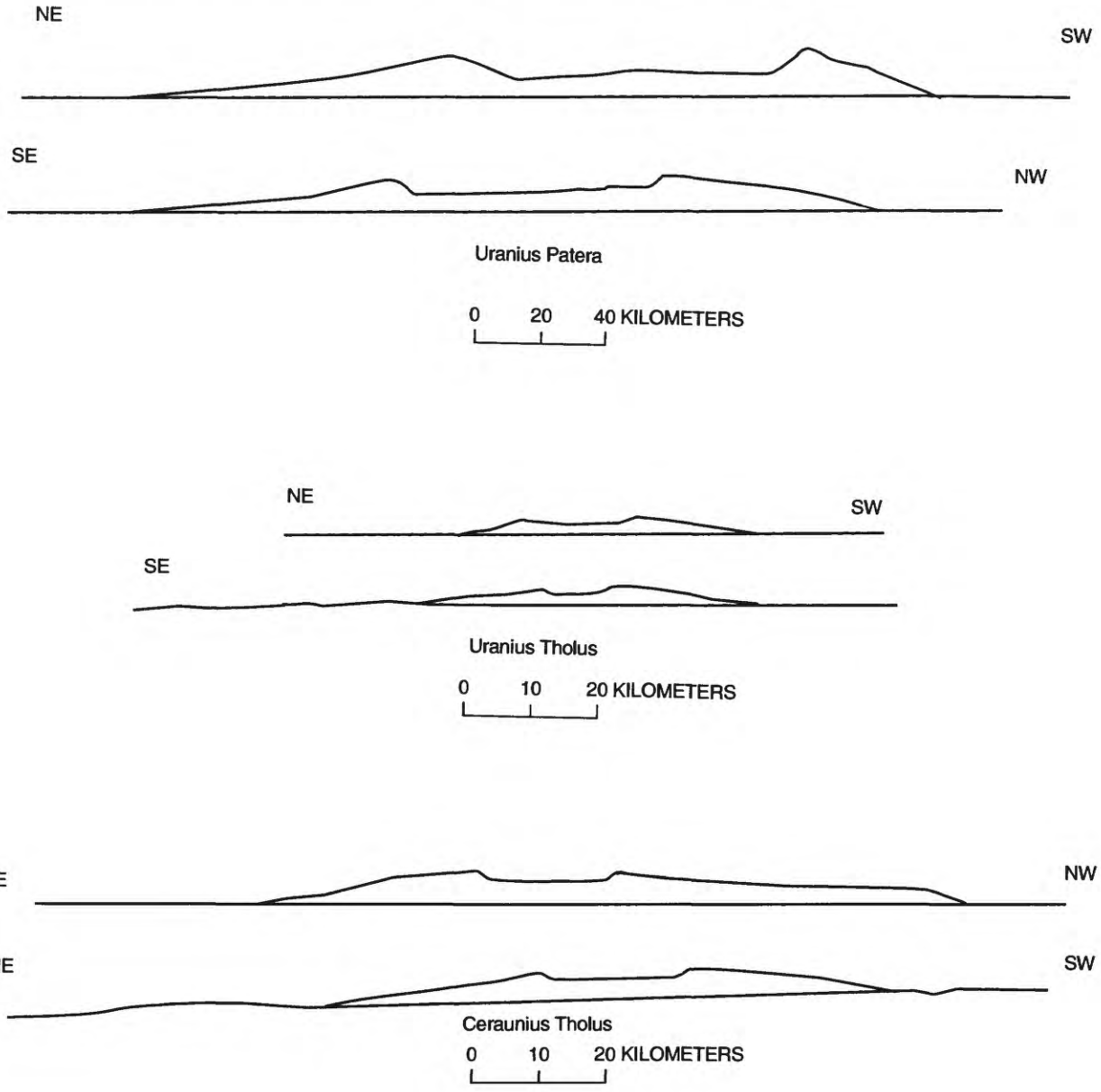

Pike and others, 1980

B, Northwest flank of Uranius Patera. Arrows denote (1) long lava flows and (2) one conspicuous, parasitic low shield. Sun illumination from left. Viking Orbiter frame 516A21.

URANIUS THOLUS

Mosaic: 211–5639 MC: 9C Coordinates: 26° N., 98° W.

Approximate dimensions (km):	
Base diameter	60
Summit elevation	7–8
Relief	2.4
Caldera diameter	10
Depth	0.4
Height/base ratio	0.04
Estimated relative age (10^{-3} craters/km^2):	
Plescia and Saunders (1979)	2.5±0.8
	7±3
Inferred age (Ga):	
Model 1	3.6–3.9
Model 2	1.5–3.7
Stratigraphic age:	
Undesignated	

DISTINCTIVE CHARACTERISTICS

(1) Caldera nested in older summit caldera (20 km diam) that filled to overflowing on south rim (fig. 7).
(2) Chains of collapse pits on flank (arrow, fig. 7).
(3) Conspicuous radial channels incised in flanks.

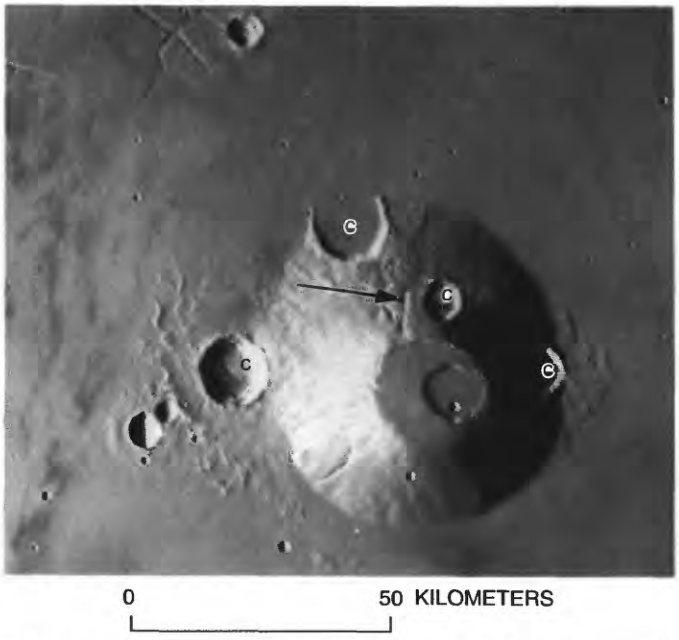

Figure 7. Uranius Tholus. Large summit caldera apparently filled and overflowed, forming radial lava channels as in many terrestrial calderas; later volcanic activity produced smaller caldera. Chains of collapse pits (arrow) probably mark fissures. Several impact craters (c) scar flanks and base of volcano. Sun illumination from left. Viking Orbiter frame 516A23, rectilinear.

CERAUNIUS THOLUS

Mosaic: 211–5639 MC: 9C Coordinates: 24° N., 97° W.

Approximate dimensions (km):	
Base diameter	90 by 130
Summit elevation	10–11
Relief	6
Caldera diameter	25
Depth (U.S. Geological Survey, 1981b)	2
Height/base ratio (110 km)	0.05
Estimated relative age (10^{-3} craters/km^2)	6.4±2.1
Inferred age (Ga):	
Model	13.8–3.9
Model	23.3–3.6
Stratigraphic age:	
Undesignated	

DISTINCTIVE CHARACTERISTICS

(1) Caldera with low domical or flowlike structure on floor.
(2) Highly dissected flanks (fig. 8).
(3) Large channel (50 km long, avg 3 km wide) beginning near caldera rim dissects rim of elongate impact crater at base of north flank and terminates in fanlike deposit on crater floor; this channel developed where caldera appears to have overflowed (fig. 6*A*).
(4) Chains of collapse pits on flanks (arrow, fig. 6*A*).

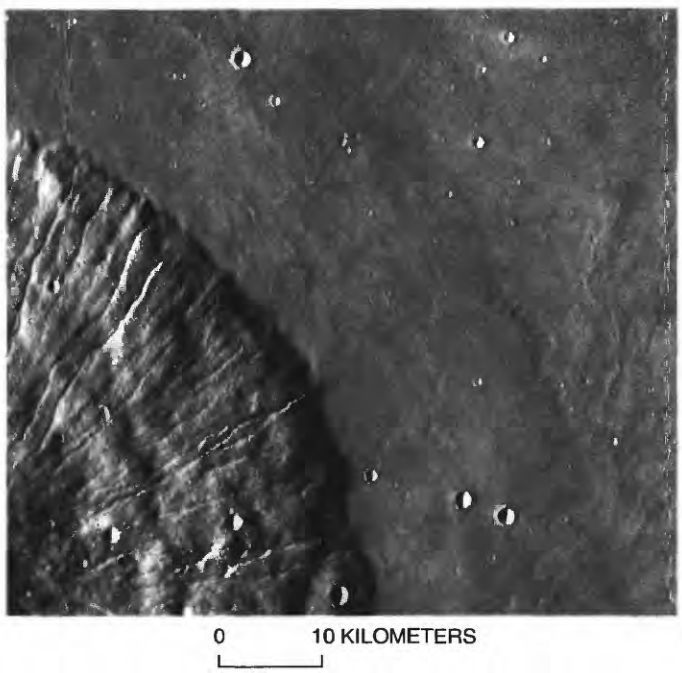

Figure 8. Northeast flank of Ceraunius Tholus, showing lava channels and fissures that characterize shield, and truncation by younger lava plains. Sun illumination from left. Viking Orbiter frame 662A06.

THARSIS THOLUS

Mosaic: 211–5904 *MC: 9C* *Coordinates: 13° N., 91° W.*

Approximate dimensions (km):	
Base diameter	120 by 150
Summit elevation	10
Relief	5
Caldera diameter	48
Height/base ratio	0.04
Estimated relative age (10^{-3} craters/km^2):	
Plescia and Saunders (1979)	3.8±1.4
Inferred age (Ga):	
Model 1	3.7–3.8
Model 2	2.2–3.5
Stratigraphic age:	
Undesignated	

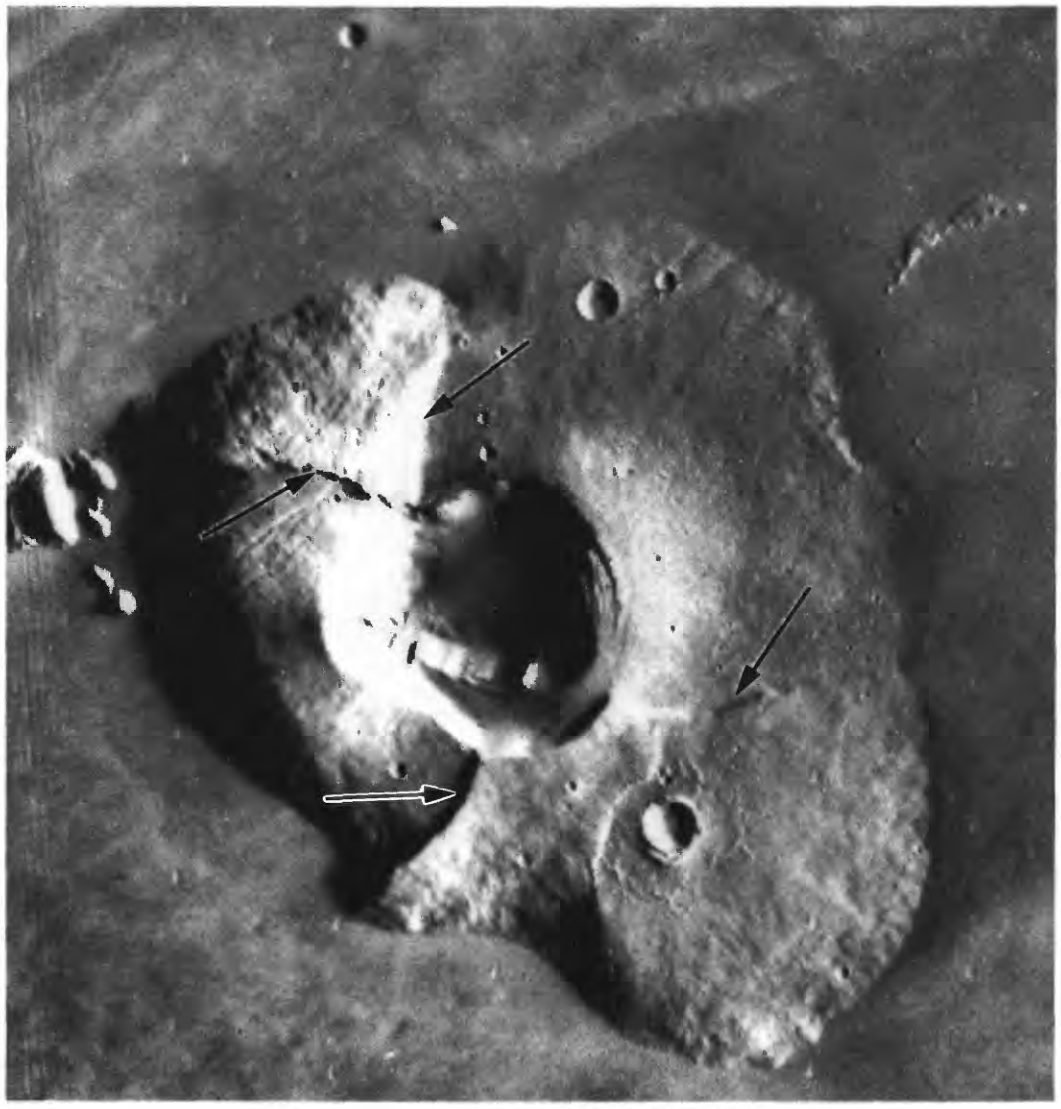

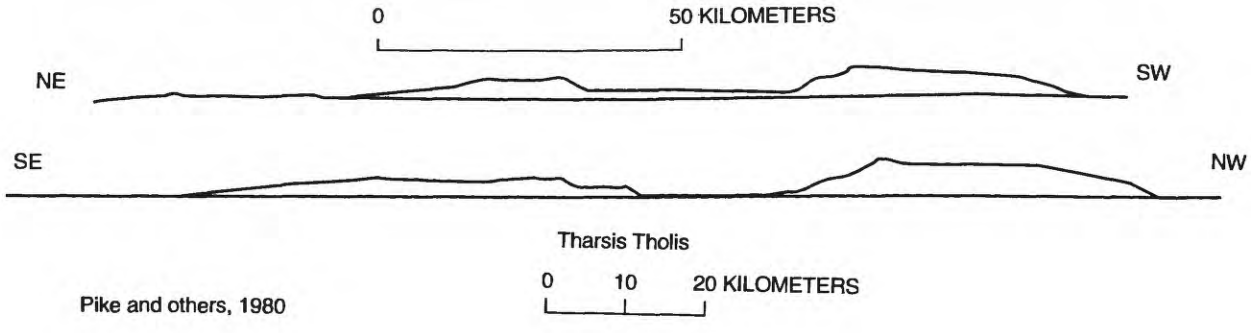

Pike and others, 1980

DISTINCTIVE CHARACTERISTICS

(1) Terraced caldera (fig. 9*A*).
(2) Structurally modified shield volcano (fig. 9*A*); four major normal faults (arrows, fig. 9*B*) transect flanks and intersect caldera rim, forming pie-shaped sector grabens.
(3) Flanks relatively smooth, conspicuously convex; individual lava flows not discernible.

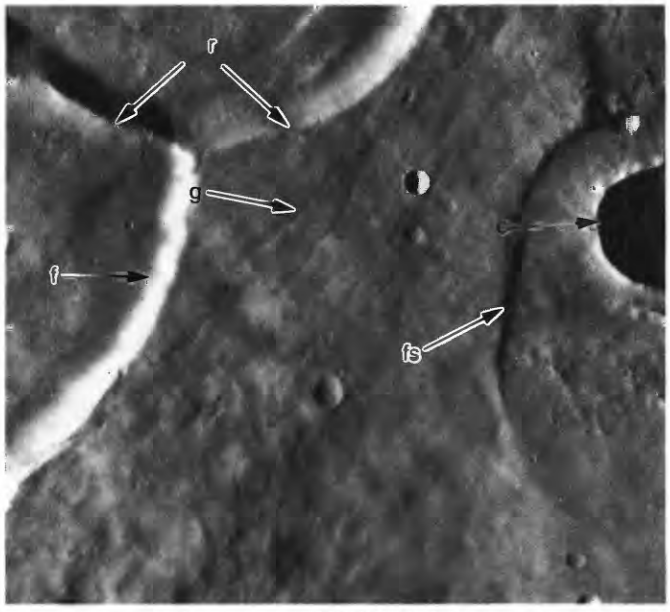

◄ **Figure 9.** Tharsis Tholus. *A*, Tharsis Tholus, with representative profile. Arrows denote fault scarps described in text. Sun illumination from right. Viking Orbiter frame 858A23. Profile from Pike and others (1980); no vertical exaggeration. *B*, Southeast flank of Tharsis Tholus. Arrows denote intersection of fault scarp (f) with caldera rim (r), smaller fault (fs) between impact crater (c) and caldera rim, and fissures and grabens (g) tangent to caldera rim. Sun illumination from left. Viking Orbiter frame 699A15.

JOVIS THOLUS

Mosaic: 211–5430 MC: 9D Coordinates: 18° N., 118° W.

Approximate dimensions (km):	
Base diameter	50 by 60
Summit elevation	6
Relief	1
Caldera diameter	20 by 40
Depth	0.6
Height/base ratio	0.02
Estimated relative age (10^{-3} craters/km^2):	
Plescia and Saunders (1979)	4.4±1.4
Inferred ages (Ga):	
Model 1	3.7–3.8
Model 2	2.7–3.5
Stratigraphic age:	
Undesignated	

DISTINCTIVE CHARACTERISTICS

(1) Anomalously low height-to-base ratio.
(2) Caldera diameter large relative to base diameter; scalloped outline, suggesting a complex sequence of collapse events (fig. 10*A*).
(3) Position of caldera highly asymmetric with respect to flanks; northeast flank is 20 km wide, southwest flank less than 1 km wide.
(4) Smooth flanks, with ridges and valleys parallel to slope direction; individual lava flows can be distinguished in figure 10*B*.

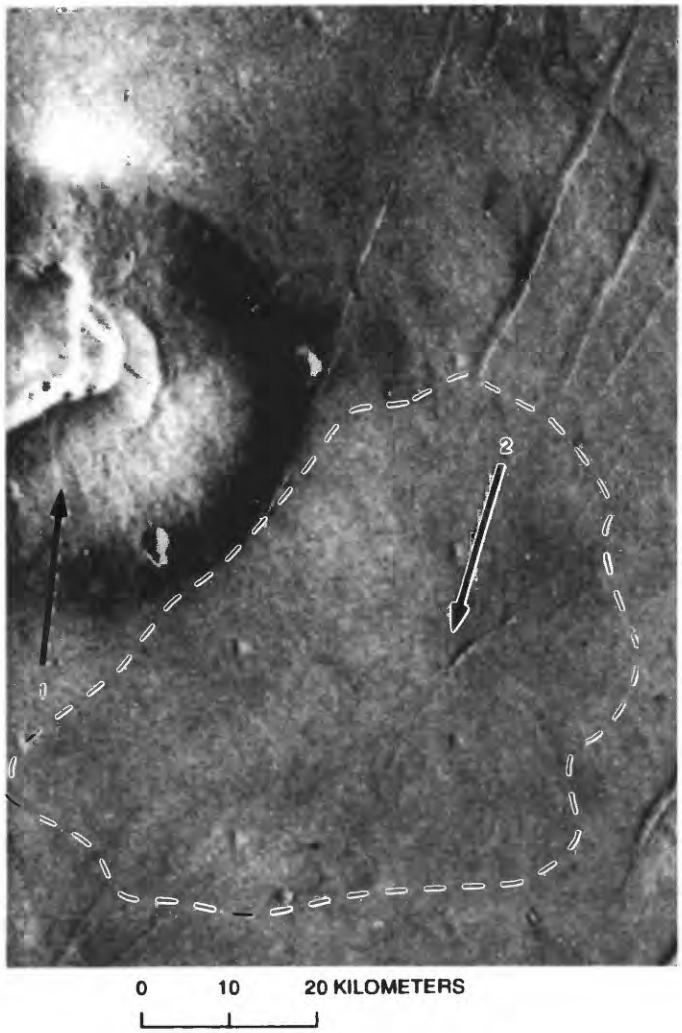

Figure 10. Jovis Tholus. *A*, Jovis Tholus. Shield volcano is deeply embayed by subsequent lava flows, obscuring original relief. Arrow indicates center of figure 10*B*. Sun illumination from left. Viking Orbiter frame 041B19.

B, East flank of Jovis Tholus. Arrows denote probable lava flows (1) emanating from summit caldera, and outline marks outer margin of lavas from small, low shield volcano (2) superposed on fractures and on base of Jovis Tholus. Sun illumination from left. Viking Orbiter frame 516A36.

BIBLIS PATERA

Mosaic: 211–5513 MC: 9E Coordinates: 2° N., 124° W.

Approximate dimensions (km):	
Base diameter	123 by 170
Summit elevation	9–10
Relief	3
Caldera diameter	55
Caldera depth	3.5
Height/base ratio (150 km)	0.02
Estimated relative age (10^{-3} craters/km^2):	
Plescia and Saunders (1979)	1.7±0.6
Inferred ages (Ga):	
Model 1	3.5–3.7
Model 2	1.0–2.1
Stratigraphic age:	
Undesignated	

DISTINCTIVE CHARACTERISTICS

(1) Asymmetric profile (fig. 11*A*); northwest flank of volcano (nearly 100 km in greatest dimension) on downslope side of Tharsis ridge is more than 4 times longer than upslope southeast flank (approx 22 km).
(2) Multiply-terraced caldera, with conspicuous concentric fractures surrounding caldera rim (fig. 11*B*).
(3) Regional grabens cutting flanks.
(4) Shield embayed by flows from Arsia Mons.
(5) Probable lava flows discernible as small ridges on flanks (fig. 11*B*).

Figure 11. Biblis Patera and Ulysses Patera. *A*, Biblis and Ulysses Paterae shield volcanoes, deeply embayed by subsequent lava flows that obscure original relief. Sun illumination from left. Digital-image mosaic.

ULYSSES PATERA

Mosaic: 211–5513 *MC: 9F* *Coordinates: 3° N., 121° W.*

Approximate dimensions (km):	
Base diameter	100
Summit elevation	8–9
Relief	1.7
Caldera diameter	55
Caldera depth	2.1
Height/base ratio	0.02
Estimated relative age (10^{-3} craters/km^2):	
Plescia and Saunders (1979)	3.4±0.8
Inferred age (Ga):	
Model 1	3.7–3.8
Model 2	2.5–3.3
Stratigraphic age:	
Undesignated	

DISTINCTIVE CHARACTERISTICS

(1) Base nearly circular, in contrast to elongate northwest flank of adjacent Biblis Patera (fig. 11*A*); shape may reflect position on somewhat flatter part of Tharsis ridge (figs. I–1, I–2).
(2) Flanks scarred by two relatively large craters (15, 25 km diam) of obvious impact origin (fig. 12).
(3) U-shaped array of 14 cratered cones on caldera floor (fig. 12).
(4) Shield embayed by lava flows from Arsia Mons.
(5) Lava flows visible on flanks (fig. 12).

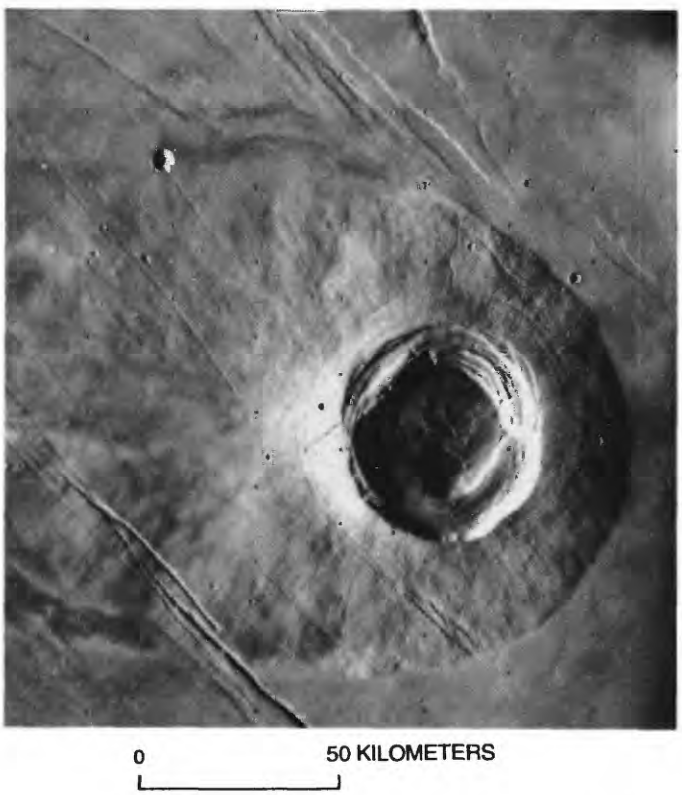

B, Biblis Patera, showing details of circular summit caldera and surrounding ring fractures, elliptical shape of shield, and lava flows originating at caldera rim. Sun illumination from left. Viking Orbiter frame 44B50.

Figure 12. Ulysses Patera, showing U-shaped array of low shields on caldera floor (arrow), as well as ejecta from two large impact craters on rim. Lava flows from Arsia Mons embay base of Ulysses Patera shield. Sun illumination from left. Viking Orbiter frame 49B85.

DISCUSSION (MINOR SHIELD VOLCANOES)

The seven shield volcanoes of these provinces form a distinct population whose dimensions are as small as a tenth those of the major Tharsis volcanoes (fig. I–1). General morphology among these shields is similar, but their relief ranges from about 1 to as much as 6 km, and their basal diameters from 60 to 240 km. The shields are surrounded and embayed by lava plains (fig. I–2) that evidently obscure their original base and height dimensions. Morphologic distinctions permit grouping the volcanoes for discussion purposes as follows: (1) Uranius Tholus and Ceraunius Tholus (fig. 6*A*), with height-to-base (*h/b*) ratios of 0.04 to 0.05; and (2) Uranius Patera (fig. 6*A*), Jovis Tholus (fig. 10*A*), Ulysses Patera, and Biblis Patera (fig. 11*A*), with *h/b* ratios about 0.01 to 0.02. Tharsis Tholus (fig. 9*A*;), with an *h/b* ratio of about 0.04, is unique in being conspicuously faulted.

Reimers and Komar (1979) contended that Uranius and Ceraunius Tholi, together with Uranius Patera, differ morphologically from shield volcanoes and more closely resemble terrestrial pyroclastic cones and composite volcanoes, particularly in the pattern of radial dissection on the flanks, which they attributed to explosive volcanic density currents. Flank-slope angles, however, of 3°–12° for the above-named features are within the range 2°–12° characteristic of shield volcanoes (Pike and Clow, 1981b). Furthermore, each of these calderas has clearly been flooded with lava, unlike terrestrial stratocones, whose last stages of eruption commonly result in extrusive rhyolitic domes and a central resurgent dome of tilted fault blocks on the caldera floor (Williams and McBirney, 1979). Dissection of the volcanoes' flanks can be attributed to lava channels, collapsed lava tubes, and pit-crater chains, all of which are characteristic of terrestrial shield volcanoes. Analogy with basaltic shields seems more persuasive than a pyroclastic or stratocone interpretation. Uranius Tholus is unique among the entire group in having filled and overflowed its caldera, with a subsequent smaller caldera forming in the lava fill, as is common in basaltic shields. The presence of several conspicuous, large impact craters on its flank suggests that Uranius Tholus may be the oldest of these seven volcanoes.

Biblis and Ulysses Paterae, each with an *h/b* ratio of 0.02, have a characteristic shield morphology, although flank widths are narrow relative to caldera diameters except on the northwest side of Biblis Patera, where the flank is elongate downslope on the Tharsis ridge (figs. 11*A*, 11*B*, 12). The bases of these shields are embayed by an unknown thickness of lava.

The northeast flank of Uranius Patera (*h/b* ratio, 0.007), like Biblis Patera, is elongate downslope at the northeast end of the Tharsis ridge (fig. 6*A*). Its large caldera and low *h/b* ratio distinguish it from nearby Ceraunius and Uranius Tholi, as do the lava flows and small edifices on the flanks of the volcano. Jovis Tholus (*h/b* ratio, 0.02) has the least relief of all the shields and the largest caldera diameter relative to its base diameter (figs. 10*A*, 10*B*), probably owing to substantial embayment by lava flows around its base.

Tharsis Tholus (*h/b* ratio, 0.04) is distinguished by the structural modification that has formed conspicuous fault scarps on its flanks (figs. 10*A*, 10*B*). Several narrow, linear grabens cross the northwest flank, but otherwise the edifice has smooth and notably convex flanks, embayed by surrounding lava.

Like the major Tharsis volcanoes, these more modest features also are interpreted here as basaltic shields, whose dimensions are more nearly analogous to their terrestrial counterparts. At about 1 to 6 km, more or less, the heights of these volcanoes relative to the caldera diameters, together with embayment relations, suggest that the true bases of each have been somewhat buried by the surrounding lava flows. Although the data are much too limited to speculate extensively, the observed differences in *h/b* ratios and morphologies among these seven volcanoes may reflect differences in eruptive style attributable to compositional variations within the basaltic regime. Pike (1978) noted a clear geometric distinction between martian tholi, paterae, and montes, and suggested that these smaller features correspond more closely to terrestrial subaerial shield volcanoes, composed of alkaline or mixed lavas, than to tholeiitic oceanic shield volcanoes. He maintained that primary-magma compositions on Mars could differ from those on Earth and that the geometry of martian shield volcanoes could reflect differences in chemical composition unlike those expected on Earth. For these seven volcanoes, however, the evidence is weak because of the unknown but substantial depth of lava flooding around their bases.

The surfaces of all the volcanoes in this group are older than the surface flows of the four major Tharsis volcanoes (Neukum and Hiller, 1981), where eruptive activity either began later or, more likely, continued

much longer. This relation is demonstrated by both superposition and crater-count data. Stratigraphic ages of these minor shields range from Noachian to Hesperian (fig. I–5); Ceraunius and Uranius Tholi appear to be Noachian, whereas the others appear to be Hesperian, although Jovis and Tharsis Tholi may be Noachian according to the wide variation in the relative-age estimates. The sequence of relative ages shown in figure I–5 agrees well with the sequence of Landheim and Barlow (1991). Inferred ages suggest that these shield volcanoes formed between about 3.9–3.5 and 3.7–1.0 Ga, depending on the model.

REFERENCES

Landheim and Barlow (1991)
Neukum and Hiller (1981)
Pike (1978)
Pike and Clow (1981b)
Pike and others (1980)
Plescia and Saunders (1979)
Reimers and Komar (1979)
Scott and Tanaka (1986)
Williams and McBirney (1979)

MAJOR PLAINS PROVINCES

THARSIS REGION

SMALL VOLCANIC FEATURES


N
0
50 KILOMETERS

TEMPE-MAREOTIS

Mosaic: 211–5813 MC: 3B Coordinates: 31°–40° N., 79°–91° W.

Province description:
Small shield volcanoes and associated lava flows amid highly fractured terrain; probable vents associated with edifices and fissures localized along fractures trending mainly 50°–60° NE. Collapse pits along grabens are probably related to volcanic activity.

Elevation (km)	2–3
Approximate dimensions (m):	
Base diameter	2,000–10,000
Summit-crater diameter (circular to slot shaped)	300–1,000
Estimated relief	35–400
Crater-diameter/base-diameter ratio	0.06–0.17
Height/base ratio	0.01–0.03
Estimated relative age (10^{-3} craters/km^2):	
associated lava plain (Plescia, 1981)	2.3±1.1
Inferred age (Ga):	
Model 1	3.5–3.7
Model 2	1.1–3.0

Stratigraphic age:
Hesperian; Tempe Terra Formation

DISCUSSION

The small, low shield volcanoes of the Tempe-Mareotis province (fig. 13*A*), at the northwest margin of the highlands (fig. I–2), are remarkable in their morphologic resemblance to features on Earth (Hodges, 1979, 1980a, c; Plescia, 1981). Unlike many other martian features, these low shields are similar in dimension to their terrestrial counterparts. In places, lava flows clearly emanate from summit craters, spreading out in broad aprons around the bases of the shields. Lava levees and flow fronts visible along some fractures indicate that fissure eruptions also occurred (figs. 13*A*, 13*B*), and dikelikelinearridgesexistaswell.

The Tempe-Mareotis province appears to be somehow related to the large-scale deformation and shield building atop the Tharsis bulge, inasmuch as the province is at the northeast end of that bulge amid terrain intensely dissected by fractures and grabens trending predominantly N. 30°–40° E., parallel to the trend of the Tharsis volcanoes (pl. 1; fig. I–1). A subsidiary fracture set that dominates the western part of the province (fig. 13*A*) trends N. 50°–60° E., and the Tempe-Mareotis volcanoes appear to be localized primarily along this trend (Hodges, 1980a). Intersection relations suggest that the two fracture sets formed essentially contemporaneously.

The most persuasive analogs for the Tempe-Mareotis shields (figs. 13*B*, 13*C*, 13*E*) are the low shield volcanoes characteristic of the Snake River Plain in Idaho (figs. 13*D*, 13*F*; Greeley, 1977b, 1982) and similar features in Iceland and Hawaii (fig. 13*G*). Pike (1978) distinguished subclasses of terrestrial small shield volcanoes according to dimensional ratios; small but significant differences occur in the crater-diameter-to-base-diameter (*c/b*) and height-to-base (*h/b*) ratios that characterize each group, resulting in a morphologic distinction as follows: (1) low shield volcanoes (all those on the Snake River Plain and a few in Hawaii and Iceland), with an average *c/b* ratio of 0.08 and *h/b* ratios ranging from 0.014 to 0.02; (2) Icelandic shield volcanoes (in Iceland, Oregon, and California), with an average *c/b* ratio of 0.06 and an average *h/b* ratio of 0.06; and (3) steep shield volcanoes (in Iceland and Hawaii), with an average *c/b* ratio of 0.12 and an average *h/b* ratio of 0.04.

Relief of the martian features can be estimated only by using photoclinometry; horizontal dimensions provide more reliable ratios. *C/b* ratios ranging from 0.06 to 0.17 suggest closest affinity with groups 1 and 3, as exemplified by Mauna Ulu in Hawaii (figs. 13*G*, 14*D*) and numerous shield volcanoes on the Snake River Plain. Although this analogy fails to consider planetary differences in gravity, the effects may be insignificant in the absence of pyroclastic activity.

Quantitative and morphologic comparisons support an interpretation of the Tempe-Mareotis province, with its thin lava flows, lava tubes, and attendant collapse pits, as probably a site of basaltic volcanism. Where such volcanism has prevailed, the lava plains are lower than the highly fractured mesas, and the N. 30°–40° E.-trending fracture set is far less evident; a few vents with limited associated lava flows appear isolated within the uplands (southeastern part of fig. 13*A*), locally obscuring the dominant fractures. The progressive invasion of volcanic activity has caused flooding and apparent foundering of the highlands in this borderland region.

Crater counts (Plescia, 1981) indicate that the terrain of the Tempe-Mareotis province is among the oldest of the Tharsis volcanic units (fig. I–5), and superposition relations demonstrate that it is older even than Alba Patera, suggesting that the activity which culminated in the enormous shield volcanoes may have been preceded by volcanism in this peripheral region, where it lasted a much shorter time. Reasons for the stunted growth of these low shields, as well as of those on the Snake River Plain, remain enigmatic,

◄ **Figure 13.** Tempe-Mareotis. *A*, Area northeast of Tharsis ridge. Arrows denote shield volcanoes; arrows with dots denote especially persuasive examples, strongly resembling terrestrial shield volcanoes on the Snake River Plain, Idaho (figs. 13*D*, 13*F*), and in Hawaii (fig. 13*G*). Sun illumination from left. Mosaic compiled from Viking Orbiter frames 627A01 through 627A58.

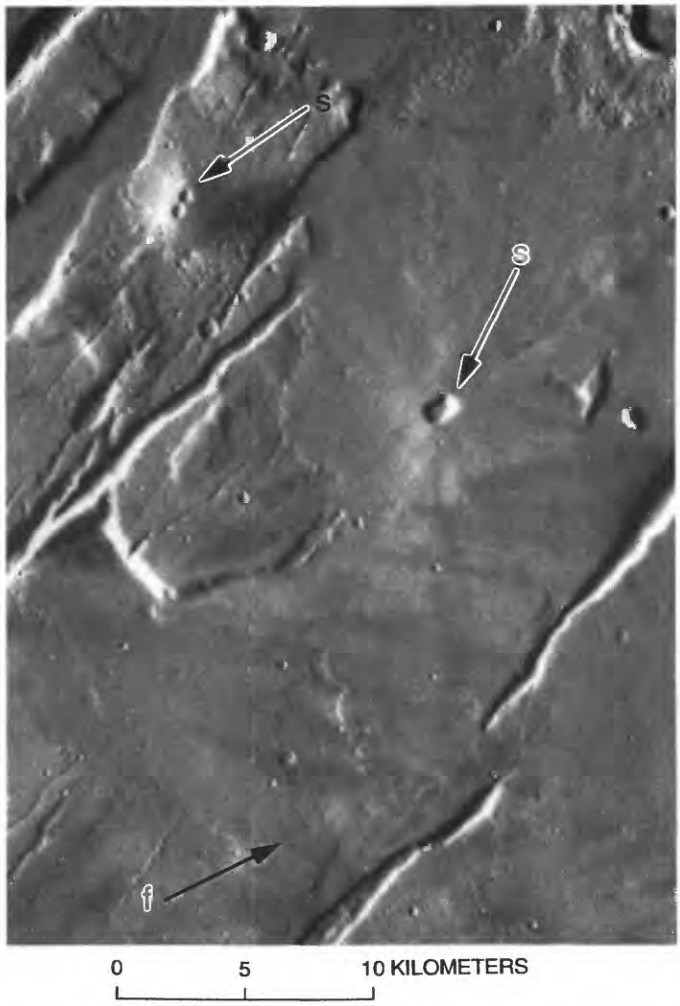

B, Two particularly well developed shield volcanoes with summit craters (arrows s). Some lava flows (arrow f) issued from fissures. Sun illumination from left. Viking Orbiter frame 627A41.

but such variables as lava viscosity, eruption rate, and conduit configuration may be more significant under some circumstances in limiting edifice height on both Earth and Mars than depth to magma chamber (Hodges, 1980a). The volcanism in the Tempe-Mareotis province, about 3.7–1.1 Ga, was evidently contemporaneous with that of such nearby shield volcanoes as Uranius Patera (fig. I–5).

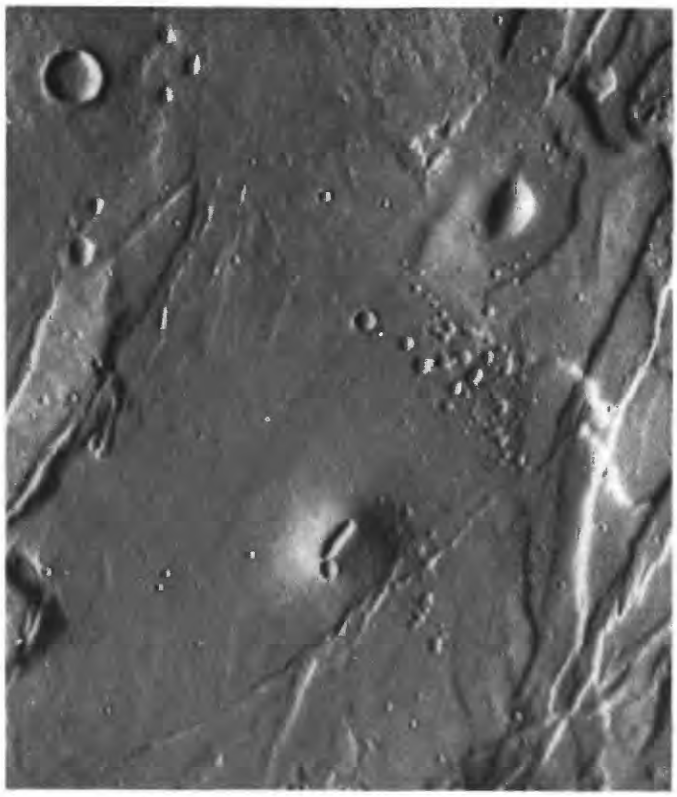

◄ *C*, Slot-shaped vent, similar to Cottrells Blowout on the Snake River Plain, Idaho (fig. 13*D*). Small crater at south end of vent is of probable impact origin. Sun illumination from left. Viking Orbiter frame 627A28.

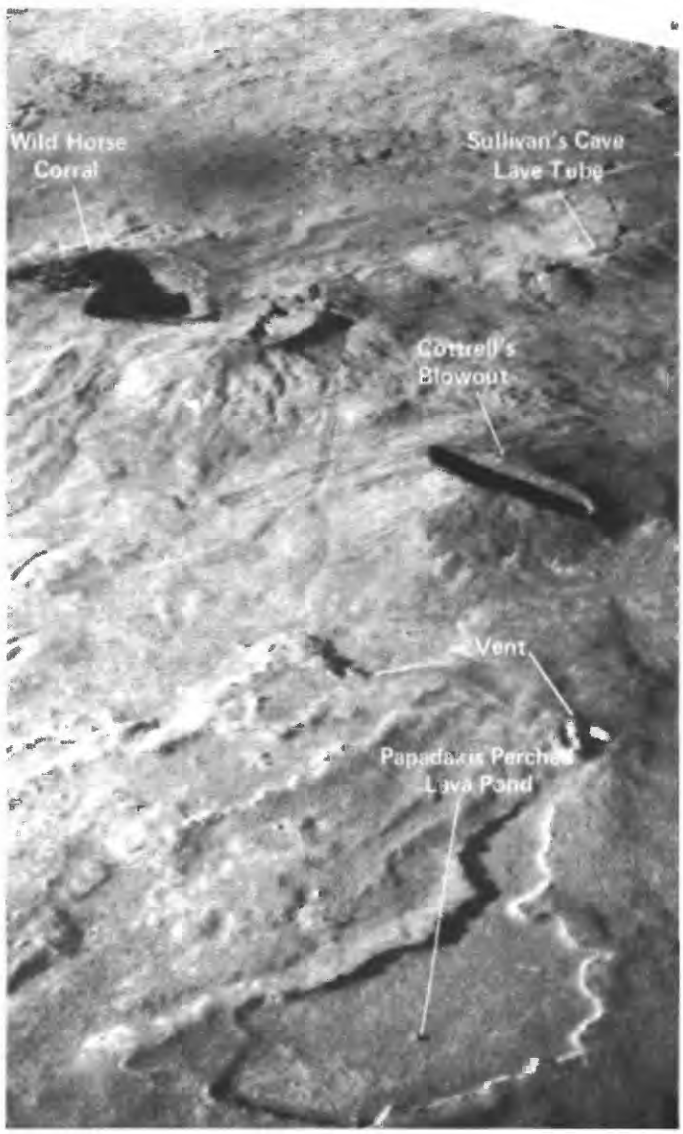

► *D*, Inferno Chasm rift zone, Snake River Plain, Idaho (from Greeley, 1977b). Cottrells Blowout (approx 500 m long) exemplifies a slot-shaped vent like that in figure 13*C*. View northeastward; Sun illumination from left.

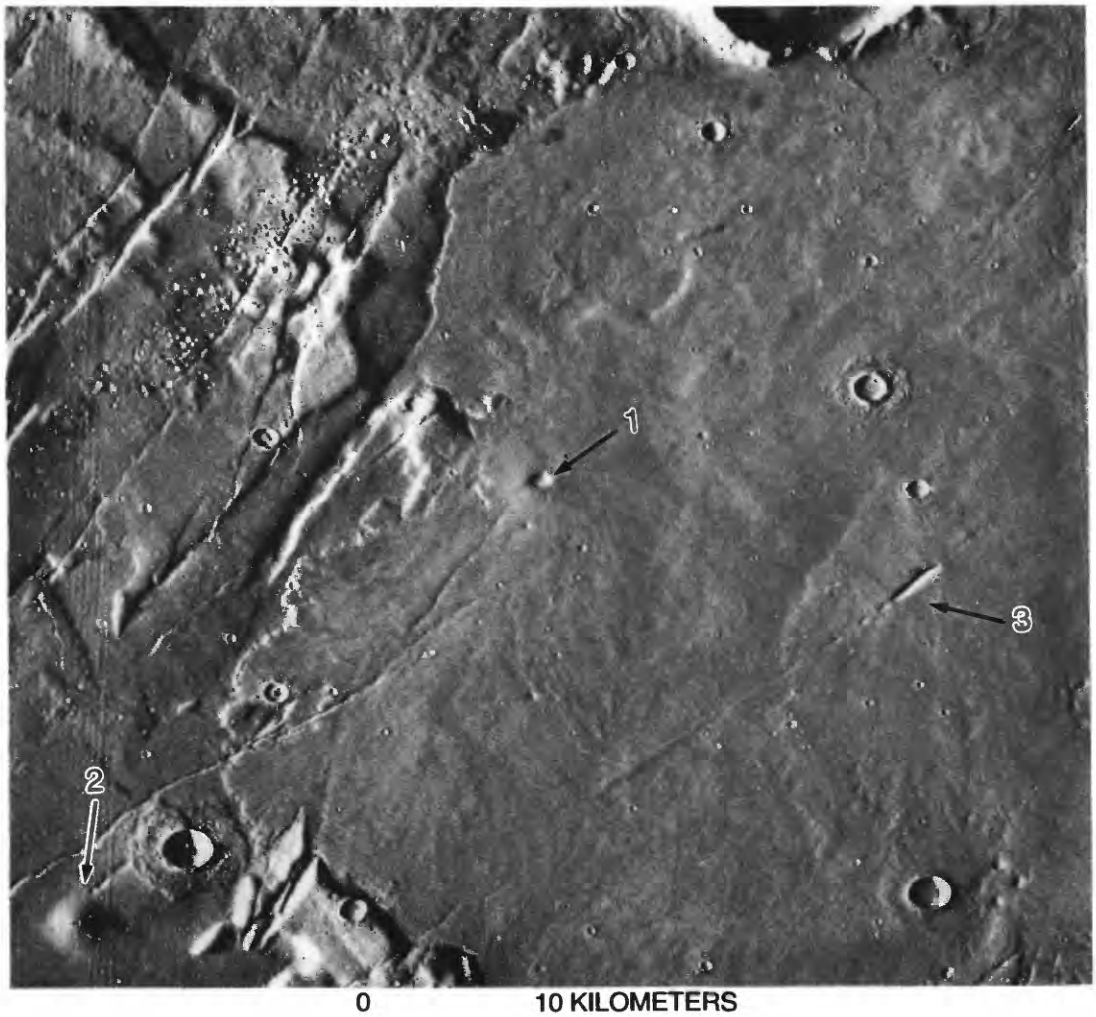

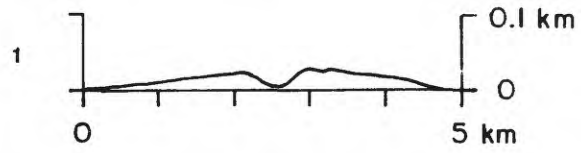

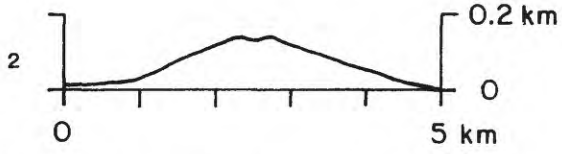

E, Three shield volcanoes of different morphologies (arrows), with representative profiles. Sun illumination from left. Viking Orbiter frame 627A27. Profile 1 dimensions: crater diameter (*c*), about 800 m; base diameter (*b*), about 4.8 km; relief (*h*), about 34 m; crater-diameter-to-base-diameter (*c*/*b*) ratio, 0.17; height-to-base-diameter (*h*/*b*) ratio, 0.01. Profile 2 dimensions: *c*, about 400 m; *b*, about 4.4 km; *h*, about 140 m; *c*/*b* ratio, 0.09; *h*/*b* ratio, 0.03. Vertical exaggeration, 10×.

F, Pillar Butte lava field, showing convex profile typical of low shield volcanoes on the Snake River Plain, Idaho. Although most of surrounding lava field is pahoehoe, numerous short aa flows were erupted from summit, building up steeper gradient around vent. Profile, which is similar to that of Mauna Ulu, Hawaii (fig. 13*G*), probably typifies that of low shield volcanoes in Tempe-Mareotis province. Photograph by Mike Lovas, taken in 1969 (from Greeley, 1977b); courtesy of Ronald Greeley.

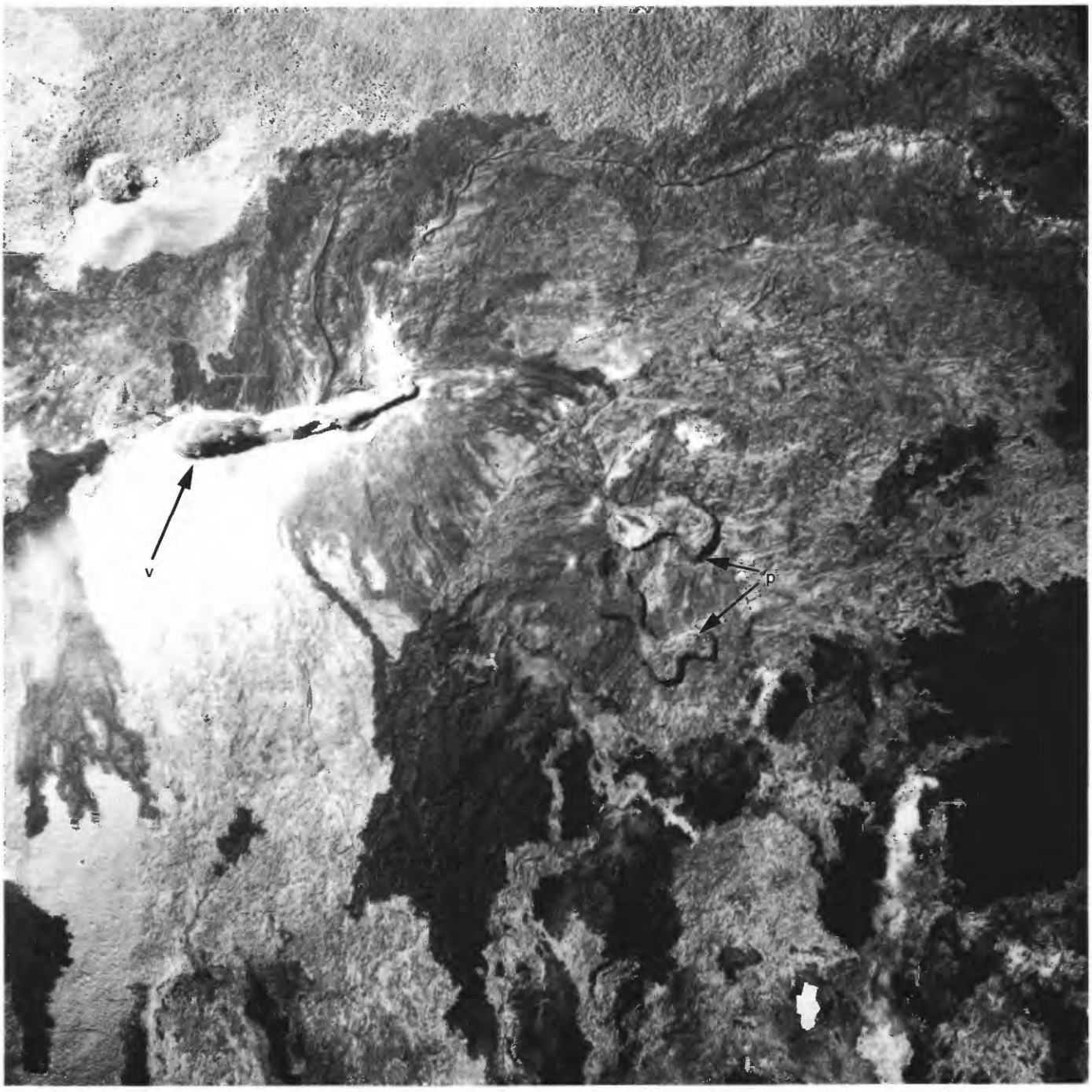

G, Mauna Ulu, Hawaii. Low shield volcano is marked by slot-shaped summit vent (arrow v), about 450 m long. Irregular collapse pits (arrows p) formed around rootless vents at site of an older crater (landscape was subsequently obliterated). Both slot-shaped and irregular craters characterize probable vents in Tempe-Mareotis province (fig. 13*A*). Sun illumination from lower right. Towhill Corp., Honolulu, photograph 5815–9, taken in October 1972 (from Carr and Greeley, 1980); courtesy of Ronald Greeley.

REFERENCES

Carr and Greeley (1980)
Greeley (1977b, 1982)
Hodges (1979, 1980a, c)
Pike (1978)
Plescia (1981)

CERAUNIUS FOSSAE

Mosaic: 211–5391 MC: 3C–9 Coordinates: 16°–40° N., 92°–117° W.

Province description:
Small shield volcanoes, lava flows, and collapse pits along fractures and grabens in highly fractured terrain.

Elevation (km)	3–5
Approximate dimensions (km):	
Base diameter	2–5
Estimated relative age (10^{-3} craters/km^2):	
Associated lava plains	0.3±0.2
Inferred age (Ga):	
Model 1	0.5–2.2
Model 2	0.1–0.5

Stratigraphic age:
Amazonian-Hesperian; Ceraunius Fossae Formation

DISCUSSION

The low shield volcanoes of the Ceraunius Fossae province are circular to elliptical features with pits, craters, and slot-shaped vents (figs. 14*A*, 14*B*); these shields probably have profiles similar to that of Mauna Ulu in Hawaii (fig. 14*D*). Faint ridges and valleys radiate from summit depressions, forming aprons superposed on an extensive system of fractures and grabens (fig. 14*C*) that trend north, merge with the somewhat-arcuate fractures around the caldera of Alba Patera, and veer northeast. The ridges probably are lava flows and tube-fed flows (Moore and Hodges, 1980); lava channels are also visible. The fractured terrain is similar to that of the Tempe-Mareotis province, but the small shield volcanoes are not so conspicuous. The surface appears to have foundered where volcanism was most active (fig. 14*A*). Flows from Ascraeus Mons embay the area, but the Ceraunius Fossae shield volcanoes and flows are superposed on fractures and grabens that transect flows from Alba Patera, and one large flow from Ceraunius Fossae is superposed on adjoining lava plains to the south (fig. I–2), supporting the young relative ages based on crater counts. Unlike the Tempe-Mareotis province, both superposition relations and crater-count data show that the volcanism in the Ceraunius Fossae province was contemporaneous with late-stage activity at the large Tharsis volcanoes (fig. I–5); thus, lava was erupting from features with both little and great relief and at moderate to high elevations during Amazonian time.

REFERENCES

Decker and others (1987) Moore and Hodges (1980)

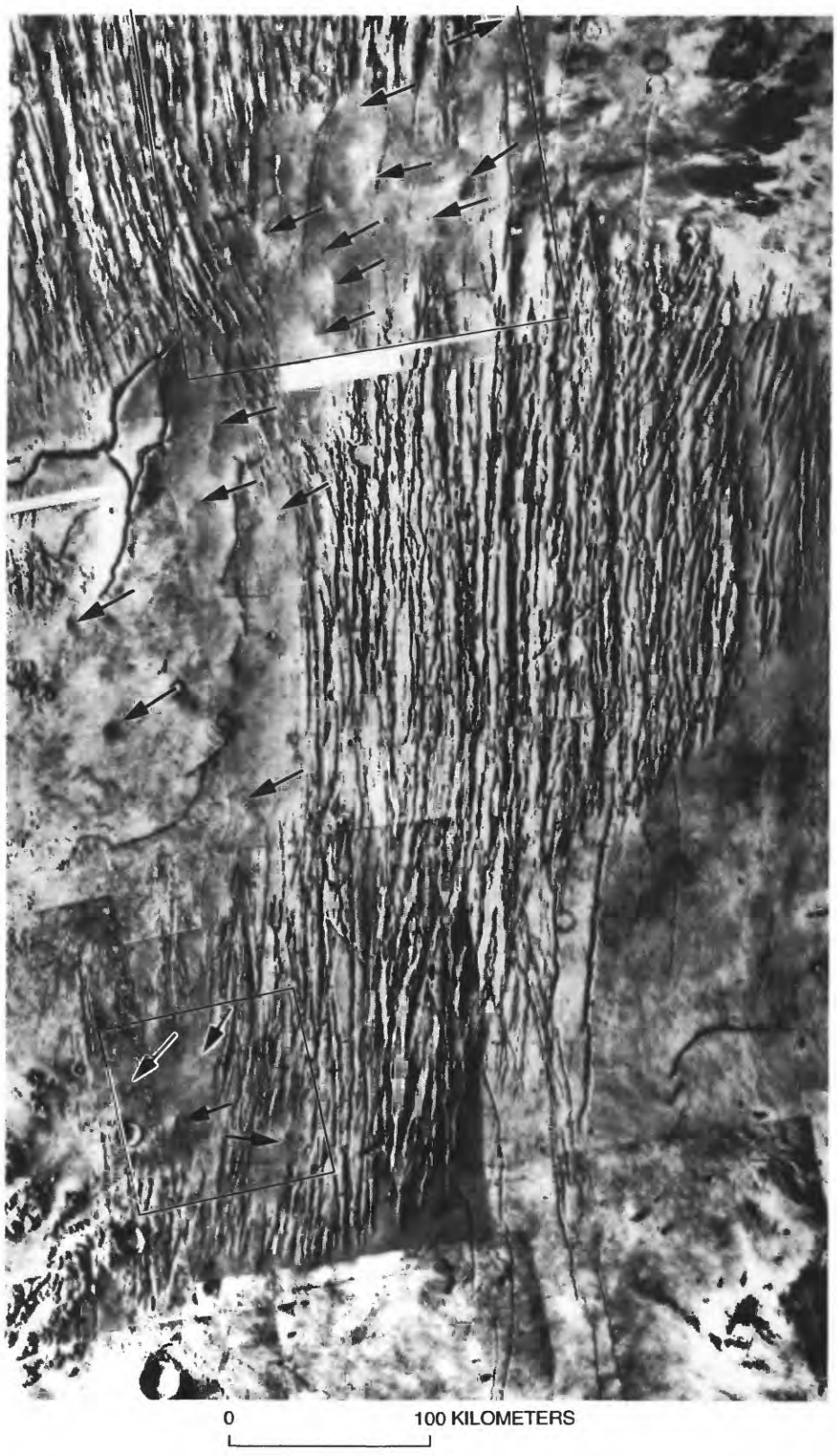

Figure 14. Ceraunius Fossae. *A*, Small shield volcanoes (arrows), representative of numerous examples in this area. Box at upper center outlines area of figure 14*B*; box at lower left outlines area of figure 14*C*. Sun illumination from left. Part of Viking Orbiter photomosaic subquadrangle MC–9NE (U.S. Geological Survey, 1980b).

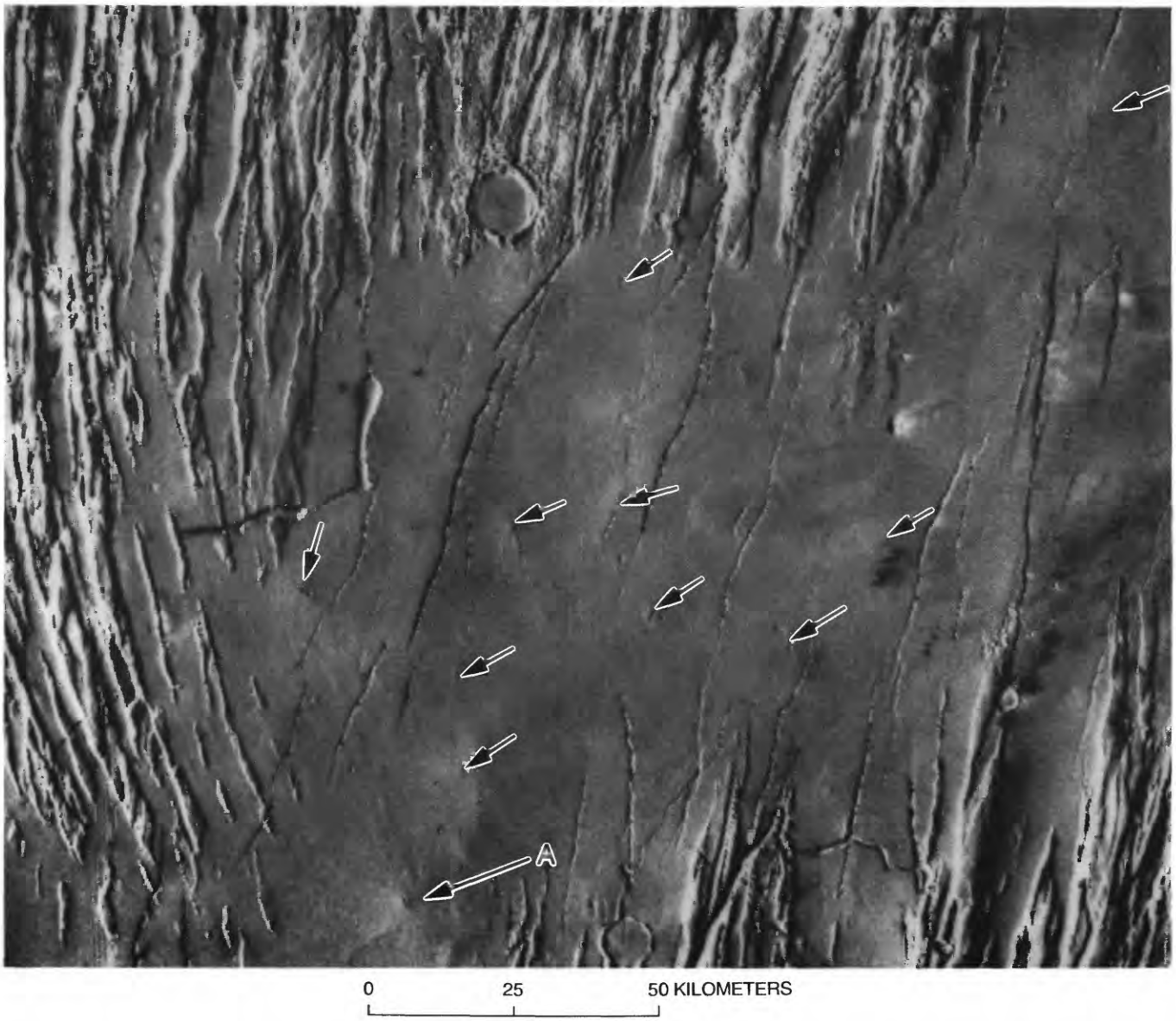

B, Small shield volcanoes (arrows). Faint radial ridges and valleys are visible around low shield volcano at arrow A. Sun illumination from left. Viking Orbiter frame 516A10.

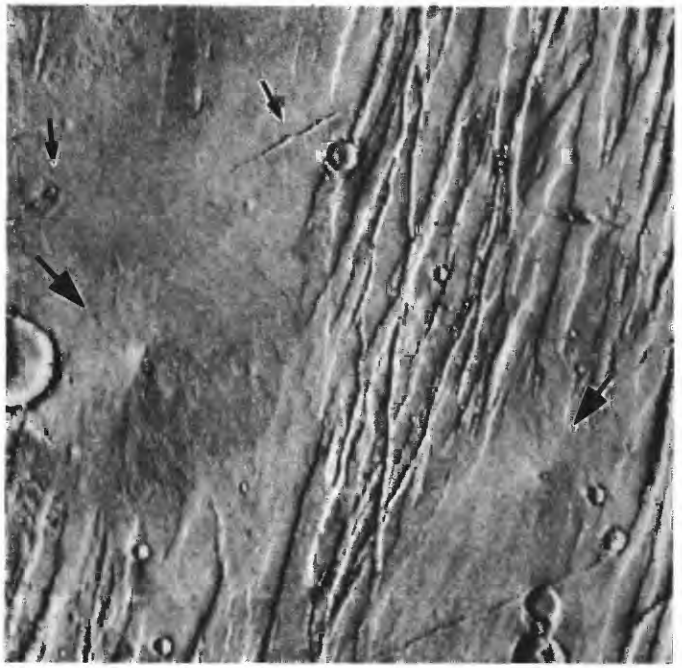

◄ *C*, Low shield volcanoes at scale barely large enough to identify lava flows emanating from summit craters (large arrows). Small arrows denote fissure eruption and crater chain. Sun illumination from left. Viking Orbiter frame 516A32.

D, Mauna Ulu, Hawaii, presumably analogous and thus similar in profile to small martian shield volcanoes. Prominent knob is a 10-m-high spatter cone. Shield of Mauna Loa is visible on horizon. Composite photograph by R.T. Holcomb, taken February 6, 1972 (from Decker and others, 1987, fig. 16.10).

URANIUS PATERA NORTH

Mosaic: 211–5787 MC: 9F–10 Coordinates: 27°–30° N., 87°–97° W.

Province description:
Low, domical shield volcanoes amid lava flows, grabens, and cone chains.

Elevation (km)	3–4
Approximate dimensions (km):	
Base diameter	5–10
Estimated relief	0.06–0.12
Summit-crater diameter (circular to slot-shaped)	0.5–1
Height/base ratio (see profiles)	~0.02
Estimated relative age (10^{-3} craters/km^2)	2.4±0.7
Inferred age (Ga):	
Model 1	3.6–3.7
Model 2	1.5–2.9

Stratigraphic age:
Hesperian member of the Tharsis Montes Formation

DISCUSSION

Like the small shield volcanoes in the Tempe-Mareotis province (figs. 13*A*–13*C*), those in the Uranius Patera North province are remarkably similar to low shields on Earth in dimension as well as morphology (Moore and Hodges, 1980). They appear as cratered "blisters" surrounded and embayed by lava flows (fig. 15*A*), some of which issued from grabens or fissures (fig. 15*B*). Also in the vicinity are several long, linear chains of craters and conelets (fig. 15*C*) that strongly resemble terrestrial spatter-cone chains, like those on the Snake River Plain in Idaho (fig. 15*D*; Greeley, 1977a). These shield volcanoes appear to have formed contemporaneously with Uranius Patera (fig. I–5).

REFERENCES

Greeley (1977a)

Moore and Hodges (1980)

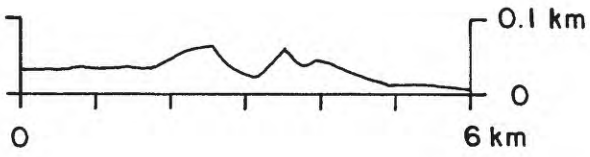

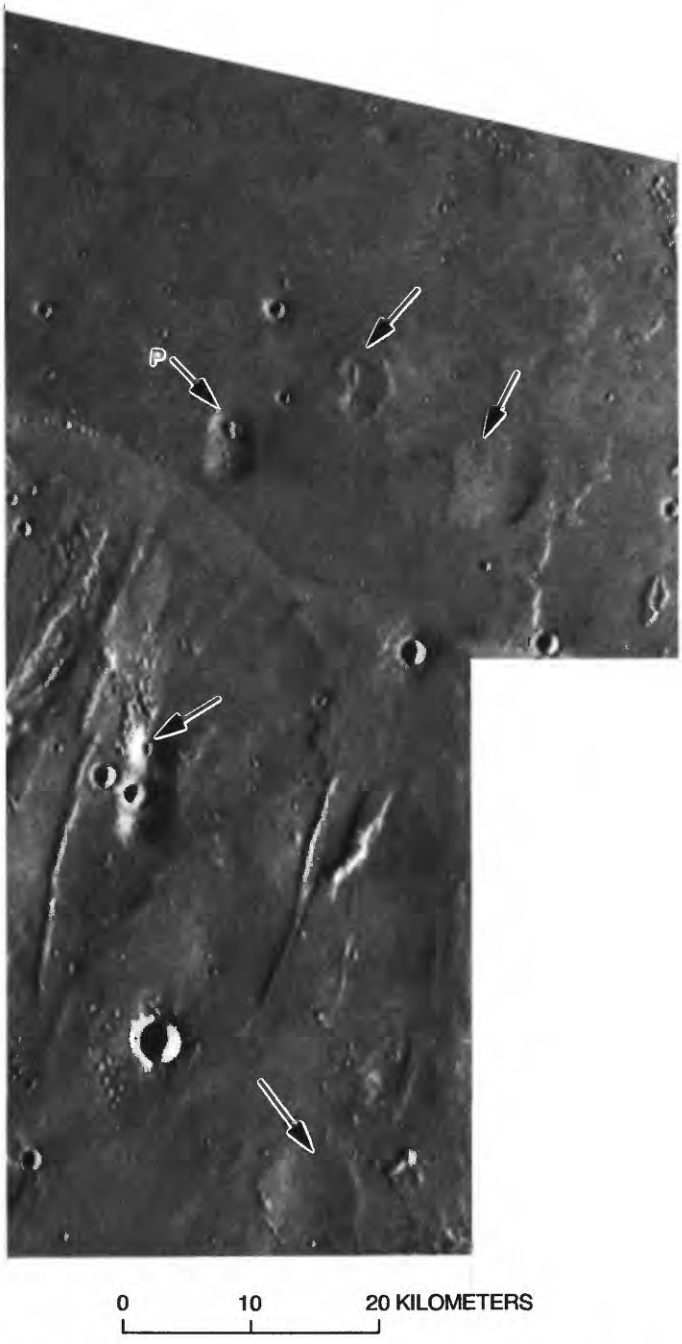

Figure 15. Uranius Patera North. *A*, Small domical shield volcanoes (arrows) embayed by lava flows from Uranius Patera (to south), with representative profile of dome at arrow p. Sun illumination from left. Viking Orbiter frames 626A64 and 626A65. Profile dimensions: crater diameter (*c*), 1,000 m; base diameter (*b*), 3.0 km; relief (*h*), 60 m; crater-diameter-to-base-diameter (*c*/*b*) ratio, 0.33; height-to-base (*h*/*b*) ratio, 0.02. Vertical exaggeration, 10×.

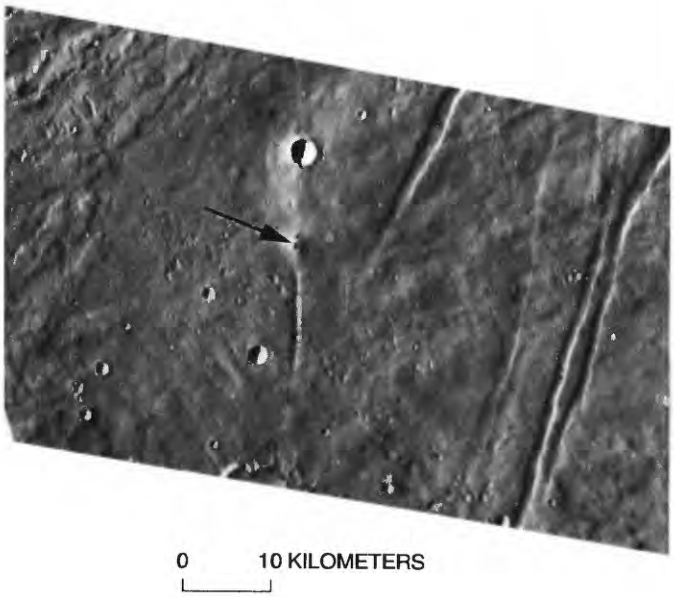

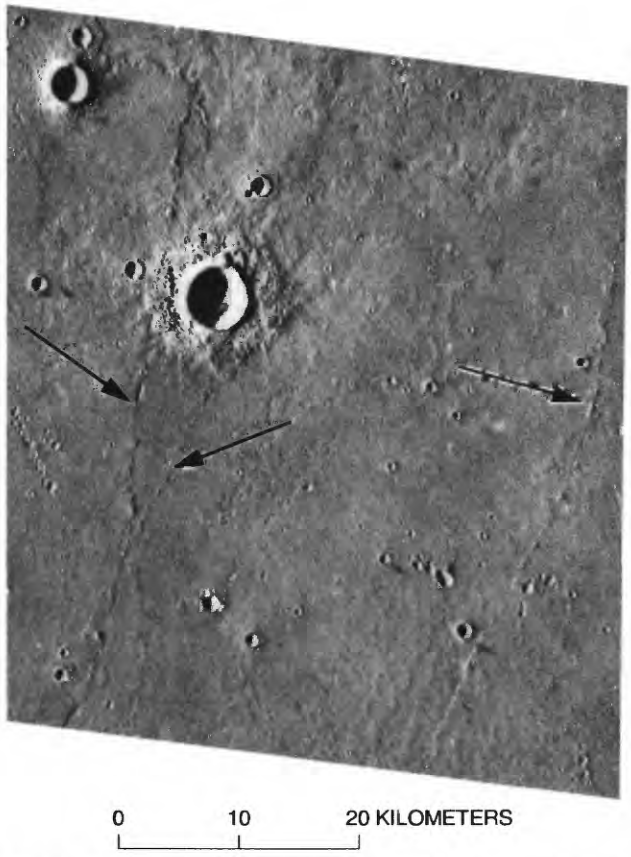

C, Linear crater-cone chains (arrows), no more than about 500 m wide, that resemble terrestrial chains of spatter vents (fig. 15*D*). Sun illumination from left. Viking Orbiter frame 626A69.

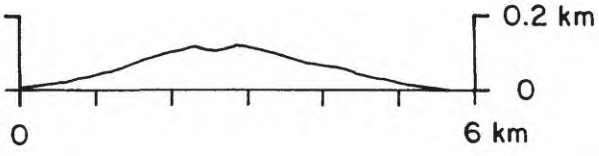

B, Low shield volcano (arrow) atop fissure, with representative profile. Sun illumination from left. Viking Orbiter frame 626A41. Profile dimensions: *c*, 550 m; *b*, 5.5 km; *h*, 120 m; *c*/*b* ratio, 0.33; *h*/*b* ratio, 0.02. Vertical exaggeration, 5×.

D, Snake River Plain, Idaho, showing lava field and chain of spatter cones along fissure, similar to martian crater-cone chains in figure 15*C*. Largest cone is about 100 m wide at base. From Greeley (1977a); photograph courtesy of Ronald Greeley.

SYRIA PLANUM

Mosaic: 211–5780 MC: 17B–18 Coordinates: 8°–30° S., 82°–109° W.

Province description:

Eruptive center marked by small shield volcanoes, conspicuous lava flows emanating from fissures, tube-fed flows, collapse pits, and numerous knobs and blisters.

Elevation (km)	5–10
Approximate dimensions (km):	
Low shield, base diameter	5–30
Estimated relief	0.3–0.6
Estimated relative age (10^{-3} craters/km^2)	2.5±0.5
Inferred age (Ga):	
Model 1	3.6–3.7
Model 2	1.9–2.8

Stratigraphic age:

Hesperian; Syria Planum Formation

DISCUSSION

Syria Planum, marginal to the Tharsis bulge and distinguished by intensely fractured terrain at its north and west borders, is a relatively smooth "thumb" of the highlands projecting into the Tharsis region at equally high elevation (fig. 16*A*). Long, digitate lava flows extend southeastward about 1,600 km across a width of nearly 1,100 km from an eruptive center at about 10°–15° S. (fig. I–2). Several low shield volcanoes at elevations near 10 km, with basal diameters of 10 to 45 km and relief of as much as about 0.6 km, show height-to-base ratios corresponding to those of terrestrial low shield volcanoes (0.01–0.03). Arcuate chains of collapse pits suggest lava conduits, but they merge with the peculiar pattern of Noctis Labyrinthus—a network of huge depressions and troughs, many of which are closed, that form the "headwaters" of Valles Marineris. Some of these collapse pits may be related to graben formation, but those near the shields appear to be volcanic. Lava flows are unmistakable, and clustered knobs and blisters may be volcanic vents (fig. 16*B*).

A distinctive texture at 15°–20° S., 95°–100° W., where nearly equidimensional protuberances abut one another, forms a mosaiclike pattern (fig. 16*C*). These landforms appear to be unique on Mars; they are somewhat domical, with relief as much 70 m (as determined by photoclinometry). Each protuberance may represent radial flows erupted from a point source, but the images do not provide an adequate basis for assessing their origin. Several flows clearly emanate from fissures (Moore and Hodges, 1980; Ward and Spudis, 1984). Analogous relations occur on the Snake River Plain in Idaho, where lava flows arising from fissures are conspicuous (fig. 16*D*; Greeley and King, 1977; Greeley, 1982). Ridges formed by tube-fed lava flows also are conspicuous in the Syria Planum province (fig. 16*C*), where volcanism apparently occurred nearly contemporaneously with that in the Tempe-Mareotis province, earlier than the eruptions that formed the present surfaces of the Tharsis volcanoes (fig. I–5).

REFERENCES

Greeley (1982)
Greeley and King (1977)
Moore and Hodges (1980)
Ward and Spudis (1984)

Figure 16. Syria Planum. *A*, Syria Planum, bounded on north by fractures and collapse structures of Noctis Labyrinthus. Dashed outlines encircle clusters of low shield volcanoes and collapse craters shown in figure 16*B*. Arrows denote isolated examples of shield volcano (s) and collapse crater (c). Sun illumination from right. Part of Viking Orbiter photomosaic subquadrangle MC–17NE (U.S. Geological Survey, 1979).

B, Clusters of shield volcanoes (arrows) and collapse craters (dashed outline), with representative profiles. Features at numbered arrows correspond to profiles; height-to-base (*h*/*b*) ratios: 1, 0.01; 2, 0.02; 3, 0.03; 4, 0.02. Dimensions and *h*/*b* ratios of martian shields are similar to those of terrestrial low shields. Sun illumination from right. Viking Orbiter frame 643A59.

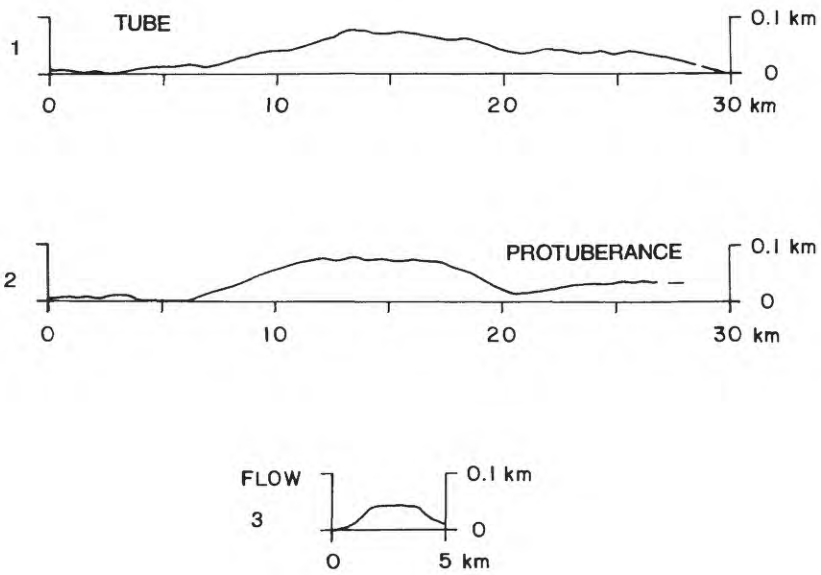

C, Distinctive volcanic features in southern part of Syria Planum, with representative profiles. Arrows denote lava flows erupted from fissures (fe), lava-tube ridges (tr), and flow lobes (f); coalescing protuberances (arrows p) form mosaic pattern in upper right. Inferred fissure eruption resembles that shown in figure 16*D*. Features at numbered arrows correspond to profiles: 1, lava tube; 2, protuberance; 3, lava flow. Sun illumination from right. Viking Orbiter frame 643A64.

D, Kings Bowl lava field, Snake River Plain, Idaho, consisting of multiple fissure-fed flows. Arrows denote swarms of extensional fractures. Flow pattern is similar to that of inferred fissure eruption in figure 16*C*. Light irregular line is jeep trail. Sun illumination from lower right. U.S. Department of Agriculture photograph CYN–7B–103, taken August 31, 1946.

HALEX FOSSAE

Mosaics: 211–5537, 211–5771 MC: 9G Coordinates: 25°–31° N., 123°–130° W.

Province description:

Arcuate fractures and grabens partly surrounding depressed central area, mostly flooded by lava flows from Olympus Mons; four small edifices, probably low shield volcanoes, with distinctive radial-flow patterns; lava flows extend outward from central depression on north, east, and south flanks.

Elevation (km)	2
Approximate dimensions (km):	
Base diameter of pinnacles	3–8
Estimated relief (m)	300–500
Estimated relative age (10^{-3} craters/km^2)	3.6±0.8
Inferred age (Ga):	
Model 1	3.7–3.8
Model 2	2.6–3.2

Stratigraphic age:

Hesperian; Halex Fossae materials (Morris and Tanaka, in press)

DISCUSSION

In the Halex Fossae province, the arcuate configuration of fractures surrounding a depression as deep as 1 km (figs. 17*A*, 17*B*) suggests the existence of an old volcanotectonic collapse structure (Schaber and others, 1978) or caldera that has been flooded and embayed by lavas from Olympus Mons, Alba Patera, and elsewhere (Morris and Tanaka, in press). The area central to this arcuate graben is depressed and contains four small buttes that appear to be the sources for short, stubby lava flows (Moore and Hodges, 1980); the largest butte has a relief of about 230 m, and its base is 5 to 10 km across (fig. 17*C*). Flows radiating outward from the center of the depression (fig. 17*B*) suggest that it may be the vestige of a caldera, but the preexisting relief—if any—has been obliterated by crustal subsidence and flooding.

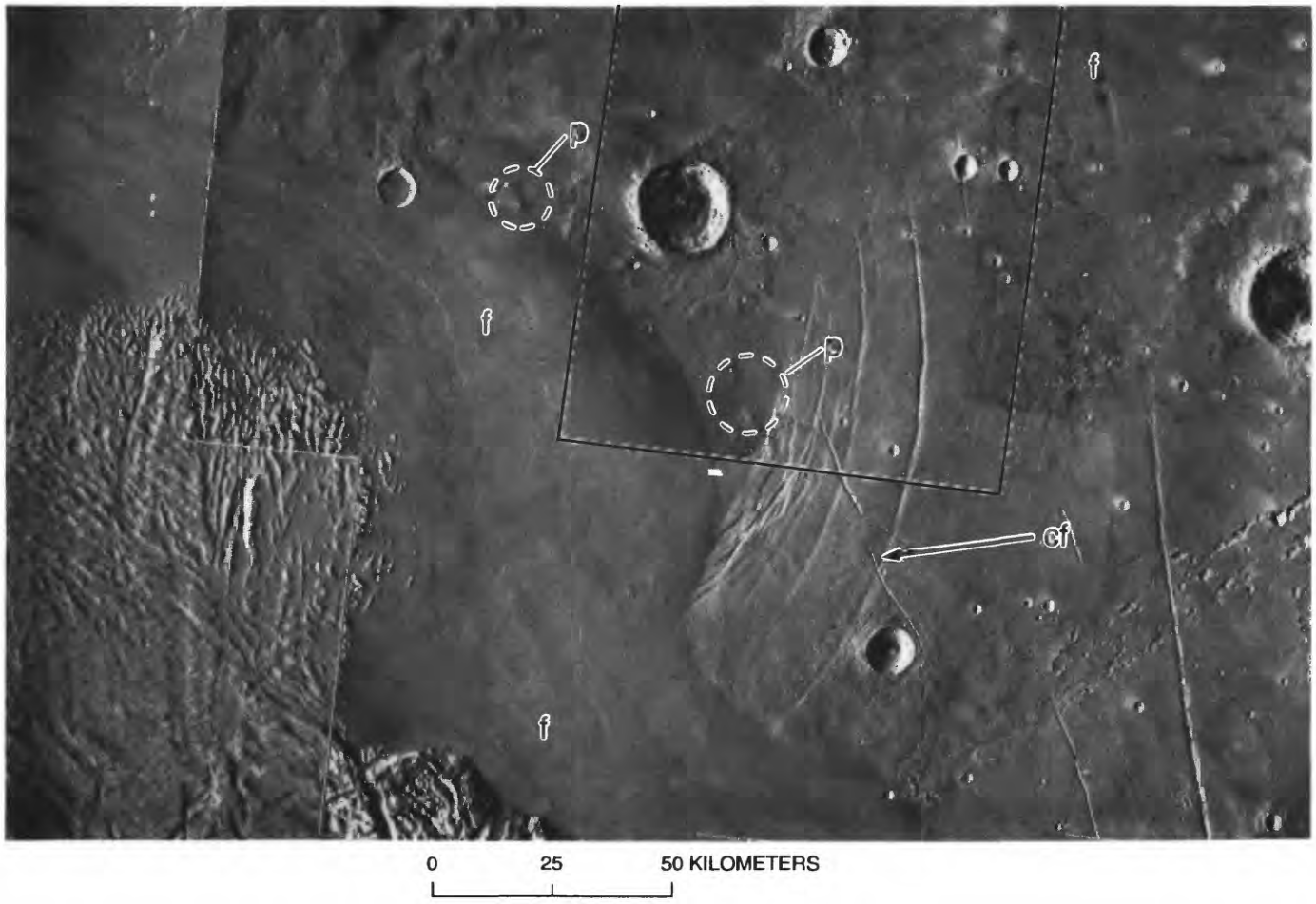

Figure 17. Halex Fossae. *A*, Halex Fossae caldera, northeast of Olympus Mons aureole materials (textured terrain), is defined by arcuate fractures (arrow cf) but is partly buried by younger lava flows (f). Dashed outlines enclose areas of small pinnacles (p) within main depression that may be vents. Box at upper center outlines area of figure 17*C*. Sun illumination from left. Mosaic of Viking Orbiter frames 43B18 through 43B26.

The precursors of the great Tharsis volcanoes may have resembled this Halex Fossae structure rather than the small, low shield volcanoes of the Tempe-Mareotis province.

Superposition of subsequent lava flows shows that this depression is relatively old. Flows from Alba Patera to the north buried the northern and eastern parts of the depression (Scott and Tanaka, 1986), flows from the general area of Ceraunius Fossae streamed westward and buried the southern parts of the depression, and the youngest lava flows, which appear to have issued from vents near the base of Olympus Mons, flowed northwestward and buried the southwest half of the depression (figs. I–2, 17B). Superposition relations are consistent with relative ages determined from crater counts, which indicate that the Halex Fossae materials formed during the Hesperian period (fig. I–5).

REFERENCES

Moore and Hodges (1980)
Morris and Tanaka (in press)
Schaber and others (1978)
Scott and Tanaka (1986)

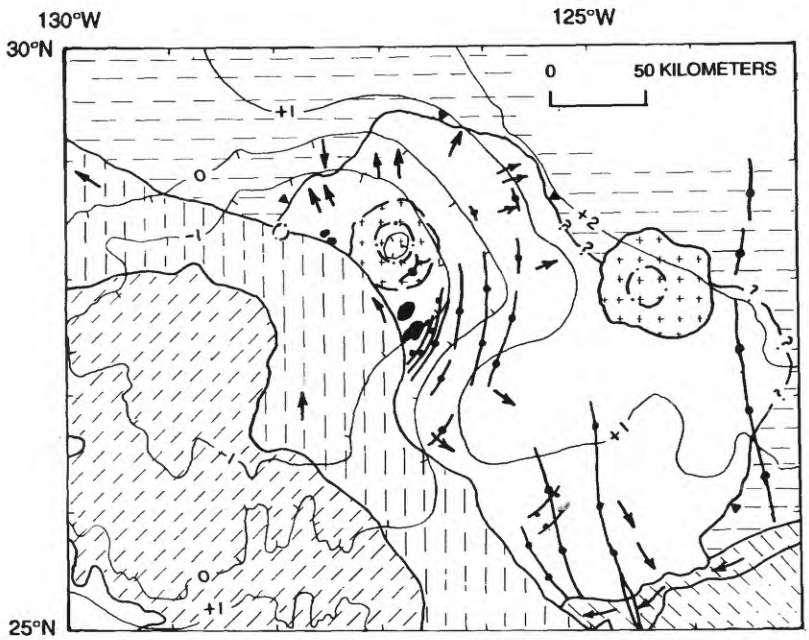

EXPLANATION

- Young flows
- Crater materials
- Aureole materials
- Ceraunius Fossae flows
- Alba Patera and old flows
- Halex Fossae materials
- Volcanoes
- Contact—Queried where questionable
- Crater rim
- Fault—Ball on downthrown side
- Graben
- Flow scarp—Barbs on elevated side
- Paleoflow direction
- Contours—Number is elevation above (+) or below (-) datum (0), in kilometers

B, Geologic sketch map of Halex Fossae caldera. Paleoflow directions radiate from center of structure. Area is larger than that in figure 17*A* (see fig. I–2).

C, Part of Halex Fossae, as outlined in figure 17*A*. Large arrows denote discrete flow lobes (f) oriented radial to main structure, pinnacles (p) that may be low shield volcanoes with attendant lava flows, and substantially younger flows from base of Olympus Mons (fo, lower left) and Alba Patera (fa, upper right corner); small arrows indicate flow directions. Sun illumination from left. Viking Orbiter frame 43B23.

OLYMPUS MONS AUREOLE NORTH

Mosaic: 211–5327 MC: 2B Coordinates: 33°–35° N., 133°–137° W.

Province description:
Field of densely populated small cones or domes with barely discernible summit craters.

Elevation (km)	–1 to 0
Approximate dimensions (m):	
Base diameter	300–1,000

Stratigraphic age:
Noachian; subdued cratered unit of the Plateau Sequence

DISCUSSION

This relatively small province at the north margin of the Olympus Mons aureole appears to contain densely clustered, cratered cones (figs. 18*A*, 18*B*), for which resolution does not permit adequate description or interpretation. However, their population, shape, and apparently random distribution suggest a possible analogy with rootless pseudocraters (fig. 18*C*), which, best developed in Iceland (Thorarinsson, 1953), formed in lava

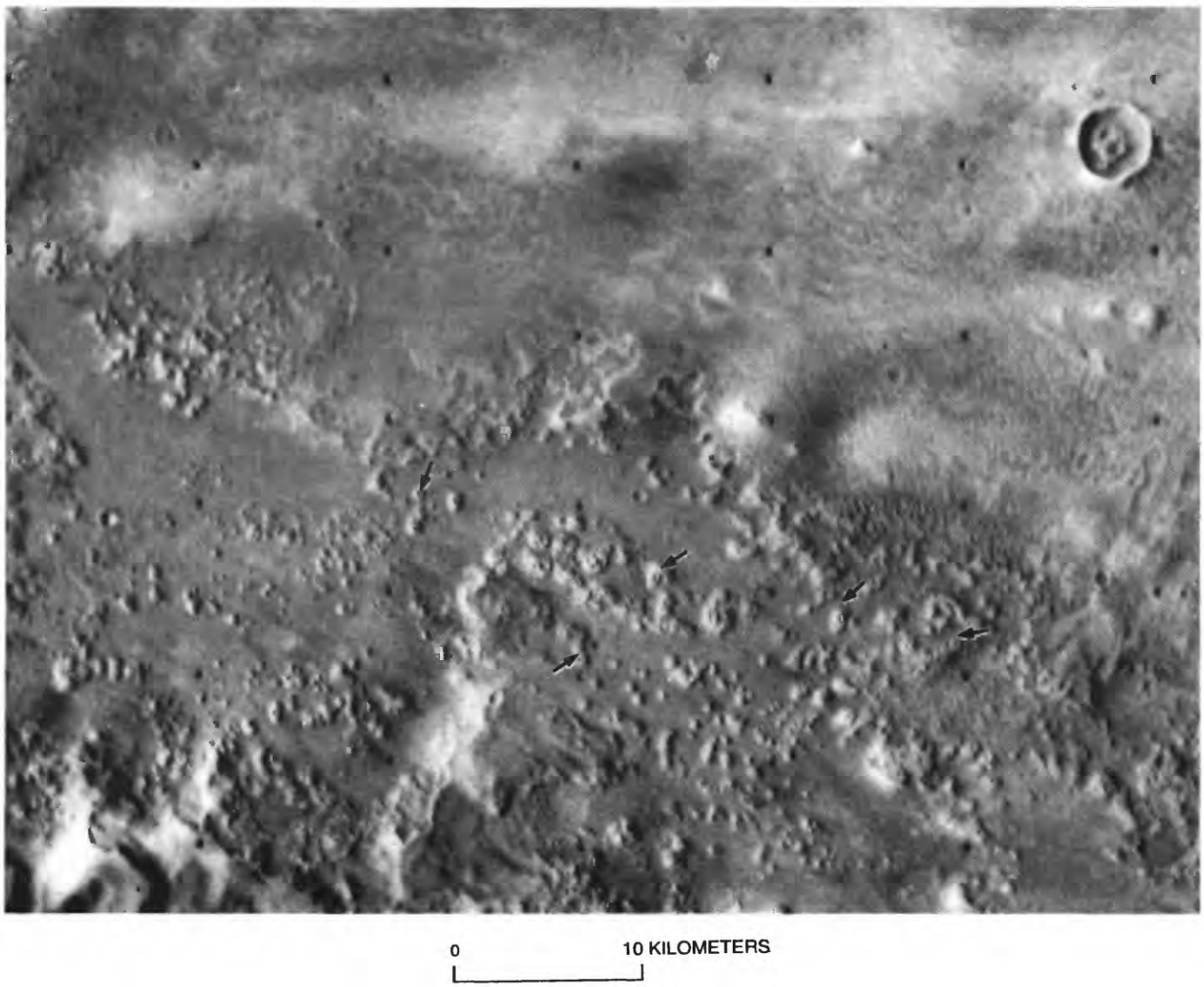

Figure 18. Olympus Mons Aureole North. *A*, Field of small cones, each about 0.5 to 1.0 km across, most of which are cratered. Arrows denote several particularly good examples. Sun illumination from left. Viking Orbiter frame 49B06.

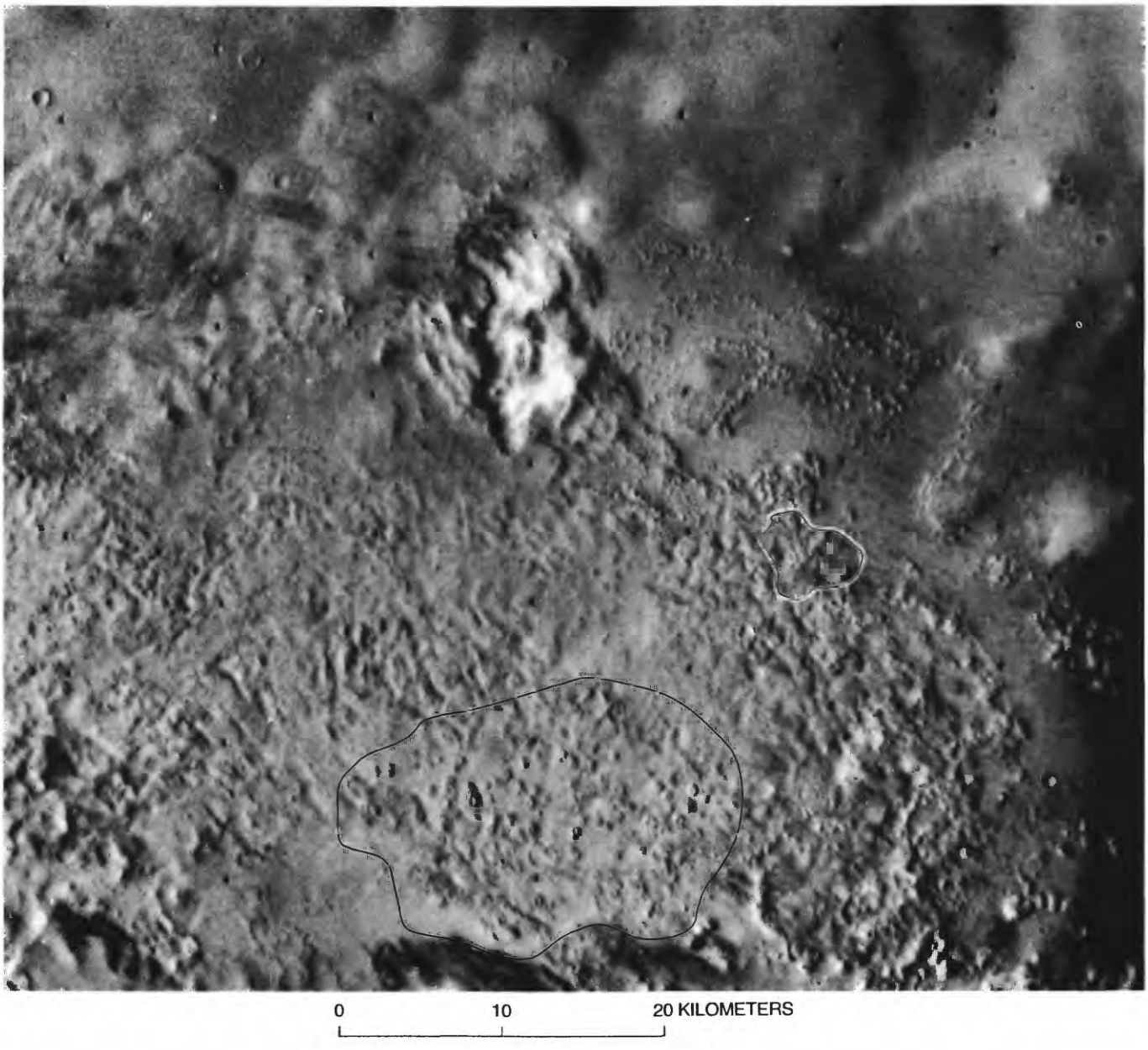

B, Clusters of small cones (outlined), each about 0.5 to 1.0 km across. Sun illumination from left. Viking Orbiter frame 49B04.

C, Pseudocraters on west shore of Lake Mývatn, Iceland (from Thorarinsson, 1953). Arrows denote several conspicuous examples. Craters range in size from "miniature" (3–5 m diam, 1–2 m high) to large, with base diameters of more than 300 m and relief of 20 to 25 m. Sun illumination from upper right.

flowing over water-saturated ground—conditions that could reasonably have occurred in this area. The province is embayed by eolian deposits and is adjacent to an outlier of old cratered plains, marked by large-scale faulting and fracturing, with no apparent relation, other than spatial, to the aureole of Olympus Mons.

REFERENCE

Thorarinsson (1953)

OLYMPUS MONS SOUTH

Mosaics: 211–5512, 211–5513 MC: 8B–9 Coordinates: 0°–11° N., 120°–150° W.

Province description:

Windswept terrain, including eroded southernmost remnant of Olympus Mons aureole materials; minor and enigmatic landforms include tablemountain-like features, collapse pits, probable etch pits, grabens, fractures, and sinuous channels.

Elevation (km)	0–5
Approximate dimensions (km):	
Tablemountain-like features	~15–20

Stratigraphic age:

Amazonian; Medusae Fossae Formation

DISCUSSION

This province, which is marginal to the oldest aureole deposits of Olympus Mons, exhibits an apparently erosional landscape of eolian derivation (fig. 19*A*). Parallel striations in a friable material, with mesalike remnants and etch pits in layered materials intermingled with narrow, digitate lava flows, present several interpretative options. Scott and Tanaka (1982) postulated that these deposits and similar ones elsewhere (Medusae Fossae Formation) are ignimbrites, a conclusion disputed by Francis and Wood (1982). Evidence for volcanism consists of collapse pits, isolated domes (fig. 19*B*), and buttes and mesas (fig. 19*A*), some of which have summit fractures or craters (fig. 19*C*; Hodges and Moore, 1979) and resemble Icelandic tablemountains (fig. 19*D*). Proximity to Olympus Mons and Biblis and Ulysses Paterae supports a volcanic interpretation, but diagnostic criteria are absent.

REFERENCES

Francis and Wood (1982)
Hodges and Moore (1979)
Scott and Tanaka (1982)

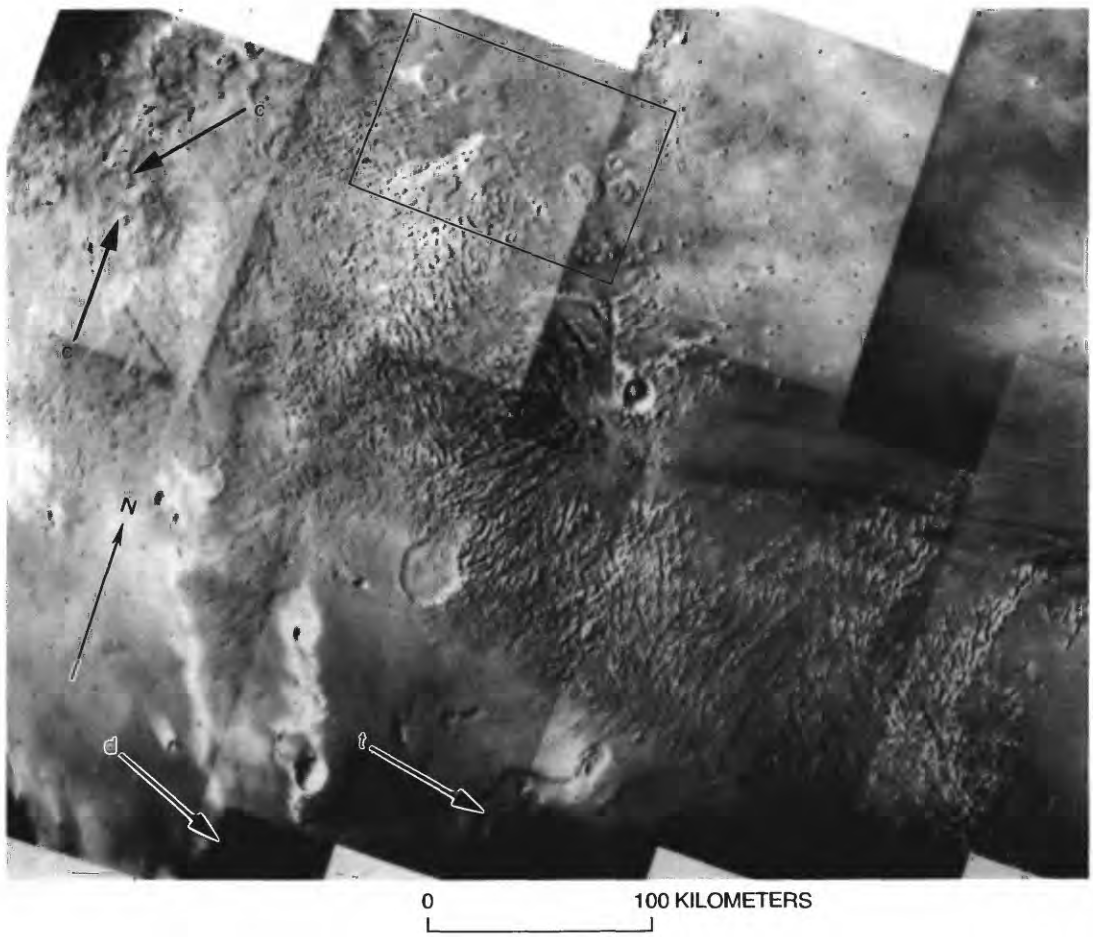

Figure 19. Olympus Mons South. *A*, Aureole materials and Medusae Fossae Formation south of Olympus Mons. Arrows denote landforms of possible volcanic origin, such as domes (d), inferred lava tubes (t), and small cratered cones (c). Box at upper center outlines area of figure 19*C*. Sun illumination from left. Part of Viking Orbiter mosaic 211–5512.

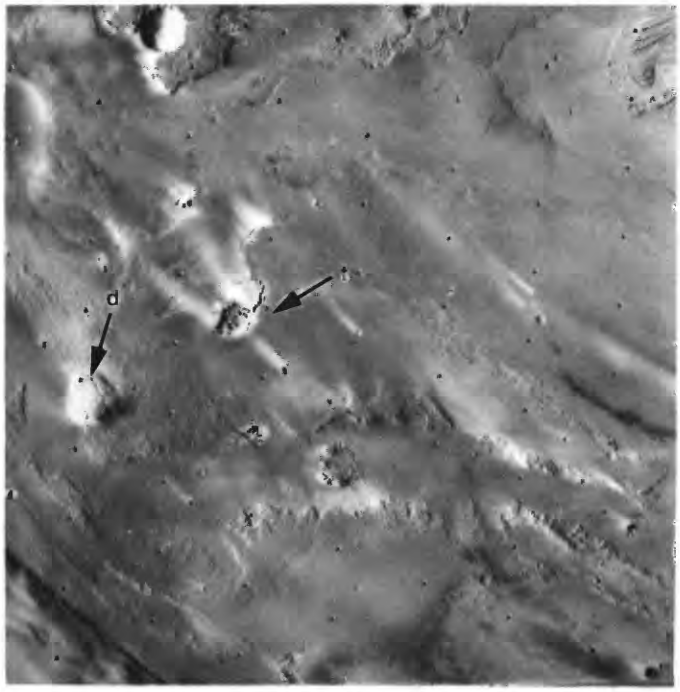

B, Possible collapse pit with lava tube (t) and lava dome (d) at 5° N., 143° W., in Medusae Fossae Formation. Sun illumination from left. Viking Orbiter frame 44B35.

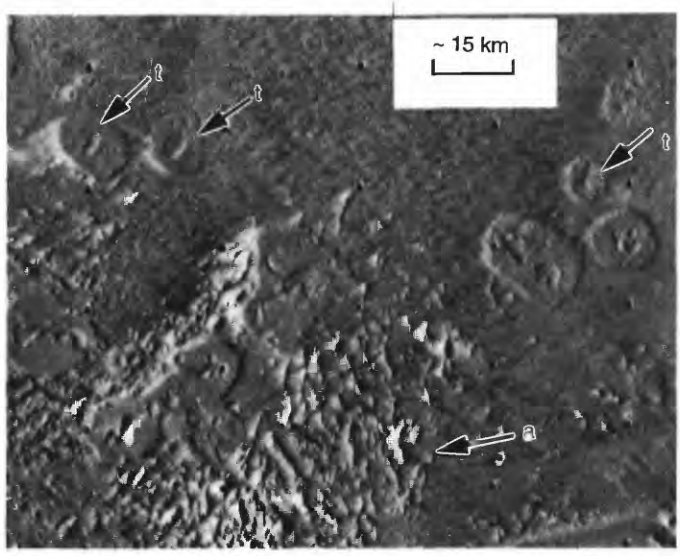

C, Cratered mesas (arrows t) that somewhat resemble Icelandic tablemountains (fig. 19*D*) but could be isolated erosional remnants of textured Olympus Mons aureole materials (arrow a) to south. Sun illumination from left. Part of Viking Orbiter frame 44B13 (from Hodges and Moore, 1979).

► *D*, Icelandic tablemountain Gæsafjöll, showing summit crater (arrow c), collapse pits (arrows p), and subaerial lava flows capping a pedestal of moberg (hyaloclastite) exposed in perimeter scarp (arrow m), somewhat similar to features in figure 19*C*. Sun illumination from left. U.S. Air Force photograph AF55–AM–3, roll 127, frame 14125, taken August 28, 1960.

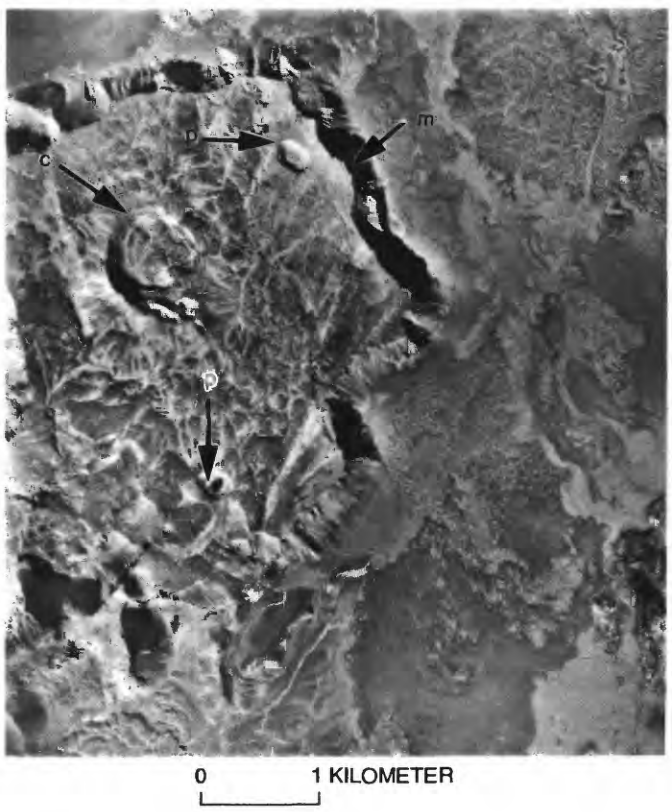

Figure 20. Tempe Volcano. *A*, Tempe Volcano, northeast of Tempe-Mareotis province, at 37° N., 76° W. Summit caldera (arrow c) was source of numerous long lava flows, many of which are faulted (arrows f). Sun illumination from left. Viking Orbiter frame 519A15.

TEMPE VOLCANO

Mosaic: 211–5866 *MC: 3D* *Coordinates: 38° N., 76° W.*

Province description:
Isolated butte with distinctive narrow, ribbonlike flows forming radial pattern around base.

Elevation (km)	2
Approximate dimensions:	
Base diameter	25
Relief	<0.5
Estimated relative age (10^{-3} craters/km^2)	3.0±0.7
Inferred ages (Ga):	
Model 1	3.7–3.8
Model 2	2.1–3.1

Stratigraphic age:
Undesignated

DISCUSSION

Conspicuous flows radiate away from Tempe Volcano (fig. I–2), indicating that it is a vent (Moore and Hodges, 1980); individual flows can be traced as far as 120 km. Detailed morphology is difficult to see on the images available, but the edifice appears to be a rugged, irregular structure, with a relatively flat summit about 6 km across (fig. 20*A*). The flows are offset by grabens and fractures (fig. 20*B*). The fractures form an arcuate pattern around this edifice, suggesting that their position was influenced by the subsurface structure or, alternatively, that the fracture pattern may have been caused by formation of the volcano and accompanying subsurface intrusion of melt. The narrow widths and long lengths of lava flows suggest a fluidity typical of basalt, also indicated by the numerous tube-fed flows that occur from 50 to 300 km southeast of the volcano.

Lava flows from Tempe Volcano are superposed on materials mapped as the upper part of the Hesperian Tempe Terra Formation. The contemporaneity of this volcano with Halex Fossae and other Hesperian features is illustrated in figure I–5.

REFERENCES

Moore and Hodges (1980)

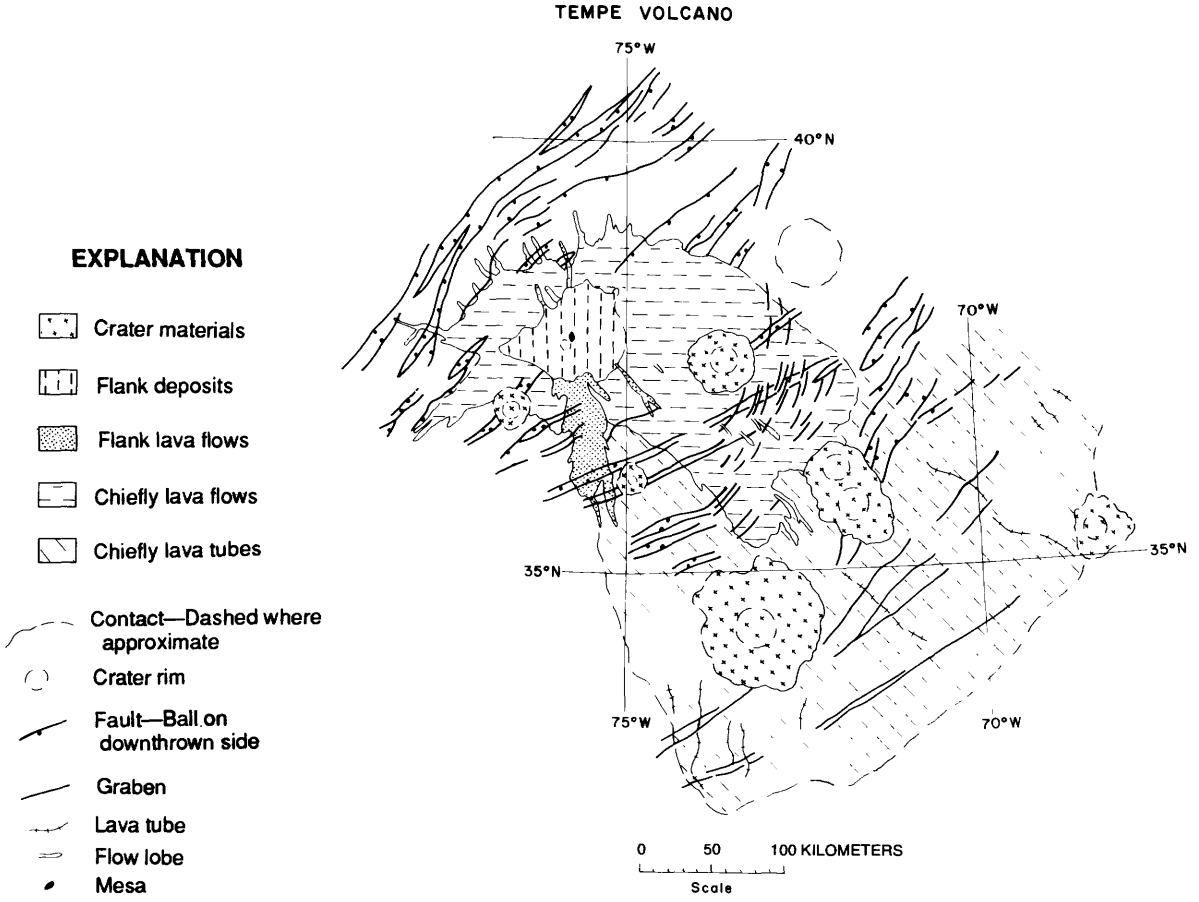

B, Geologic sketch map of Tempe Volcano area, including area of abundant lava-tube ridges not shown in figure 20*A* (see fig. I–2).

MAJOR PLAINS PROVINCES

ELYSIUM REGION

MAJOR SHIELD VOLCANOES

ELYSIUM MONS

Mosaics: 211–5906, 211–5643 MC: 7B–15 Coordinates: 25° N., 214° W.

Approximate dimensions (km):	
Base diameter	415
Summit elevation	16
Relief	12.5
Caldera diameter	14.5
Caldera depth	1
Height/base ratio	0.03
Estimated relative age (10^{-3} craters/km^2)	1.5±0.5
Inferred age (Ga):	
Model 1	3.4–3.6
Model 2	0.9–1.9
Stratigraphic age:	
Amazonian; Elysium Formation	

DISTINCTIVE CHARACTERISTICS

(1) Symmetrical shield with circular caldera (figs. 21*A*, 21*B*).
(2) Concentric graben segments and fractures around base (fig. 21*A*).
(3) Radial channel and fracture systems with extensive collapse pits (Elysium Fossae).
(4) Long digitate radial flows with channels and ridges formed by lava tubes (fig. 21*C*).
(5) Broad cobrahead rilles.
(6) Spongy-appearing distal terrain (figs. 21*A*, 22*A*).
(7) Well-defined positive gravity anomaly (Sjogren, 1979).

DISCUSSION

The three volcanoes of the Elysium Mons region—Elysium Mons, Albor Tholus, and Hecates Tholus—surmount a localized topographic high, the Elysium bulge, which rises about 5 km above adjacent Elysium Planitia to the west (U.S. Geological Survey, 1989, 1991). Despite their relative proximity (pl. 1; fig. I–3), each of these shield volcanoes differs morphologically from the others (figs. 21*A*, 22*A*). As in the Tharsis region, a significant positive gravity anomaly coincides with the Elysium bulge (Sjogren, 1979).

Elysium Mons has a single, remarkably circular summit caldera (fig. 21*B*). Unlike the Tharsis calderas, it has only one narrow terrace around half its rim, suggesting that collapse was limited to a single major event. Lava flows, covering an area of 1,300 by 2,200 km, are associated with conspicuous channels, pit craters, large cobrahead rilles, and ridges formed by tube-fed flows. Greeley (1973) drew an analogy with similar-appearing structures on Mauna Loa in Hawaii for many of these features. Several small rilles originate near the caldera rim and extend downslope 10 km or so. Rille segments also are present on the steep flanks; a three-tined array of pit-crater chains occurs on the west flank, about 20 km from the caldera (arrow c, fig. 21*A*). Conspicuous concentric grabens around the base of the volcano on the northeast and west probably resulted from tensional stress caused by loading of the volcanic pile (Solomon and Head, 1982).

Characteristics of the channel-and-rille systems of Elysium Mons indicate that low-viscosity fluids were involved in their formation. Linear, closed depressions attain widths of 12 km and lengths of 300 km; they may be isolated, aligned in chains, or interconnected. Several of the smaller depressions are aligned radially from the caldera, and several others are concentric, but most trend northwest. These linear depressions were interpreted as tectonic by Hall and others (1983). Four box canyons, as much as 28 km across, 1 km deep, and 190 km long, occur on the west and northwest edges of the Elysium Mons deposits (fig. 21*A*). A tongue of flow deposits extends northwestward from two of these box canyons, suggesting that the flows issued from the canyons. One rille-channel system consists of a cobrahead rille, 9 km across at the head and tapering to about 3 km across, that feeds into a distributary system of incised channels, some of which can be traced 800 km to the northwest. Isolated channel segments with streamlined islands occur as far as 1,200 km to the northwest. Typical widths of these channels range from 3 to 12 km, and depths from 0.1 to 0.6 km. One channel becomes progressively filled to the northwest, yielding flow deposits of some kind that terminate against hills and craters (Moore, 1982a) and as thick lobes 1,400 to 1,500 km from the channelhead (fig. 21*C*).

The northwest flank of the Elysium rise was inundated by lava flows from the volcano, but the terrain exhibits a spongy appearance riddled by pits, fractures, and channels (fig. 22*A*). Water, derived either during eruption or by melting of ground ice as lava encroached, may have contributed to erosional scarring (Moore, 1982b), resulting in deposition of mudflows or lahars (Christiansen, 1989). Mouginis-Mark and others (1984) suggested that the Elysium Fossae region of channels (fig. 21*A*) marks a complex vent area in which the channels and rilles are attributable to both lava and fluvial erosion. Moore (1982b) suggested that some hills and ridges (arrows h, r, fig. 21*D*; fig. 22*A*) strongly resemble the moberg (hyaloclastite) hills and ridges of Iceland that formed during subglacial eruptions (figs. 21*E*, 21*F*; Thorarinsson and others, 1973). Many of the hills and scarps appear to be rounded and muted. Other nearby places topographically resemble

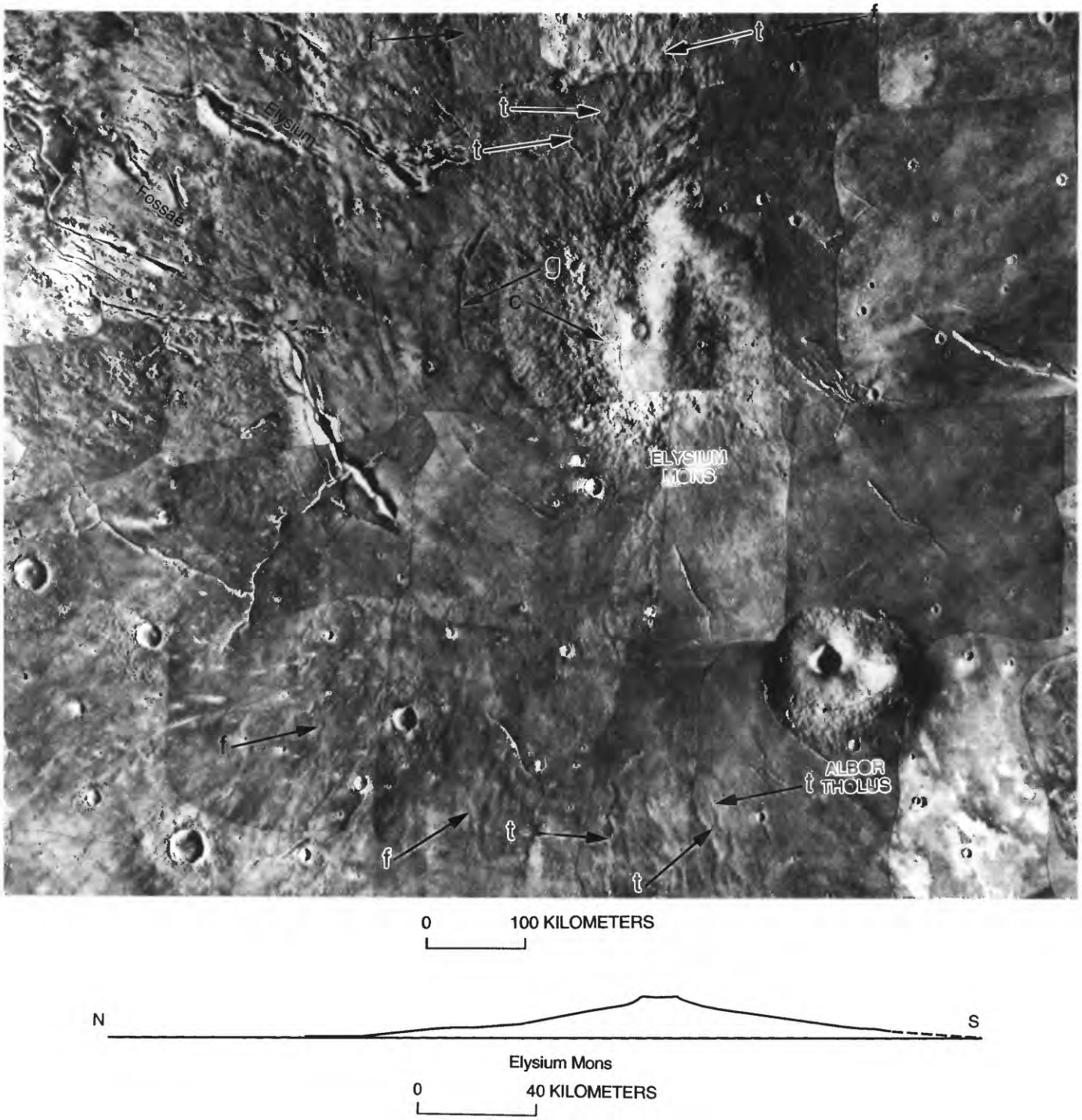

Figure 21. Elysium Mons and Albor Tholus. *A*, Elysium Mons and Albor Tholus, with representative profile of Elysium Mons. Arrows denote characteristic volcanic features: long, digitate lava flows (f), zigzag lava-tube ridges (t), pit-crater chains (c), and concentric grabens (g); collapse pits, box canyons, and extensive channels and rilles are also visible. Sun illumination from left in upper left quadrant, from right elsewhere. Part of Viking Orbiter photomosaic subquadrangle MC–15NW (U.S. Geological Survey, 1984). Profile from Pike and others (1980); no vertical exaggeration.

B, Elysium Mons caldera, about 13 km in diameter. Principal superposed craters are of impact origin. Simplicity of caldera suggests a single collapse episode, in marked contrast to complex calderas of Tharsis region. Radial furrows appear at least partly to be collapse features. Subdued appearance of flanks suggests presence of pyroclastic deposits, according to Malin (1977). Dark ring at bottom center of photograph is an artifact. Sun illumination from left. Viking Orbiter frames 106A85 and 106A86, rectilinear.

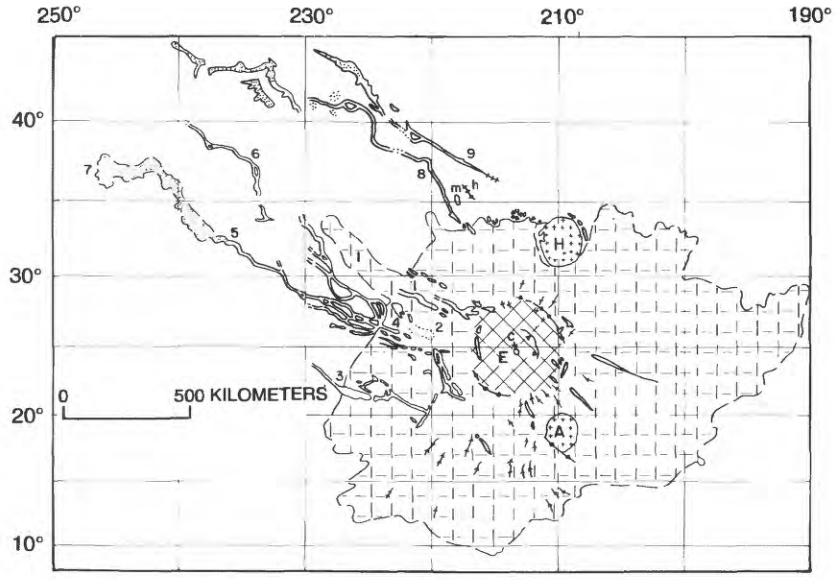

EXPLANATION

- Elysium mons
- Lava flows and tubes
- Tholus
- Channel deposits
- Summit caldera
- Moberg hill
- Hyaloclastite ridge
- Ridge
- Contact—Dashed where approximate
- Channel system
- Cobrahead rille
- Buried rille
- Rilles, closed
- Graben
- Scarp—Barbs on elevated side
- Lava-tube ridge

C, Sketch map of Elysium region, showing major edifices Elysium Mons (E), Hecates Tholis (H), and Albor Tholus (A). Flow deposits occur at 1, buried cobra-head rille at 2, and cobra-head rille at 3; channel originating at 4 extends to 5, where it becomes filled with deposits terminating at 7. Disconnected channels occur at 6 and 8; channel at 9 begins as a ridge. Corresponding images shown in figures 21*A* and 22*A*..

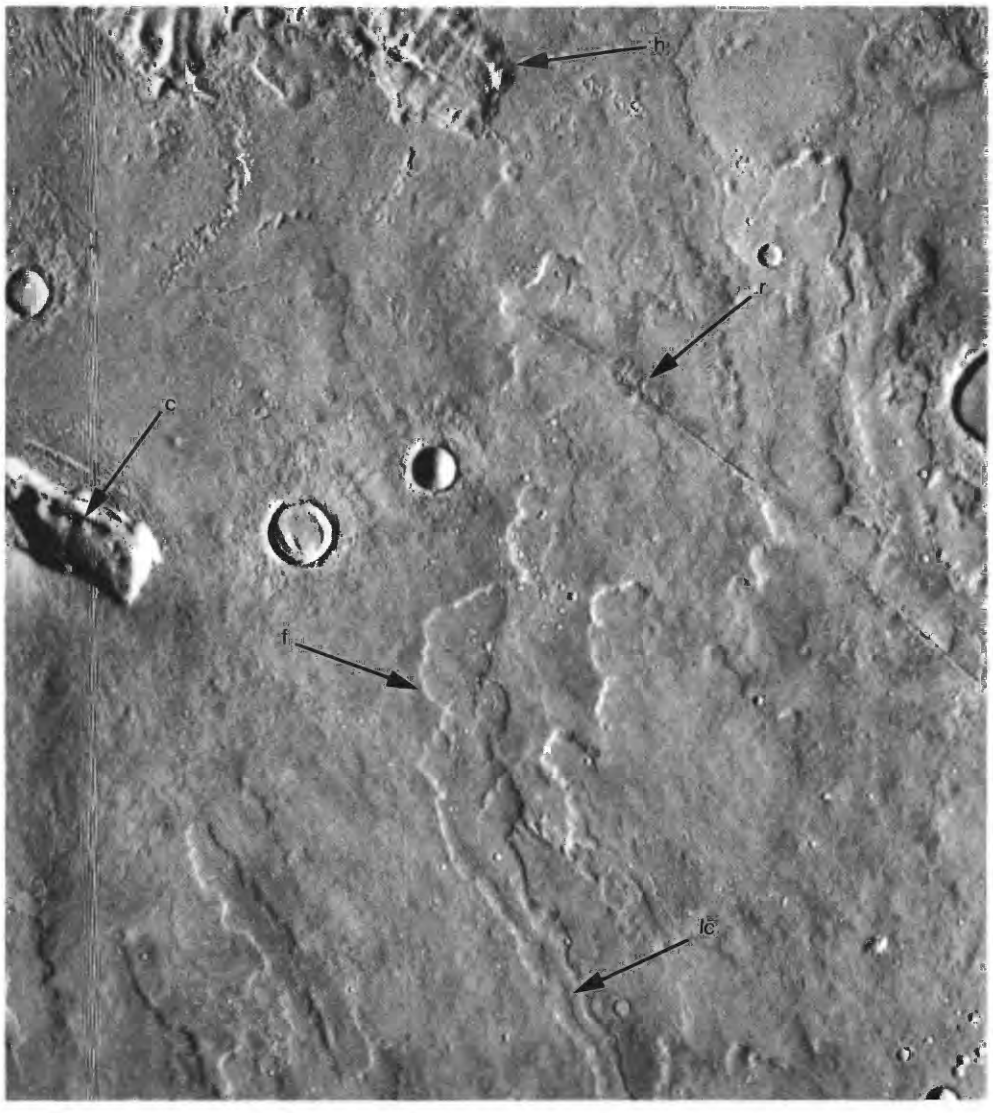

D, Area north of Elysium Mons, approximately at transition in terrain type from one dominated by discrete lava flows (arrow f), commonly with leveed channels (arrow lc), to one more chaotic and spongy appearing, characterized by deposits that resemble moberg (hyaloclastite) mounds and ridges (arrow h) in Iceland formed by subglacial eruptions (fig. 21*E*) and possible mudflows. Apparent fissure eruption (arrow r) formed ridge that strongly resembles Icelandic moberg ridges (fig. 21*F*); collapse depressions (arrow c) occur in one ridge. Sun illumination from left. Viking Orbiter frame 651A04.

E, Moberg (hyaloclastite) ridges (arrow h) in Iceland formed by subglacial fissure eruption, and adjacent tablemountain (arrow t) that consists of hyaloclastite pedestal capped by subaerial lava flows. Sun illumination from lower right. U.S. Air Force photograph AF55–AM–3, roll 120, frame 13304, taken August 24, 1960.

badlands with intervening flood plains that have disconnected channel segments, incised channels with streamlined islands, and broad, flat plains. Christiansen (1989) interpreted these channels and associated deposits as lahars formed by the interaction of lava with trapped volatile materials, probably water ice.

Because the shape of Elysium Mons appeared in Mariner 9 images to differ markedly from that of the Tharsis volcanoes (Scott and Allingham, 1976), Malin (1977) suggested a composite as opposed to basaltic-shield origin for the edifice. He drew an analogy with Emi Koussi Volcano (in the Tibesti area of Chad, Africa), largely on the basis of caldera configuration and flank morphology, though noting a significant difference in flank slope: Mariner data indicated that the average flank slope of Elysium Mons was about 10°–12°, in contrast to that of Emi Koussi at about 2°–5°. This apparent steepness of Elysium Mons' slopes, together with his interpretation that pyroclastic material blanketed the flanks of the volcano, led Malin (1977) to conclude that viscous (silicic) lavas and ash had governed the volcano's shape. Subsequent Viking topographic data compiled by Pike and others (1980) and Pike and Clow (1981b) suggest, however, that the average slope angle of Elysium Mons is no more than 3°–6°, similar to that of the slopes of the Tharsis volcanoes (2°–6°; Olympus Mons' average slope is about 4°) but unlike the steeper slope angles (10°–35°) and concave profiles normally characteristic of terrestrial composite cones (Macdonald, 1972). Diagnostic evidence of substantial pyroclastic activity is not apparent on Viking images, and the large number, extreme length, and continuity of lava channels are characteristic of low-viscosity basaltic lavas (figs. 21*A*, 22*A*). The uppermost flanks of Elysium Mons do appear to be steeper than those of the Tharsis volcanoes (fig. 21*A*), however (Scott and Allingham, 1976; Blasius and Cutts, 1981), and may indicate that the latest lavas erupted became increasingly differentiated, much as in the waning stages of eruption at terrestrial shield volcanoes, as exemplified by the steep summit slopes and late pyroclastic activity of Mauna Kea in Hawaii (Macdonald, 1972).

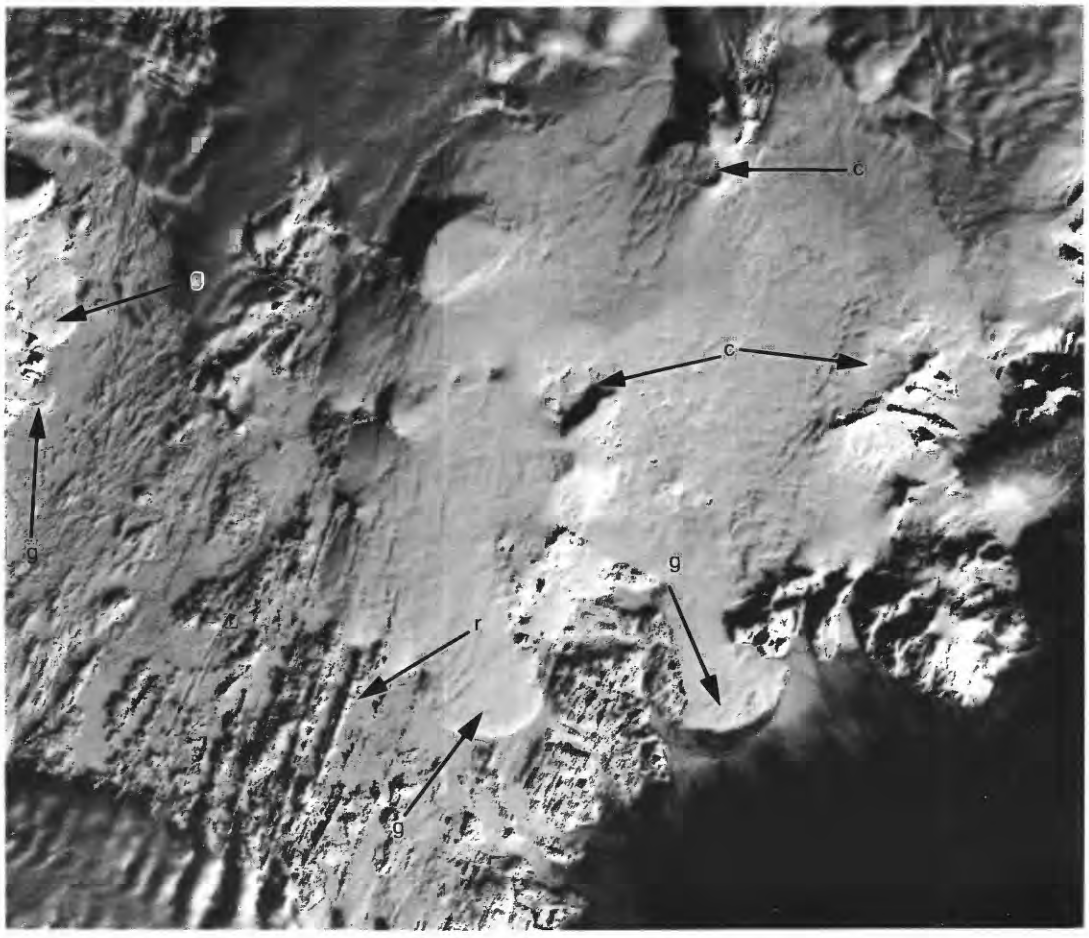

F, Snow-covered Vatnajökull area, Iceland, showing three calderas (arrows c) and lobate fronts of glacial tongues (arrows g). Linear northeast-trending features (arrow r) are structurally controlled hyaloclastite ridges and crater rows formed by fissure eruptions that were subglacial when moberg (hyaloclastite) was produced. These features strongly resemble long narrow ridges on northwest flank of Elysium Mons that may have formed by eruption in ice-rich materials (arrows r, h, fig. 21*D*). Sun illumination from right. Landsat I image E–1192–12084–7, taken January 31, 1973; approximate scale 1:1,000,000; photograph courtesy of R.S. Williams.

Plescia and Saunders (1979) obtained crater counts showing Elysium Mons to be the oldest of the three Elysium volcanoes, and Albor Tholus the youngest. The extensive flows around Elysium Mons, however, embay the flanks of both Hecates and Albor Tholi, and so the latest activity at Elysium Mons postdates the final eruptions from the other two volcanoes. These stratigraphic relations were recognized and formalized in the nomenclature by Greeley and Guest (1987), and H.J. Moore obtained consistent crater counts. Relative ages are compatible with a late Hesperian to early Amazonian stratigraphic age (fig. I–5). Elysium Mons appears to be older than the large Tharsis volcanoes (see Landheim and Barlow, 1991), predating Olympus Mons by 1.3 to 3.1 Ga and the shield of Arsia Mons by 0.4 to 0.6 Ga, depending on the model used (fig. I–5).

REFERENCES

Blasius and Cutts (1981)
Christiansen (1989)
Greeley (1973)
Greeley and Guest (1987)
Hall and others (1983)
Landheim and Barlow (1991)
Macdonald (1972)
Malin (1977)
Moore (1982a, b)
Mouginis-Mark and others (1984)
Pike and Clow (1981a)
Pike and others (1980)
Plescia and Saunders (1979)
Scott and Allingham (1976)
Sjogren (1979)
Solomon and Head (1982)
Thorarinsson and others (1973)
U.S. Geological Survey (1989, 1991)

ALBOR THOLUS

Mosaic: 211–5906 MC: 7B–15 Coordinates: 19° N., 210° W.

Approximate dimensions (km):	
Base diameter	160
Summit elevation	9
Relief	5–6
Caldera diameter	32
Depth	3
Height/base ratio	0.03
Estimated relative age (10^{-3} craters/km^2)	~5
Inferred age (Ga):	
Model 1	3.8
Model 2	3.5
Stratigraphic age:	
Amazonian-Hesperian; Albor Tholus Formation	

DISTINCTIVE CHARACTERISTICS

(1) Convex flanks, with discernible ridges that are possibly lava tube ridges and lava flows (fig. 21*A*).
(2) Circumferential fractures with collapse pits.
(3) Caldera slightly off center.
(4) Positive gravity anomaly coincident with Elysium Mons anomaly (Sjogren, 1979).

DISCUSSION

Albor Tholus (fig. 21*A*) is similar in size and morphology to the small shield volcanoes of the Tharsis province and probably is also basaltic. Its broadly convex shape led Scott and Allingham (1976) to suggest that Albor Tholus is composed of more viscous, silica-rich flows than those of Elysium Mons, but long, narrow ridges on its hummocky surface, interpreted as lava flows, are more indicative of a basaltic composition. The rim of the caldera appears to be surrounded by a collar of smooth material, varying in albedo, that may be a late-stage ash-flow deposit (C.A. Wood, written commun., 1991). Relative ages suggest that Albor Tholus is Noachian, possibly early Hesperian, but not Amazonian (fig. I–5).

REFERENCES

Scott and Allingham (1976) Sjogren (1979)

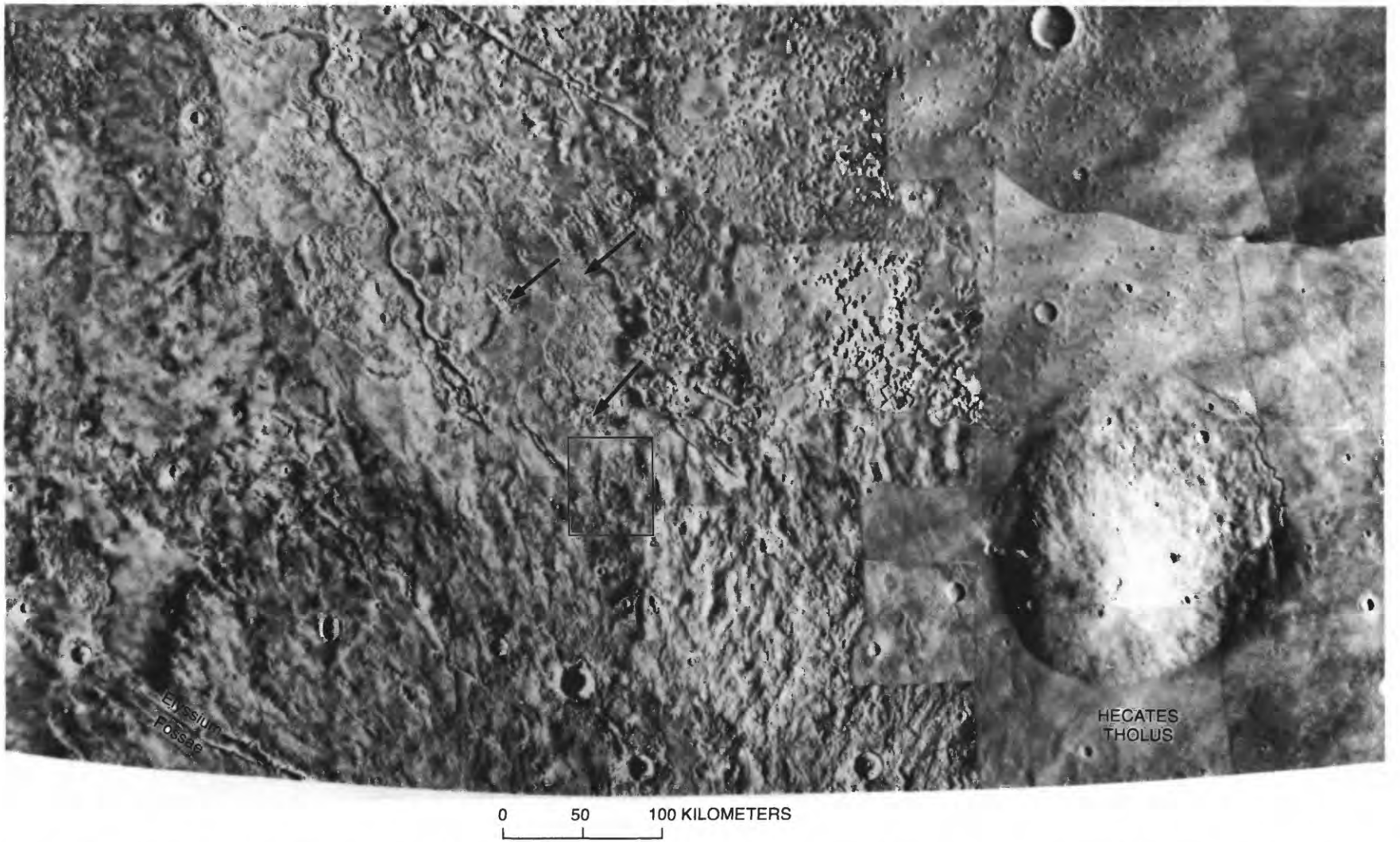

Figure 22. Hecates Tholus. *A*, Hecates Tholus and north flanks of Elysium Mons. Terrain immediately northwest of Hecates Tholus appears to have calved, much as if ground ice had dissipated from subsurface. Spongy-looking terrain farther to northwest, which resembles ground moraine, may have resulted in part from lava/ice interaction, followed by fluvial or mudflow erosion and deposition. Arrows denote deposits that resemble moberg (hyaloclastite) ridges in Iceland (fig. 21*E*). Box at center outlines area of figure 21*D*. Sun illumination from right in east third of image, from left elsewhere. Part of Viking Orbiter photomosaic subquadrangle MC–7SC (U.S. Geological Survey, 1981a).

HECATES THOLUS

Mosaic: 211–5906 MC: 7B–15 Coordinates: 32° N., 210° W.

Approximate dimensions (km):	
Base diameter	200
Summit elevation	8
Relief	6–7
Caldera (nested)	11 by 9
Caldera depth (Mouginis-Mark and others, 1981)	0.47
Height/base ratio	0.03
Estimated relative age (10^{-3} craters/km^2)	2.7±0.6
Inferred age (Ga):	
Model 1	3.6–3.7
Model 2	1.9–3.0
Stratigraphic age:	
Hesperian; Hecates Tholus Formation	

DISTINCTIVE CHARACTERISTICS

(1) Caldera unusually small relative to base diameter (fig. 22*A*).
(2) Caldera located asymmetrically with respect to base; flank longer on north, downslope side of Elysium ridge.
(3) Flanks slightly convex.
(4) Flanks scored by numerous radial grooves and channels, commonly with dendritic elements; no distinguishable lava flows.
(5) No apparent gravity anomaly (Sjogren, 1979).

DISCUSSION

Hecates Tholus (fig. 22*A*) has a domelike shape and an unusually small caldera relative to its size. Unlike Elysium Mons, its flanks are scored by radial striations and channels with dendritic upper reaches. Several investigators (Elston, 1979; Mouginis-Mark and others, 1981, 1982a; Wilson and others, 1981) suggested that part of the west flank of the caldera is surfaced by pyroclastic deposits, accounting for the smooth morphology and low frequency of impact craters. Reimers and Komar (1979) suggested that the volcano may be composed of both lava and ash and that the radial scoring of its flanks is attributable to erosion by base-surge density currents. Except for the anomalously small size of its caldera, Hecates Tholus resembles Ceraunius Tholus (figs. 6*A*, 8), for which Reimers and Komar (1979) proposed a pyroclastic origin. Gulick and Baker (1990a, b), however, suggested that the generally radial network of valleys on both Hecates and Ceraunius Tholi is fluvial in origin and that their degree of development is consistent with a Noachian age, rather than with the Hesperian age assigned to Hecates Tholus by Greeley and Guest (1987). Our relative-age estimate above, however, supports the Hesperian designation. Like Ceraunius Tholus, Hecates Tholus also morphologically resembles terrestrial basaltic shield volcanoes (Pike and Clow, 1981a, b). Pyroclastic activity may have contributed to the bulk of the volcano, particularly if ground ice were prevalent, but basaltic magma was probably the major component. Both its relative age (fig. I–5) and superposition relations (figs. I–3, 21*C*) demonstrate that Hecates Tholus is older than Elysium Mons and its related volcanic materials.

REFERENCES

Elston (1979)
Greeley and Guest (1987)
Gulick and Baker (1990a, b)
Mouginis-Mark and others (1981, 1982a)
Pike and Clow (1981a, b)
Reimers and Komar (1979)
Sjogren (1979)

B, Hecates Tholus caldera, 9 by 11 km across. Smooth materials around rim were interpreted as pyroclastic deposits by Mouginis-Mark and others (1981, 1982a) and Wilson and others (1981). Sun illumination from left. Viking Orbiter frame 651A19.

APOLLINARIS PATERA

Mosaic: 211–5213 MC: 23A Coordinates: 8.5° S., 186° W.

Approximate dimensions (km):	
Base diameter	180 by 280
Summit elevation	5
Relief (Robinson, 1990)	5
Caldera diameter	85
Caldera depth (Robinson, 1990)	0.8
Height/base ratio	~0.02
Estimated relative age (10^{-3} craters/km^2)	1.5–3.1
Inferred age (Ga):	
Model 1	3.6–3.7
Model 2	1.4–2.9
Stratigraphic age:	
Hesperian-Amazonian; Apollinaris Patera Formation	

DISTINCTIVE CHARACTERISTICS

(1) Shield volcano, with caldera breached on the southeast by lava or ash flows that formed a large dissected fan on southeast flank.
(2) Multiple stages of collapse, as shown by scalloped caldera rim.
(3) Low scarp encircling base of volcano, obscured by superposed volcanic flows on the southeast and elsewhere draped by lava or ash flows.

DISCUSSION

Apollinaris Patera is at the margin of the highlands plateau, isolated from the volcanoes of Elysium Planitia to the northwest (fig. I–3), and was described as a basaltic shield volcano by Scott and others (1978). Impact craters as large as 20 km across are superposed on the volcano. Though not nearly so high as the Tharsis volcanoes, Apollinaris Patera is similar in general morphology; however, its large caldera relative to the base diameter as now exposed (fig. 23*A*) suggests that the volcano may have been significantly higher before caldera collapse. Individual lava flows are not readily identifiable, and the southeastern fan more nearly resembles the flanks of the highlands volcano Hadriaca Patera than the Tharsis volcanoes' flanks; the former have been interpreted as eroded ash flows and pyroclastic deposits by Crown and Greeley (1990a). The complex caldera was subjected to at least three stages of collapse (Scott and others, 1978), the earliest of which may be represented by the subdued arcuate remnant about 25 km west of the present rim.

The rim of the caldera exhibits an array of closely spaced radial rilles or channels, one of which crosses the rim from inside and appears to have been the conduit for flows that formed the fan deposit. The scarp encircling the base of the volcano is somewhat reminiscent of that around Olympus Mons, although it is not nearly so conspicuous. Evidence for ground failure and breakup into chaotic terrain beyond the south flank suggests that degradation of underlying, ice-rich plateau materials has formed the scarp, which was subsequently draped by the latest Apollinaris Patera deposits. Above the scarp, the flanks of the volcano show a break in slope, becoming steeper toward the summit (Scott and others, 1978); Robinson (1990) suggested that the upper slope may reflect a change in eruptive style from early pyroclastic activity to a later effusive stage. The conspicuous southern fan, however, appears to comprise the youngest deposits, and its dissection and the absence of identifiable lava-flow ribbons and lobes are more suggestive of ash-flow deposits than effusive lavas. The extent of collapse implied by the size of the caldera and the evidence for ground ice around the base of the volcano suggest that a pyroclastic eruption could have been charged by magma/ice interaction.

Barcena Volcano (fig. 23*B*), in the eastern Revillagigedos Islands off the west coast of Mexico, exhibits both a profusion of radial furrows that could be analogous in general origin to those on Apollinaris Patera, and a late-stage lava fan (fig. 23*C*). According to Moore (1967), the closely spaced rilles on Barcena Volcano were eroded by base-surge density flows, and dunes were deposited at the lower ends of the furrows as a result of a change in slope (fig. 23*D*). Base-surge clouds and their attendant effects are particularly common during phreatomagmatic eruptions where water has access to the conduit. At Apollinaris Patera, ground ice could have supplied water to the eruptions, accounting for the radial rilles around the caldera rim and the large fan, subsequently or syngenetically dissected. Distal ends of the furrows may have been smoothed by deposition of base-surge debris. Although the deltalike lava fan at Barcena Volcano (fig. 23*C*) somewhat resembles the conspicuous fan at Apollinaris Patera (notwithstanding the enormous difference in scale), the Barcena fan is silicic (J.G. Moore, oral commun., 1991), whereas the Apollinaris fan is presumed to be basaltic. Nevertheless, the geographic and morphologic similarities are pronounced, indicating once again the uncertainties sometimes inherent in extrapolation.

Gulick and Baker (1990a, b) concluded from their analyses of valley formation on martian volcanoes that the valleys on Apollinaris Patera display features suggestive of mixed fluvial and lava origins, and that the stage of valley development indicates a Noachian age. Relative ages suggest that Apollinaris Patera is

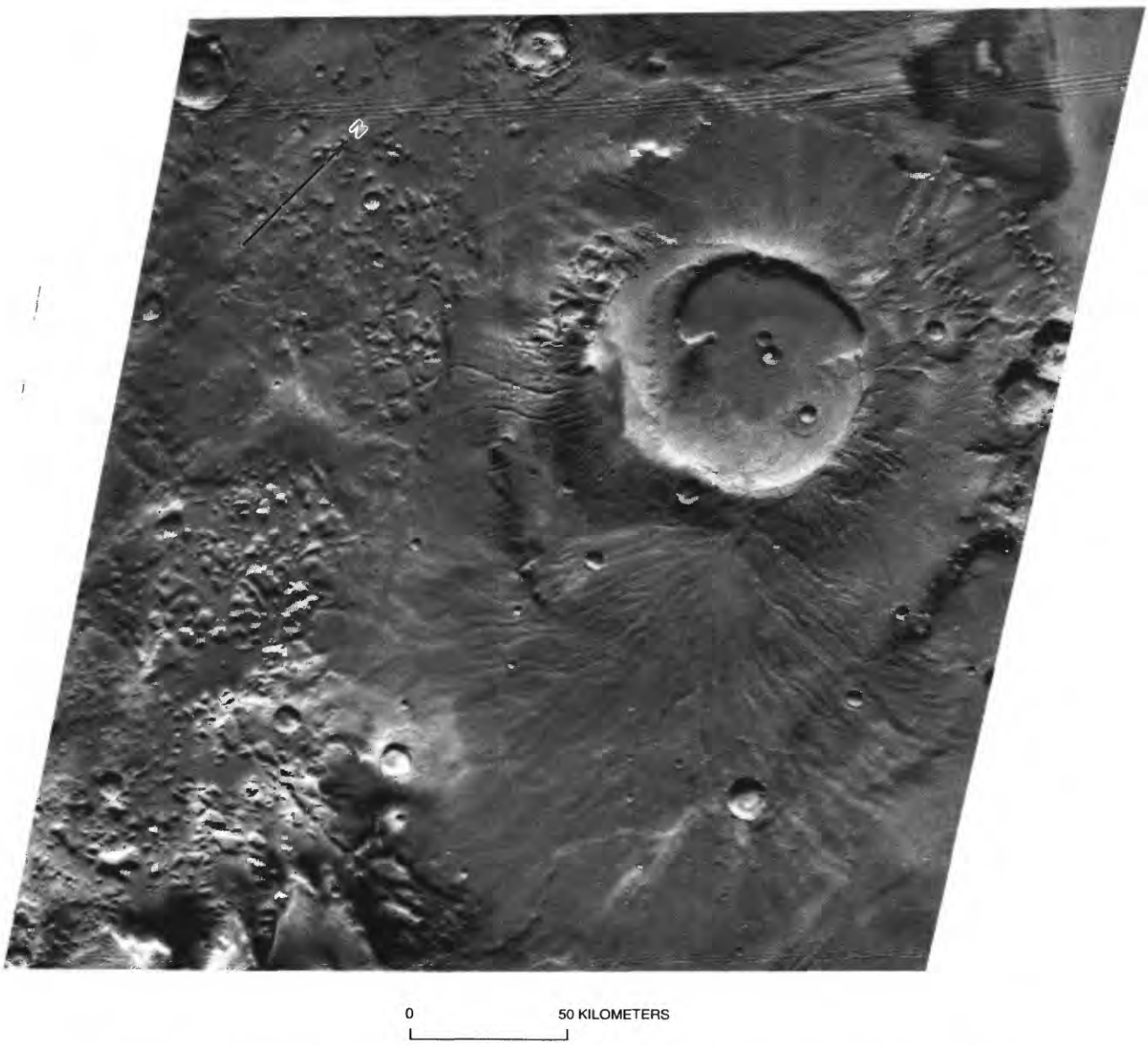

Figure 23. Apollinaris Patera. *A*, Apollinaris Patera and shield, relatively isolated at northern margin of old cratered highlands. Caldera apparently overflowed extensively on southeast side, forming broad fan of ash or lava that obscured basal escarpment surrounding volcano; fan displays dendritic network of distributary channels. Flanks of shield are highly dissected. Sun illumination from top. Viking Orbiter frame 372S56.

B, Barcena Volcano (tephra cone), eastern Revillagigedos Islands, off west coast of Mexico. Closely spaced radial channels, which were eroded by tephra avalanches or density flows as base-surge clouds radiated from main crater, have been slightly modified and incised by meteoric runoff (Richards, 1959; Moore, 1967). Radial pattern on flanks of Apollinaris Patera may have originated similarly or may be entirely attributable to lava channels. Prominent escarpment somewhat resembles that at south and east base of Apollinaris Patera, but their origins probably are not analogous. Barcena Volcano scarp presumably is remnant of earlier erosional seacliff, although mechanism of uplift is unclear. Cone is approximately 380 m high; flank slope is steeper than at Apollinaris Patera. U.S. Navy photograph, courtesy of J.G. Moore.

C, Barcena Volcano, side opposite view in figure 23*B*, showing late-stage, silicic lava flow (J.G. Moore, oral commun., 1991) that emerged from base of tephra cone. Lava-flow ridges and channels, and relation of flow to cone and crater, somewhat resemble those of lava fan (probably basaltic) at Apollinaris Patera, albeit orders of magnitude smaller. U.S. Navy photograph, courtesy of J.G. Moore.

Hesperian, older than the Tharsis volcanoes and, probably, than Elysium Mons as well, but approximately equivalent in age to the highlands volcanoes Tyrrhena and Hadriaca Paterae (fig. I–5).

REFERENCES

Crown and Greeley (1990a)
Gulick and Baker (1990a, b)
Moore (1967)
Richards (1959)
Robinson (1990)
Scott and others (1978)

D, Barcena Volcano, showing furrows eroded by base-surge density flow of tephra and gases from crater (approx 750 m diam) at bottom left. Furrows on right transform into dunes at change in slope where base-surge clouds lost erosional energy and began to deposit ash. Sun illumination from upper right. From Moore (1967); photograph courtesy of J.G. Moore.

MAJOR PLAINS PROVINCES

ELYSIUM REGION

SMALL VOLCANIC FEATURES

HEPHAESTUS FOSSAE

Mosaic: 14NE MC: 14A Coordinates: 21°–25° N., 234°–239° W. (no 211 series available)

Province description:
Field of small cratered domes.

Elevation (km)	2
Approximate dimensions (m):	
Base diameter	500
Crater diameter	≤200

Stratigraphic age:
Amazonian; knobby-plains material

DISTINCTIVE CHARACTERISTICS

(1) Some domes contiguous, but generally at least 1 km apart.
(2) Featureless plains, presumed to be volcanic because of their proximity to Elysium Mons.

DISCUSSION

The field of cratered cones or domes in the Hephaestus Fossae province (fig. 24) is associated spatially with fractures or rilles but appears to be unrelated to them genetically. These features are similar to other fields or clusters farther west (in Elysium Planitia), for which Frey and Jarosewich (1981) suggested Icelandic pseudocraters (fig. 18*C*; Thorarinsson, 1953) as the most likely terrestrial analog. A volcanic interpretation of their origin is inconclusive, but their morphology, as well as their proximity to Elysium Mons and other apparently volcanic features, is suggestive.

REFERENCES

Frey and Jarosewich (1981) Thorarinsson (1953)

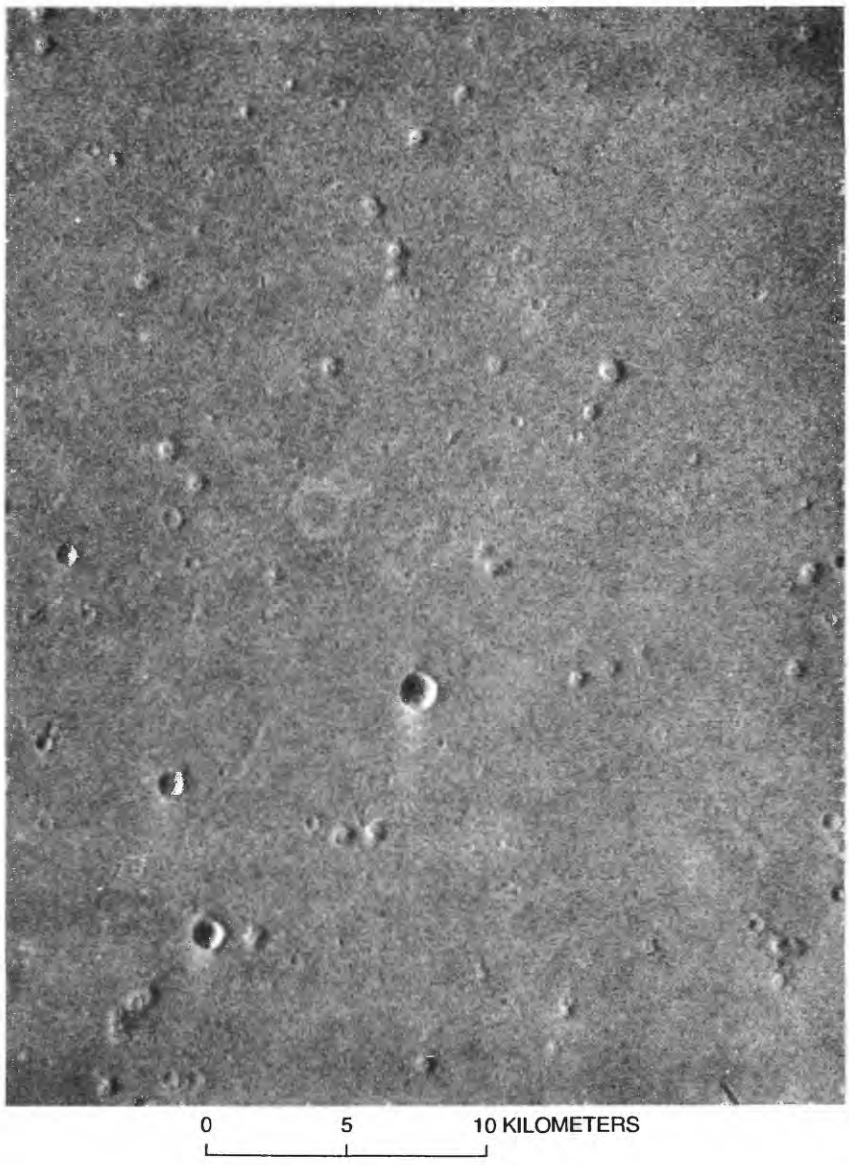

Figure 24. Hephaestus Fossae province, showing small cratered domes near Hephaestus Fossae rilles. Light hexagonal ring near center of photograph is an artifact. Sun illumination from left. Viking Orbiter frame 647A42.

ELYSIUM SOUTH

Mosaic: 211–5813 MC: 23C Coordinates: 2° S.–0.5° N., 209°–218° W.

Province description:
Two cratered cones associated with long, narrow, curvilinear ridge segments.

Elevation (km)	0–1
Approximate dimensions (m):	
Cone base diameter	700, 1,500
Cone crater diameter	250
Ridge width	100
Ridge length	10,000–40,000
Ridge height (shadow measurement)	20

Stratigraphic age:
Amazonian; lower member of the Medusae Fossae Formation

DISCUSSION

These possibly volcanic features of the Elysium South province occur at the margins of fluted deposits that appear to have been eroded by wind and may have been entirely removed from the area to the south (figs. 25*A*, 25*B*). One cone is symmetrical, and the crater of the other cone is offset from the summit; both cones resemble terrestrial cinder cones. Only one of these cones overlaps a ridge

The origin of the ridges is enigmatic; they somewhat resemble esker segments but could be dikes etched in relief, similar to the spectacular dikes exposed by erosion around Ship Rock volcanic neck in New Mexico (see fig. 30*D*). Pitted terrain immediately to the south has been interpreted as a result of volcano/ground-ice interaction (Squyres and others, 1987).

REFERENCES

Squyres and others (1987)

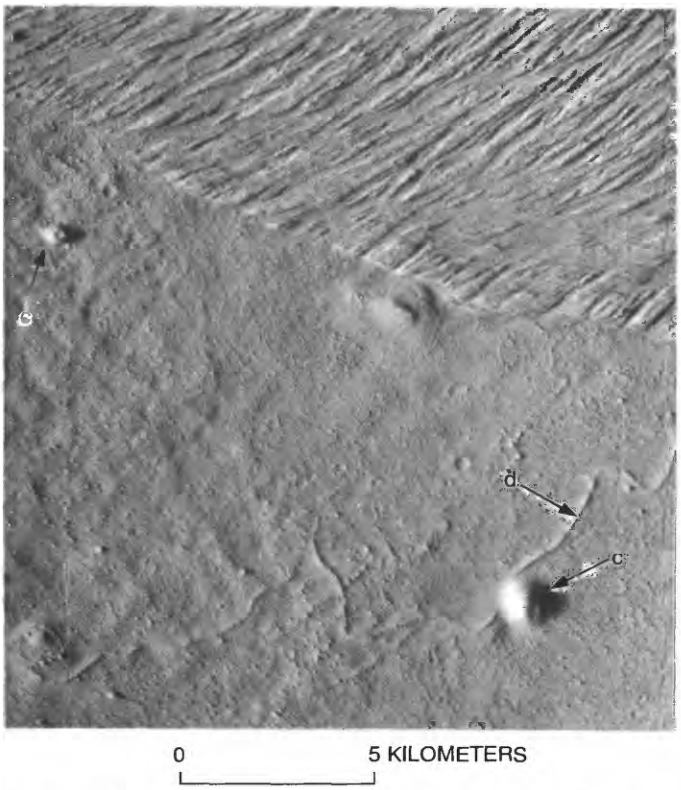

Figure 25. Elysium South. *A*, Area in southern Elysium Planitia near margin of old cratered highlands. Arrows denote cones (c) and dikelike ridges (d). Fluted deposits at top appear to have been eroded by wind. Sun illumination from left. Viking Orbiter frame 724A20.

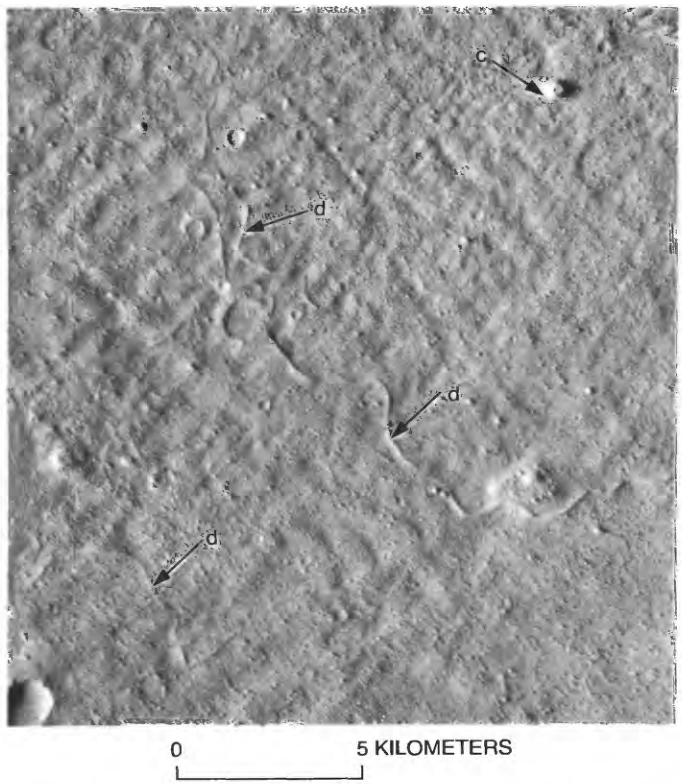

B, Area west of that in figure 25*A*. Arrows denote cones (c) and segmented, dikelike ridges (d). Sun illumination from left. Viking Orbiter frame 724A16.

CERBERUS

Mosaic: 211–6075 MC: 15A Coordinates: 1° S.–9° N., 194°–208° W.

Province description:

About nine low shield volcanoes with circular to linear vents, associated with extensive lava flows.

Elevation (km)	–2 to –1
Approximate dimensions (Plescia, 1990) (km):	
Shield diameter	50–100
Circular-vent diameter	1–5
Linear-vent length	max 15
Estimated relative age (10^{-3} craters/km^2):	
Plescia (1990)	0.09±0.02
	0.08±0.05
Inferred age (Ga):	
Model 1	0.11–0.6
Model 2	0.03–0.11

Stratigraphic age:

Late Amazonian; younger channel and flood-plain material, undivided

DISCUSSION

The Cerberus province and its associated lava flows (figs. I–3, 26) are particularly interesting because the density of superposed craters suggests that these flows are among the youngest volcanic features on Mars (Moore, 1982a; Scott and Tanaka, 1986; Greeley and Guest, 1987; Plescia, 1990). According to Plescia (1990), at least nine vents and low shield volcanoes in the Cerberus province erupted low-viscosity lava that flowed generally eastward and then northeastward. Much of this lava was likely erupted from fissure vents that are now buried. The adjacent Cerberus Rupes fissures may have been the site of some eruptions, but no evidence thereof has been identified (Plescia, 1990). The lavas are typically thin and fill preexisting channels; flow fronts are indistinct. One channel, informally called the Amazonis Channel (Moore, 1982a), contains thin dark lavas about 1,260 km east of the Cerberus vent area (fig. I–3) that progressively thickened as they flowed north-northeastward, eventually filled the channel, and poured into Amazonis Planitia (Moore, 1982a; Plescia, 1990). About 2,600 km from the vent area, these lavas terminate against mountains and as thick lobes; the terminal lobes are as much as 30 to 45 m thick.

The volcanic features in the Cerberus province are not specifically identified on geologic maps, but the area is mapped as younger fluvial-channel and flood-plain materials (units Ach, Achp, Achu; Scott and Tanaka, 1986; Greeley and Guest, 1987), and there is general agreement that these deposits are among the youngest on Mars (see fig. I–5).

REFERENCES

Greeley and Guest (1987)
Moore (1982a)
Plescia (1990)
Scott and Tanaka (1986)

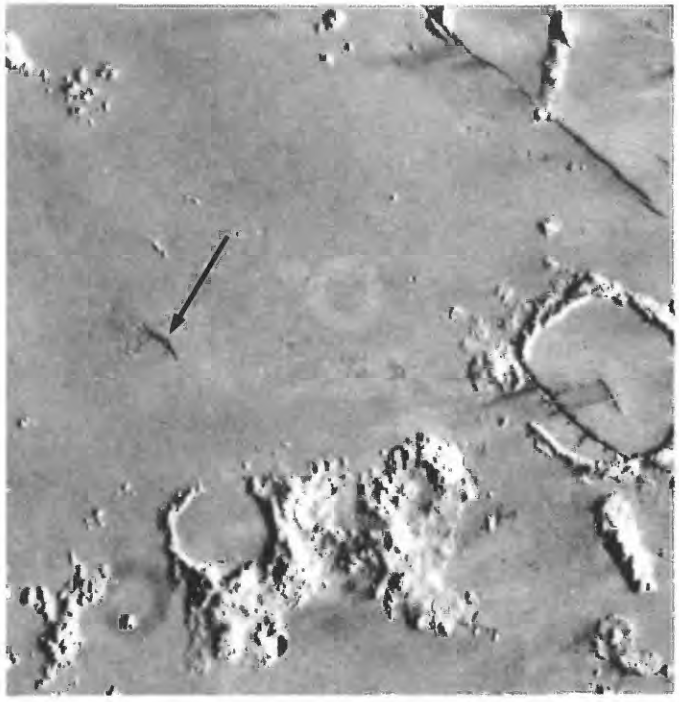

Figure 26. Cerberus province, south of Elysium Mons in Cerberus Planitia region (Plescia, 1990) at about 7° N., 200° W. Elongate vent (arrow) is surrounded by radially textured deposits that suggest a low shield volcano. Vent is about 0.6 by 10 km across; shield is about 30 to 35 km in diameter. Sun illumination from right. Light circle at center is artifact. Viking Orbiter frame 385S46.

MINOR PLAINS PROVINCES

ARCADIA-AMAZONIS REGION

SMALL VOLCANIC FEATURES

ARCADIA PLANITIA

Mosaic: 211–5558 MC: 2A Coordinates: 42°–50° N., 140°–162° W.

Province description:

Low convex domes atop a textured deposit characterized by arcuate ridges.

Elevation (km)	–2 to –1
Approximate dimension (km):	
Dome base diameter	1–8
Relief (shadow measurements)	0.4–0.5

Stratigraphic age:

Amazonian; Arcadia Formation

DISCUSSION

The symmetrical domes in the Arcadia Planitia province are distinguished by circular summit depressions that do not resemble true craters of either volcanic or impact origin (figs. 27*A*, 27*B*); in some domes, radial fractures give a "puckered" appearance to these depressions. The domes are most prominent on the peculiarly textured ridged terrain but are not confined exclusively thereto. The textured deposits are enigmatic; this is the only known occurrence of such terrain on the planet. The pattern of arcuate ridges is interrupted by a conspicuous, nearly linear, north-trending trough, with one branch to the southwest. Both the main trough and its "tributary" contain an axial ridge (figs. 27*A*, 27*B*); however, the resolution of the images south of those shown here is poor, and thus the characteristics of the "headward" extension of the deposits are unknown.

Both glacial or periglacial and volcanic hypotheses can be invoked to explain this complex terrain, which somewhat resembles a ground moraine with superposed recessional moraines, transected by an esker, and associated with pingoes (Hodges, 1980b). Rossbacher and Judson (1981) suggested that similar ridges may result from solifluction of ice-rich materials or ice-cored ridges. Adjacent terrain to the west is also depositional but more chaotically patterned, somewhat resembling disorganized glacial debris.

The crescentic-ridge pattern may be equally reminiscent of arcuate pressure ridges on silicic lava flows, suggesting a volcanic interpretation for these features (Hodges, 1980b). The puckered domes are similar in morphology to terrestrial tholoid domes, such as Glass Mountain, Calif. (fig. 27*C*). Using a model based on ridge height and spacing and an as-

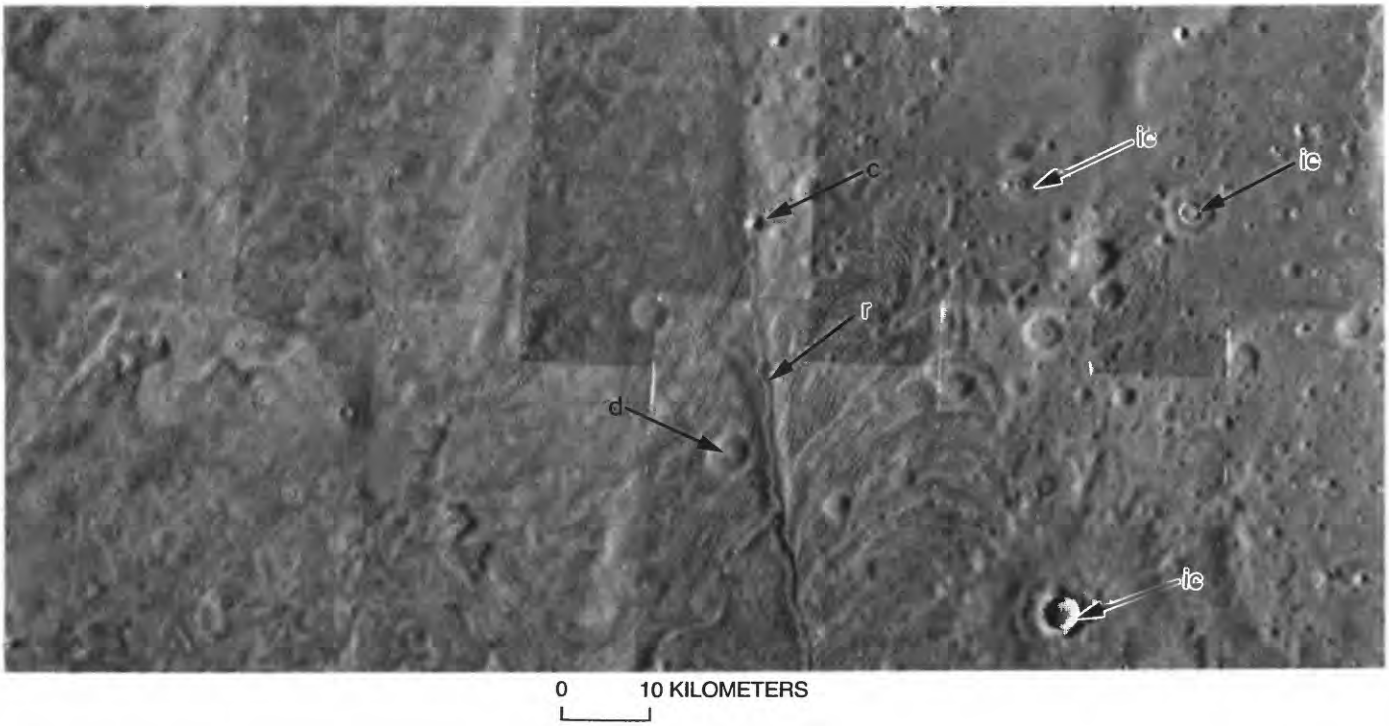

Figure 27. Arcadia Planitia. *A*, Festoonlike, textured deposits of concentric, arcuate ridges and troughs associated with low convex domes (arrow d). Ridges are transected by north-trending trough and southwest "tributary" with conspicuous axial ridge (arrow r) and superposed cone (arrow c). Some domes appear to be morphologically transitional from those with shallow, fractured summit depression to those more nearly resembling impact craters (arrows ic). Sun illumination from left. Part of Viking Orbiter mosaic 211–5558.

sumed strain rate, Fink (1980) calculated the viscosities of the martian lava flows to fall within the range for rhyolite. As he noted, the presence of rhyolite on Mars would imply a more highly differentiated planetary crust than has heretofore been evident. However, no volcanic edifice exists in the province to serve as an obvious source for such a silicic flow, and the ridge patterns show no relation to the superposed domes. Nevertheless, the patterned terrain (figs. 27*A*, 27*D*) and the domes somewhat resemble the rhyolite-obsidian complex at Glass Mountain and other terrestrial silicic centers, such as Mono Craters, Calif.

REFERENCES

Fink (1980)
Hodges (1980b)
Rossbacher and Judson (1981)

B, Textured deposits, showing details of central trough with axial ridge and domes with fractured craters. Sun illumination from left. Viking Orbiter frame 115A24.

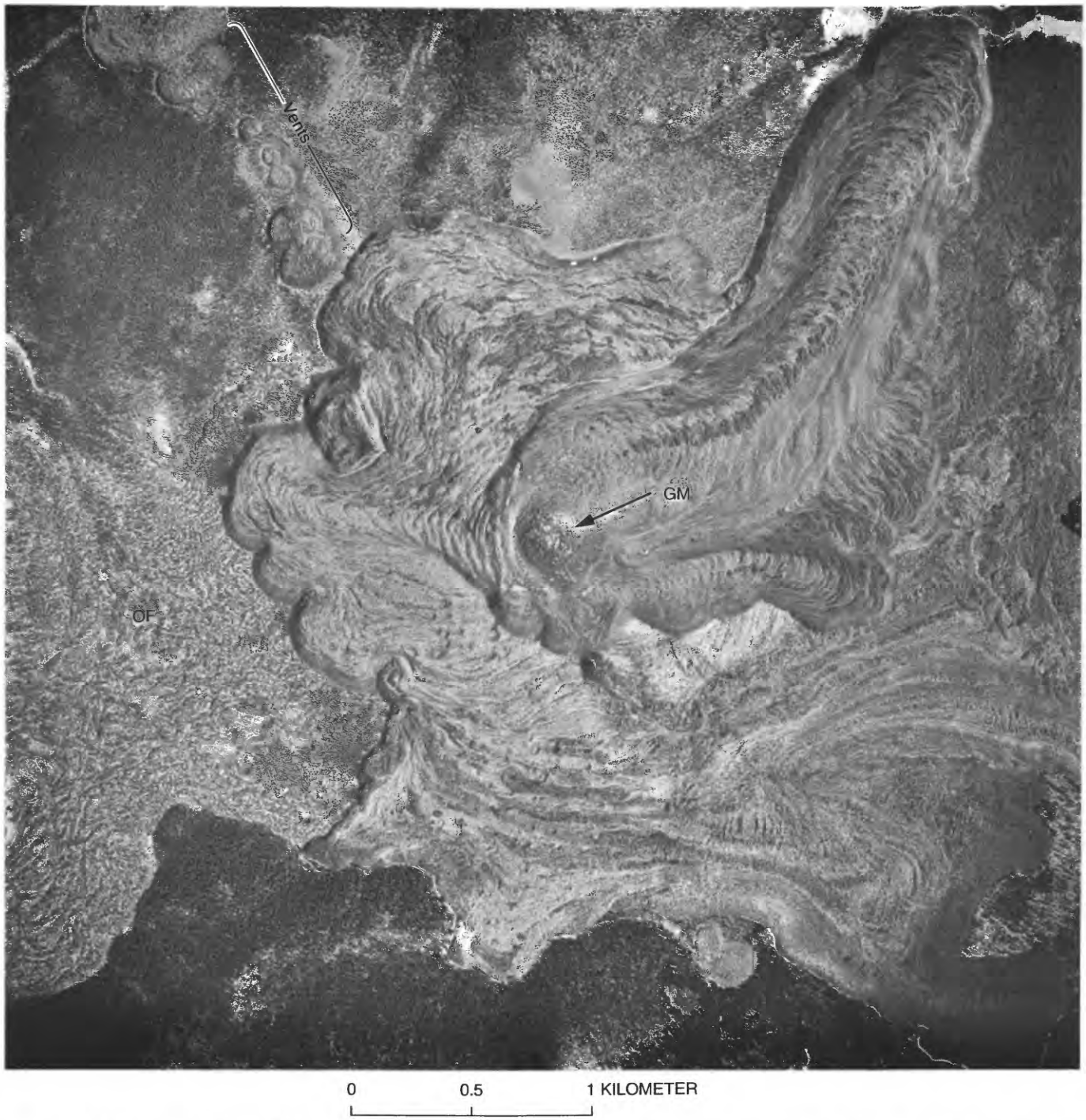

C, Glass Mountain rhyolite-obsidian complex in Medicine Lake Highlands east of Mount Shasta, Calif. Steep lava-flow fronts and ropy, festoonlike textures are typical of blocky silicic flows. Dome of Glass Mountain (arrow GM) and independent vents aligned northwest of main lava flows are morphologically similar to those in Arcadia Planitia (figs. 27*A*, 27*B*). Older, partly vegetated lava flow (OF) somewhat resembles terrain in figure 27*D*. Sun illumination from right. U.S. Forest Service photograph DDC–3P–28, taken July 31, 1955.

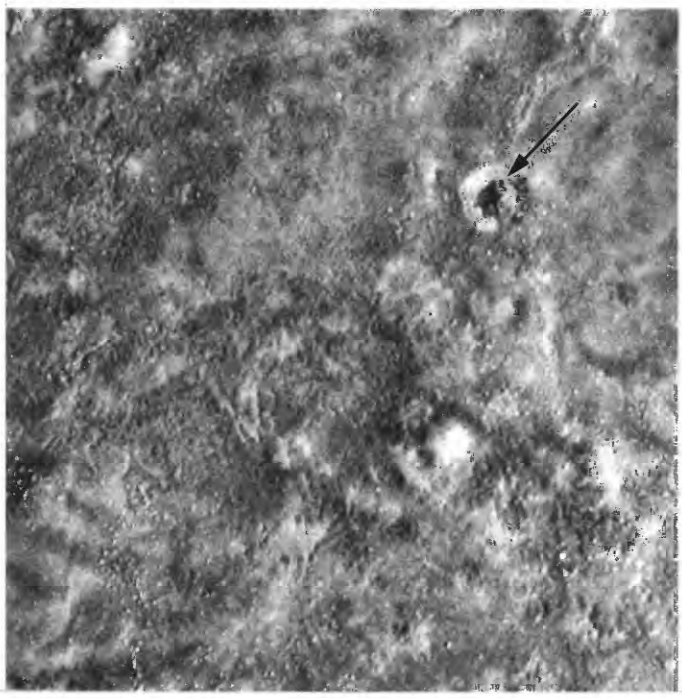

D, Cratered dome (arrow) about 100 km west of area in figure 27*A*. Unusually textured plains materials are of unclear origin but appear to be related genetically to more definite, ridged terrain to east and, despite differences of scale, are remarkably similar in texture to older lava flow west of Glass Mountain rhyolite (fig. 27*C*). Both cratered dome and surrounding plains materials may be volcanic. Sun illumination from left. Viking Orbiter frame 115A11.

AMAZONIS PLANITIA

Mosaic: 211–5845 MC: 8C Coordinates: 16° N., 171° W.

Province description:
Two symmetrical cones with summit craters.

Elevation (km)	–2
Approximate dimensions (km):	
Base diameter	2–3
Crater diameter	0.6–1
Relief (shadow measurement)	0.3
Height/base ratio	0.1–0.15

Stratigraphic age:
Hesperian; ridged-plains materials

DISCUSSION

The cratered cones of the Amazonis Planitia province are amid volcanic plains, and one is astride a lunar-mare-type ridge (fig. 28*A*). The most conspicuous cone has two lobate deposits at its base that appear to be associated genetically with the cone (fig. 28*B*); these deposits resemble thick, viscous lava flows, and they are morphologically similar to the symmetrical cone and basaltic andesite flow at S.P. Crater (fig. 28*C*) in the San Francisco volcanic field, Ariz. (Hodges, 1962). The deposits could also be landslides, but there is no evident landslide scar on the cone from which they might have derived. Conceivably, these lobate ridges might also be preexisting terrain, but their shape and coincidence with the cone make that interpretation seem less likely. The dimensions of these cones are similar to those of possible analogs on Earth, although they have broader base diameters than most terrestrial cones as high as 300 m, which commonly are 1 to 2 km wide (Pike and Clow, 1981b). The approximate height-to-base (*h*/*b*) ratios of these martian cones, however, fall within the range for terrestrial cinder cones (Pike, 1978). Wood (1979) concluded that extrapolation of the *h*/*b* ratios of pyroclastic cones to Mars is invalid because the lower gravity and atmospheric density (relative to Earth) would cause a wider distribution of ballistic ejecta. He suggested that a crater-width-to-cone-width ratio is more reliable, in that both components are equally affected by atmospheric or gravitational effects. For these two cones, this ratio ranges from 0.2 to 0.5, encompassing the average of 0.41 that Wood (1979) calculated for 21 other martian cones. A volcanic origin is plausible, regardless of which dimensions are compared.

REFERENCES

Hodges (1962)
Pike (1978)
Pike and Clow (1981b)
Wood (1979)

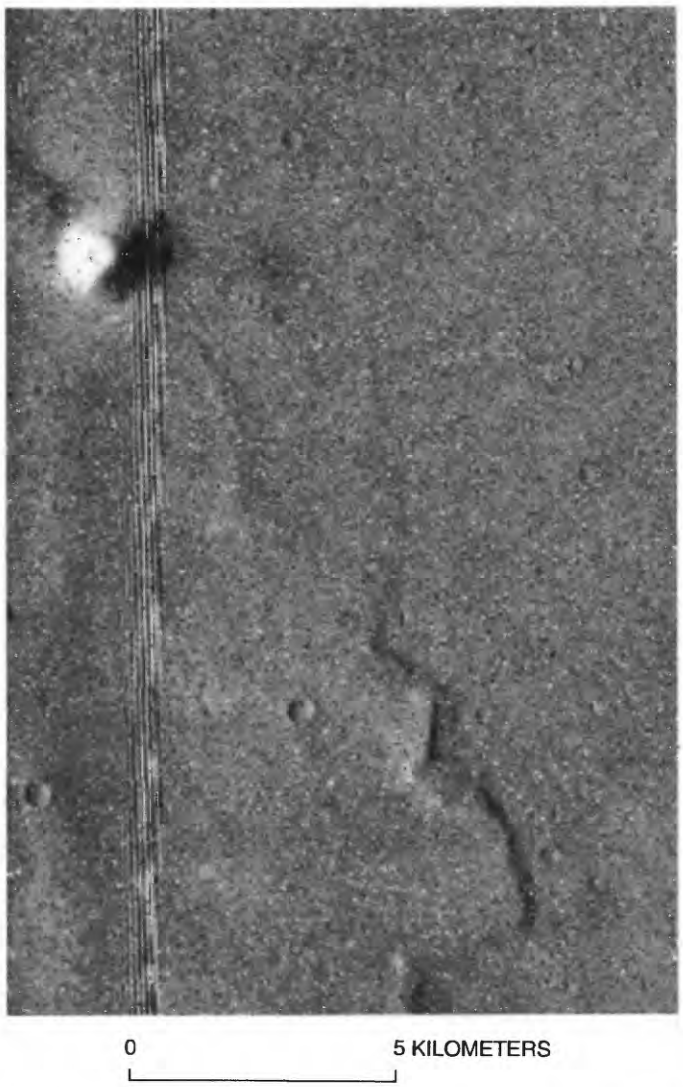

Figure 28. Amazonis Planitia. *A*, Cratered cone atop mare-type ridge. Vertical band on left side of photograph is an artifact. Sun illumination from left. Viking Orbiter frame 691A44.

B, Symmetrical cratered cone in volcanic plains. Basal deposits may be landslides, but absence of cone disruption suggests they more probably are lava flows that predated cone, as at S.P. Crater, Ariz. (fig. 28*C*). Sun illumination from left. Viking Orbiter frame 691A43.

C, S.P. Crater and basaltic andesite flow, San Francisco volcanic field, Ariz. Flow preceded final stages of cone building. Crater rim is preserved by collar of large bombs and agglutinate (Hodges, 1962). Sun illumination from lower right. U.S. Geological Survey photograph VV HU M 16 AMS 134, frame 2000, taken February 23, 1954.

MINOR PLAINS PROVINCES

ACIDALIA-CHRYSE REGION

SMALL VOLCANIC FEATURES

ACIDALIA PLANITIA

Mosaics: 211–5025, 211–5036, 211–5557 *MC: 4A* *Coordinates: 34°–48° N., 3°–31° W.*

Province description:

Small cones or domes with summit craters amid remnants of highlands plateau at northern margin; small ridges and mesas, some with craters.

Elevation (km)	–2 to 0
Approximate dimensions (km):	
Base diameter	0.5–1.5 (avg 0.8)
Crater diameter	0.25–0.45
Relief (shadow measurements)	0.3–0.7

Stratigraphic age:

Amazonian-Hesperian; member of the Arcadian Formation, grooved member of the Vastitas Borealis Formation

DISCUSSION

The Acidalia Planitia province hosts various small landforms, several of which may be volcanic. The most likely candidates are the numerous cratered cones and domes clustered amid ragged remnants of the highlands plateau at its margin (figs. 29*A*–29*C*). These features have been interpreted both as cinder cones (Wood, 1979) and as pseudocraters (Frey and others, 1979; Frey and Jarosewich, 1981, 1982; Frey, 1986), analogous to those in Iceland that formed by explosive action when lava flowed over marshy, water-saturated ground (Thorarinsson, 1953). Additionally, mesas, both cratered and uncratered (fig. 29*F*), are present that have been interpreted as tablemountains (Hodges and Moore, 1978a, 1979), as well as ridges interpreted as products of subglacial fissure eruptions (Allen, 1979). The distinctiveness of the cratered cones and their relatively restricted, clustered occurrence are strong evidence for a non-impact origin. The absence of any large impact crater nearby precludes their being eroded secondary-impact craters. The cratered cones are most commonly individual, but doublets and short chains also occur (figs. 29*B*, 29*C*), characteristics common in terrestrial cinder-cone fields (figs. 29*D*, 29*E*); pseudocraters in Iceland occur similarly. The larger ridges and mesas that resemble tablemountains (figs. 29*E*, 29*G*) may be older than the smaller cratered cones, and if their interpretation as products of subglacial eruption is correct, they suggest the earlier presence of glacial ice in the region (Hodges and Moore, 1978b, 1979). Disintegration of the plateau by apparent calving at its margins is compatible with the presence of ground ice. The interaction of volcanic extrusions with surface and (or) ground ice to form tablemountains and (or) pseudocraters is a plausible explanation for some of these landforms.

Several plateaulike features with apparently collapsed centers (fig. 29*C*) could be analogous to the pressure plateaus (fig. 29*H*) that form in terrestrial volcanic plains as a result of opposing pressures within moving lava flows (Greeley, 1977a). An uplifted crust may have been left unsupported when the lava chilled.

REFERENCES

Allen (1979)
Frey (1986)
Frey and Jarosewich (1981, 1982)
Frey and others (1979)
Greeley (1977a)
Hodges and Moore (1978a, b, 1979)
Thorarinsson (1953)
Wood (1979)

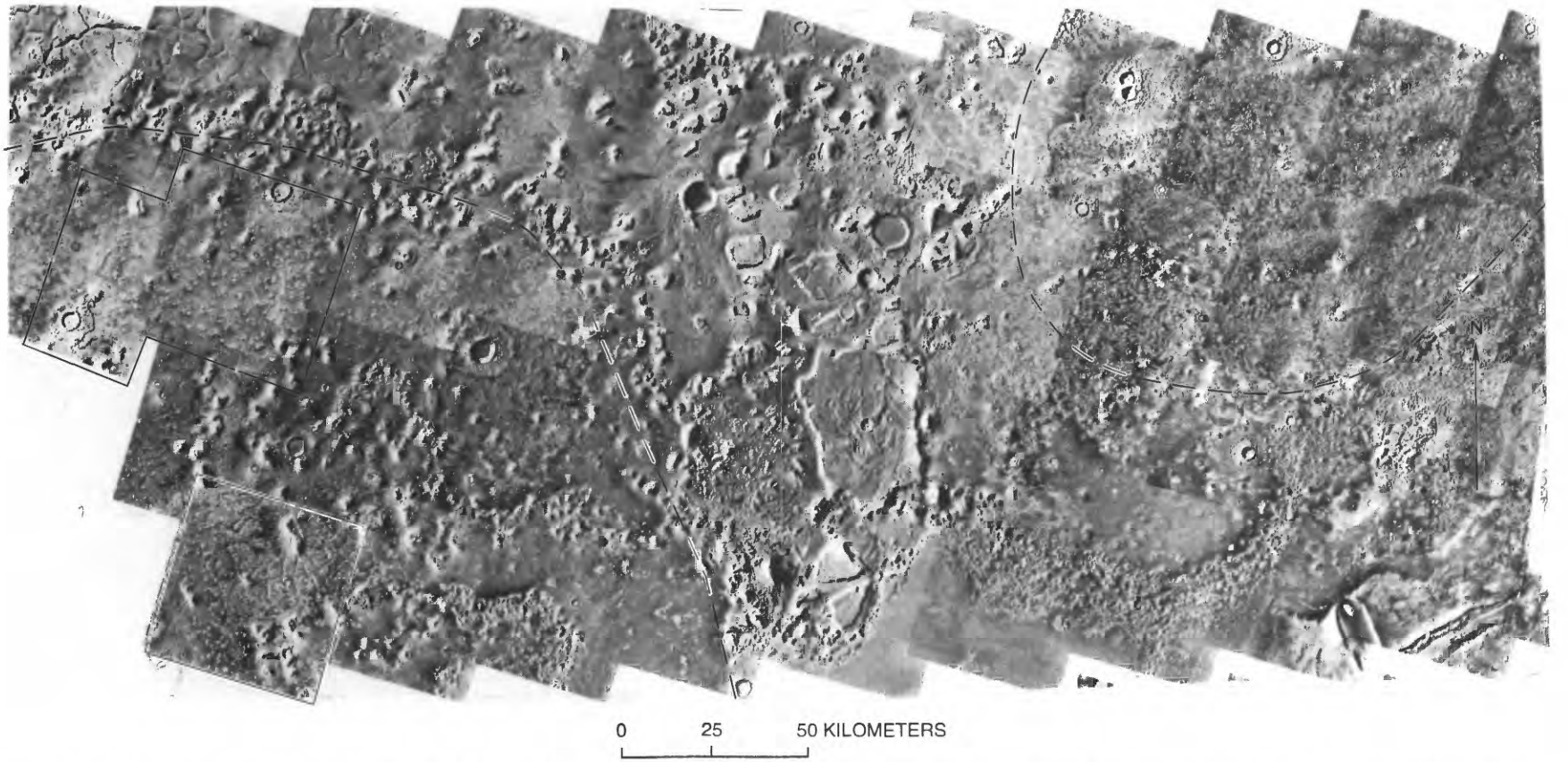

Figure 29. Acidalia Planitia. *A*, Eastern part of Acidalia Planitia, showing clusters of small cratered cones amid scattered remnants of highlands plateau. Dashed lines enclose areas containing especially conspicuous cones. Boxes at left outline areas of figures 29*B* (lower) and 29*C* (upper). Sun illumination from left. Part of Viking Orbiter mosaic 211–5557.

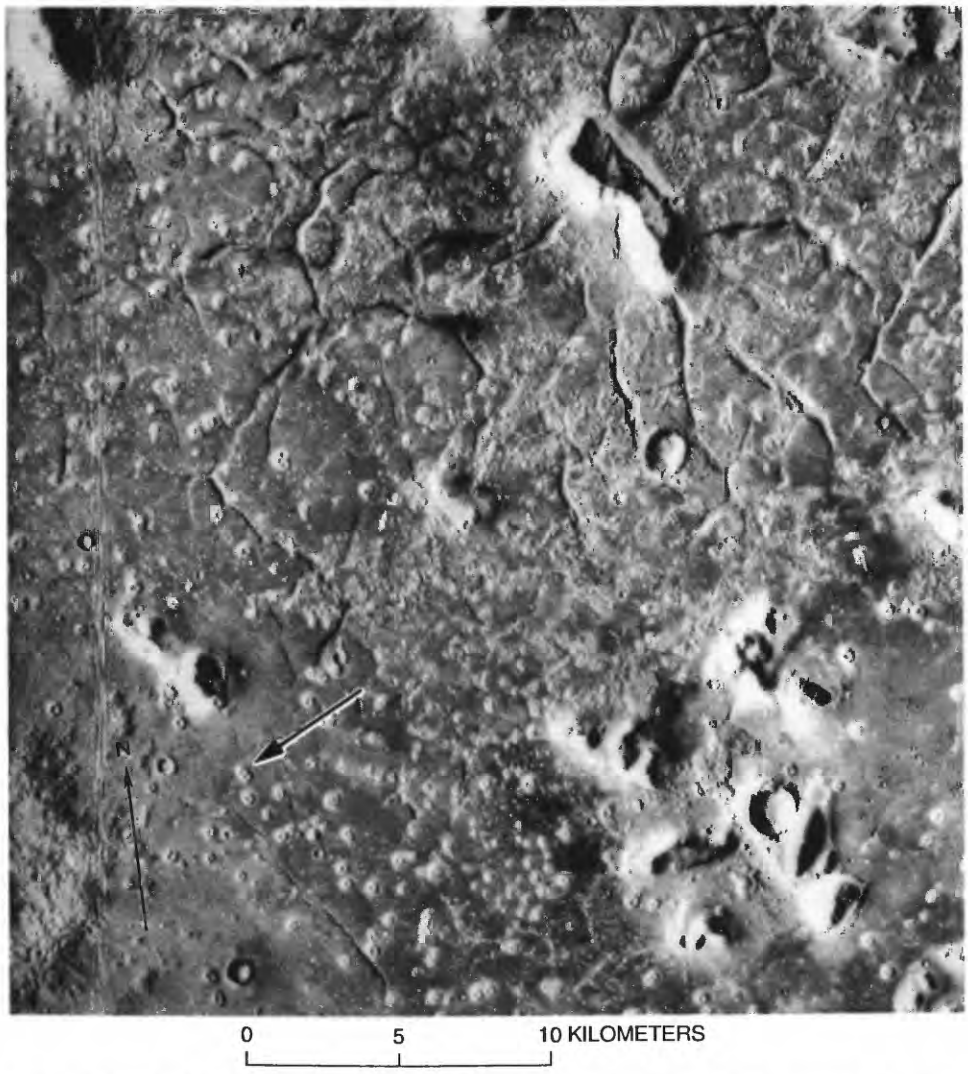

B, Small cratered cones and highlands plateau remnants. Arrow denotes well-developed doublet crater that resembles terrestrial doublet cinder cones (fig. 29*E*) and pseudocraters (fig. 18*C*). Sun illumination from left. Viking Orbiter frame 72A02.

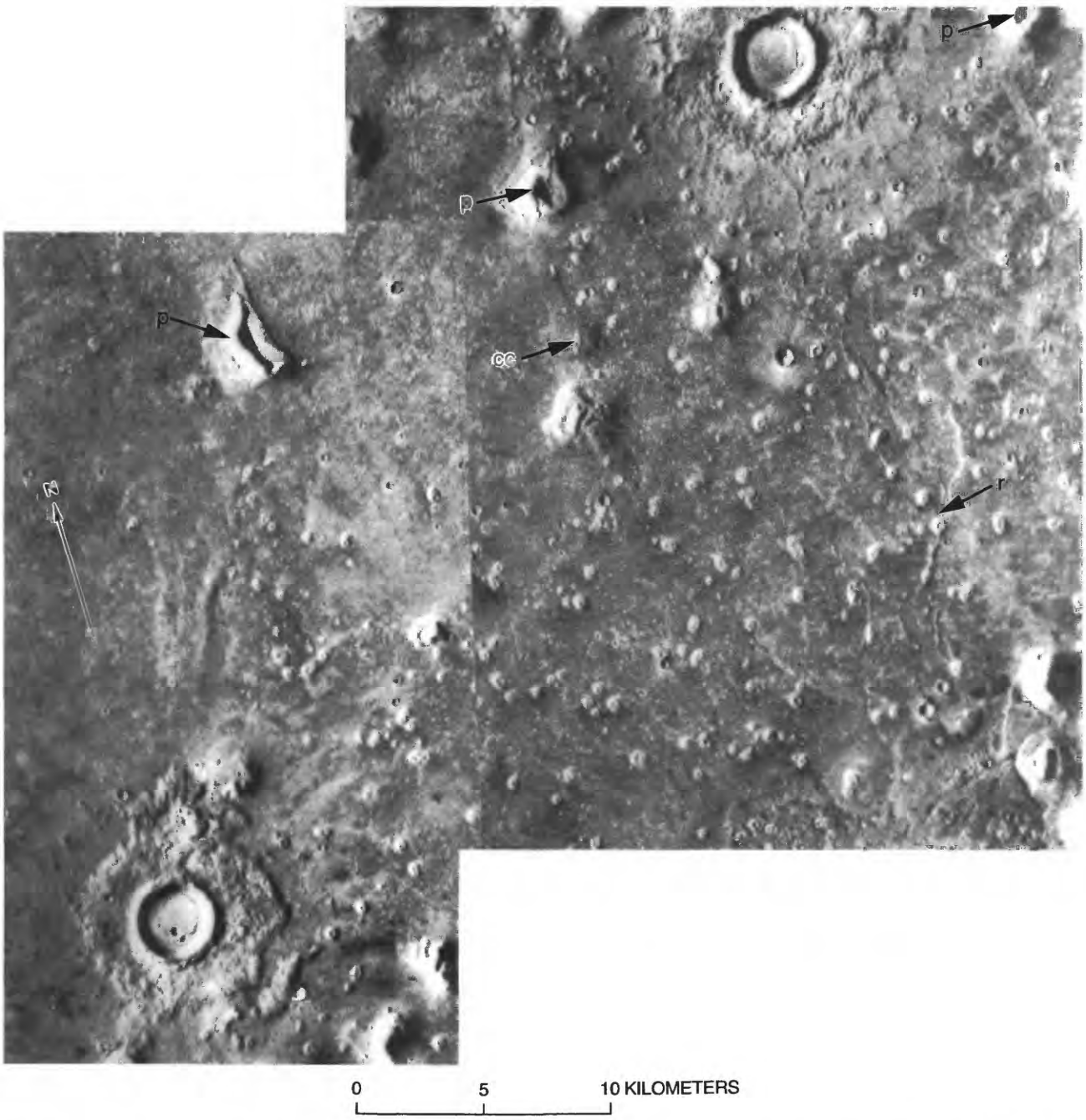

C, Cratered cones occurring singly and in chains (arrow cc). Some cones are astride a small wrinkle ridge (arrow r); several plateau-like features (arrows p) have apparently collapsed centers. Sun illumination from left. Viking Orbiter frames 70A02 and 70A04.

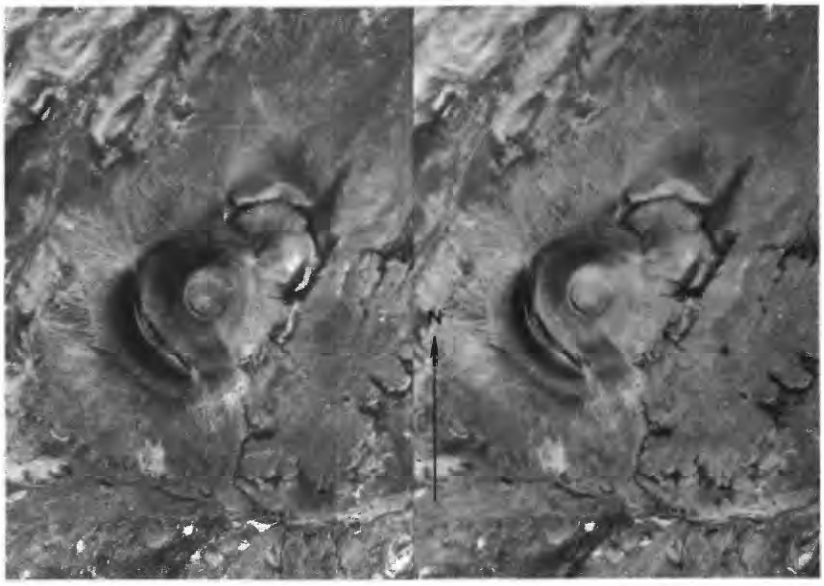

D, Stereopair of Roden Crater and associated basalt flow (f), San Francisco volcanic field, Ariz. Vent producing this unusually symmetrical cinder cone, with its somewhat-convex flanks, destroyed a preexisting tuff cone, an arcuate remnant of which is visible at southwest base. Cinder cone is morphologically similar to many cones in Acidalia Planitia province. Sun illumination from left. U.S. Geological Survey photograph VV HU M 18 AMS 134, frames 2278 and 2279, taken February 25, 1954.

◄ *E*, Somewhat-eroded cinder cones in San Francisco volcanic field, Ariz., southeast of Sunset Crater. Doublet, elongate, and aligned vents, as well as isolated cinder cones, are common throughout this sparsely forested area. Light band at right is path of transmission line. Sun illumination from right. U.S. Geological Survey photograph VV HU M 18 AMS 134, taken February 25, 1954.

► *F*, Rectangular to subcircular mesas that resemble Icelandic tablemountains with (arrow tc) and without (arrow t) summit craters. Features in Iceland, formed by subglacial eruptions, are morphologically diverse (fig. 29*G*), but all have steep scarps and pedestals composed largely of moberg (hyaloclastite). Crater floor higher than surrounding plain in cone at arrow c is indicative of volcanic origin; feature resembles cinder cone (arrow cc) of figure 29*G*. Sun illumination from left. Viking Orbiter frame 26A30.

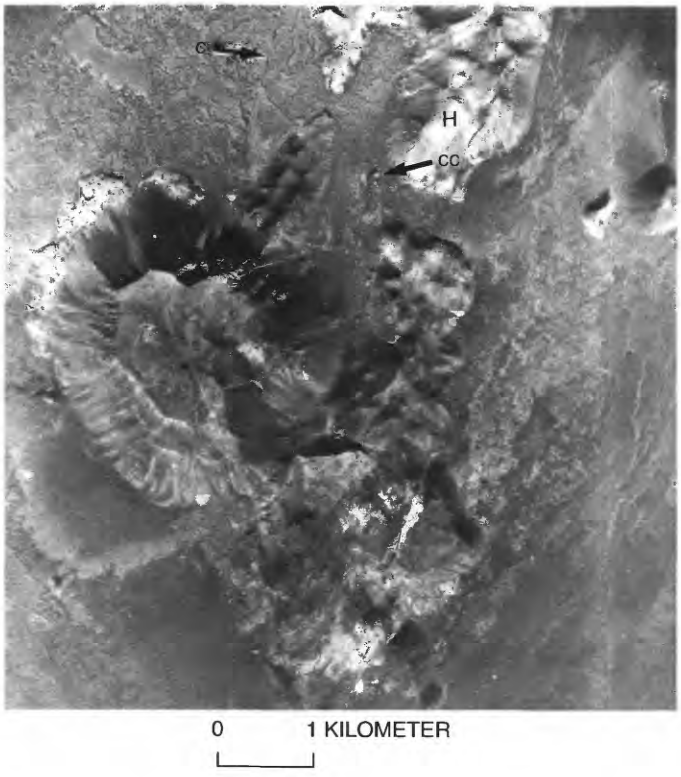

◄ *G*, Búrfell tablemountain (T) and hyaloclastite ridges (H) formed by Pleistocene subglacial eruptions at single vents and fissures in Iceland. Arrows denote recent cinder cone (cc) and lava channel (c). Features resemble those of cinder cone in figure 29*F*. Sun illumination from bottom. U.S. Air Force photograph 55–AM–3, roll 120, frame 13305, taken August 1960.

► *H*, Snake River Plain, Idaho, showing pressure plateau several hundred meters long that may be analogous to collapsed plateaus in Acidalia Planitia province (arrows p, fig. 29*C*). Sun illumination from right. From Greeley (1977a); photograph courtesy of Ronald Greeley.

CHRYSE PLANITIA

Mosaics: *211–4989, 211–4990, 211–5051* *MC: 11A* *Coordinates: 18°–25° N., 34°–44° W.*

Province description:

Pancake-like shield volcanoes, associated with long narrow ridges, buttes, knobs, and etched terrain.

Elevation (km)	–2
Approximate dimension (km):	
Shield diameter	<1–4
Ridges length	10–20
Buttes width	0.5
Estimated relative age (10^{-3} craters/km^2):	
Dial (1978)	1.6±0.4
Inferred ages (Ga):	
Model 1	3.5–3.6
Model 2	1.1–1.9

Stratigraphic age:

Hesperian; older channel and flood-plain materials

DISCUSSION

The Chryse Planitia province has attracted particular interest because of its proximity to the Viking I Lander site, at 22° N., 48° W. Greeley and others (1977) interpreted the light circular patches as low shield volcanoes; some have summit craters, but their relief is almost negligible (figs. 30*A*, 30*B*). Such features may be analogous to some low shield volcanoes on the Snake River Plain in Idaho (fig. 30*C*). The narrow linear ridges have been interpreted as dikes (Greeley and others, 1977). Three buttes that occur along one ridge (fig. 30*B*) resemble volcanic necks with a connecting dike, somewhat reminiscent of Ship Rock, N.Mex. (fig. 30*D*); other buttes are scattered among the shields. Several small cratered cones (fig. 30*E*) have profiles characteristic of volcanoes.

The etched terrain (fig. 30*A*) could have been caused by fluvial erosion from outflow channels to the south and west. Many etch pits have linear boundaries that may reflect a geometric fracture pattern in bedrock.

The low circular pedestals and narrow ridges appear to be unique to this area of the planet. The buttes could be erosional remnants of the highlands plateau, but the dikelike ridges and circular pedestals are not so easily explained. These three landform types appear to be genetically related and are included here as questionably volcanic.

REFERENCES

Dial (1978)

Greeley and others (1977)

Greeley and Schultz (1977)

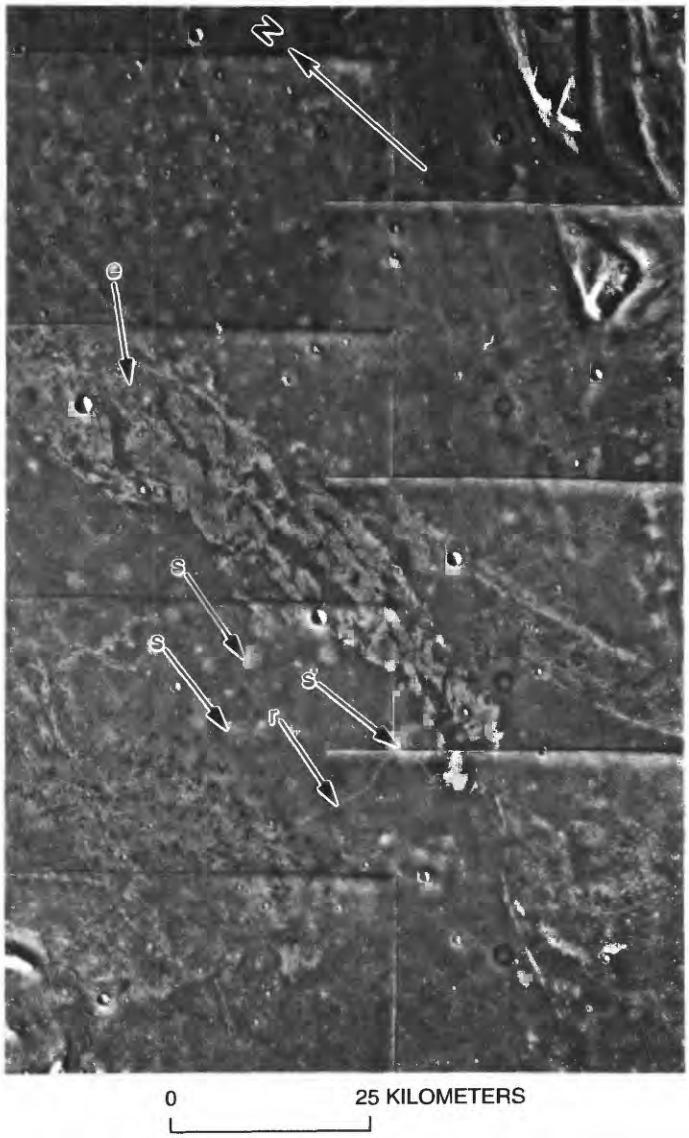

Figure 30. Chryse Planitia. *A*, Low, pancake-like shields (arrows s) and narrow, dikelike ridges (arrow r) associated with unusual, geometrically patterned, etched terrain (arrow e). Highland remnants at upper right appear to have been streamlined by fluvial erosion. Sun illumination from left. Part of Viking Orbiter mosaic 211–4990.

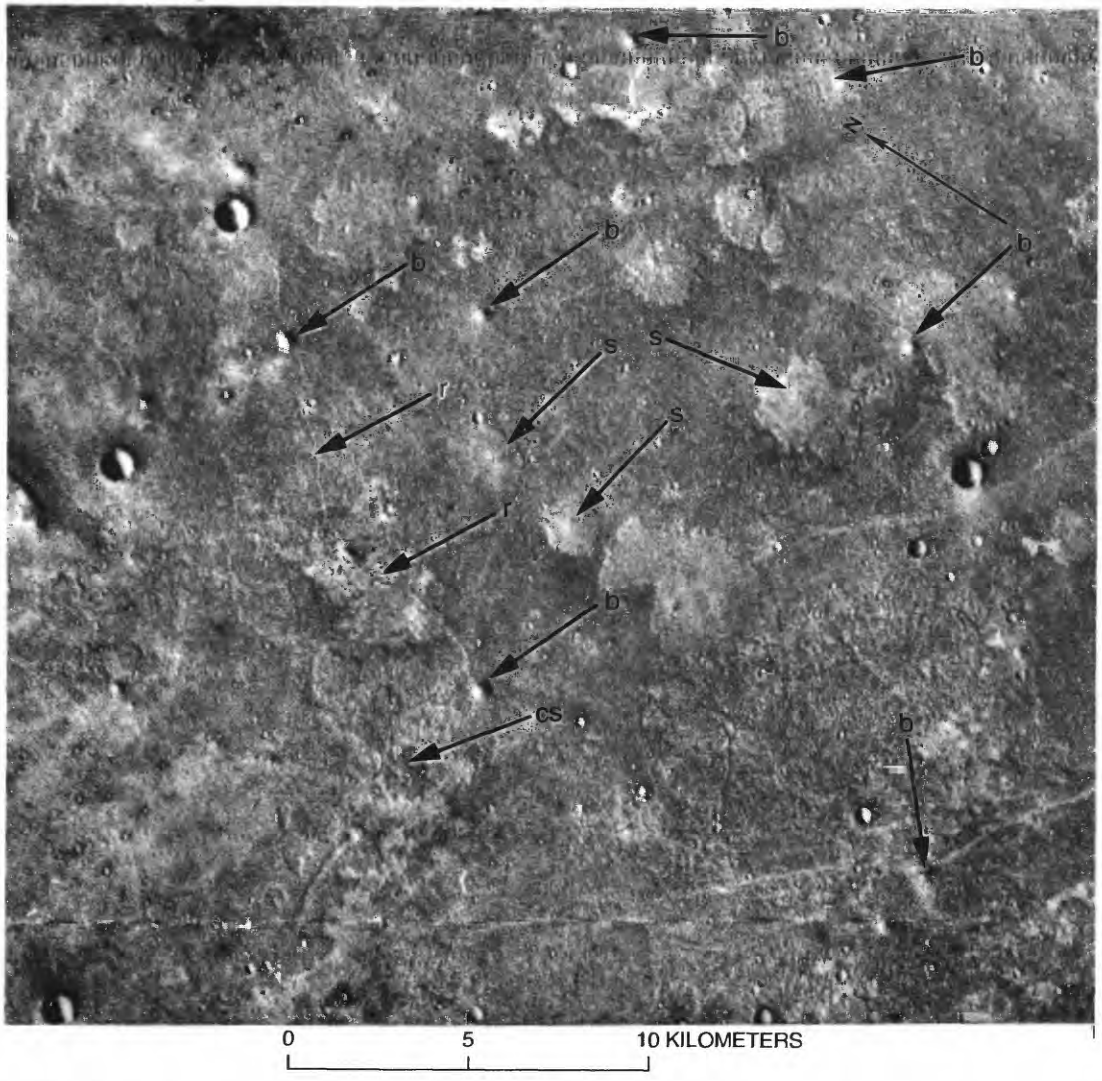

B, Shields (arrows s), buttes (arrows b), and narrow, linear ridges (arrows r) that may be volcanic. Low, pancake-like shields, some of which are cratered (arrow cs), are morphologically similar to lava shields on the Snake River Plain in Idaho (fig. 30*C*). Buttes, reminiscent of terrestrial volcanic necks, are astride ridges that could be dikes etched in relief, much as at Ship Rock, N.Mex. (see fig. 30*D*). Horizontal lines at top and bottom of photograph are artifacts. Sun illumination from left. Viking Orbiter frame 6A35.

◄ *C*, Snake River Plain, Idaho, showing small shield volcano with summit crater. Irregular line is jeep trail. Sun illumination from lower right. From Greeley and Schultz (1977); photograph courtesy of Ronald Greeley.

► *D*, Ship Rock, N.Mex., about 540 m high. Erosion has stripped away pyroclastic cone, leaving only volcanic neck and radiating dikes. Photograph by Donald L. Baars, courtesy of the photographer.

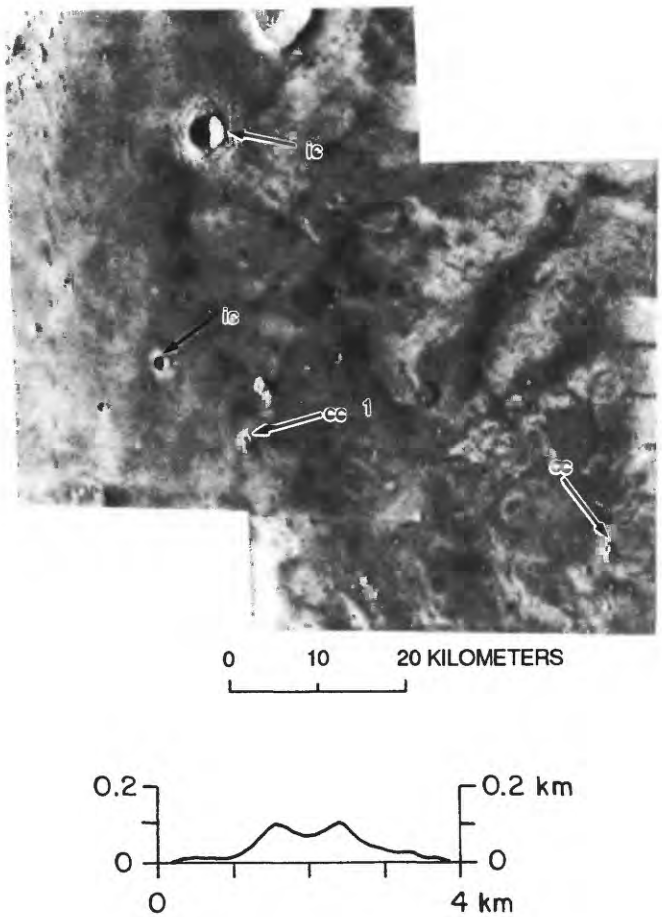

E, Cratered cones, with representative profile. Arrows denote cratered cones (cc) that are probably volcanic, as evidenced by summit craters whose floors lie well above surrounding plain, in contrast to impact craters (ic), which are initially deeper than rim is high above plain on which impact occurred. This relation is demonstrated by respective shadow lengths of rim and crater walls. Breached volcanic cone (at 1) shown in profile; vertical exaggeration, 5×. Sun illumination from left. Viking Orbiter frames 3A01 and 3A02.

MINOR PLAINS PROVINCES

UTOPIA-ISIDIS REGION

SMALL VOLCANIC FEATURES

UTOPIA PLANITIA NORTHWEST

Mosaic: 211–5078 MC: 6A Coordinates: 47°–51° N., 284°–291° W.

Province description:
Arcuate, parallel, narrow, segmented ridges.

Elevation (km)	0
Approximate dimensions (ridge segments)	commonly 5–10 km long, from several hundred meters to 1 km wide

Stratigraphic age:
Hesperian; ridged member of the Vastitas Borealis Formation

DISCUSSION

Carr and Schaber (1977) suggested that the stripes or segmented ridges in the Utopia Planitia Northwest province are remnants of ice-rich mantles, produced by melting of ground ice and deflation of the mantles by wind. Rossbacher and Judson (1981) preferred to interpret these features as solifluction lobes or ice-cored ridges, whereas Parker and others (1989) suggested that similar ridges in Deuteronilus Mensae, to the west, could be analogous to strandlines formed at the shore of a standing body of water subject to multiple floods. The pattern of these segmented ridges somewhat resembles that of recessional moraines, but no cause for localization of a relatively small ice mass in this area is apparent.

Although resolution is not high enough to discern fine details, some ridge segments appear to consist of rows of cratered cones or domes (arrows, fig. 31). Thus, these chains may be similar to the chains of cratered cones visible at higher resolution in the Isidis Planitia province (see figs. 34*B*, 34*C*). The regular, curvilinear pattern indicates probable fracture control of the cone chains. No other obviously volcanic features are associated with these ridges.

Terrestrial cinder cones, though commonly localized along fractures, are not known to occur in so large a field with so regular a curvilinear pattern. The cone chains in the Utopia Planitia Northwest and Isidis Planitia provinces, if volcanic, appear to reflect an eruptive style or structural control different from that prevalent within cinder-cone fields on Earth.

REFERENCES

Carr and Schaber (1977)
Parker and others (1989)
Rossbacher and Judson (1981)

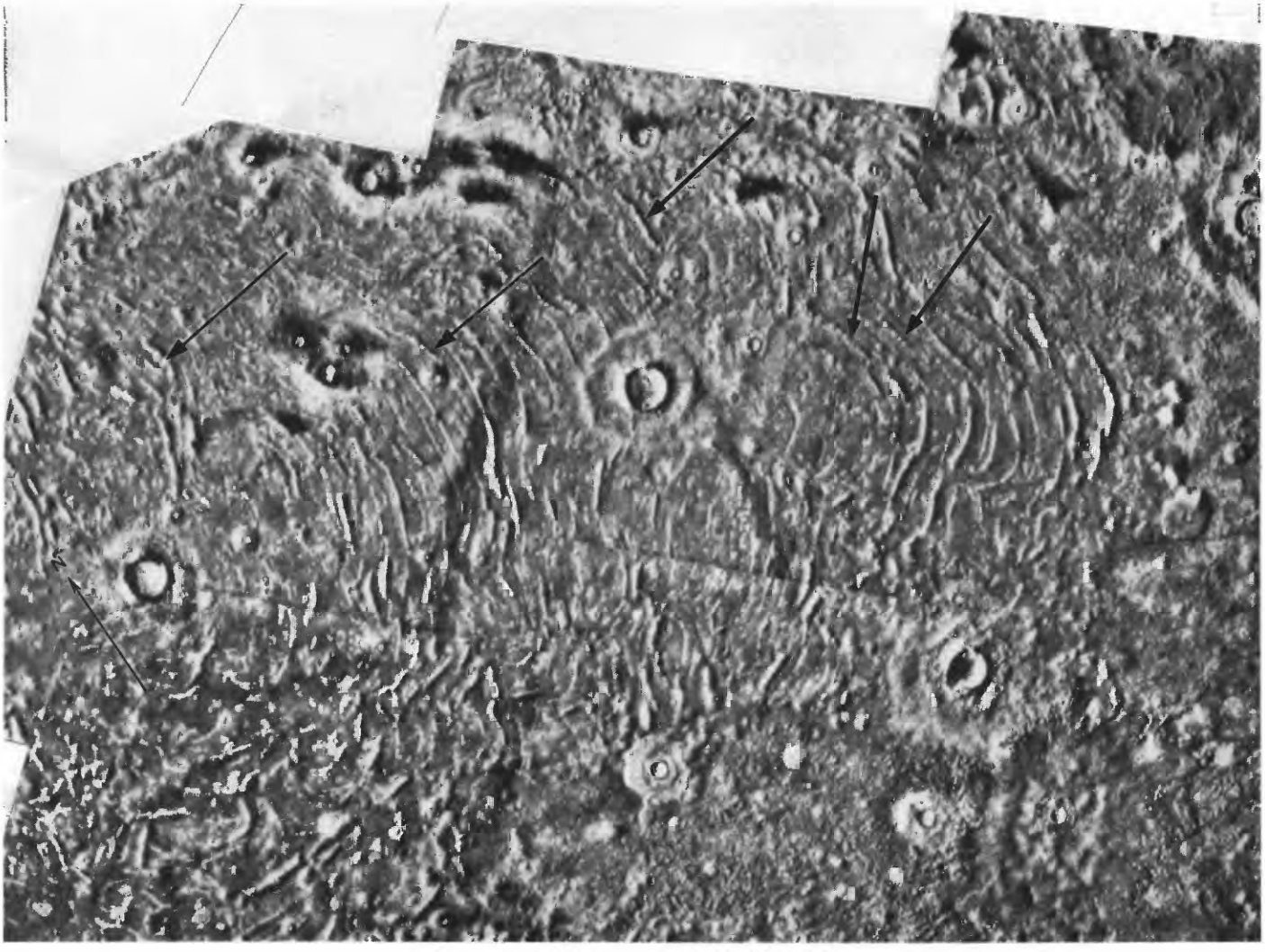

Figure 31. Utopia Planitia Northwest province, showing parallel, curvilinear ridges. Morphology of some of these ridges suggests they are actually contiguous cratered cones (arrows), but this interpretation is controversial. Sun illumination from left. Part of Viking Orbiter mosaic 211–5078.

UTOPIA PLANITIA

Mosaics: 211–5072, 211–5080 MC: 6B–7 Coordinates: 40°–50° N., 223°–273° W.

Province description:

Terrain flooded by lava that embays impact craters; includes cratered mesas that may be analogs of Icelandic tablemountains.

Elevation (km)	–2 to –1
Approximate dimensions (km):	
Tablemountain pedestal width	5–15
Relief	0.1–0.5
Estimated relative age (10^{-3} craters/km^2):	
Masursky and Crabill (1976)	1.3–4.0
Inferred age (Ga):	
Model 1	3.5–3.8
Model 2	1.2–3.4

Stratigraphic age:

Amazonian-Hesperian; members 3 and 4 of the Elysium Formation, plains and channel materials; grooved, knobby, and mottled members of the Vastitas Borealis Formation

DISCUSSION

The Utopia Planitia province contains lava flows, fractured ground, numerous impact craters, and several enigmatic features that may be related to volcanic processes (figs. 32*A*, 32*B*). Smooth dark bands and patches generally confined to channels and local depressions are here interpreted as volcanic, probably lava flows, because of their morphology, low albedo, and proximity to Elysium Mons; Christiansen (1989) interpreted them as intrachannel debris flows produced by draining of lahar deposits from the Elysium Mons area. In places, these materials are superposed on impact ejecta as lobes (fig. 32*C*). At the east edge of the province, the topography is dominated by the impact crater Mie and its ejecta. Several small, near-circular mesas with shallow, nearly rimless summit craters (figs. 32*A*, 32*D*, 32*E*) resemble Icelandic tablemountains (figs. 32*F*, 32*G*), which formed by eruption of lava beneath a Pleistocene icecap (Van Bemmelen and Rutten, 1955; Kjartansson, 1960; Einarsson, 1968; Jones, 1969, 1970). Association of the martian features with lava flows at these northern latitudes suggests that the polar icecap once extended far enough southward to permit lava/ice interaction (Hodges and Moore, 1978a, b, 1979, 1980).

In some places, however, a gradational sequence of landforms is apparent, from obvious impact craters with upraised rims and surrounding ejecta blankets of low relief, through craters whose rims and ejecta blankets merge in a domical flank shape, to craters whose ejecta blankets appear to form pedestals (fig. 32*H*). Thus, the cratered mesas here interpreted as tablemountains may be only a morphologic end member in the impact-crater series, reflecting some unique set of target conditions. McCauley (1973) attributed similar pedestals to the armoring effect of impact-crater ejecta that protected underlying terrain from erosion by wind; a scarp formed where the surrounding material had been deflated. In any case, the occurrence of lava flows indicates that volcanism was active in this area, and the terrain is highly fractured, with a mottled appearance reminiscent of patterned ground in periglacial or permafrost regions on Earth. It is at least tenable that lava could have interacted with ice in this area, and the mesas pictured are considered good candidates for volcanic features whose pedestals were formed by subglacial eruption. A possible lava cone with filled crater also has been identified (fig. 32*H*).

The Viking 2 landing site is in the northeast corner of the province at 48° N., 226° W. Estimated relative ages suggest that Utopia Planitia is Hesperian or possibly early Amazonian, but geologic relations (Greeley and Guest, 1987) suggest that this complex area is mainly Amazonian. This province is not plotted in figure I–5 because of uncertainties in the crater counts.

REFERENCES

Christiansen (1989)
Einarsson (1968)
Greeley and Guest (1987)
Hodges and Moore (1978a, b, 1979, 1980)
Jones (1969, 1970)
Kjartansson (1960)
Masursky and Crabill (1976)
McCauley (1973)
Van Bemmelen and Rutten (1955)

► **Figure 32.** Utopia Planitia. *A*, Cratered mesas and domes (arrows tm) amid probable lava flows (arrows lf) and patterned ground (pg) are promising candidates for tablemountains, analogous to those in Iceland formed by subglacial eruptions. Boxes at lower left and upper right outline areas of figures 32*D* and 32*E*, respectively. Sun illumination from left. Part of Viking Orbiter mosaic 211–5072.

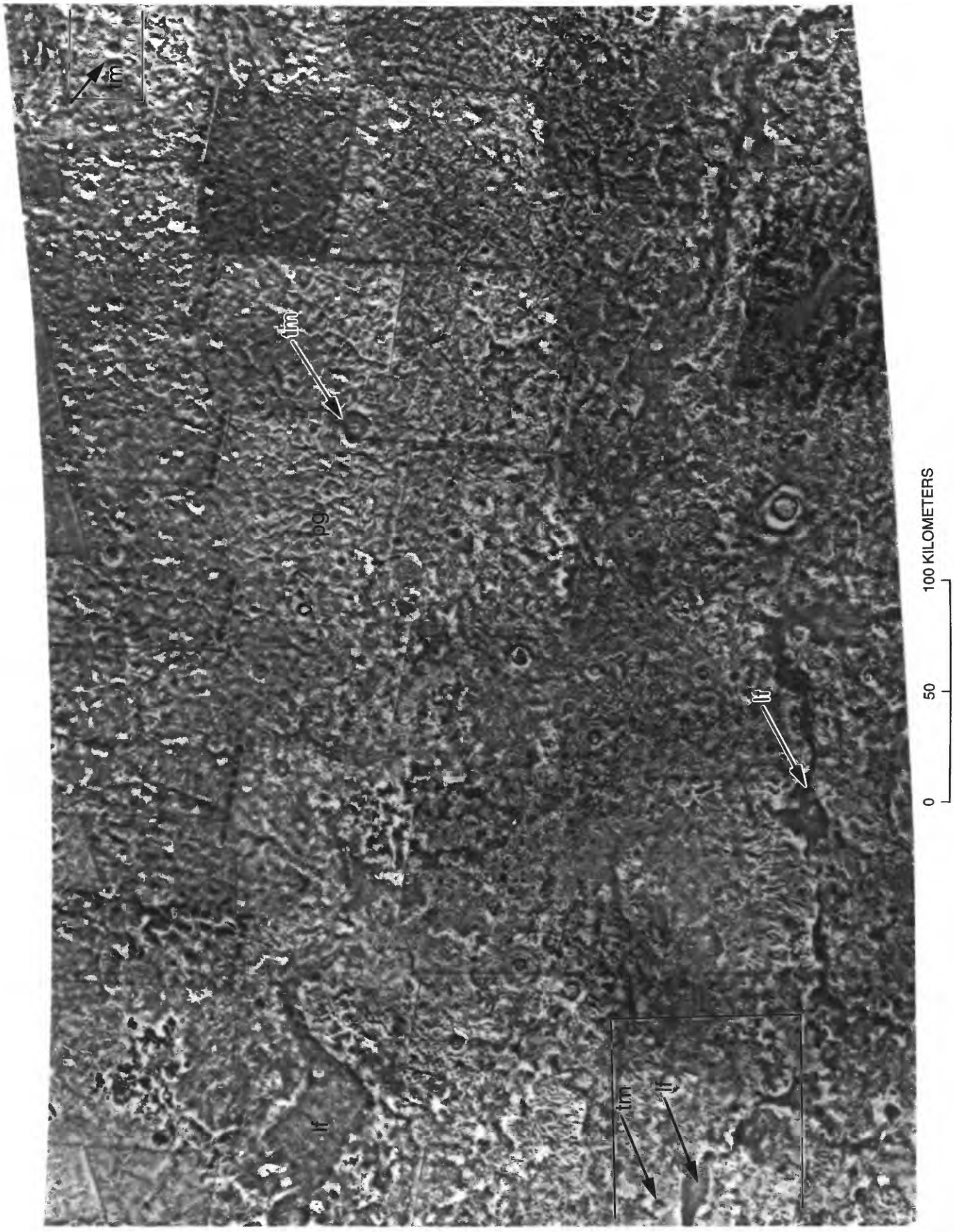
tm
pg
lf
lf
lf
tm
lf
0
50
100 KILOMETERS

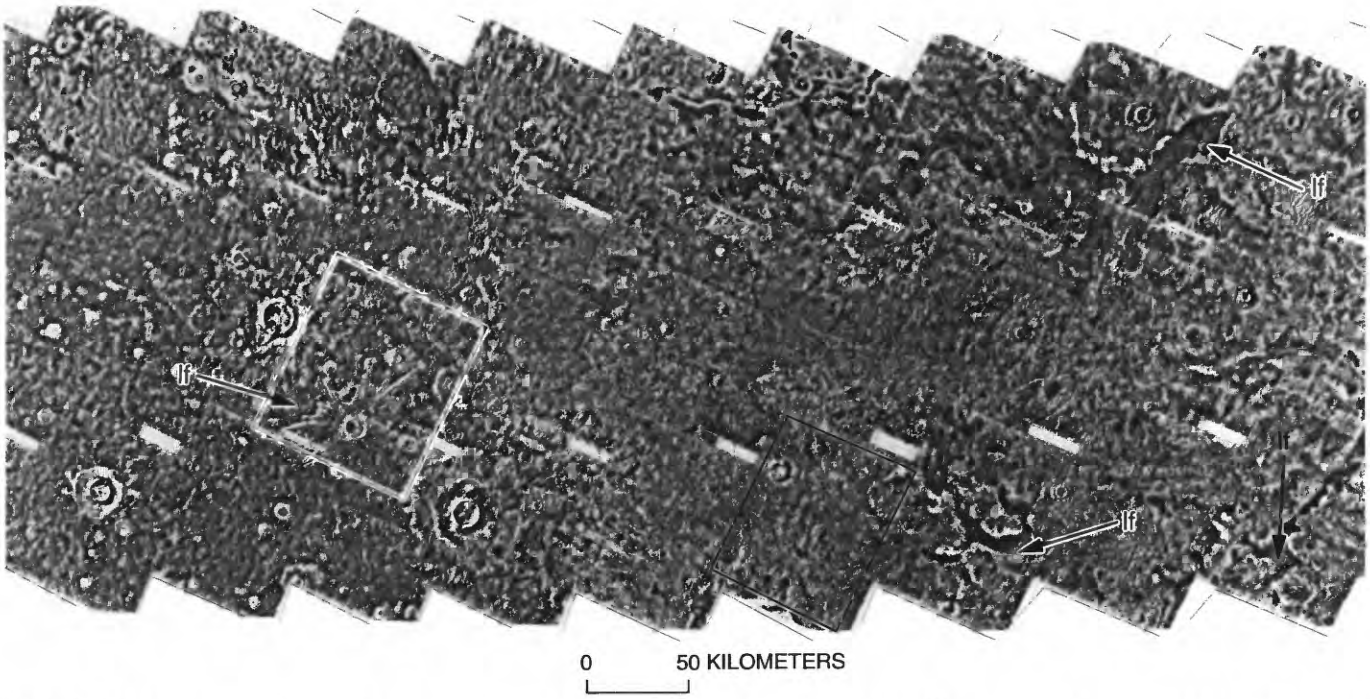

B, Probable lava flows (arrows lf) characterized by low albedo and narrow, ribbonlike pattern in topographically low pathways. Boxes at left and lower center outline areas of figures 32*C* and 32*H*, respectively. Sun illumination from left. Part of Viking Orbiter mosaic 211–5080.

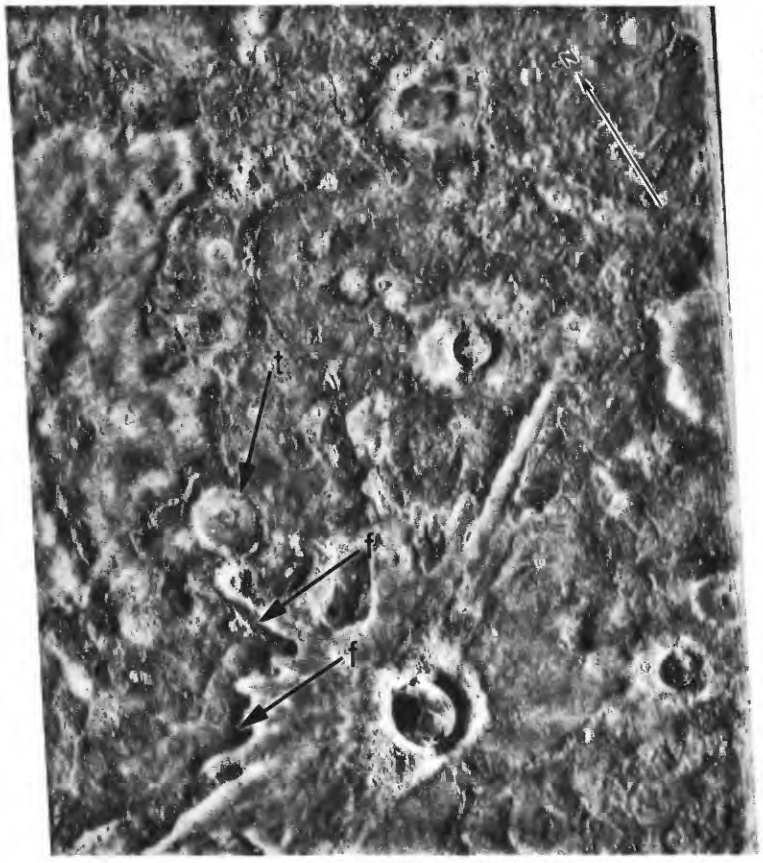

◄ *C*, Flow material (arrows f), probably volcanic, that appears to have overridden impact-crater ejecta. Mesa (arrow t) is plausible candidate for tablemountain. Sun illumination from left. Viking Orbiter frame 10B52.

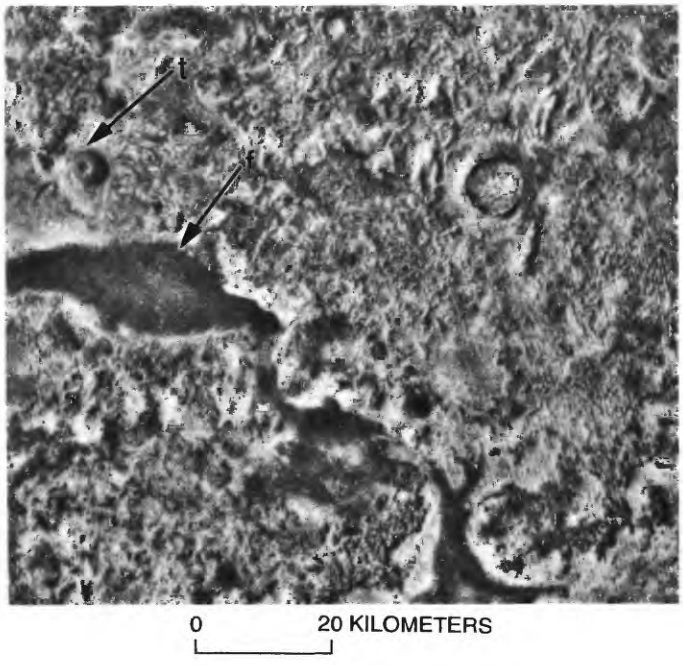

► *D*, Probable lava flow (arrow f), as suggested by low albedo and morphology indicative of fluid emplacement, and possible tablemountain (arrow t). Sun illumination from left. Viking Orbiter frame 9B22.

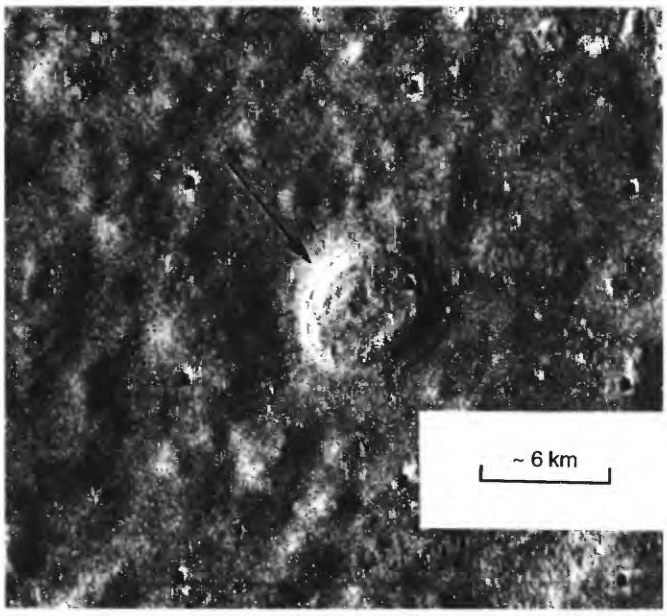

◄ *E*, Type example of possible tablemountain, analogous to those in figures 32*F* and 32*G* (from Hodges and Moore, 1979). Sun illumination from left. Viking Orbiter frame 9B15.

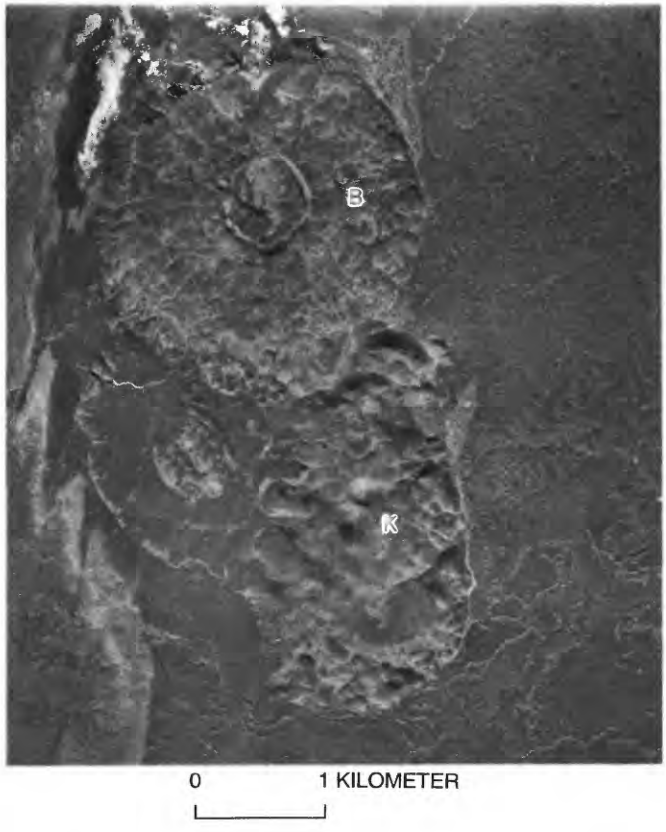

► *F*, Bæjarfjall (B) and Kvíhólafjöll (K), two Icelandic tablemountains composed almost entirely of moberg (hyaloclastite). These features, not capped by subaerial lava flows, either formed entirely subglacially or were eroded after emplacement so that basaltic caprocks were largely removed. Both tablemountains have summit depressions. Sun illumination from lower left. U.S. Air Force photograph AF–55–AM–3, roll 121, frame 13394, taken August 24, 1960; courtesy of R.S. Williams.

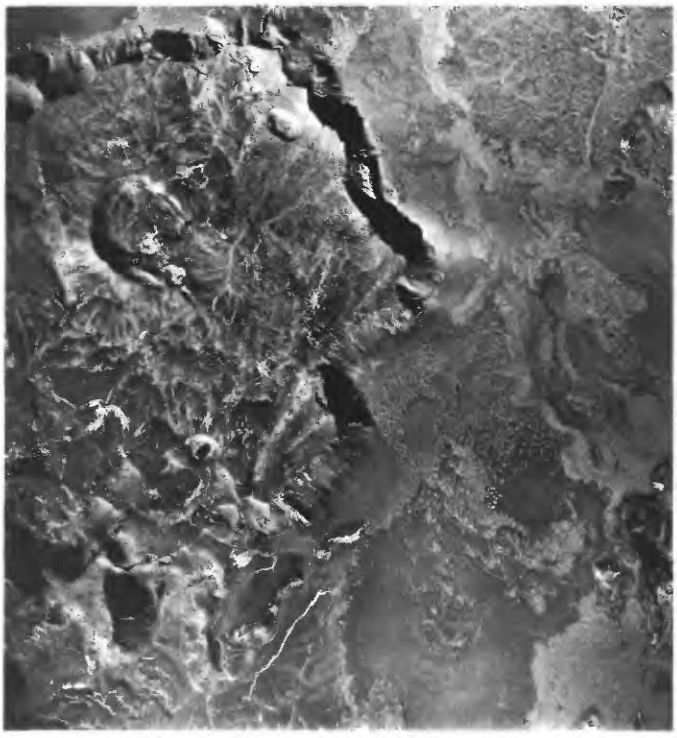

◄ *G*, Gæsafjöll, Iceland, excellent example of a tablemountain capped by subaerial lava flows, with well-preserved summit crater and secondary collapse depressions. Both tablemountain and surrounding terrain are morphologically similar to features in Utopia Planitia province (figs. 32*A*, 32*D*). Sun illumination from lower left. U.S. Air Force photograph AF55–AM–3, roll 127, frame 14125, taken August 28, 1960.

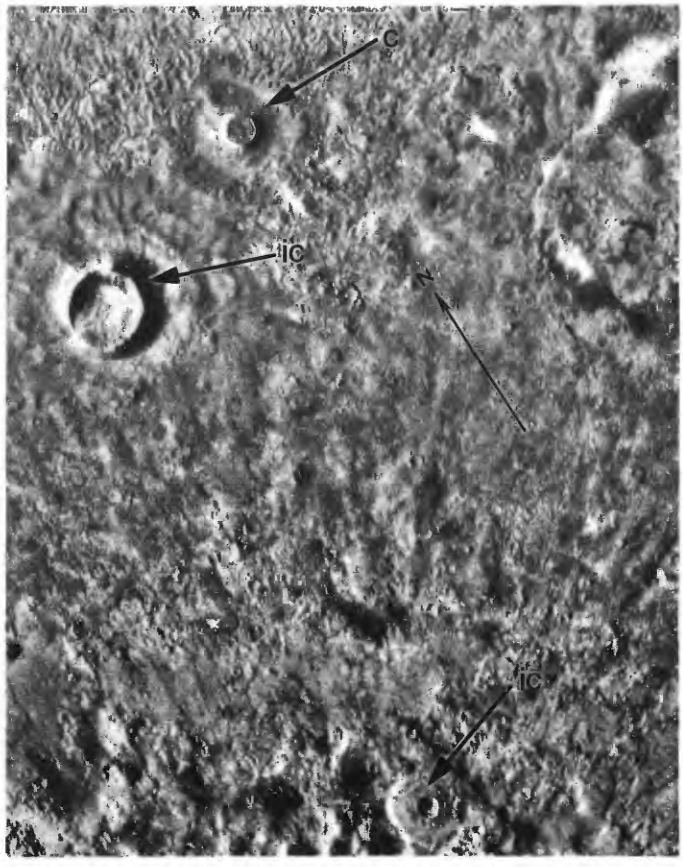

► *H*, Possible lava cone (arrow c) with filled summit crater. Typical impact craters (arrows ic) have floors below or at level of surrounding terrain, depending on degree of postimpact erosional modification, whereas summit crater of lava cone before filling appears to have been higher than surrounding terrain. A demonstrably broad spectrum of impact-crater morphologies on Mars, however, lends uncertainty to volcanic interpretations in this part of northern plains. Ejecta around impact crater at bottom center appears to have formed a slight pedestal. Sun illumination from left. Viking Orbiter frame 10B59.

UTOPIA PLANITIA SOUTH

Mosaics: 211–5781, MC: 6C–14 Coordinates: 24°–36° N., 254°–277° W. 211–5884

Province description:

Arcuate, segmented ridges, and furrows with axial ridges; cratered cones occurring singly, as doublets, as triplets, in longer chains, and atop mesas or platforms.

Elevation (km)	–2 to 0
Approximate dimensions (m):	
Ridge length	1,000–5,000
Ridge width	1,000
Mesa width	1,000–5,000
Base diameter (cones or domes)	300–1,000
Relief (shadow measurement)	70–80

Stratigraphic age:

Amazonian-Hesperian; smooth- and knobby-plains materials; ridged and grooved members of the Vastitas Borealis Formation

DISCUSSION

The localized concentration of wormlike ridges in the Utopia Planitia South province (fig. 33*A*) is puzzling. Small remnants of plateau materials (to the southwest) are scattered about the area, but the ridges are distinctive, and some appear to be composed of conelike or domelike elements (fig. 33*B*). No summit craters are visible on these ridges, but the entire area appears to be mantled by unconsolidated material. The ridges may be coalescent volcanic cones or domes, similar to those in the Utopia Planitia Northwest province (fig. 31). The relation, if any, of these rounded ridges to the curvilinear troughs with narrow axial ridges (fig. 33*B*) is unclear. Lucchitta and others (1986) pointed out the striking resemblance of these ridges-in-troughs to features in Antarctica that form where ice streams converge, and they suggested that in this area of Mars, ice-related mechanisms are likely responsible for much of the landscape.

Some cratered cones or domes are similar to those in the Acidalia Planitia province (fig. 29*C*) but far less numerous and less densely clustered (fig. 33*C*). Fractures are not evident, but the linear and arcuate chains of cones (arrows, figs. 33*C*, 33*D*) probably reflect some type of structural control. Some small mesas also support knobs and cratered cones (arrows m, figs. 33*C*, 33*D*). The tops of a few of these mesas have marginal fractures, giving them the appearance of pressure plateaus within lava flows, as in the Acidalia Planitia province (fig. 29H), rather than erosional remnants. Those mesas topped by knobs and cratered cones somewhat resemble the two-story tablemountains in Iceland that have subaerial shields atop steep-sided pedestals of hyaloclastite, formed by subglacial eruptions (figs. 33*E*, 33*F*). A superficially similar morphology can be produced by an entirely different terrestrial mechanism, however (fig. 33*G*): At Syowa Sinsan, Japan, upward heaving of the ground surface by intrusion created a mesalike mountain, about 200 m high and 1 km across at the base. Explosive venting along a ring fracture culminated in the central protrusion of a dacite dome that eventually rose 110 m above the mesa (Williams and McBirney, 1979). Although the relatively silicic composition of this dome makes it an unlikely analog for martian landforms, clearly, interpretations of some extraterrestrial features on the basis of morphology alone cannot be considered conclusive.

REFERENCES

Lucchitta and others (1986)
Van Bemmelen and Rutten (1955)
Williams and McBirney (1979)

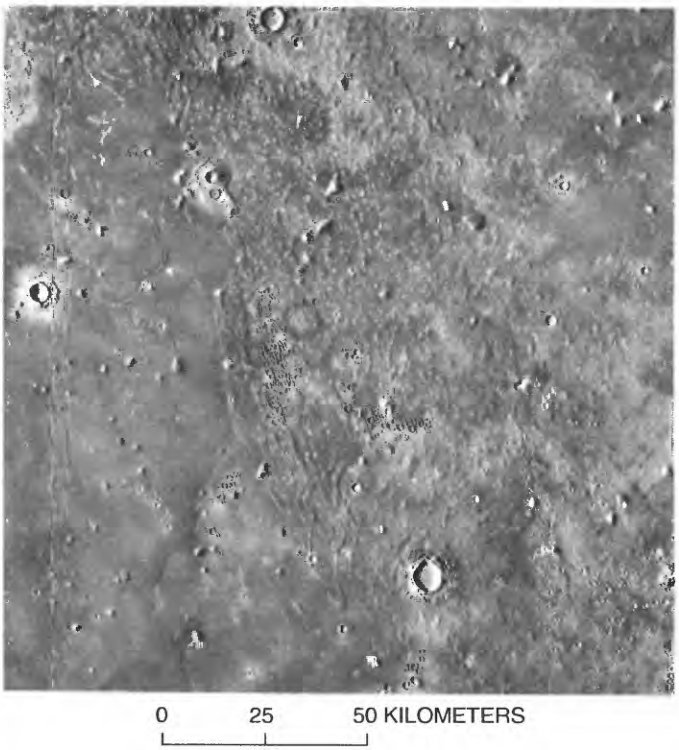

◄ **Figure 33.** Utopia Planitia South. *A*, Lava plains in southern part of province, showing narrow arcuate ridges that may be composed of coalescent volcanic cones. Dark ring in center and vertical band on left side of image are artifacts. Sun illumination from left. Viking Orbiter frame 572A06.

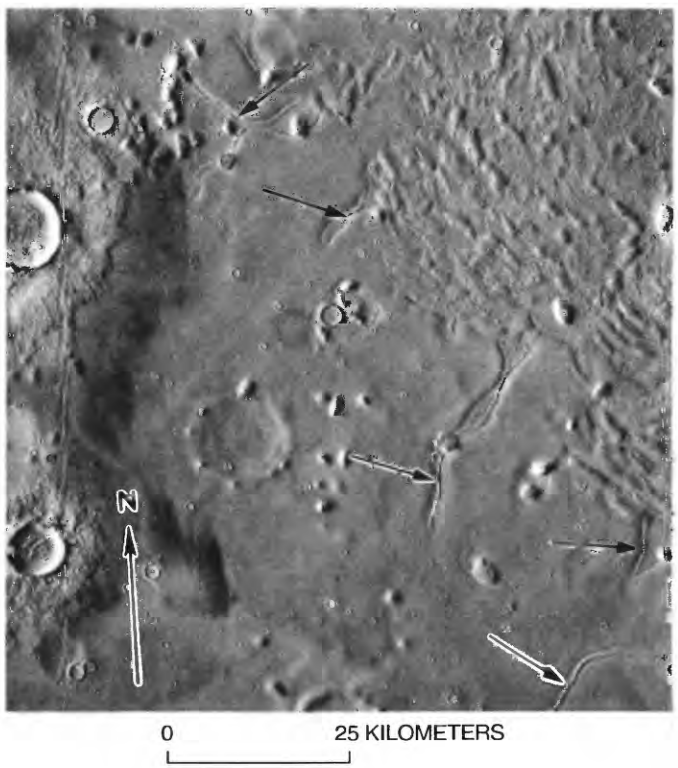

► *B*, Transition from curvilinear-ridge field to adjacent plain. Meandering troughs and narrow axial ridges (arrows) may be ice related (Lucchitta and others, 1986). Dark ring in center and vertical bands on left and right sides of image are artifacts. Sun illumination from left. Viking Orbiter frame 608A06.

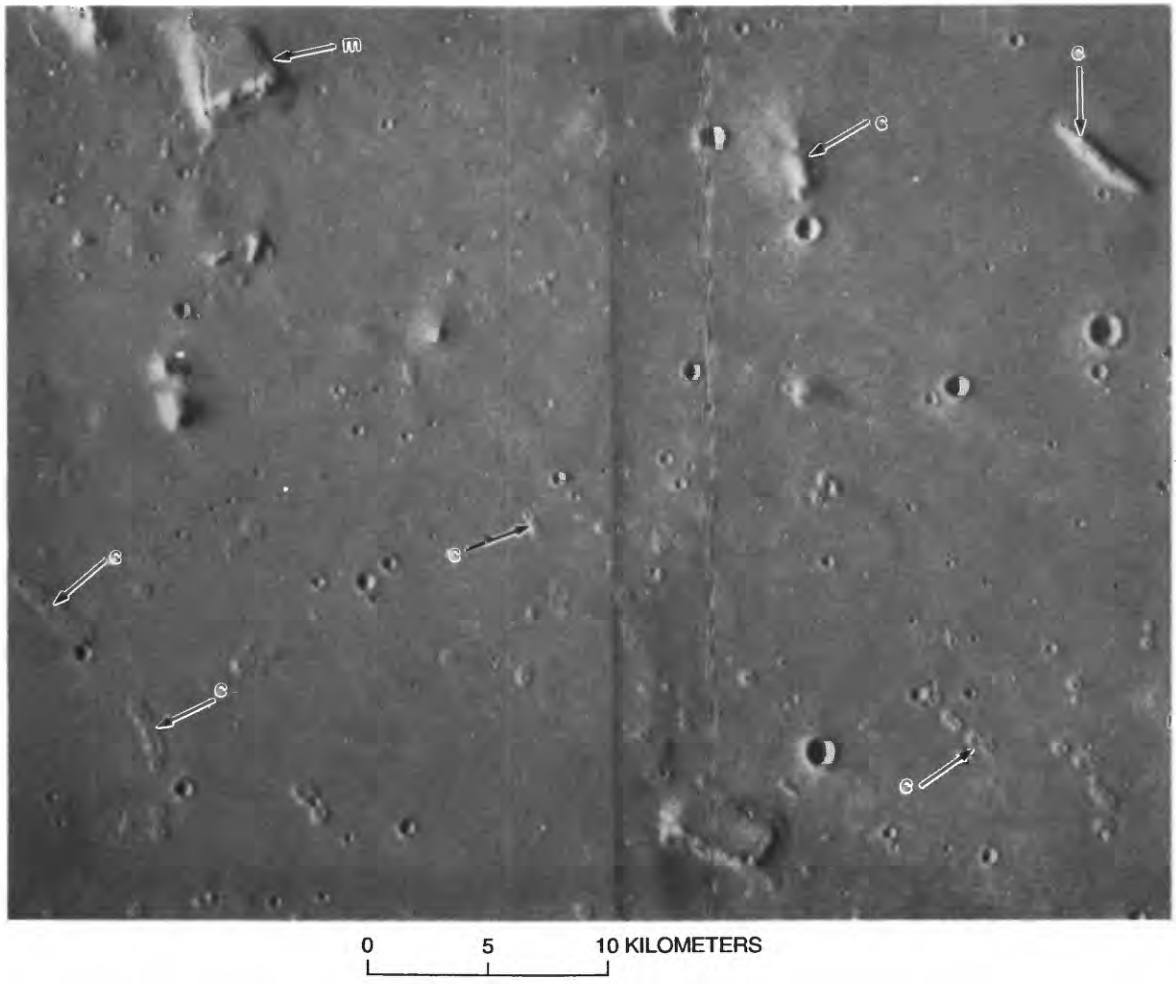

C, Lava plains in southern part of province, showing chains and clusters of cratered cones (arrows c) and mesas (arrow m) with marginal fractures that resemble terrestrial pressure plateaus (see fig. 29*H*). Sun illumination from left. Viking Orbiter frames 645A10 and 645A12.

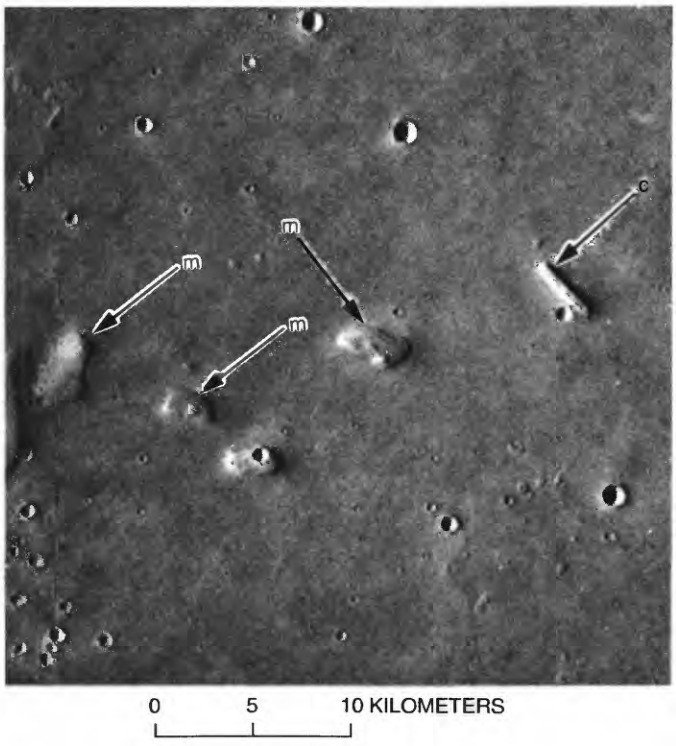

D, Cratered cone chains (arrow c) and mesas (arrows m) with superjacent cratered cones or knobs. Such mesas are morphologically similar to two-story Icelandic tablemountains (subaerial shield volcanoes atop pedestals of hyaloclastite), which were formed by subglacial eruptions (figs. 33*E*, 33*F*). A terrestrial structure of similar morphology but very different origin is shown in figure 33*G*. Sun illumination from left. Viking Orbiter frame 645A07.

E, Herdubreid, highest tablemountain in Iceland, with more than 1,000 m of relief. Shield volcano is superposed on subaerial lava flows at top of cliff; intercalated palagonite tuff breccia (moberg or hyaloclastite) and columnar basalt form basal pedestal, as shown in figure 33*F*. Photograph by C.A. Wood, courtesy of the photographer.

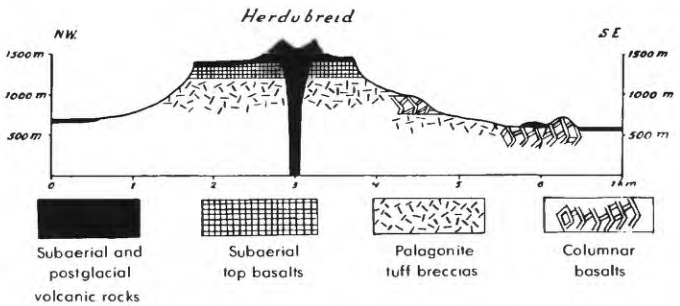

F, Diagrammatic cross section through Herdubreid. From Van Bemmelen and Rutten (1955); copyright © 1955 by E.J. Brill, Inc., used with permission.

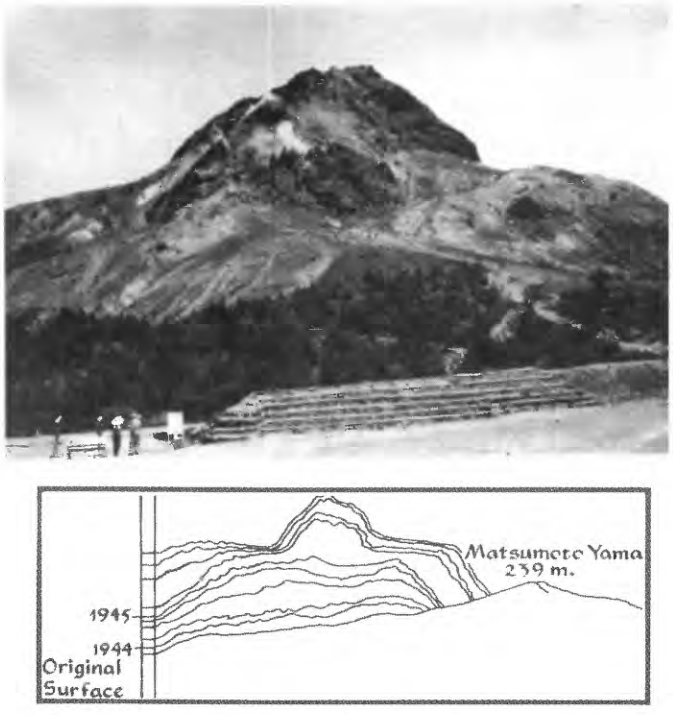

G, Dome of Syowa Sinsan, Japan, in 1962, with profiles during successive stages of its growth. Overall morphology appears to be superficially similar to that of some tablemountains, but dome is of totally different origin and thus exemplifies the difficulty of drawing analogies for extraterrestrial features on the basis of morphology alone. From Williams and McBirney (1979); copyright © 1979 by Jones and Bartlett, Inc., used with permission.

ISIDIS PLANITIA

Mosaics: 211–5579, MC: 13B–14 Coordinates: 5°–25° N., 262°–282° W. 211–6054

Province description:

Long, curvilinear chains of coalescent cratered cones in a distinctive semiparallel arrangement; individual cones, doublets, and short chains also prevalent.

Elevation (km)	–2 to 0
Approximate dimensions (m):	
Individual cone diameter	200–400
Chain length	2,000–20,000+
Relief	30–100

Stratigraphic age:

Amazonian-Hesperian; smooth- and knobby-plains materials; ridged member of the Vastitas Borealis Formation

DISCUSSION

The cone chains in the Isidis Planitia province are visible as narrow arcuate ridges on Viking Orbiter B images (fig. 34*A*), but their distinctive morphology was not apparent until high-resolution Orbiter A images (figs. 34*B*, 34*C*) became available during the extended Viking mission. The ridges clearly are composed of coalescent cones within a densely populated field of cratered cones. Grizzaffi and Schultz (1989) suggested that these arcuate, segmented ridges and cratered cones are residua from ice-rich deposits that covered the Isidis Basin (fig. I–4), and that the craters atop knobs and ridges were formed by ablation of ice cores, a mechanism also suggested by Rossbacher and Judson (1981). The pattern of the ridges at low resolution (fig. 34*A*) is reminiscent of recessional moraines, but high-resolution images seem to preclude such an origin.

The cratered surfaces of the cones (figs. 34*C*) and their configuration in chains support a volcanic interpretation. Although Frey (1986) suggested that these cones could be pseudocraters, distinct chains are not characteristic of terrestrial pseudocrater fields, and the mechanism of their formation (lava flowing over wet ground; Thorarinsson, 1953) seems to dictate a random orientation. Ronald Greeley (written commun., 1990) noted that some pseudocraters in Iceland appear to be related to lava tubes and thus could be aligned, but the parallel and arcuate configuration of so many ridges in this area on Mars makes such an explanation unlikely. Neither are such arcuate patterns and long cone chains duplicated in terrestrial cinder-cone fields or groups of low shield volcanoes, although doublet, elongate, and aligned vents are common (fig. 34*D*). If these extensive curvilinear chains are volcanic and their pattern is governed by crustal fracturing, such structural control is apparently unique to Mars. Because volcanism seems best able to explain these features, it also is favored, by extrapolation, in other areas where high-resolution images are unavailable and only the arcuate pattern of similar, closely spaced ridges is observed—for example, in the Utopia Planitia Northwest, Utopia Planitia South, and Phlegra Montes provinces.

REFERENCES

Carr and Greeley (1980)
Frey (1986)
Grizzaffi and Schultz (1989)
Rossbacher and Judson (1981)
Thorarinsson (1953)

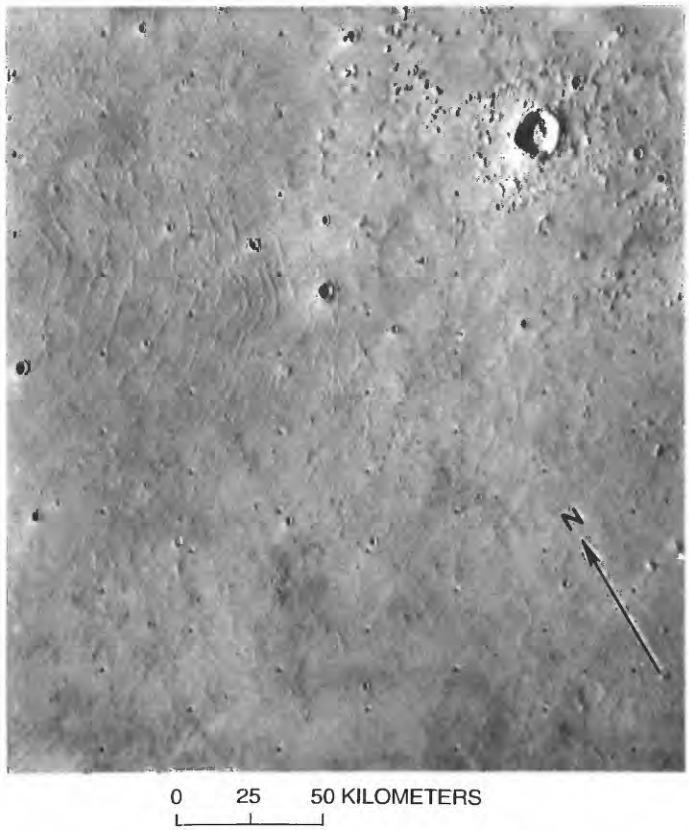

Figure 34. Isidis Planitia. *A*, Narrow curvilinear ridges. At this resolution (220 m/pixel), cratered-cone components of ridges are unresolved, and ridges resemble those in Utopia Planitia Northwest, Utopia Planitia South, and Phlegra Montes provinces. Sun illumination from left. Viking Orbiter frame 67B55.

B, High-resolution image of Isidis Planitia ridges. At this resolution (26 m/pixel), ridges clearly are composed of coalescent cratered cones, and a volcanic origin appears to be plausible. Sun illumination from left. Viking Orbiter frame 146S21.

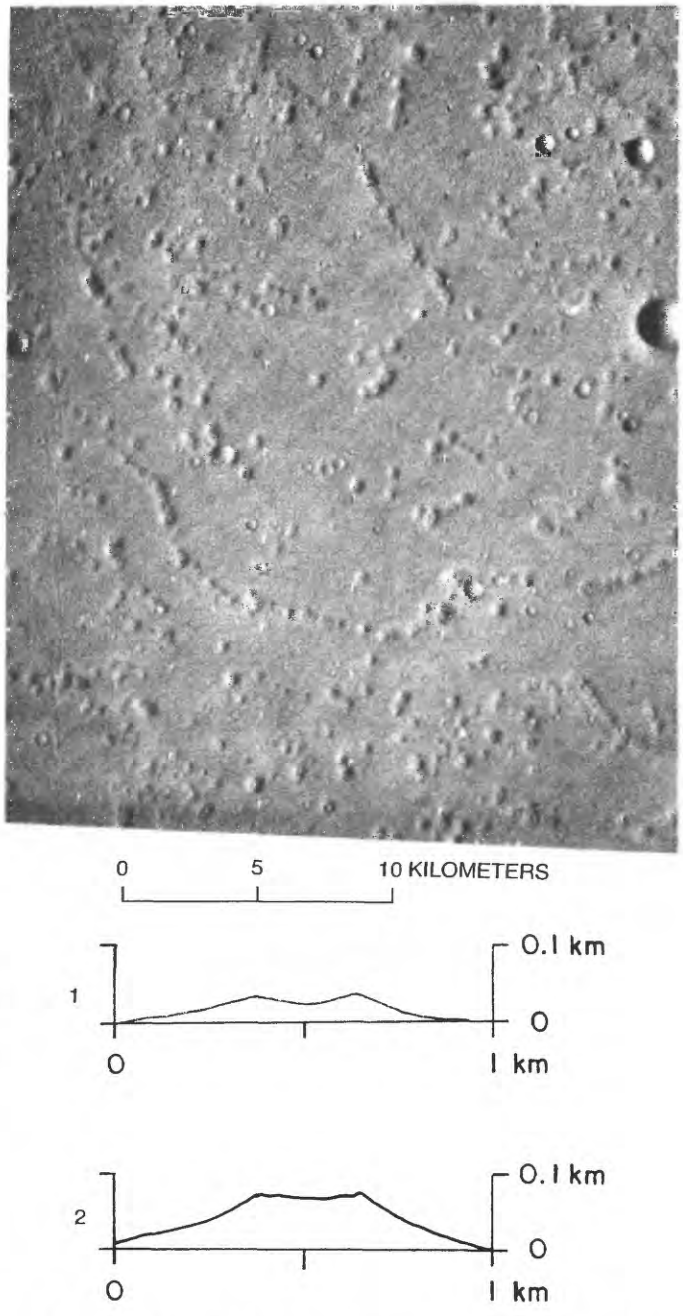

C, Cones and crater chains, with representative profiles. Features are morphologically similar to vents in the San Francisco volcanic field, Ariz., that are structurally aligned (fig. 29*E*), and to chains of cinder cones along southwest rift zone of Mauna Loa, Hawaii (fig. 34*D*). Sun illumination from left. Viking Orbiter frame 146S13. Profile 1 dimensions: crater diameter (*c*), 270 m; base diameter (*b*), 800 m; relief (*h*), 33 m; crater-diameter-to-base-diameter (*c*/*b*) ratio, 0.33; height-to-base (*h*/*b*) ratio, 0.04. Profile 2 dimensions: *c*, 270 m; *b*, 1,000 m; *h*, 72 m; *c*/*b* ratio, 0.27; *h*/*b* ratio, 0.07.

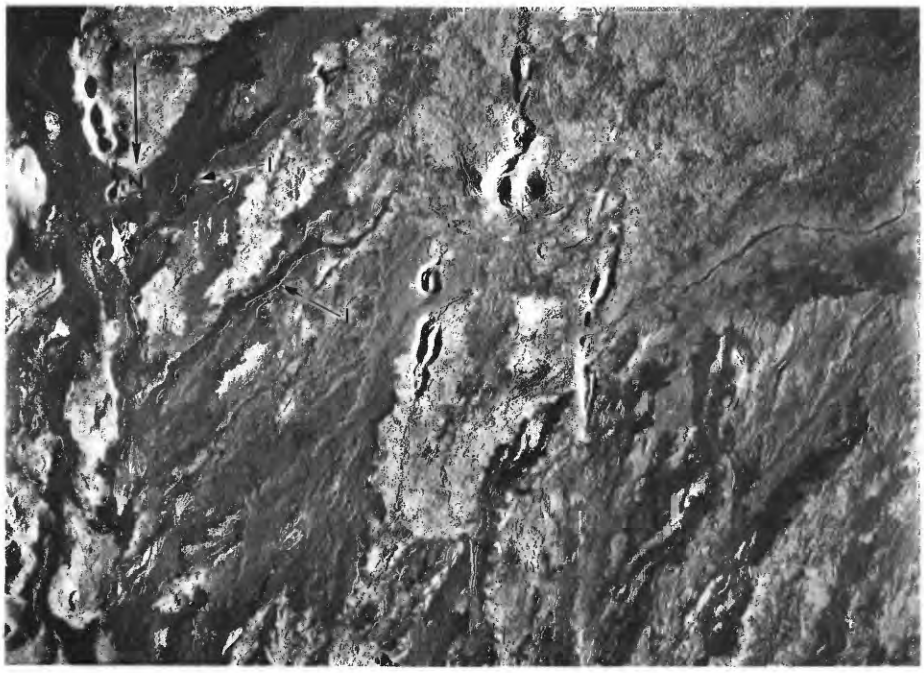

D, Southwest rift zone of Mauna Loa, Hawaii, showing characteristic elongate cinder cones and cone chains aligned along fissures. Lavas (arrows) flowed southward (toward top). Sun illumination from left. From Carr and Greeley (1980); photograph courtesy of Ronald Greeley.

PHLEGRA MONTES

Mosaics: 211–5579 MC: 7A Coordinates: 43°–55° N., 178°–210° W.

Province description:

Localized region of narrow curvilinear ridges; irregular pattern of rilles and troughs, some with axial ridges and cones.

Elevation (km)..... –2 to 0

Approximate dimensions:

Ridge segments, 10–30 km long by a few hundred meters to 1 km wide; troughs, tens of kilometers long by 2–4 km wide

Stratigraphic age:

Amazonian-Hesperian-Noachian; knobby- and smooth-plains materials; grooved, knobby, ridged, and mottled members of the Vastitas Borealis Formation; undivided material

DISCUSSSION

Narrow, arcuate, segmented ridges in the Phlegra Montes province (fig. 35*A*) appear at high resolution to be composed of cone elements, resembling ridges in the Isidis Planitia province that are better photographed and more widely distributed (figs. 34*B*, 34*C*). These features may be volcanic cones and domes; the curvilinear chains may be structurally controlled, but no such patterns have been described on Earth. Alternative interpretations for somewhat-similar features are ice-cored ridges or solifluction lobes, as in the Utopia Planitia Northwest province (Rossbacher and Judson, 1981), or beach ridges and bars, as in Deuteronilus Mensae (Parker and others, 1989).

The meandering troughs are even more enigmatic (fig. 35*B*). At 50° N., this landscape could be the product of glacial phenomena or ground ice. Such troughs and their included mesas may reflect topography buried by thin, overlying sedimentary deposits that contained substantial amounts of water and contracted on freezing at temperatures as low as –110°C at this latitude (Lucchitta and others, 1986; McGill, 1989). If volcanism occurred locally, however, and ground ice were prevalent, lava/ice interaction could have caused melting of ice and consequent ground failure along bedrock fractures. Cones are superposed on some of the troughs (figs. 35*B*, 35*C*), and an axial ridge or linear flow pattern is also discernible (fig. 35*C*). Lucchitta and others (1986) described a similar ridge-in-trough topography in Antarctica where iceflows converge. The troughs probably are not exclusively volcanic in any case, whereas the curvilinear, segmented ridges (fig. 35*A*) may be.

REFERENCES

Greeley and Guest (1987)
Lucchitta and others (1986)
McGill (1989)
Parker and others (1989)
Rossbacher and Judson (1981)

Figure 35. Phlegra Montes. *A*, Segmented, arcuate ridges (lower half of image) at about 51° N., 182° W., possibly composed of coalescent cones similar to those in Isidis Planitia province that may be volcanic. Area was mapped as ridged member of the Vastitas Borealis Formation by Greeley and Guest (1987), who suggested that ridges may be products of periglacial or erosional processes or, in the Isidis Basin, eruption of spatter cones along lines of vents. Sun illumination from right. Viking Orbiter frame 810A29.

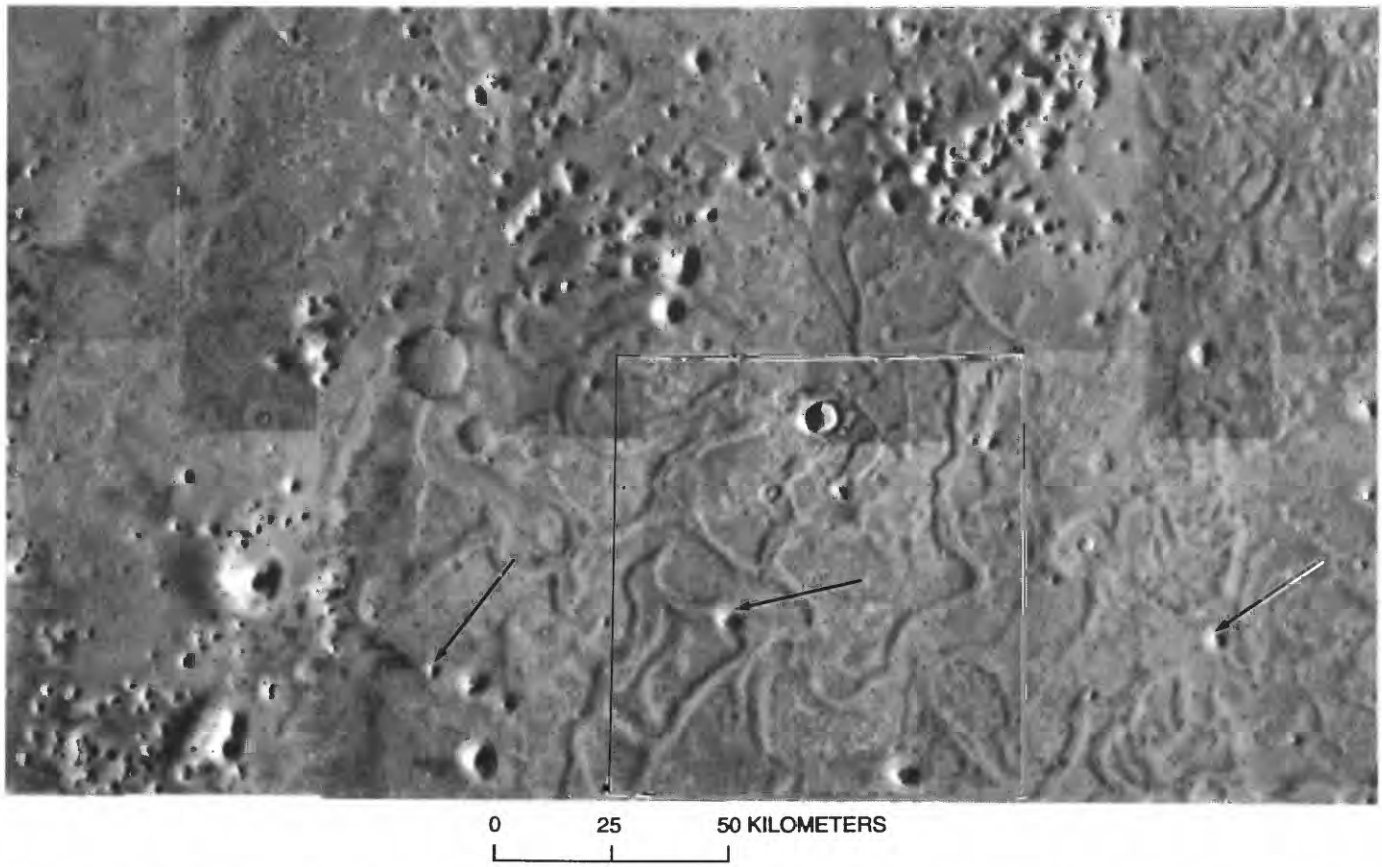

B, Network of broad, meandering troughs; arcuate ridges (fig. 35*A*) are visible to north. Cluster of knobs at top center appears to comprise eroded remnants of crater ejecta. Arrows denote a few similar, conelike features that interrupt troughs and thus could be younger and, conceivably, volcanic. Landscape may be partly attributable to interaction of volcanism with glacial phenomena or permafrost. Box at bottom right outlines area of figure 35*C*. Sun illumination from left. Part of Viking Orbiter photomosaic subquadrangle MC–7SE (U.S. Geological Survey, 1981b).

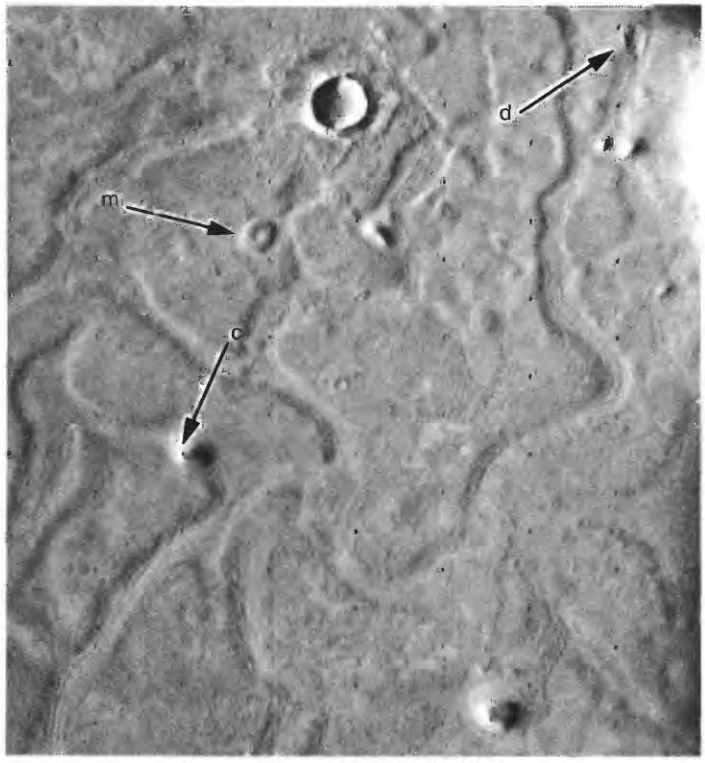

C, Troughs and superposed cone (arrow c). Possible collapse depression (arrow d) may be volcanic in origin; cratered mesa (arrow m) lacks typical impact morphology. Sun illumination from left. Viking Orbiter frame 76B86.

HIGHLANDS PROVINCES

LARGE CALDERAS

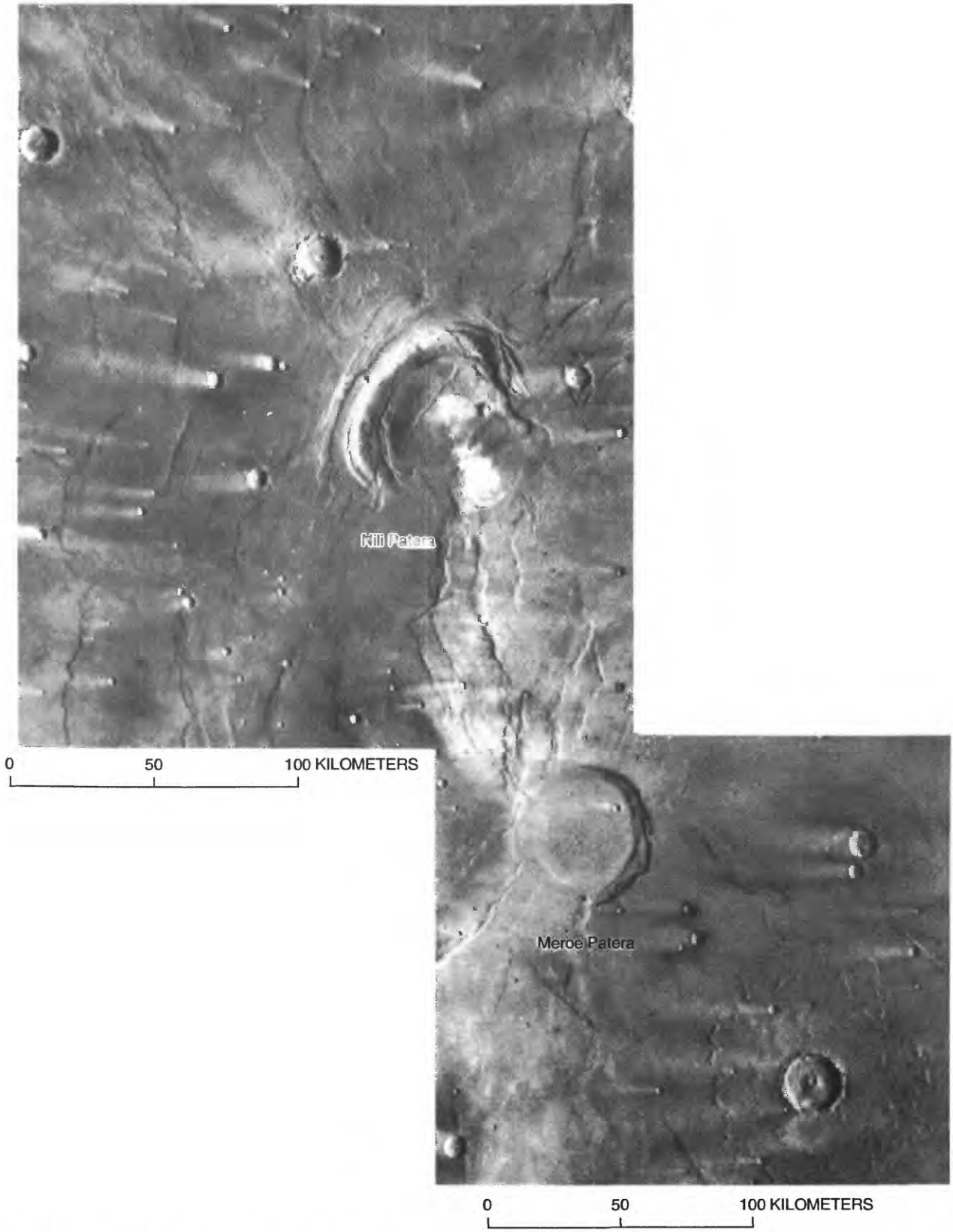

Figure 36. Syrtis Major. *A*, Two calderas, Nili and Meroe Paterae, within volcanic plain. Conspicuous light streaks extending westward from small impact craters are caused by wind. Sun illumination from right. Viking Orbiter frames 375S13 and 375S32.

SYRTIS MAJOR—NILI AND MEROE PATERAE

Mosaics: 211–5862, 211–6059 MC: 13A Coordinates: 7°–9° N., 292°–293° W.

Province description:
Two adjacent large calderas, partly foundered.

Elevation (km)	4
Approximate dimensions (km):	
Nili Patera (NW) diameter	60 by 70
Meroe Patera (SE) diameter	50
Shield diameter (Schaber, 1982)	1,100
Estimated relief	0.5
Estimated relative age (10^{-3} craters/km^2)	2
Inferred age (Ga):	
Model 1	3.6
Model 2	1.9

Stratigraphic age:
Hesperian; Syrtis Major Formation

DISCUSSION

Two calderas (fig. 36*A*) occur within the volcanic plain of Syrtis Major (fig. I–4), which appears to be essentially a broad, shieldlike lava plateau (or planum). According to Schaber (1982), there is no evidence of a preexisting impact basin, although Schultz and Frey (1990) proposed that the west juncture of the plateau with the cratered highlands marks the outer ring of a basin overlapped on the northeast by the younger Isidis Basin (Wilhelms, 1973). The northwest vent (Nili Patera) was recognized and mapped by Scott and Carr (1978), but the shieldlike morphology of Syrtis Major first became evident in a radar topographic profile (Schaber and others, 1981; Schaber, 1982; Simpson and others, 1982) that showed the two calderas nearly coincident with a broader summit depression, 280 km in diameter. The gentle flanks of the shield are characterized by numerous radial and concentric mare-type ridges, lava flows (figs. I–4, 36*B*), and lava channels or collapsed lava tubes surrounding the calderas (Schaber, 1982). Several concentric faults mark the caldera rims. Meroe Patera is nearly circular, but Nili Patera appears to have partly foundered in the surrounding flood lavas, which probably emanated from the two calderas.

The low relief of this shield contrasts strikingly with that of the Tharsis and Elysium volcanoes. Relief is, however, comparable to that of the highlands paterae, Tyrrhena, Hadriaca, and Amphitrites, on the flanks of the Hellas Basin. Evidently, either the calderas within the highlands plateau failed to sustain eruption long enough to construct large edifices, or the viscosity of the lavas was so low, or the rate of eruption so high, that flood basalts were produced instead. An additional factor may have been lithospheric thickness, which, by mid-Hesperian time, may have been insufficient in this region to provide the pressure necessary for magma to rise to extreme heights above datum. According to crater counts, the Syrtis Major calderas are approximately equivalent in age to Hadriaca Patera and may be slightly younger than Tyrrhena Patera, but all fall within the Hesperian interval (fig. I–5).

On Earth, also, the large basaltic shield volcanoes on the continents (for example, Medicine Lake and Newberry in the Western United States, and several in Africa) have extremely low height-to-base ratios (0.01–0.02) and more gentle slopes than the large oceanic shield volcanoes. Sustained mafic outpourings on both the terrestrial continents and martian highlands appear to have produced broad, low shield volcanoes and extensive fissure flows, resulting in flood-basalt plateaus.

REFERENCES

Schaber (1982)
Schaber and others (1981)
Schultz and Frey (1990)
Scott and Carr (1978)
Simpson and others (1982)
Wilhelms (1973)

B, Lava flows (arrows f) and mare-type ridges (arrows r) northwest of Nili Patera. Sun illumination from right. Viking Orbiter frame 341S47.

TYRRHENA PATERA

Mosaics: 211–5213, 211–5730 MC: 22A Coordinates: 22° S., 253.5° W.

Elevation (km)	5
Approximate dimensions (km):	
Base diameter	160–170
Relief (Downs and others, 1975; Zisk and others, 1991)	1–1.5
Caldera diameter	6–20 by 40
Caldera depth	0.5–1
Estimated relative age (10^{-3} craters/km^2)	3.4±1.8
Inferred age (Ga):	
Model 1	3.6–3.8
Model 2	1.5–3.5
Stratigraphic age:	
Amazonian-Hesperian; Tyrrhena Patera Formation	

DISTINCTIVE CHARACTERISTICS

(1) Dumbbell-shaped caldera.
(2) Radial channels scoring flanks of shield volcano, with lava flows extending from caldera rim to more than 125 km away on ridged plains.
(3) Unusually broad channels, 3 to 8 km wide.
(4) Circumferential channel segments following grabens at north base of shield volcano.
(5) Concentric grabens and fractures with beaded series of collapse pits around parts of caldera.

DISCUSSION

Tyrrhena Patera, on the northeast flank of the Hellas Basin (fig. I–4), attracted much attention when first seen in Mariner 9 images because of its unusual caldera shape and broad radial channels (fig. 37*A*). The volcano's morphology and caldera configuration are quite distinct from those of the Tharsis and Elysium volcanoes, although King (1978) identified it as a basaltic shield volcano. Relief, negligible relative to the diameter of the volcano, is manifested by the radial pattern of the channels. Early radar data indicated that the caldera rim is about 1 km higher than the surrounding lava flows of Hesperia Planum (Downs and others, 1975); more recent data show that relief of the east rim is 1.5 km (Zisk and others, 1991). On Earth, somewhat similar, linear, slotlike vents also produce low shield volcanoes, as in Hawaii (Mauna Ulu, fig. 13*G*) and on the Snake River Plain in Idaho (fig. 37*B*), albeit orders of magnitude smaller than Tyrrhena Patera.

Curious channels and flowlike features occur at considerable distances from Tyrrhena Patera. The dumbbell-shaped caldera, the channel that drained it, and the lavas that flowed through the channel onto the ridged plains appear to be the youngest volcanic features in the province. The caldera drainage channel, initially 6 km wide, can be traced 100 km southwestward, where it becomes a partly filled, leveed channel that continues southwestward an additional 85 km, whereupon the lava that issued from this channel was deposited (fig. 37*C*). Other south-trending flows occur to the east, south, and southwest of the channel flow (fig. 37*D*). Although these flows are related to Tyrrhena Patera, their sources are unclear. Some of the flows have leveed channels with lobate termini, 5 to 50 km across, whereas others are simply tongues, as much as 20 to 50 km across. Most of the flows are transected by mare-type ridges. The array of flows, as much as 100 km wide, terminates about 800 km southwest of the Tyrrhena Patera summit. Crown and others (1991) concluded from morphologic analyses of these flows that viscosities, yield strengths, and effusion rates were lower at Tyrrhena Patera than at Alba Patera and the Tharsis volcanoes, and they suggested "a temporal evolution in the nature of martian magmas."

Greeley and Spudis (1981) concluded that the morphology of the radial channels indicates low erosional resistance of the volcano's flank deposits, which they therefore interpreted as ash flows; they considered Tyrrhena Patera to be typical of the several low shield volcanoes identifiable within the cratered highlands that exhibit channels with similar configurations. The postulated development begins with phreatomagmatic eruptions of ash, generated by invasion of magma into a water-charged regolith. Volcanism in the Hesperia Planum region probably was localized, if not induced, by formation of the Hellas impact basin (Greeley and Spudis, 1981; Schultz, 1984; Crown and Greeley, 1990b; Crown and others, 1990) and preceded formation of the Tyrrhena Patera shield (Greeley and Crown, 1990). Greeley and Crown (1990) suggested that the volcanic deposits and smooth plains that extend to the north and southwest consist of phreatomagmatic ash, whereas the flows within the caldera and extending southward from it are effusive lavas.

By analogy with Earth, the width and vertical walls of the channels suggest easily eroded materials (for example, loess and volcanic-ash deposits), but these attributes may also result from spring sapping in such competent rocks as limestone, sandstone, and basalt. The channel draining the caldera appears to be a primary lava conduit, and older channels elsewhere around the caldera could have formed similarly. The northeast flank of Mauna Kea in Hawaii (fig. 37*E*) is channeled in a pattern similar to that on the

Figure 37. Tyrrhena Patera. *A*, Tyrrhena Patera, a highlands shield volcano with unique (on Mars) dumbbell-shaped caldera (arrow). Sun illumination from right. Mosaic of Viking Orbiter frames 87A12 through 87A17.

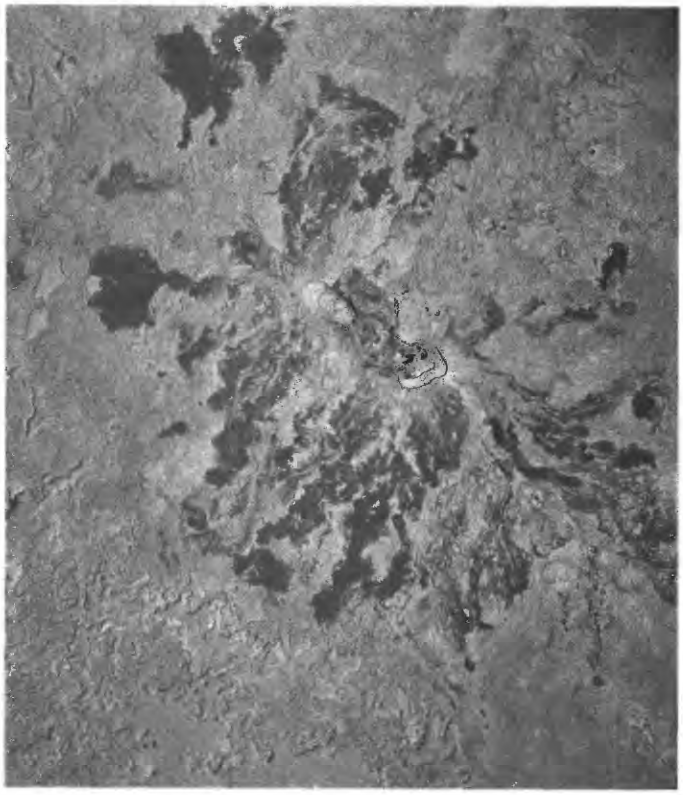

◄ *B*, Hells Half Acre vent area, Snake River Plain, Idaho, showing elongate caldera-like crater surrounded by radial lava flows and channels. Crater is aligned with other features that suggest localization of eruptions along a fracture zone. Area has low relief, like Tyrrhena Patera shield, but central vent is about 50 times smaller. Sun illumination from right. U.S. Department of Agriculture photograph CXO–1GG–31, taken May 2, 1966.

► *C*, Area southwest of Tyrrhena Patera, showing lava channel (arrow c), flows (arrows f), and mare-type ridges (arrows r). Channel at upper right develops into a flow deposit. Sun illumination from left. Viking Orbiter frame 365S42.

D, Lava plain southeast of Tyrrhena Patera. Conspicuous lava flow appears to emanate from ridge at upper left but is apparently deformed by ridges that it crosses along its path of about 200 km southward (arrows). Sun illumination from left. Viking Orbiter frame 365S62.

flanks of Tyrrhena Patera; although the flat floors of large Hawaiian channels are formed by alluvial fill, their depth and width are largely attributable to spring sapping, common in porous and permeable basalt flows. Such a process could also have operated on Mars where, as at this locality, magmatic heat may have interacted with frozen ground. The weight of evidence, however, suggests that the broadly dissected units at both Tyrrhena and Hadriaca Paterae were more likely ash-flow sheets (Crown and Greeley, 1990a, b; Greeley and Crown, 1990).

Tyrrhena Patera, like the other highlands shields, is among the oldest volcanoes on Mars (Crown and others, 1991); Gulick and Baker (1990a, b) placed it in the Noachian system, in contrast to the Amazonian-Hesperian age (see above) assigned by Greeley and Guest (1987). Relative ages imply that Tyrrhena Patera is probably Hesperian and was contemporaneous with some of the older, smaller Tharsis volcanoes (fig. I–5).

REFERENCES

Downs and others (1975)
Crown and Greeley (1990a, b)
Crown and others (1990, 1991)
Greeley (1974)
Greeley and Crown (1990)
Greeley and Guest (1987)
Greeley and Spudis (1981)
Gulick and Baker (1990a, b)
King (1978)
Schultz (1984)
Zisk and others (1991)

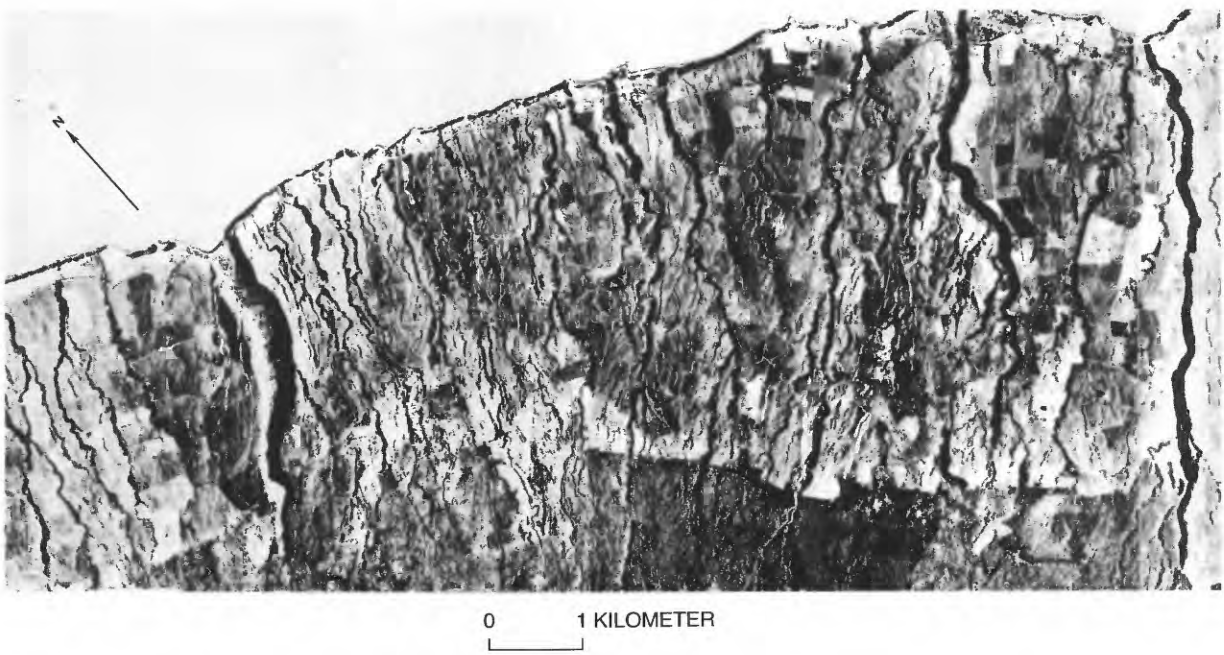

E, Mauna Kea Volcano, Hawaii, showing broad, flat-floored valleys on flanks formed largely by spring sapping. Channels are morphologically similar to those at Tyrrhena Patera. Sun illumination from right. From Greeley (1974); photograph courtesy of Ronald Greeley.

HADRIACA PATERA

Mosaics: 211–5211, 211–5213 MC: 28A Coordinates: 31° S., 267° W.

Elevation (km)	2
Approximate dimensions (km):	
Shield diameter	300 by 500
Relief	1–2
Caldera diameter	70–75
Estimated relative age (10^{-3} craters/km^2)	2.7±0.4
Inferred ages (Ga):	
Model 1	3.7
Model 2	2.1–2.9

Stratigraphic age:
Amazonian-Hesperian; older channel material of the Hadriaca Patera Formation

DISTINCTIVE CHARACTERISTICS

(1) Circular caldera.
(2) Prominent mare-type ridge on caldera floor.
(3) Radial array of densely spaced valleys.
(4) Broad, shallow depressions, some closed, with scalloped margins, near base of volcano.

DISCUSSION

As at Tyrrhena Patera, the relief of the Hadriaca Patera shield (Potter, 1976) is negligible relative to the volcano's diameter. In contrast to the flat-floored

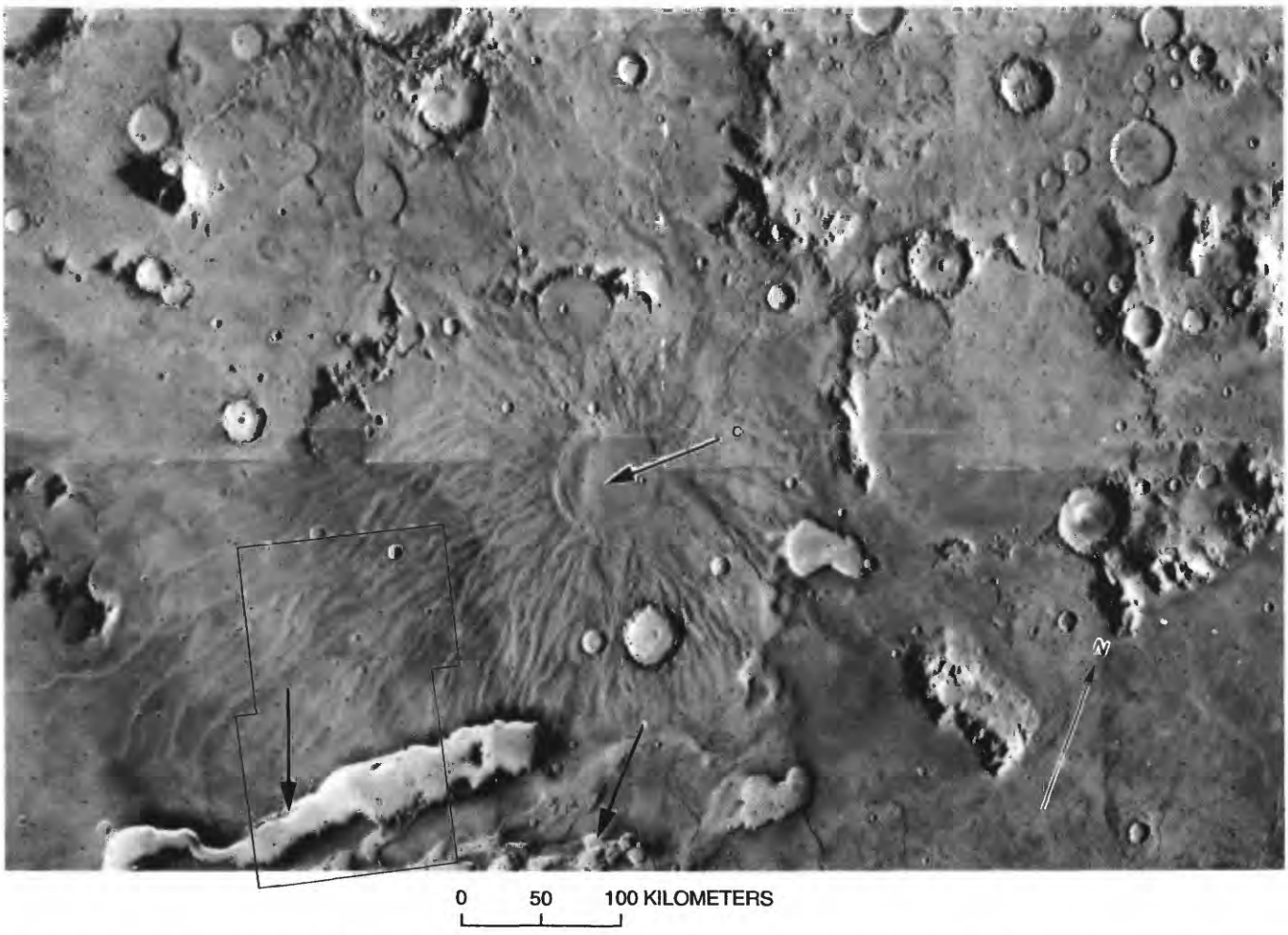

Figure 38. Hadriaca Patera. *A*, Summit caldera (arrow c) surrounded by radial channels. Broad, boxlike canyons (arrows) are localized on lower south flanks of shield; some of these canyons appear to have been modified by fluvial activity. Box at lower left outlines area of figure 38*B*. Sun illumination from right. Part of Viking Orbiter mosaic 211–5213.

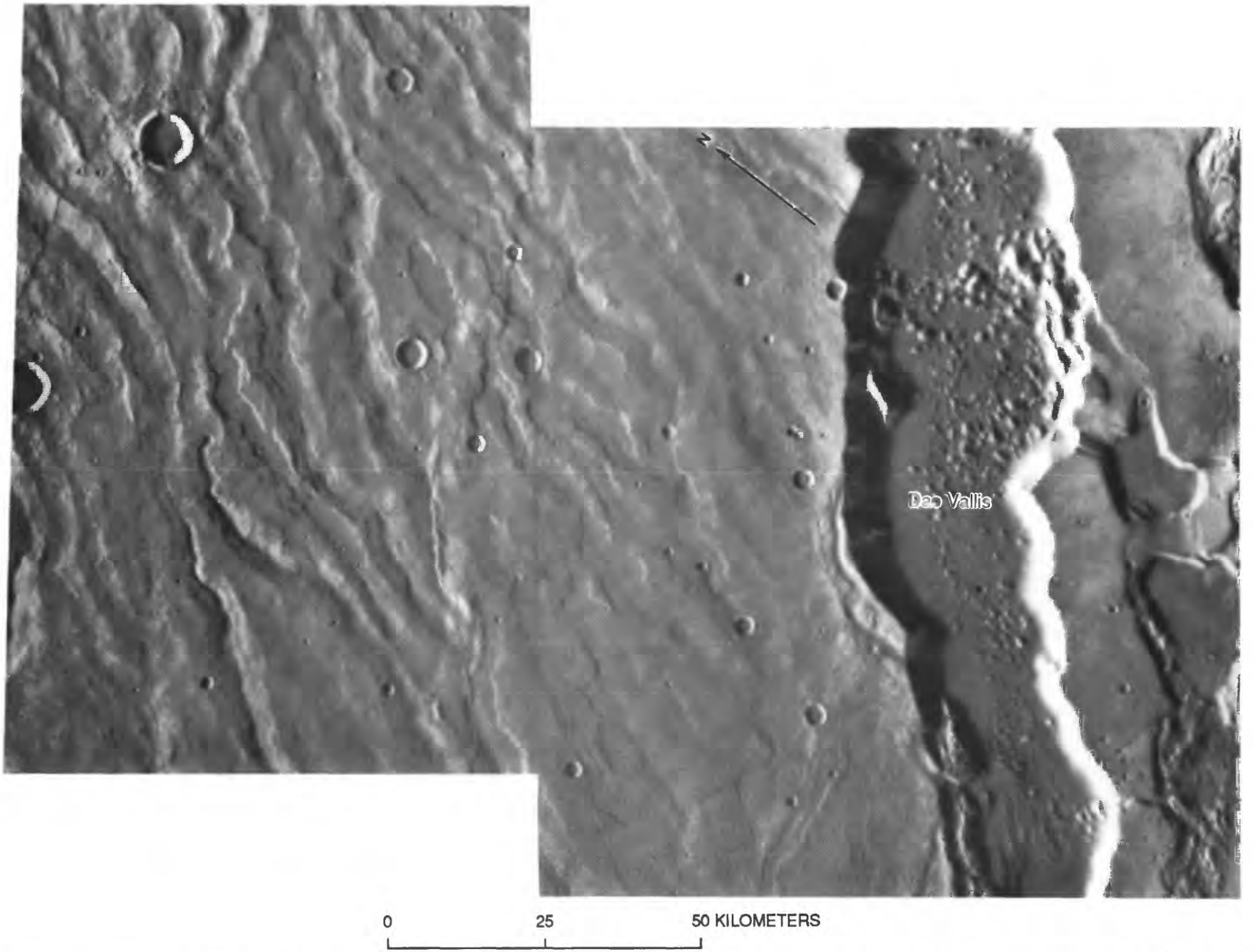

B, Southwest flank of Hadriaca Patera, showing lava flows and channels and fluvially modified (Crown and others, 1990) channel of Dao Vallis. Configuration of Dao Vallis may be attributable to interaction of magmatic heat and ground ice, resulting in collapse within ash-flow deposits (Squyres and others, 1987; Crown and Greeley, 1990a, b), or to spring sapping, similar to that on the Snake River Plain in Idaho (fig. 38*C*). Sun illumination from left. Viking Orbiter frames 408S67 and 408S69.

channels at Tyrrhena Patera, more subdued, V-shaped valleys form a pronounced radial pattern surrounding the caldera rim (fig. 38*A*); sharp walls and rims do not characterize either the valleys or the caldera. The valley walls exhibit subtle scarps and other erosional remnants that suggest layering in the volcanic materials. The morphology of the shield's flanks and the valleys is consistent with a pyroclastic origin of the flank materials, and quantitative analyses by Crown and Greeley (1990a, b) indicated that the deposits may be attributable to gravity-driven pyroclastic flows generated by phreatomagmatic eruptions.

The broad depressions of Dao Vallis, marginal to the base of the volcano, closely resemble coalescent collapse features (figs. 38*A*, 38*B*), modified in one place by fluvial erosion (Crown and others, 1990), that formed an extensive dendritic network entering the Hellas Basin and petering out on its floor (Greeley and Guest, 1987). Several similar channels that occur elsewhere in the layered materials of this quadrangle (MC 28) appear unrelated to eruptive activity, suggesting that their origin is nonvolcanic. As at Tyrrhena Patera, the morphology of these channels, which head in "box canyons" or "amphitheaters," could be due to spring sapping in competent rock (ash flows or lava, for example) caused by the interaction of magmatic heat with ground ice. Similar types of canyons occur in terrestrial basaltic plains, such as the Snake River Plain in Idaho (fig. 38*C*), where they formed by spring sapping. Squyres and others (1987), however, attributed these large depressions on Mars to collapse due to melting of ground ice by surface and subsurface volcanism.

Volcanism at Hadriaca Patera, on the rim of the Hellas Basin (fig. I–4), may have been localized by the crustal disruption caused by the extremely large impact that produced the basin (Peterson, 1977, 1978). Relative ages (see also Landheim and Barlow, 1991) show that Hadriaca Patera is approximately contemporaneous with, or slightly younger than, Tyrrhena Patera (fig. I–5).

REFERENCES

Crown and Greeley (1990a, b)
Crown and others (1990)
Greeley and Guest (1987)
Landheim and Barlow (1991)
Peterson (1977, 1978)
Potter (1976)
Squyres and others (1987)

C, Lake Channel, Snake River Plain, Idaho, showing fluvial channel and tributaries widened and extended headward by spring sapping in basalt. Sun illumination from right. Photograph courtesy of Ronald Greeley.

AMPHITRITES AND PENEUS PATERAE

Mosaics: 211–5335, 211–5524 *MC: 27A–28* *Coordinates: 59° S., 299° W.; 58° S., 307° W.*

Elevation (km)	3–4
Approximate dimensions (km):	
Caldera diameters	120 (each)
Shields	poorly defined
Relief	0
Estimated relative age (10^{-3} craters/km^2)	2–4
Inferred age (Ga):	
Model 1	3.6–3.8
Model 2	1.9–3.2

Stratigraphic age:
Hesperian; patera and dissected members of the Amphitrites Formation

DISTINCTIVE CHARACTERISTICS

(1) Two circular, calderalike depressions on southwest rim of the Hellas impact basin: Amphitrites, consisting of nested shallow, indistinct depressions with ill-defined rims, surrounded by a conspicuous, high-density radial-channel system; and Peneus, distinguished by concentric fractures and rim grabens.
(2) Extensive plains, with numerous mare-type ridges surrounding calderas.

DISCUSSION

Evidence that Amphitrites and Peneus Paterae (fig. 39*A*) are volcanic is largely circumstantial: They are flooded and surrounded by what appear to be lava plains, and neither the radial-channel system around Amphitrites Patera nor the concentric grabens at the rim of neighboring Peneus Patera are characteristic of old impact craters. Although they are probably volcanic (Potter, 1976), Wood (1984a) found no evidence of collapse and thus questioned their interpretation as calderas. The radial-channel system suggests that the rim was higher than the surrounding plain at some time, although there is little relief apparent in Viking images (figs. 39*B*, 39*C*). Peterson (1977, 1978) considered these features to be part of a shield complex including as many as five or six calderas, but identification of these older calderas is inconclusive.

A few channels head near the rims of the calderas at steep, cirquelike walls, suggestive of spring sapping or sudden breakouts of confined fluids. The surrounding lava plains are vast. If they were fed by sheet floods from the calderas or associated fissures, extrusion rates were probably high (Greeley and Spudis, 1981); channels could have developed within lava flows, or the channel system could be due to postvolcanic erosional dissection.

No other conclusively volcanic landforms exist in the province, although a few cratered domes on the plains could be small shield volcanoes or lava cones (fig. 39*D*). Several conspicuous impact craters have prominent central peaks with summit craters (fig. 39*E*), which were interpreted by Peterson (1977) as volcanoes triggered by the impacts. These features may, however, be simply variants of the central-pit type of impact craters that are common on Mars (Hodges, 1978; Hodges and others, 1980), exhibiting center morphologies ranging from rimless pits to symmetrical peaks with summit craters, like those here. The formation of this type of crater presumably reflects varying characteristics of the substrate impacted.

Peterson (1978) suggested that the Amphitrites Patera shield complex was localized by the second ring of the Hellas impact basin.

The relative ages of Amphitrites and Peneus Paterae are difficult to obtain from crater counts because the resolutions of available images are too low and the smaller craters appear to be eroded and filled. The presence of large (more than 2.6 km diam) superposed craters suggests a Hesperian age comparable to that of Hadriaca and Tyrrhena Paterae (fig. I–5), but Amphitrites and Peneus Paterae could be older.

REFERENCES

Greeley and Spudis (1981)
Hodges (1978)
Hodges and others (1980)
Peterson (1977, 1978)
Potter (1976)
Wood (1984a)

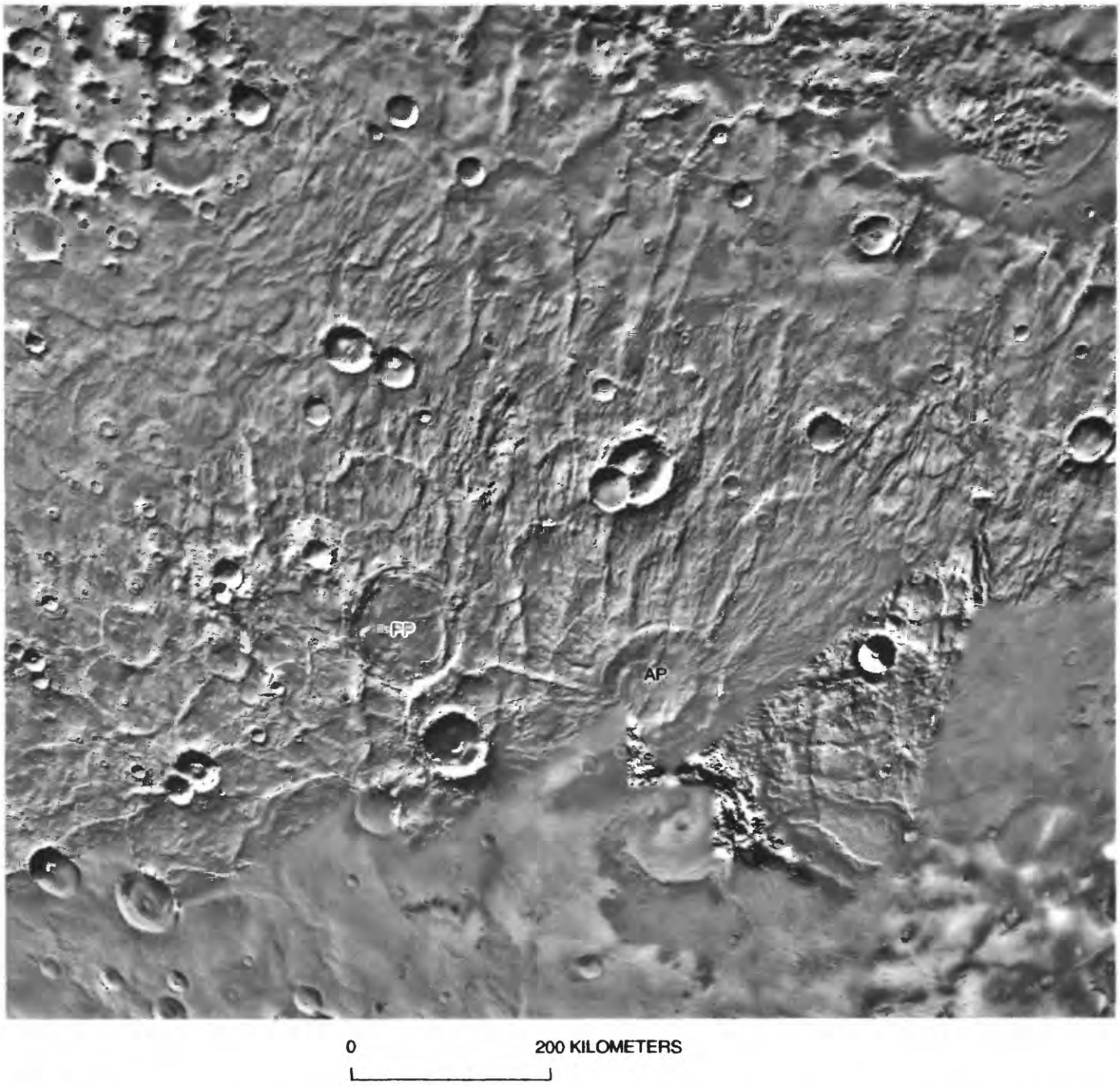

Figure 39. Amphitrites and Peneus Paterae. *A*, Amphitrites Patera (AP) and Peneus Patera (PP), both about 120 km across. Sun illumination from top. Digital-image mosaic.

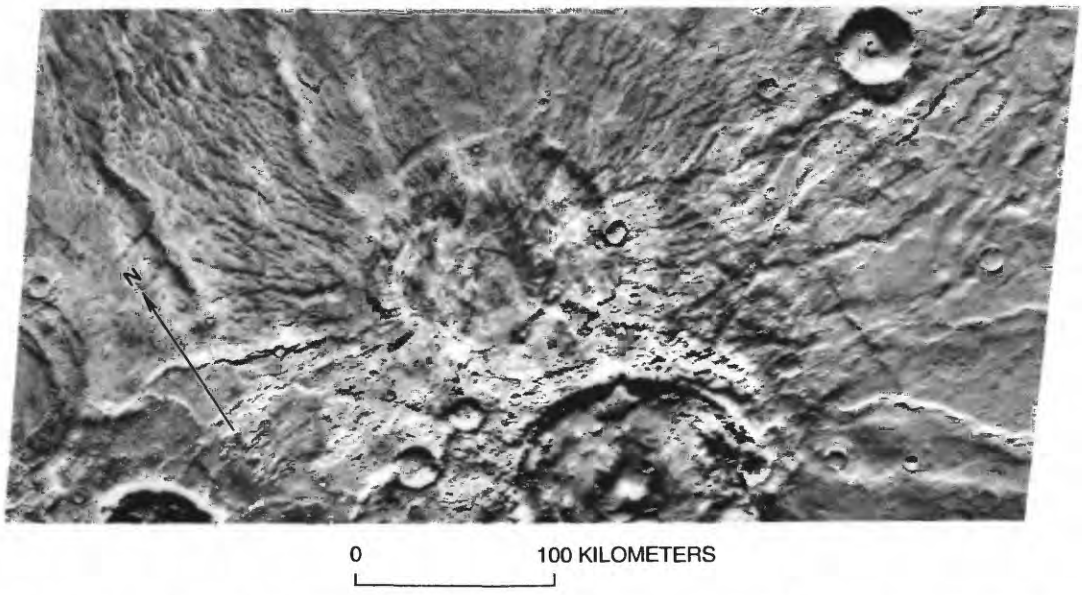

B, Amphitrites Patera (center), showing conspicuous channels radiating from caldera, although rim does not now have significant relief. Crater at lower right is poorly resolved in figure 39*A*. Sun illumination from top. Viking Orbiter frame 94A75.

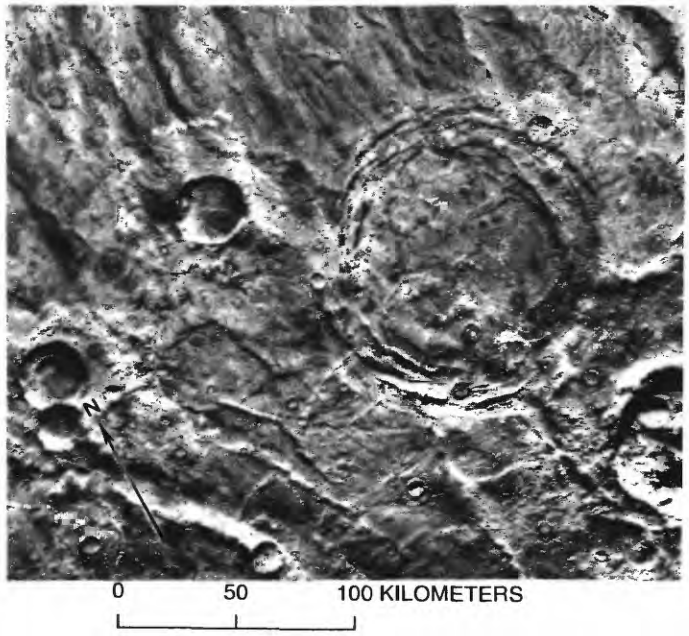

C, Peneus Patera, apparently flooded by volcanic materials. Sun illumination from top. Viking Orbiter frame 94A74.

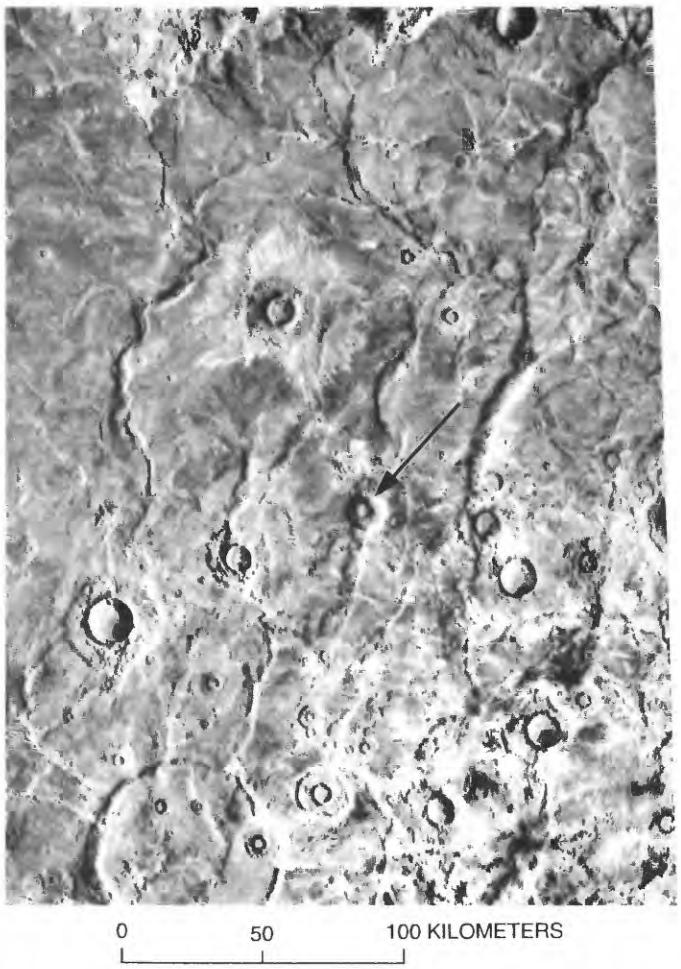

◄ *D*, Volcanic plains surrounding Amphitrites Patera. Arrow denotes one of several cratered, domelike features (at approx 57° S., 318° W.) astride mare-type ridge that could be of volcanic origin; crater floor is higher than surrounding plain. Sun illumination from right. Viking Orbiter frame 94A65.

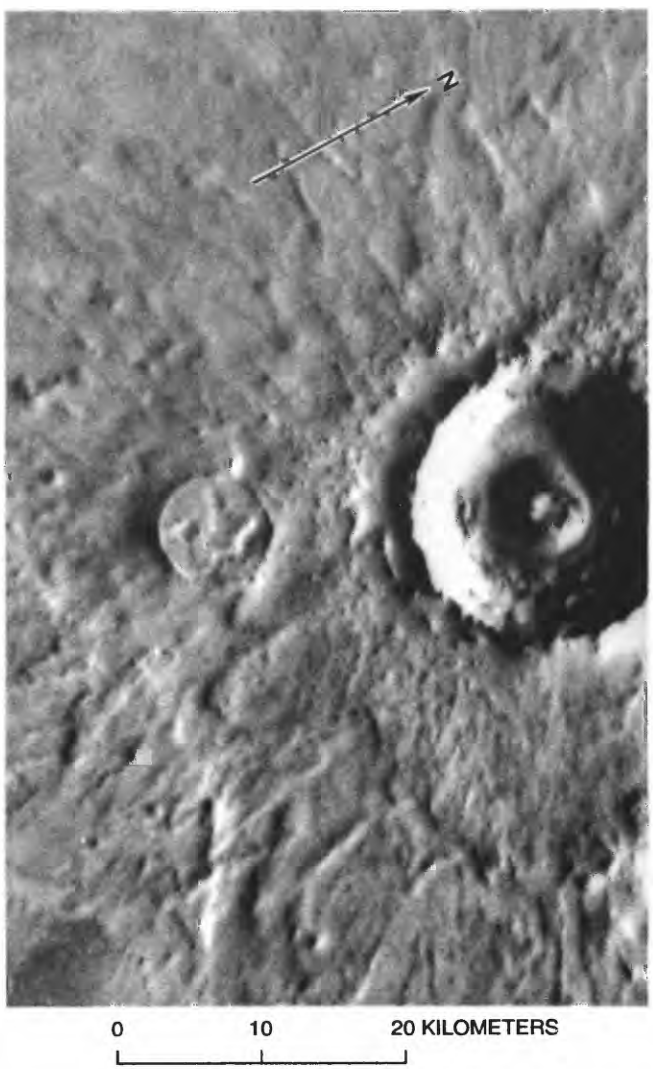

► *E*, Impact crater with large central peak and summit crater near Amphitrites Patera at approximately 59° S., 322° W. Peterson (1977) interpreted peak as a volcano; alternatively, it could be an exceptionally well formed end member in central-pit-crater morphologic series of Hodges and others (1980), as exemplified by more typical impact craters in Coprates Chasma South province (fig. 42*A*). Sun illumination from right. Viking Orbiter frame 539B49.

HIGHLANDS PROVINCES

SMALL VOLCANIC FEATURES

ARRHENIUS

Mosaic: 211–5870 MC: 29A Coordinates: 40°–45° S., 235°–240° W.

Province description:
Densely populated field of small hills and buttes, many with summit depressions.

Elevation (km)	3–4
Approximate dimensions (m):	
Butte base diameters	100–1,000
Relief (shadow measurements)	100

Stratigraphic age:
Amazonian; knobby-plains materials

DISTINCTIVE CHARACTERISTICS

(1) Circular to oblong buttes and hills.
(2) Some evidence of short lava flows among buttes.
(3) Apparently random distribution.
(4) Relatively low albedo.

DISCUSSION

The cluster of buttes in the Arrhenius province (fig. 40*A*) is evidently unique on the planet. These buttes do not appear to be erosional remnants of a highland plateau, nor are they similar to the erosional remnants of ejecta blankets common around old impact craters. Their random distribution, low albedo, round to oblong shapes, and common but not ubiquitous summit craters (fig. 40*B*) suggest a possible analogy with the basalt-capped diatremes of the Hopi Buttes, Ariz. (Shoemaker and others, 1962; Sutton, 1974), although the martian buttes are far more numerous. In aerial photographs, the Hopi Buttes contrast sharply with the Mesozoic and Tertiary strata through which they were erupted (figs. 40*C*, 40*D*); their relief is due largely to differential erosion. Also plausible are interpretations of the martian features as cinder cones, tablemountains, or pseudocraters (Hodges, 1979). Frey and others (1981) favored their interpretation as pseudocraters, analogous to the rootless pyroclastic cones in Iceland (fig. 40*E*), so named because they formed as lava flowed over saturated ground (Thorarinsson, 1953). The buttes and cones also resemble the cinder-cone field of the San Francisco Mountains near Flagstaff, Ariz., where pyroclastic cones and ridges lacking any vestige of a crater are common (fig. 40F), in association with normal, cratered cinder cones (Hodges, 1979). Minor mare-type ridges and lobate scarps that resemble flow fronts suggest that the buttes occur on a volcanic plain, although their low albedo contrasts sharply with that of the underlying terrain; subsequent eolian deposition on the plain could possibly account for this contrast. The plains materials may be flood basalts from Hadriaca and (or) Tyrrhena Paterae on the flanks of the Hellas Basin.

REFERENCES

Frey and others (1981)
Greeley and Guest (1987)
Hodges (1979)
Thorarinsson (1953)
Shoemaker and others (1962)
Sutton (1974)

Figure 40. Arrhenius province. *A*, Field of knobs, buttes, and cratered hills clustered on plain within cratered highlands east of the Hellas Basin. Mare-type ridges suggest that plain may be volcanic. Area was mapped by Greeley and Guest (1987) as knobby-plains material (unit Apk) of diverse origin. Sun illumination from right. Viking Orbiter frame 518A50.

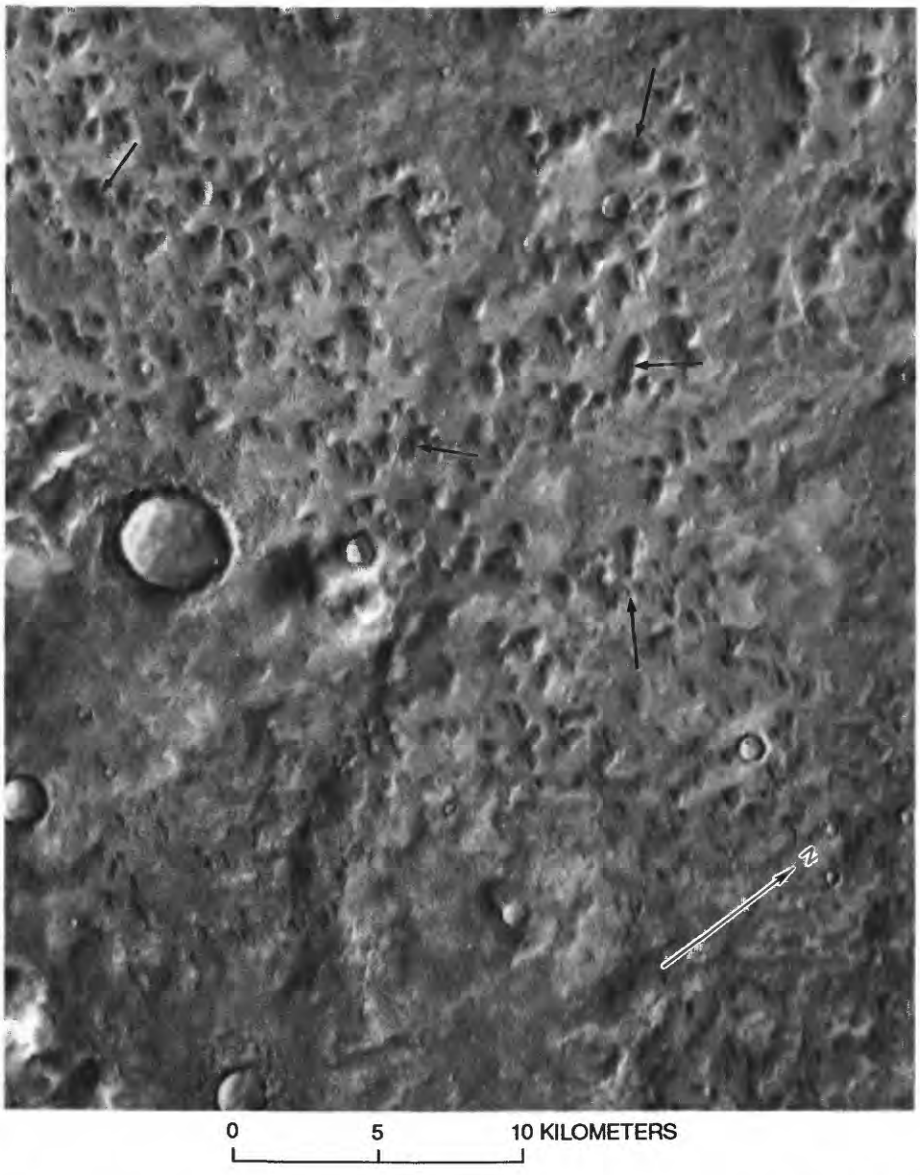

B, Buttes and mesas, many with summit craters (arrows). Characteristically random orientation and low albedo suggest several possible analogs: diatremes of the Hopi Buttes, Ariz. (figs. 40*C*, 40*D*), pseudocraters in Iceland (fig. 40*E*), tablemountains reflecting subglacial origin (figs. 29*F*, 29*G*), or cratered and craterless cinder cones (fig. 40*F*). Sun illumination from right. Viking Orbiter frame 586B33.

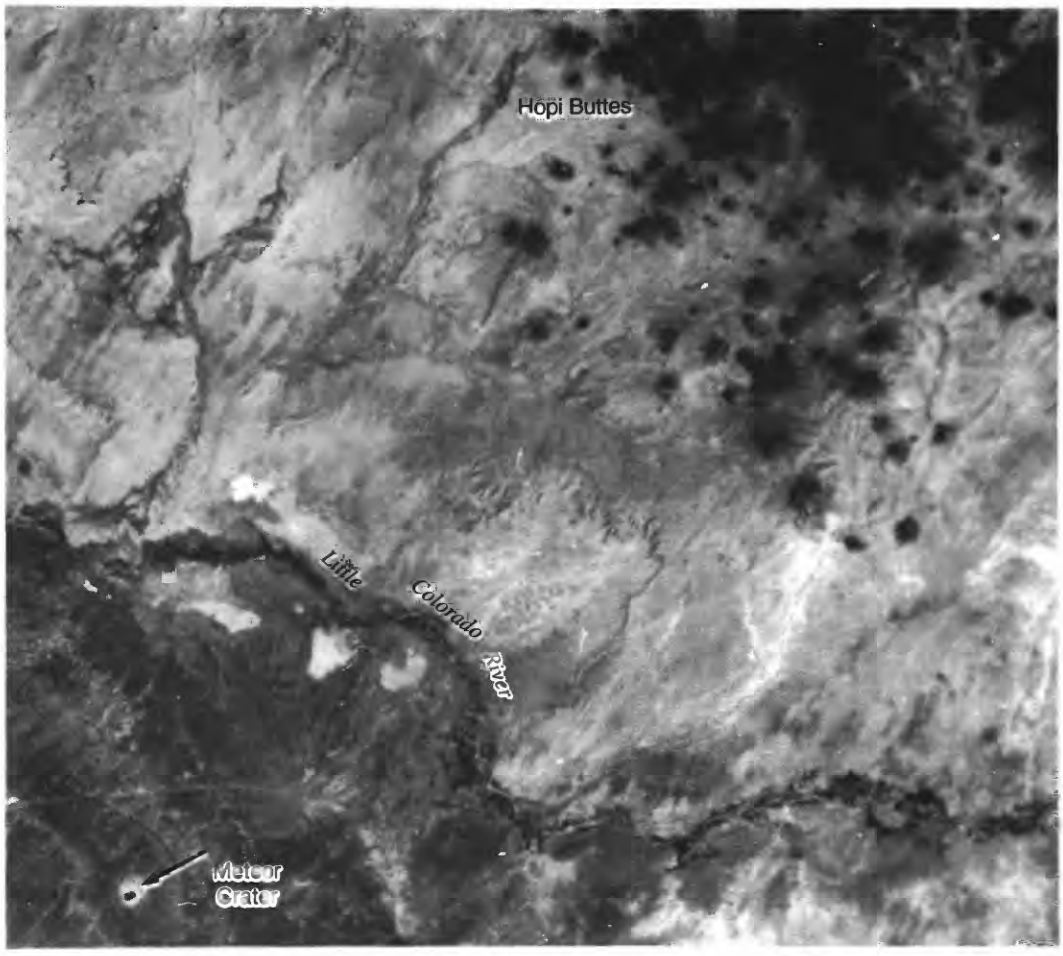

C, Hopi Buttes, Ariz., showing field of Pleistocene diatremes and maars, most of which were filled with mafic lava (monchiquite) and subsequently etched in relief by differential erosion. Buttes somewhat resemble clustered features in Arrhenius province. Meteor Crater (arrow) is about 1 km across. Sun illumination from right. Part of Landsat image 1103–17323, band 5.

D, One of the many Hopi Buttes, at which mafic lava flows filled diatreme craters. Photograph by C.A. Hodges.

E, Pseudocraters of the Alftaver group, Iceland, composed of hundreds of mostly symmetrical tephra cones, both with and without craters (Thorarinsson, 1953). Photograph by Ronald Greeley, courtesy of the photographer.

F, Merrill Crater cinder cone, San Francisco volcanic field, Ariz. Despite its name, Merrill does not have a crater but is a ridge of cinder and scoria, about 1.5 km long and 250 m high. Several such craterless cones occur in this field. Photograph by C.A. Hodges.

AEOLIS

Mosaic: 211–5760, 211–5945 MC: 23B Coordinates: 20° S., 187° W.

Province description:
Single cratered cone in highlands.

Elevation (km)	~3
Approximate dimensions (km):	
Base diameter	30
Relief (shadow measurement)	2
Caldera diameter	8

Stratigraphic age:
Noachian; hilly unit of the Plateau sequence

DISTINCTIVE CHARACTERISTICS

(1) Unusually symmetrical cone.
(2) Flooded circular summit crater.
(3) Conspicuous radial dissection of flanks.

DISCUSSION

Its symmetrical shape and circular summit crater make this feature in the Aeolis region the best candidate yet observed for a highlands-type composite cone or stratovolcano (fig. 41*A*); it was first identified by Greeley and Spudis (1978), and its apparently unique characteristics were also acknowledged by Francis and Wood (1982) and Wood (1984a). The superficial resemblance of this cone to Tongariro Volcano in New Zealand (fig. 41*B*) is striking. Tongariro is a truncated composite cone of andesitic ash and lava flows; erosion of its flanks has been augmented by glaciers and streams (Gregg, 1960). The martian feature is surrounded by intercrater plains that exhibit mare-type ridges, suggestive of volcanism; deep ravines on the structure's flanks are reminiscent of those commonly sculptured in the flanks of composite volcanoes by ash-flow erosion and subsequent meteoric processes, and there is some evidence of debris deposition at the base. A slight rise occurs at the center of the crater floor.

Age estimates based on crater counts are impossible for this feature because of its small size, isolation, and rugged topography.

REFERENCES

Decker and Decker (1981)
Francis and Wood (1982)
Greeley and Spudis (1978)
Gregg (1960)
Wood (1984a)

Figure 41. Aeolis province. *A*, Possible highlands composite volcano south of Apollinaris Patera. Filled crater and dissected flanks are morphologically similar to truncated, eroded, composite cone of Tongariro Volcano, New Zealand (fig. 41*B*). Sun illumination from left. Viking Orbiter frame 430S23.

B, Tongariro (foreground), Ngauruhoe, and Ruapehu Volcanoes, New Zealand. Snow-covered crater of Tongariro, 1.3 km across, is filled by ponded prehistoric flows and cut by small collapse crater. From Decker and Decker (1981), used with permission; photograph by S.N. Beatus, New Zealand Geological Survey.

COPRATES CHASMA SOUTH

Mosaic: 211–5750 *MC: 18A* *Coordinates: 19° S., 59° W.*

Province description:
Possible caldera and resurgent dome.

Elevation (km)	6
Approximate dimensions (km):	
Base of caldera edifice	75
Caldera diameter	20
Base of dome	50 by 65

Stratigraphic age:
Undesignated

DISTINCTIVE CHARACTERISTICS

(1) Conical mountain with large summit crater (caldera); elongate block without crater.
(2) Dense radial dissection of both features.

DISCUSSION

The cratered edifice and uncratered block south of Coprates Chasma (fig. 42*A*) are among several mountainous blocks at the eastern margin of the Sinai Planum and Solis Planum lava plains, which are distinguished by a succession of parallel mare-type ridges, trending generally north-south. The highlands in this area are densely fractured, and conspicuous radial dissection is characteristic of impact-crater rims as well as mountainous outliers. The relatively symmetrical shape of feature "a" and its summit crater (fig. 42*A*) led to its interpretation by Saunders and others (1980) as a highlands shield volcano with radiating lava channels on its flanks. The feature is near the crest of the north-south-trending Coprates rise, which has about 2 km of relief on its west side and about 3 km of relief on the east (Roth and others, 1980). A volcanic origin for the cratered edifice is uncertain because of the superposition of several impact craters on it and the general density of impact craters in the area, suggesting that the apparent summit crater may be of impact origin. Nevertheless, the crater does not appear to intersect the substrate; its depth is less than its rim height, an attribute typical of volcanic craters but not of impact craters.

Numerous other mountainous blocks in the vicinity (arrow b, fig. 42*A*; fig. 42*B*) are equally irregular and dissected but show no evidence of a summit crater. They somewhat resemble the resurgent central domes of such old, eroded terrestrial calderas as Cerro Galán in Argentina (fig. 44D; Francis, 1982; Sparks and others, 1985), but in this province on Mars there is no evidence of a surrounding caldera rim. This feature, like those in the Thaumasia province, is included here only as possibly volcanic.

REFERENCES

Francis (1982)
Roth and others (1980)
Sparks and others (1985)
Saunders and others (1980)

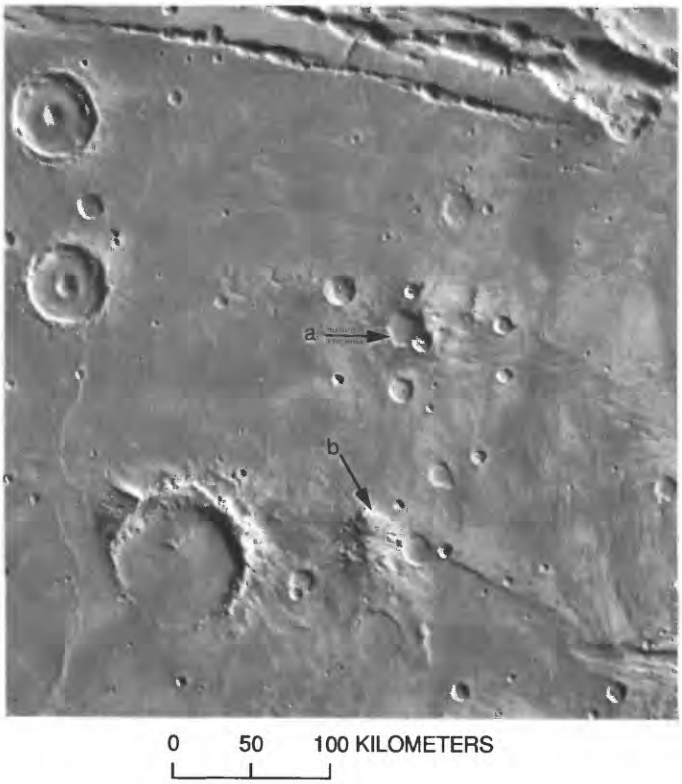

◄ **Figure 42.** Coprates Chasma South province. *A*, Mountainous blocks south of Coprates Chasma that may be highlands volcanoes. Large summit crater and relatively symmetrical shape of upper feature (arrow a) led Saunders and others (1980) to interpret it as a highlands shield volcano with radiating lava channels. Other highlands blocks in the area, however, including flanks of impact crater west of feature at arrow b, exhibit similar channels, although elevation of crater floor of proposed shield volcano lends some support to a volcanic interpretation. Domical feature (arrow b) somewhat resembles central resurgent dome characteristic of many terrestrial calderas. Central pits of typical impact craters at upper left may be comparable in origin to central-peak crater near Amphitrites Patera (fig. 39*E*). Sun illumination from right. Digital-image mosaic.

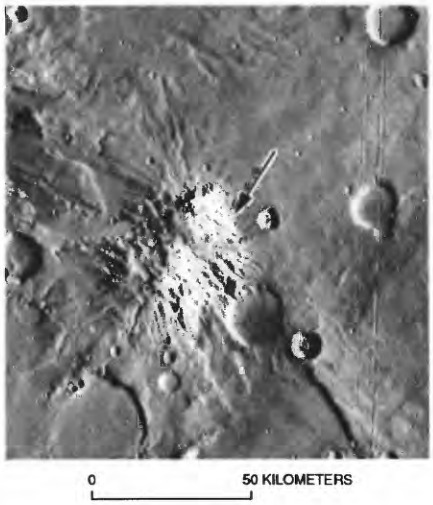

► *B,* Highly dissected mountainous block (arrow b, fig. 42*A*) resembling terrestrial resurgent dome of Cerro Galán caldera, Argentina (fig. 44*D*), but lacking any vestige of surrounding caldera rim. Appearance of adjacent crater rim, as well as of terrain to south (fig. 42*A*), suggests that such dissected features may be equally well explained as erosional remnants. Sun illumination from right. Viking Orbiter frame 610A24.

THAUMASIA

Mosaic: 211–5471 MC: 25A-D Coordinates: 37°–42° S., 88°–111° W.

Province description:
Possible highlands calderas and resurgent domes.
Elevation (km) 5–9
Approximate dimensions (km):
Base diameter 80–100
Stratigraphic age:
Pre-Tharsis, but relative age unknown

DISTINCTIVE CHARACTERISTICS

(1) Irregular mountainous blocks.
(2) Near-circular to elongate summit depressions.
(3) Radial dissection.
(4) Radial-flow materials in at least one place (25C, fig. 43*C*).

DISCUSSION

Scott (1982) and Scott and Tanaka (1981f) identified more than 30 features in the Thaumasia and Phaethontis quadrangles of Mars that they interpreted as volcanic, ranging from rugged mountainous blocks to collapse depressions, fissure vents, and nearly circular, rimless structures. Among the best examples are the four irregular features shown here, associated with Thaumasia and Claritas Fossae; a volcanic origin for each of them is questionable, but alternative explanations seem no more persuasive. All the features show distinct radial dissection away from a summit depression (figs. 43*A*–43*D*). The best candidate for a volcanic origin (arrow 25C, fig. 43*C*) shows evidence of resurfacing by lava (or lahars) on its flanks and flow fronts intermixed with dissection (arrow, fig. 43*C*). There is no diagnostic evidence of pyroclastic activity, and these features do not even remotely resemble the typical large highlands shield volcanoes Tyrrhena or Hadriaca Paterae. The features are somewhat reminiscent of the cratered cone in the Aeolis province (fig. 41*A*) in radial dissection and isolated occurrence, but they are far more irregular and less distinctive among their surroundings. The resemblance of these features, like those in the Coprates Chasma South province (figs. 42*A*, 42*B*), to the resurgent central dome of Cerro Galán caldera in Argentina (fig. 44*D*) and to the smaller (20 km diam) Valles Caldera in New Mexico (fig. 43*E*) lends some support to a volcanic interpretation. Features 25B (fig. 43*B*) and 25D (fig. 43*D*) display axial troughs that may be analogous to the graben characteristic of central domes in resurgent cauldrons (Smith and Bailey, 1968).

Scott and Tanaka (1981e, f) mapped several similar features in the Thaumasia-Phaethontis region as provisionally volcanic. Schultz and Glicken (1979), however, identified them as massifs related to a large, old impact basin centered at Syria Planum. The evidence is equivocal.

REFERENCES

Francis (1982)
Schultz and Glicken (1979)
Scott (1981, 1982)
Scott and Tanaka (1981b, e, f, 1986)
Smith and Bailey (1968)

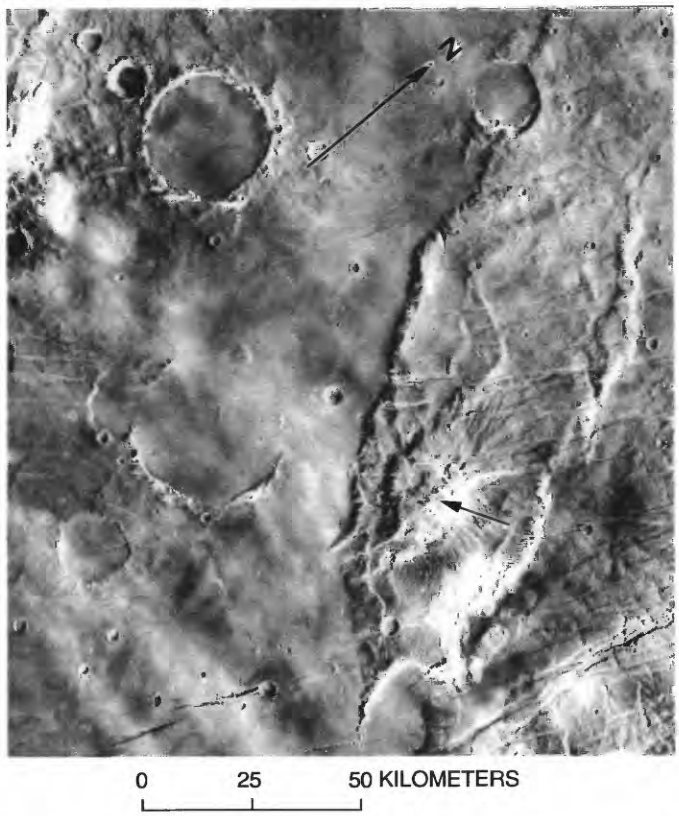

Figure 43. Thaumasia. *A*, Highlands block (arrow; 25A, pl. 1) with caldera-like morphology at summit and radial dissection. Sun illumination from right. Viking Orbiter frame 56A66.

◄ *B*, Highlands block bisected by elongate depression (arrow; 25B, pl. 1) with finely dissected outer flanks, somewhat resembling large caldera breached at both ends. Depression is possible source vent for some surrounding lava flows. Sun illumination from lower right. Viking orbiter frame 57A02.

► *C*, Dissected highlands structure (arrow; 25C, pl. 1) with distinct flow lobes (arrow f) and channels on north flank. This feature, which somewhat resembles Tempe Volcano (fig. 20*A*), is most persuasive candidate for volcanic origin in province. Topography around flow lobes is similar to channeled flanks of Tyrrhena Patera (fig. 37*A*) and Hadriaca Patera (fig. 38*A*), though on a vastly smaller scale. Sun illumination from lower right. Viking Orbiter frame 63A08.

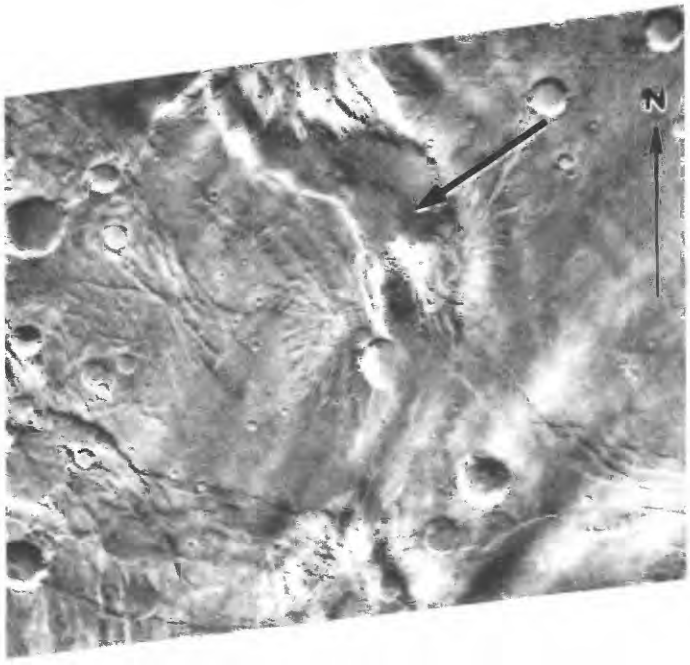

◄ *D*, Highlands block (arrow; 25D, pl. 1), possibly a breached caldera or, alternatively, a resurgent central dome with characteristic axial graben, although a candidate caldera rim is not apparent. Flanks are highly dissected, like other features in this province, and lobate deposits (probably lava or mudflows) are faintly visible on plain at base of flanks. Sun illumination from upper right. Viking Orbiter frame 63A13.

► *E*, Valles Caldera, N.Mex. (approx 22 km diam), possibly the best known example of a resurgent caldera. Catastrophic eruptions vented hundreds of cubic kilometers of felsic ash flows, now deeply gullied by radial drainage around rim. Caldera collapse was followed by intrusion of fresh magma, causing resurgence of central caldera floor and formation of broad dome with longitudinal graben (arrow g), typical of such features (Smith and Bailey, 1968). Rhyolite domes, cones, and flows, extruded after central doming, surround resurgent center. Sun illumination from right. Landsat image from Francis (1982).

TEMPE PATERA

Mosaic: 211–5866 MC: 3E–4 Coordinates: 44° N., 62° W.

Province description:

Three main features: shallow crater (Tempe Patera) surrounded by radial pattern of broad, shallow, ill-defined channels, disrupted by impact craters (fig. 44*A*); filled circular structure (unnamed) associated with somewhat less conspicuous channels (fig. 44*B*); and a possible highlands caldera with resurgent dome (fig. 44*C*).

Elevation (km)	0
Approximate dimensions (km):	
Crater diameter	16
Filled-structure diameter	40
Caldera-rim diameter	55 by 75
Estimated relative age (10^{-3} craters/km^2)	
Plescia and Saunders (1979)	4.3±0.4
Inferred ages (Ga):	
Model 1	3.8
Model 2	3.2–3.4
Stratigraphic age:	
Unknown	

DISCUSSION

Identified as a "major volcanic center" by Wise (1979), Tempe Patera has few distinguishing or diagnostic characteristics (fig. 44*A*). The channels have steep walls and broad floors, 5 to 10 km across, somewhat resembling those around Tyrrhena Patera (fig. 37*A*), where an obvious central caldera exists. They are 60 to 100 km long and appear to narrow somewhat toward their distal ends, which are closed in some places. There is no evidence of a central edifice. A similar though less conspicuous pattern of channels occurs to the northeast at approximately 46° N., 55° W., surrounding a filled circular structure (fig. 44*B*) identified by Scott (1982) as a possible shield volcano. The strong circularity and low relief, however, indicate that this feature may simply be an old impact crater subsequently inundated by lava. As pointed out by Plescia and Saunders (1979), the absence of adequate terrestrial analogs makes interpretation difficult. The pattern of channels may be erosional, possibly attributable to lava, mudflow, or surface-water runoff. Scott (1982) noted three additional, possibly volcanic ring structures, marked by concentric fractures and grabens, in this general Tempe highlands region.

A candidate for a silicic highlands caldera with resurgent dome (fig. 44*C*), similar to that described south of Coprates Chasma, occurs to the west at 45° N., 70° W.; it somewhat resembles Cerro Galán (Francis, 1982), the large Andean caldera with resurgent dome in Argentina (fig. 44*D*). Thousands of cubic kilometers of dacitic ignimbrite were erupted from Cerro Galán (Sparks and others, 1985), and the resurgent central block exposes a 1.2-km thickness of densely welded ignimbrite (de Silva and Francis, 1991). If the analogy with highlands features on Mars is apt, it poses significant implications for the composition and petrologic history of the planet, inasmuch as there is otherwise little conclusive evidence for silicic differentiation.

The relative age of Tempe Patera (not plotted in fig. I–5) suggests that it was contemporaneous with older volcanoes of moderate relief and Hesperian age.

REFERENCES

de Silva and Francis (1991)
Francis (1982)
Plescia and Saunders (1979)
Scott (1982)
Sparks and others (1985)
Wise (1979)

Figure 44. Tempe Patera. *A*, Presumed caldera (arrow) surrounded by radial system of broad, shallow channels, somewhat resembling highlands volcanoes Tyrrhena and Hadriaca Paterae. Sun illumination from left. Viking Orbiter frame 704B36.

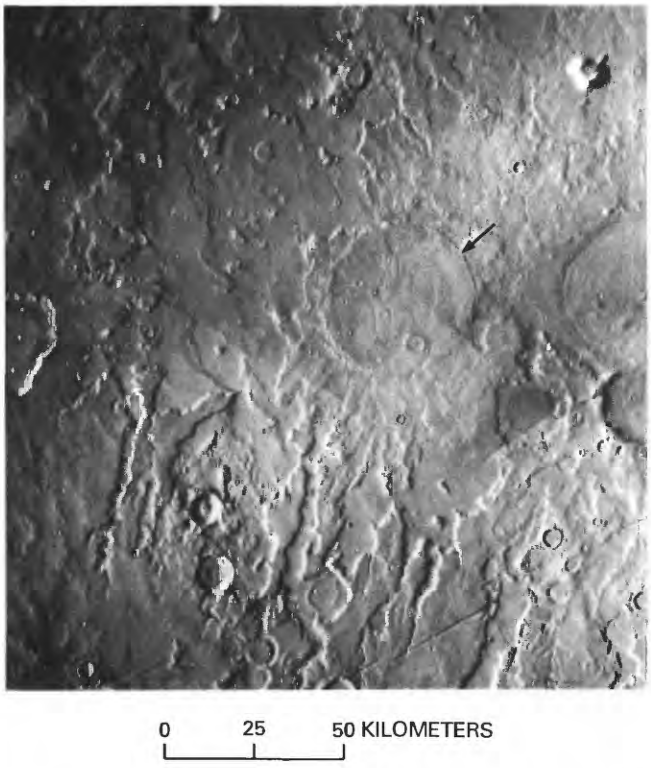

B, Filled circular structure (arrow) of possible volcanic origin northeast of Tempe Patera at 46° N., 55° W. Sun illumination from left. Viking Orbiter frame 704B39.

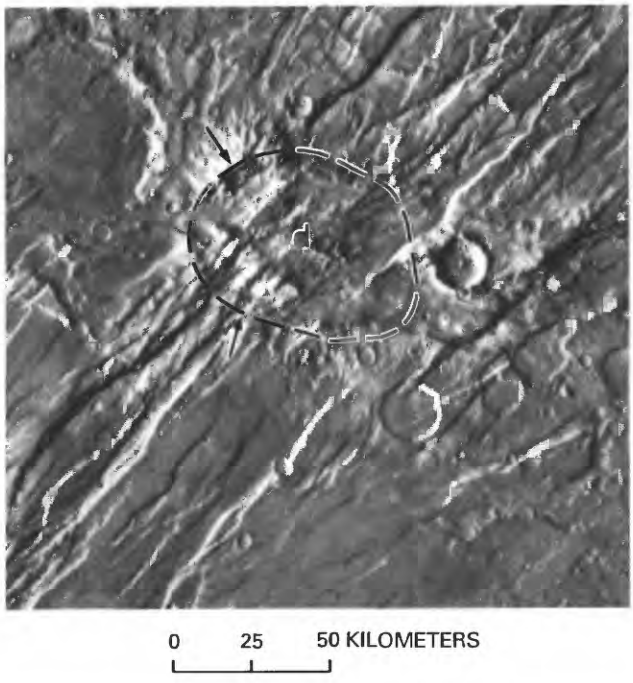

C, Candidate for highlands-type caldera with incipient resurgent dome (d) at approximately 45° N., 70° W. Raised rim (arrows), about 75 km across, with conspicuous radial channels, somewhat resembles rim of Cerro Galán caldera, Argentina (fig. 44*D*). Sun illumination from left. Viking Orbiter frames 704B30 and 704B32.

► *D*, Cerro Galán caldera, Argentina (lat 25°57′ S., long 65°57′ W.). Rim of caldera (arrows r), about 35 km across from north to south, surrounds well-defined resurgent central dome (d). Deeply gullied rocks outside rim are largely ignimbrites (ash flows) of dacitic to andesitic composition. Main caldera-forming event occurred about 2.1 Ma with eruption of thousands of cubic kilometers of ignimbrite (Sparks and others, 1985); resurgent block exposes thickness of about 1.2 km of densely welded ignimbrite (de Silva and Francis, 1991). Caldera is morphologically similar to radially dissected rim in figure 44*C* and deeply gullied blocks in figures 42*A* and 42*B* (feature b). Sun illumination from left. Landsat Thematic Mapper image, courtesy of S.L. de Silva.

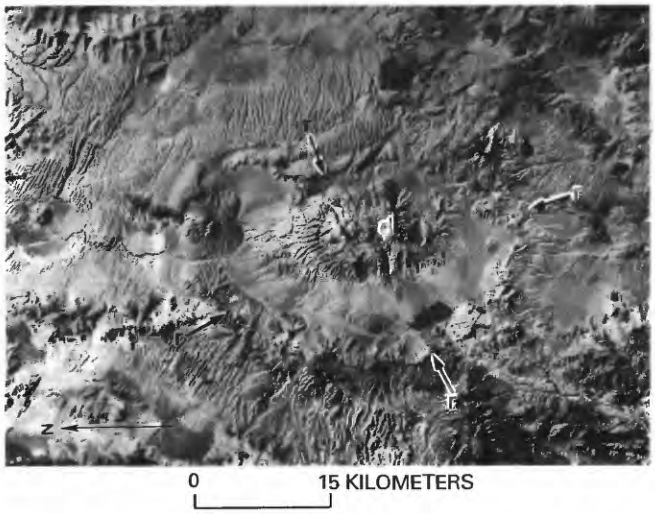

NORTH POLAR PROVINCE

SMALL VOLCANIC FEATURES

BOREALIS

Mosaics: 211–5562, 211–5869 MC: 1A Coordinates: 77°–81° N., 60°–75° W.

Province description:

Four cratered cones and two mesas associated with patterned ground near margin of north polar icecap.

Elevation (km)	–1
Approximate dimensions (km):	
Base diameter	4–16
Relief (two cones with shadows)	1.2
Crater diameters	1–8
Height/base (6 km) ratio	0.2

Stratigraphic age:

Amazonian; Mantle material and Polar layered deposits

DISTINCTIVE CHARACTERISTICS

(1) Three symmetrical cones, with summit craters clearly visible on two.
(2) Broad cratered cone in which crater diameter (8 km) is half that of base (16 km) and flank length is equal to length of crater wall.
(3) Two mesas lacking craters.

DISCUSSION

The cratered cones in the Borealis province (arrows a–c, fig. 45*A*) resemble terrestrial volcanoes. They are relatively isolated features, 70 km to several hundred kilometers apart, standing on patterned ground (fig. 45*B*). The cone nearest the icecap is on the higher of two apparently stripped surfaces, each showing a polygonal network of troughs. The westernmost cratered peak (arrow c, fig. 45*A*; fig. 45*C*) exhibits smooth flanks and a symmetrical apron of debris around its base, much like some cinder cones on Earth. South of these cones, a larger cratered cone has a flank width equal to the width of its crater wall (arrow d, fig. 45*A*; fig. 45*D*), a relation not characteristic of impact craters but typical of terrestrial tuff rings or maars; phreatomagmatic eruptions would be compatible with this location near the polar icecap.

Hodges and Moore (1979) speculated that if these cones were volcanic, as seems likely, then the two isolated mesas (arrows e, fig. 45*A*; fig. 45*E*) could be also, possibly having formed as tablemountains (fig. 29*G*) by subglacial eruption when the icecap was somewhat more extensive. Alternatively, they could be tuff cones analogous to the dish-shaped Menan Buttes in Idaho (fig. 45*F*). "Frost" appears to be present on the north-facing slopes of the mesas and the two nearest cones. The pronounced scarcity of impact craters in the entire region suggests that ice was considerably more extensive in the recent past. These features are exceptionally good candidates for volcanic landforms. No comparable landforms have been found in the south polar region.

REFERENCES

Hodges and Moore (1979)

Figure 45. Borealis. *A*, North polar icecap and adjacent terrain, showing features resembling volcanic cones (arrows a, b, c), maars (arrow d), and tablemountains or tuff cones (arrows e). Part of Viking Orbiter mosaic 211–5869.

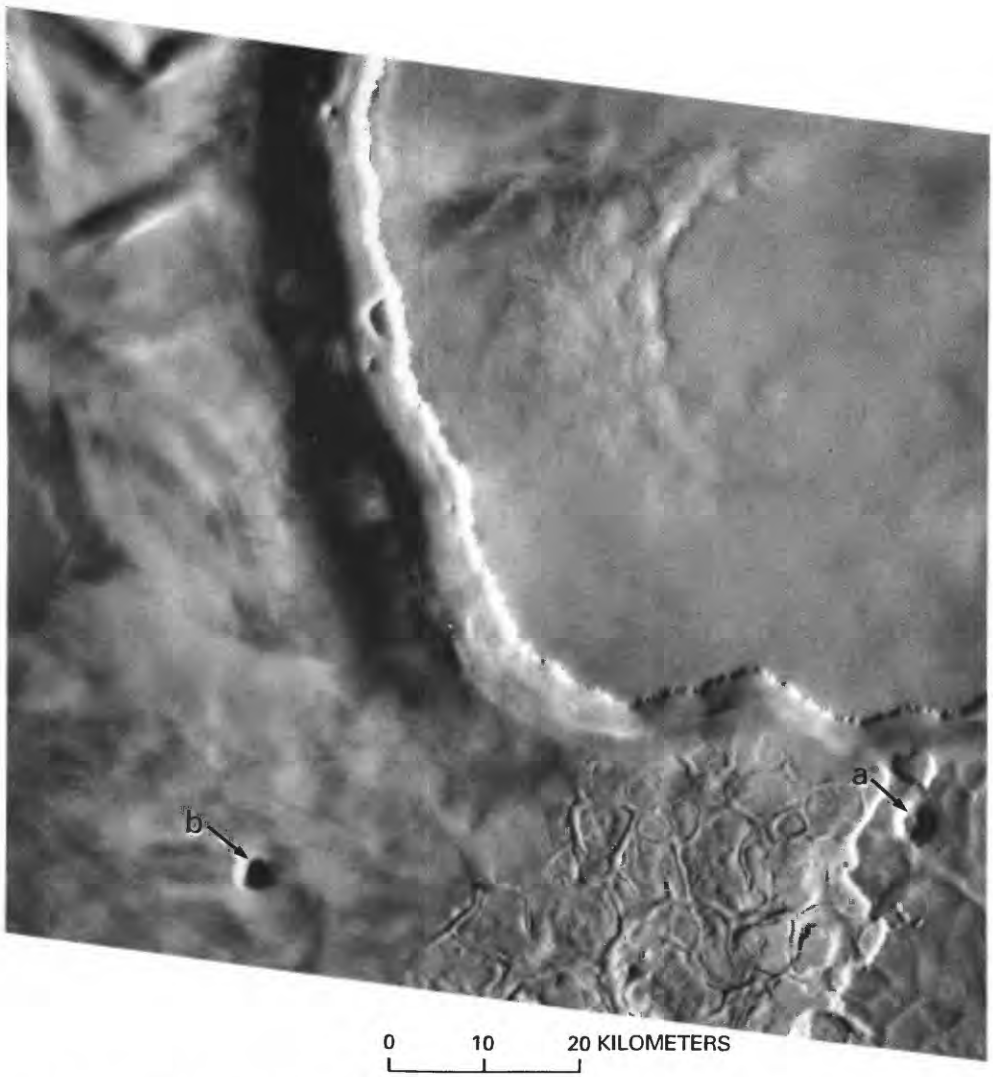

B, Two possible volcanic cones (arrows a, b; see fig. 45*A*) with summit craters on patterned ground adjacent to north polar icecap. Cones apparently postdate erosional stripping of surfaces. Sun illumination from left. Viking Orbiter frame 560B42.

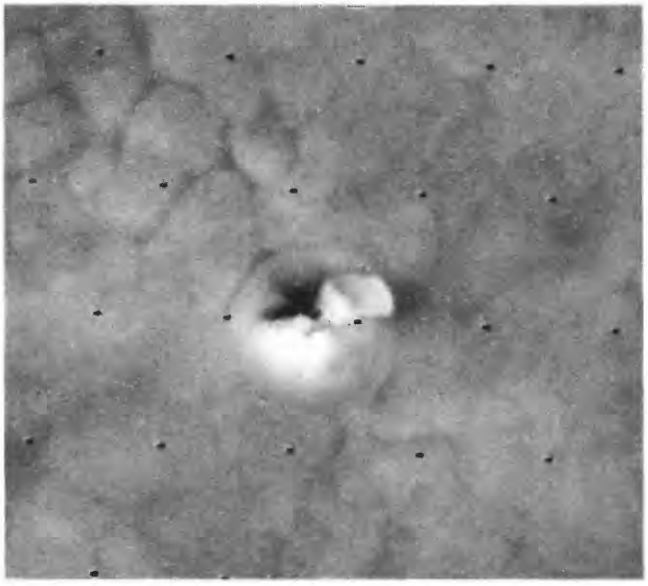

C, Cratered peak (arrow c, fig. 45*A*) strongly resembling terrestrial volcanic cone. "Frost" is visible on northeast-facing slopes. Sun illumination from lower right. Viking Orbiter frame 70B09.

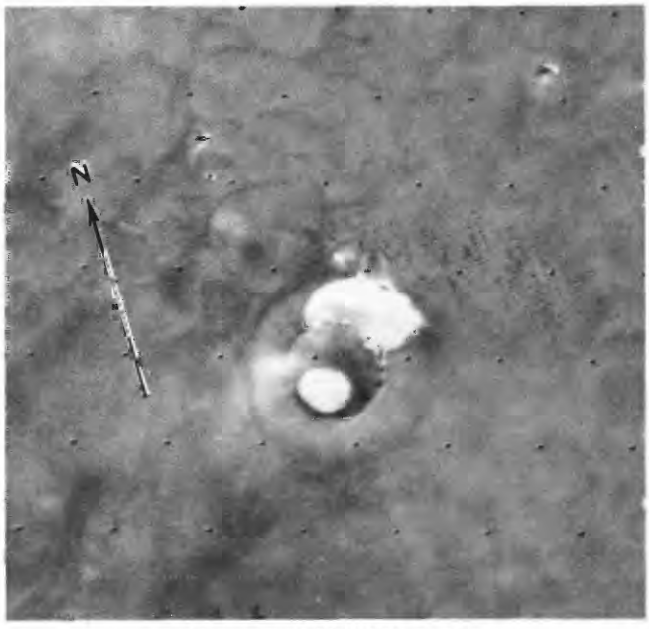

D, Possible maar crater (arrow d, fig. 45*A*). Unlike typical impact craters, this crater's outside flanks appear to be smooth and equal in length to that of inside wall. "Frost" is visible on north-facing slopes. Sun illumination from lower right. Viking Orbiter frame 70B29.

E, Mesas (arrows e, fig. 45*A*) resembling Icelandic table-mountains with subaerial lava caps or, possibly, terrestrial tuff cones like the dish-shaped Menan Buttes in Idaho (fig. 45*F*). "Frost" is visible on north-facing slopes. Sun illumination from lower right. Viking Orbiter frame 70B27.

F, Twin Menan Buttes tuff cones near Menan, Idaho. Summit craters are 760 and 900 m across and rise about 150 m above surrounding plain. These shallow, partially filled craters are possible analogs for slightly dish shaped mesas (shown at much lower resolution in fig. 45*E*) in Borealis province. Sun illumination from right. U.S. Department of Agriculture photographs CXS–6AA–50 and CXS–6AA–51, taken June 24, 1960.

REFERENCES CITED

Allen, C.C., 1979, Volcano-ice interactions on Mars: Journal of Geophysical Research, v. 84, no. B14, p. 8048–8059.

Anders, Edward, and Owen, Tobias, 1977, Mars and Earth; origin and abundance of volatiles: Science, v. 198, no. 4316, p. 453–465.

Baker, V.R., 1982, The channels of Mars: Austin, University of Texas Press, 198 p.

Baker, V.R., Strom, R.G., Croft, S.K., Gulick, V.C., Kargel, J.S., and Komatsu, G., 1990, Ancient ocean-land-atmosphere interactions on Mars; global model and geological evidence, *in* Solomon, S.C., Sharpton, V.L., and Zimbelman, J.R., eds., Scientific results of the NASA-sponsored study project on Mars; Evolution of volcanism, tectonics, and volatiles: Houston, Tex., Lunar and Planetary Institute Technical Report 90–06, p. 61–62.

Baker, V.R., Strom, R.G., Gulick, V.C., Kargel, J.S., Komatsu, G., Kale, V.S., 1991, Ancient oceans and martian paleohydrology [abs.], *in* Lunar and Planetary Science XXII: Lunar and Planetary Science Conference, 22d, Houston, Tex., 1991, Abstracts of Papers, pt. 1, p. 47–48.

Batson, R.M., Bridges, P.M., and Inge, J.L., 1979, Atlas of Mars, 1:5,000,000 map series: Washington, D.C., U.S. National Aeronautics and Space Administration, Science and Technology Branch, 146 p.

Batson, R.M., 1990, Map formats and projections used in Planetary cartography, app. 1 *of* Greeley, Ronald, and Batson, R.M., eds., Planetary mapping: New York, Cambridge University Press, p. 261–276.

Blasius, K.R., 1976, Topical studies of the geology of the Tharsis region of Mars: Pasadena, California Institute of Technology, Ph.D. thesis, 85 p.

Blasius, K.R. and Cutts, J.A., 1981, Topography of martian central volcanoes: Icarus, v. 45, no. 1, p. 87–112.

Borgia, Andrea, Burr, Jeremiah, Montero, Walter, Morales, L.D., and Alvarado, G.E., 1990, Fault propagation folds induced by gravitational failure and slumping of the central Costa Rica volcanic range; implications for large terrestrial and Martian volcanic edifices: Journal of Geophysical Research, v. 95, no. B9, p. 14357–14382.

Carr, M.H., 1973, Volcanism on mars: Journal of Geophysical Research, v. 78, no. 20, p. 4049–4062.

———1974, Tectonism and volcanism of the Tharsis region of Mars: Journal of Geophysical Research, v. 79, no. 26, p. 3943–3949.

———1975, Geologic map of the Tharsis quadrangle of Mars: U.S. Geological Survey Miscellaneous Geologic Investigations Map I–893, scale 1:5,000,000.

———1976a, Changes in height of martian volcanoes with time, *in* International Colloquium of Planetary Geology, Rome, 1975, Proceedings: Geologica Romana, v. 15, p. 421–422.

———1976b, The volcanoes of Mars: Scientific American, v. 234, no. 1, p. 32–43.

———1980, The geology of Mars: American Scientist, v. 68, no. 6, p. 626–635.

———1981, The surface of Mars: New Haven, Conn., Yale University Press, 232 p.

———1984, Mars, *in* Carr, M.H., Saunders, R.S., Strom, R.G., Wilhelms, D.E., and Carr, M.H., eds., The geology of the terrestrial planets: U.S. National Aeronautics and Space Administration Special Publication SP–469, p. 206–263.

———1986a, Mars: A water-rich planet?: Icarus, v. 68, no. 2, p. 187–216.

———1986b, Silicate volcanism on Io: Journal of Geophysical Research, v. 91, no. B3, p. 3521–3532.

———1987, Water on Mars: Nature, v. 326, no. 6108, p. 30–35.

Carr, M.H., and Clow, G.D., 1981, Martian channels and valleys; their characteristics, distribution, and age: Icarus, v. 48, no. 1, p. 91–117.

Carr, M.H., and Greeley, Ronald, 1980, Volcanic features of Hawaii, a basis for comparison with Mars: U.S. National Aeronautics and Space Administration Special Publication SP–403, 211 p.

Carr, M.H., Greeley, Ronald, Blasius, K.R., Guest, J.E., and Murray, J.B., 1977, Some martian volcanic features as viewed from the Viking Orbiters: Journal of Geophysical Research, v. 82, no. 28, p. 3985–4015.

Carr, M.H., and Schaber, G.G., 1977, Martian permafrost features: Journal of Geophysical Research, v. 82, no. 28, p. 4039–4054.

Cattermole, Peter, 1986a, Linear volcanic features at Alba Patera, Mars—probable spatter ridges: Journal of Geophysical Research, v. 91, no. B13, p. E159–E165.

———1986b, High volume volcanic flows at Alba Patera, Mars [abs.], *in* Lunar and Planetary Science XVII: Lunar and Planetary Science Conference, 17th, Houston, Tex., 1986, Abstracts of Papers, pt. 1, p. 107–108.

———1987, Sequence, rheological properties, and effusion rates of volcanic flows at Alba Patera, Mars: Journal of Geophysical Research, v. 92, no. B4, p. E553–E560.

———1990, Volcanic flow development at Alba Patera, Mars: Icarus, v. 83, no. 2, p. 453–493.

Cattermole, Peter, and Reid, Colin, 1984, The summit calderas of Alba Patera, Mars [abs.]: Lunar and Planetary Science Conference, 15th, Houston, Tex., 1984, Proceedings, p. 142–143.

Christiansen, E.H., 1989, Lahars in the Elysium region of Mars: Geology, v. 17, no. 3, p. 203–206.

Clague, D.A. and Dalrymple, G.B., 1987, The Hawaiian-Emperor volcanic chain. Part I. Geologic evolution, chap. 1 *of* Decker, R.W., Wright, T.L., and Stauffer, P.H., eds., Volcanism in Hawaii: U.S. Geological Survey Professional Paper 1350, v. 1, p. 5–54.

Crown, D.A., and Greeley, Ronald, 1990a, Hadriaca Patera; evidence for pyroclastic volcanism in the Hellas region of Mars, *in* Abstracts for the Mars: Evolution of Volcanism, Tectonics, and Volatiles Workshop on the Evolution of Magma Bodies on Mars: San Diego, Calif., Lunar and Planetary Institute, p. 12–13.

———1990b, Styles of volcanism, tectonic associations, and evidence for magma-water interactions in eastern Hellas, Mars [abs.], *in* Lunar and Planetary Science Conference XXI: Lunar and Planetary Science Conference, 21st, Houston, Tex., 1990, Abstracts of Papers, pt. 1, p. 250–251.

Crown, D.A., Porter, T.K., and Greeley, Ronald, 1991, Physical properties of lava flows on the southwest flank of Tyrrhena Patera, Mars [abs.], *in* Lunar and Planetary Science XXII: Lunar and Planetary Science Conference, 22d, Houston, Tex., 1991, Abstracts of Papers, pt. 1, p. 261–262.

Crown, D.A., Price, K.H., and Greeley, Ronald, 1990, Evolution of the east rim of the Hellas basin, Mars [abs.], *in* Lunar and Planetary Science XXI: Lunar and Planetary Science Conference, 21st, Houston, Tex., 1990, Abstracts of Papers, pt. 1, p. 252–253.

Crumpler, L.S., and Aubele, J.C., 1978, Structural evolution of Arsia Mons, Pavonis Mons, and Ascreus Mons; Tharsis region of Mars: Icarus, v. 34, no. 3, p. 496–511.

Davis, P.A., and Soderblom, L.A., 1984, Modeling crater topography and albedo from monoscopic Viking Orbiter images; 1. Methodology: Journal of Geophysical Research, v. 89, no. B11, p. 9449–9457.

Decker, R.W., and Decker, Barbara, 1981, Volcanoes: San Francisco, Calif., W.H. Freeman & Co., 244 p.

Decker, R.W., Wright, T.L., and Stauffer, P.H., eds., 1987, Volcanism in Hawaii: U.S. Geological Survey Professional Paper 1350, 2 v.

de Silva, S.L., and Francis, P.W., 1991, Volcanoes of the Central Andes: New York, Springer-Verlag, 216 p.

Dial, A.L., Jr., 1978, The Viking I landing site crater diameter-frequency distribution [abs.], *in* Strom, R.G., and Boyce, J.M., compilers, Reports of Planetary Geology Program, 1977–1978: U.S. National Aeronautics and Space Administration Technical Memorandum 79729, p. 179–181.

Downs, G.S., Reichley, P.E., and Green, R.R., 1975, Radar measurements of martian topography and surface properties; the 1971 and 1973 oppositions: Icarus, v. 26, no. 3, p. 273–312.

Dreibus, Gerlind, and Wänke, Heinrich, 1987, Volatiles on Earth and Mars; a comparison: Icarus, v. 71, no. 2, p. 225–240.

Eaton, J.P., and Murata, K.J., 1960, How volcanoes grow: Science, v. 132, no. 3432, p. 925–930.

Einarsson, Thorleifur, 1968, Jardfraedi, Saga bergs og lands [Geology, the history of rocks and landforms]: Reykjavik, Nal og Menning, 335 p.

Elston, W.E., 1979, Geologic map of the Cebrenia quadrangle of Mars: U.S. Geological Survey Miscellaneous Investigations Series Map I–1140, scale 1:4,336,000.

Evans, Nancy, 1982, The Viking mosaic catalog: U.S. National Aeronautics and Space Administration Contractor Report 3496, 2 v.

Fanale, F.P., 1976, Martian volatiles; their degassing history and geochemical fate: Icarus, v. 28, no. 2, p. 179–202.

Fanale, F.P., and Cannon, W.A., 1979, Mars; CO_2 adsorption and capillary condensation on clays—significance for volatile storage and atmospheric history: Journal of Geophysical Research, v. 84, no. B14, p. 8404–8414.

Farmer, C.B., and Doms, P.E., 1979, Global seasonal variation of water vapor on Mars and the implications for permafrost: Journal of Geophysical Research, v. 84, no. B6, p. 2881–2888.

Fink, Jonathan, 1980, Surface folding and viscosity of rhyolite flows: Geology, v. 8, no. 5, p. 250–254.

Francis, P.W., 1982, The Cerro Galán caldera, Argentina: U.S. Geological Survey Earthquake Information Bulletin, v. 14, no. 4, p. 124–133.

Francis, P.W., and Wadge, Geoff, 1983, The Olympus Mons aureole; formation by gravitational spreading: Journal of Geophysical Research, v. 88, no. B10, p. 8333–8344.

Francis, P.W., and Wood, C.A., 1982, Absence of silicic volcanism on Mars; implications for crustal composition and volatile abundance: Journal of Geophysical Research, v. 87, no. B12, p. 9881–9889.

Frey, Herbert, 1986, Pseudocraters as indicators of ground ice on Mars [abs.], *in* Lunar and Planetary Science XVII: Lunar and Planetary Science Conference, 17th, Houston, Tex., 1986, Abstracts of Papers, pt. 1, p. 239–240.

Frey, Herbert, and Jarosewich, Martha, 1981, Martian pseudocraters; searching the northern plains [abs.], *in* Lunar and Planetary Science XII: Lunar and Planetary Science Conference, 12th, Houston, Tex., 1981, Abstracts of Papers, pt. 1, p. 297–299.

———1982, Subkilometer martian volcanoes; properties and possible terrestrial analogs: Journal of Geophysical Research, v. 87, no. B12, p. 9867–9879.

Frey, Herbert, Jarosewich, Martha, and Partridge, K., 1981, Pseudocraters near Hellas? [abs.], *in* Lunar and Planetary Science XII: Lunar and Planetary Science Conference, 12th, Houston, Tex., 1981, Abstracts of Papers, pt. 1, p. 300–302.

Frey, Herbert, Lowry, B.L., and Chase, S.A., 1979, Pseudocraters on Mars: Journal of Geophysical Research, v. 84, no. B14, p. 8075–8086.

Gaskell, R.W., Synnott, S.P., McEwen, A.S., and Schaber, G.G., 1988, Large-scale topography of Io; implications for internal structure and heat transfer: Geophysical Research Letters, v. 15, no. 6, p. 581–584.

Gradie, Jonathan, and Veverka, Joseph, 1984, Photometric properties of powdered sulfur: Icarus, v. 58, no. 2, p. 227–245.

Greeley, Ronald, 1973, Mariner 9 photographs of small volcanic structures on Mars: Geology, v. 1, no. 4, p. 175–180.

———ed., 1974, Guidebook to the Hawaiian Planetology Conference, August, 1974: U.S. National Aeronautics and Space Administration Technical Memorandum TM X–62362, 257 p.

———1977a, Aerial guide to the geology of the central and eastern Snake River Plain, Idaho, *in* Greeley, Ronald, and King, J.S., eds., Volcanism of the eastern Snake River Plain; a Comparative planetary geology guidebook: Washington D.C., U.S. National Aeronautics and Space Administration, p. 61–111.

———1977b, Basaltic "plains" volcanism, *in* Greeley, Ronald, and King, J.S., eds., Volcanism of the eastern Snake River Plain, Idaho; a comparative planetary geology guidebook: Washington, D.C., U.S. National Aeronautics and Space Administration, p. 25–44.

———1982, The Snake River plain, Idaho; representative of a new category of volcanism: Journal of Geophysical Research, v. 87, no. B4, p. 2705–2712.

———1987, Release of juvenile water of Mars; estimated amounts and timing associated with volcanism: Science, v. 236, no. 4809, p. 1653–1654.

Greeley, Ronald, and Crown, D.A., 1990, Volcanic geology of Tyrrhena Patera, Mars: Journal of Geophysical Research, v. 95, no. B5, p. 7133–7149.

Greeley, Ronald, and Guest, J.E., 1987, Geologic map of the eastern equatorial region of Mars: U.S. Geological Survey Miscellaneous Investigations Series Map I–1802–B, scale 1:15,000,000.

Greeley, Ronald, and King, J.S., eds., 1977, Volcanism of the eastern Snake River Plain, Idaho; a comparative planetary geology guidebook: Washington, D.C., U.S. National Aeronautics and Space Administration, 308 p.

Greeley, Ronald, and Schultz, P.H., 1977, Possible planetary analogs to Snake River Plain basalt features, *in* Greeley, Ronald, and King, J.S., eds., Volcanism of the eastern Snake River Plain, Idaho; a comparative planetary geology guidebook: Washington, D.C., U.S. National Aeronautics and Space Administration, p. 233–251.

Greeley, Ronald, and Spudis, P.D., 1978, Volcanism in the cratered terrain hemisphere of Mars: Geophysical Research Letters, v. 5, no. 6, p. 453–455.

———1981, Volcanism on Mars: Reviews of Geophysics and Space Physics, v. 19, p. 13–41.

Greeley, Ronald, Theilig, Eilene, Guest, J.E., Carr, M.H., Masursky, Harold, and Cutts, J.A., 1977, Geology of Chryse Planitia: Journal of Geophysical Research, v. 82, no. 28, p. 4093–4109.

Gregg, D.R., 1960, The geology of Tongariro Subdivision: New Zealand Geological Survey Bulletin, new ser. 40, 152 p.

Grizzaffi, Patricia, and Schultz, P.H., 1989, Isidis Basin; site of ancient volatile-rich debris layer: Icarus, v. 77, no. 2, p. 358–381.

Gulick, V.C. and Baker, V.R., 1990a, Origin and evolution of valleys on martian volcanoes: Journal of Geophysical Research, v. 95, no. B9, p. 14325–14344.

———1990b, Valley development on Mars; a global perspective [abs.], *in* Solomon, S.C., Sharpton, V.L., and Zimbelman, J.R., eds., Scientific results of the NASA-sponsored study project on Mars; evolution of volcanism, tectonics, and volatiles: Houston, Tex., Lunar and Planetary Institute Technical Report 90–06, p. 172–173.

Hall, J.L., Solomon, S.C., Head, J.W., and Mouginis-Mark, P.J., 1983, Elysium region, Mars; characterization of tectonic features [abs.], *in* Lunar and Planetary Science XIV: Lunar and Planetary Science Conference, 14th, Houston, Tex., 1983, Abstracts of Papers, pt. 1, p. 275–276.

Harris, S.A., 1977, The aureole of Olympus Mons, Mars: Journal of Geophysical Research, v. 82, no. 20, p. 3099–3107.

Hartmann, W.K., Strom, R.G., Weidenschilling, S.J., Blasius, K.R., Woronow, Alex, Dence, M.R., Grieve, R.A.F., Diaz, Jimmy, Chapman, C.R., Shoemaker, E.M., and Jones, K.L., 1981, Chronology of planetary volcanism by comparative studies of planetary cratering, *in* Basaltic Volcanism Study Project, Basaltic volcanism on the terrestrial planets: New York, Pergamon, p. 1049–1127.

Head, J.W., Campbell, D.B., Elachi, Charles, Guest, J.E., McKenzie, D.P., Saunders, R.S., Schaber, G.G., and Schubert, Gerald, 1991, Venus volcanism; initial analysis from Magellan data: Science, v. 252, no. 5003, p. 276–288.

Head, J.W., Settle, Mark, and Wood, C.A., 1976, Origin of Olympus Mons escarpment by erosion of pre-volcano substrate: Nature, v. 263, no. 5579, p. 667–668.

Hiller, K.H., Janle, Peter, Neukum, G.P.O., Guest, J.E., and Lopes, R.M.C., 1982, Mars; stratigraphy and gravimetry of Olympus Mons and its aureole: Journal of Geophysical Research, v. 87, no. B12, p. 9905–9915.

Hodges, C.A., 1962, Comparative study of S.P. and Sunset craters and associated lava flows: Plateau, v. 35, no. 1, p. 15–35.

———1978, Central pit craters, peak rings, and the Argyre Basin [abs.], *in* Strom, R.G., and Boyce, J.M., compilers, Reports of Planetary Geology Program, 1977–1978: U.S. National Aeronautics and Space Administration Technical Memorandum 79729, p. 169–171.

———1979, Some lesser volcanic provinces on Mars [abs.], *in* Boyce, J.M., and Collins, P.S., compilers, Reports of Planetary Geology Program, 1978–1979: U.S. National Aeronautics and Space Administration Technical Memorandum 80339, p. 247–249.

———1980a, Small shield volcanoes on Mars [abs.]: Geological Society of America Abstracts with Programs, v. 12, no. 7, p. 448.

———1980b, The domes and associated flow lobes in Arcadia Planitia, Mars [abs.], *in* Wirth, P., Greeley, Ronald, and D'Alli, R.E., compilers, Reports of Planetary Geology Program, 1979–1980: U.S. National Aeronautics and Space Administration Technical Memorandum 81776, p. 184–186.

———1980c, The Tempe-Mareotis volcanic province, Mars [abs.], *in* Wirth, P., Greeley, Ronald and D'Alli, R.E., compilers, Reports of Planetary Geology Program, 1979–1980: U.S. National Aeronautics and Space Administration Technical Memorandum 81776, p. 181–183.

Hodges, C.A., and Moore, H.J., 1978a, Tablemountains of Mars [abs.], *in* Lunar and Planetary Science IX: Lunar and Planetary Science Conference, 9th, Houston, Tex., 1978, Abstracts of Papers, pt. 1, p. 523–525.

———1978b, The subglacial birth of Olympus Mons [abs.]: Geological Society of America Abstracts with Programs, v. 10, no. 7, p. 422.

———1979, The subglacial birth of Olympus Mons and its aureoles: Journal of Geophysical Research, v. 84, no. B14, p. 8061–8074.

———1980, Ice on Mars—some evidence from volcanoes [abs.]: Eos (American Geophysical Union Transactions), v. 61, no. 6, p. 69.

Hodges, C.A., Shew, N.B., and Clow, G.D., 1980, Distribution of central pit craters on Mars [abs.], *in* Lunar and Planetary Science XI: Lunar and Planetary Science Conference, 11th, Houston, Tex., 1980, Abstracts of Papers, pt. 2, p. 450–452.

Hulme, G., 1976, The determination of the rheological properties and effusion rate of an Olympus Mons lava: Icarus, v. 27, no. 2, p. 207–213.

Hunten, D.M., Donahue, T.M., Walker, J.C.G., and Kasting, J.F., 1989, Escape of atmospheres and loss of water, *in* Atreya, S.K., Pollack, J.B., and Matthews, M.S., eds., Origin and evolution of planetary and satellite atmospheres: Tucson, University of Arizona Press, p. 386–422.

Johnson, M.C., Rutherford, M.E., and Hess, P.C., 1990, Intensive parameters of SNC petrogenesis [abs.], *in* Mars; evolution of volcanism, tectonics, and volatiles; workshop on the evolution of magma bodies on Mars: Houston, Tex., Lunar and Planetary Institute Technical Report 90–04, p. 33–34.

Jones, J.G., 1966, Intraglacial volcanoes of south-west Iceland and their significance in the interpretation of the form of the marine basaltic volcanoes: Nature, v. 212, no. 5062, p. 586–588.

———1969, Intraglacial volcanoes of the Laugarvatn region, southwest Iceland—I: Geological Society of London Quarterly Journal, v. 124, p. 197–211.

———1970, Intraglacial volcanoes of the Laugarvatn region, southwest Iceland, II: Journal of Geology, v. 78, no. 21, p. 127–140.

Kasting, J.F., and Toon, O.B., 1989, Climate evolution on the terrestrial planets, *in* Atreya, S.K., Pollack, J.B., and Matthews, M.S., eds., Origin and evolution of planetary and satellite atmospheres: Tucson, University of Arizona Press, p. 423–449.

King, E.A., 1978, Geologic map of the Mare Tyrrhenum quadrangle of Mars: U.S. Geological Survey Miscellaneous Investigations Series Map I–1073 (MC–22), scale 1:5,000,000.

King, J.S., and Riehle, J.R., 1974, A proposed origin of the Olympus Mons escarpment: Icarus, v. 23, no. 2, p. 300–317.

Kjartansson, Gudmundur, 1960, The Móberg Formation, chap. 2 *of* Thorarinsson, Sigurdur, ed., On the geology and geophysics of Iceland: International Geological Congress, 21st, Copenhagen, 1960, Guide to Excursion A2, p. 21–28.

Landheim, R., and Barlow, N.G., 1991, Relative chronology of martian volcanoes [abs.], *in* Lunar and Planetary Science XXII: Lunar and Planetary Science Conference, 22d, Houston, Tex., 1991, Abstracts of Papers, pt. 2, p. 775–776.

Lopes, R.M.C., Guest, J.E., Hiller, K.H., and Neukum, Gerhard, 1981, Olympus Mons aureole; mechanism of emplacement [abs.], *in* International Colloquium on Mars, 3d, Pasadena, Calif., 1981, Papers: Houston, Tex., Lunar and Planetary Institute Contribution 441, p. 136.

———1982, Further evidence for a mass movement origin of the Olympus Mons aureole: Journal of Geophysical Research, v. 87, no. B12, p. 9917–9928.

Lopes, R.M.C., Guest, J.E., and Wilson, C.J., 1980, Origin of the Olympus Mons aureole and perimeter scarp: Moon and the Planets, v. 22, no. 2, p. 221–234.

Lucchitta, B.K., 1981, Mars and Earth; comparison of cold-climate features: Icarus, v. 45, no. 2, p. 264–303.

———1985, Geomorphologic evidence for ground ice on Mars, *in* Klinger, Jürgen, Benest, Daniel, Dollfus, Audouin, and Smoluchowski, Roman, eds., Ices in the solar system: Dordrecht, Holland, Reidel, p. 583–604.

———1987, Recent mafic volcanism on Mars: Science, v. 235, no. 4788, p. 565–567.

———1990, Young volcanic deposits in the Valles Marineris, Mars?: Icarus, v. 86, no. 2, p. 476–509.

Lucchitta, B.K., Ferguson, H.M., and Summers, C.A., 1986, Sedimentary deposits in the Northern Lowland Plains, Mars: Journal of Geophysical Research, v. 91, no. B13, p. E166–E174.

Macdonald, G.A., 1972, Volcanoes: Englewood Cliffs, N.J., Prentice-Hall, 510 p.

Malin, M.C., 1977, Comparison of volcanic features of Elysium (Mars) and Tibesti (Earth): Geological Society of America Bulletin, v. 88, no. 7, p. 908–919.

Mark, R.K., and Moore, J.G., 1987, Slopes of the Hawaiian ridge, chap. 3 *of* Decker, R.W., Wright, T.L., and Stauffer, P.H., eds., 1987, Volcanism in Hawaii: U.S. Geological Survey Professional Paper 1350, v. 1, p. 101–107.

Masursky, Harold, Batson, R.M., McCauley, J.F., Soderblom, L.A., Wildey, R.L., Carr, M.H., Milton, D.J., Wilhelms, D.E., Smith, B.A., Kirby, T.B., Robinson, J.C., Leovy, C.B., Briggs, G.A., Young, A.T., Duxbury, T.C., Acton, C.H. Jr., Murray, B.C., Cutts, J.A., Sharp, R.P., Smith, S., Leighton, R.B., Sagan, Carl, Veverka, Joseph, Noland, M., Lederberg, Joshua, Levinthal, E., Pollock, J.B., Moore, J.T., Jr., Hartmann, W.K., Shipley, E.N., de Vaucouleurs, G., and Davies, M.E., 1972, Mariner 9 television reconnaissance of Mars and its satellites; preliminary results: Science, v. 175, no. 4019, p. 294–305.

Masursky, Harold, and Crabill, N.L., 1976, Search for the Viking 2 landing site: Science, v. 194, no. 4260, p. 62–68.

McCauley, J.F., 1973, Mariner 9 evidence for wind erosion in the equatorial and mid-latitude regions of Mars: Journal of Geophysical Research, v. 78, no. 20, p. 4123–4137.

McCauley, J.F., Carr, M.H., Cutts, J.A., Hartmann, W.K., Masursky, Harold, Milton, D.J., Sharp, R.P., and Wilhelms, D.E., 1972, Preliminary Mariner 9 report on the geology of Mars: Icarus, v. 17, no. 2, p. 289–327.

McElroy, M.B., Kong, T.-Y., and Yung, Y.L., 1977, Photochemistry and evolution of Mars' atmosphere; a Viking perspective: Journal of Geophysical Research, v. 82, no. 28, p. 4379–4388.

McGill, G.E., 1989, Buried topography of Utopia, Mars; persistence of a giant impact depression: Journal of Geophysical Research, v. 94, no. B3, p. 2753–2759.

McSween, H.Y., 1985, SNC meteorites; clues to martian petrologic evolution?: Reviews of Geophysics, v. 23, p. 391–416.

Moore, H.J., 1979, Yield strengths of diverse flows on the flanks of Elysium, Ascraeus, and Arsia montes, Mars [abs.], *in* Boyce, J.M., and Collins, P.S., compilers, Reports of Planetary Geology Program, 1978–1979: U.S. National Aeronautics and Space Administration Technical Memorandum 80339, p. 63–64.

Moore, H.J., 1982a, Channel deposits on Mars [abs.], *in* Holt, H.E., compiler, Reports of Planetary Geology Program—1982: U.S. National Aeronautics and Space Administration Technical Memorandum 85127, p. 213–215.

———1982b, Mapping volcanic features on Mars [abs.], *in* Holt, H.E., compiler, Reports of Planetary Geology Program—1982: U.S. National Aeronautics and Space Administration Technical Memorandum 85127, p. 132–133.

Moore, H.J., and Ackerman, J.A., 1989a, Martian and terrestrial lava flows [abs.], *in* Lunar and Planetary Science XX: Lunar and Planetary Science Conference, 20th, Houston, Tex., 1989, Abstracts of Papers, pt. 2, p. 711–712.

———1989b, Martian and terrestrial lava flows [abs.], *in* Reports of Planetary Geology and Geophysics Program, 1988: U.S. National Aeronautics and Space Administration Technical Memorandum 4130, p. 387–389.

Moore, H.J., Arthur, D.W.G., and Schaber, G.G., 1978, Yield strengths of flows on the Earth, Mars, and Moon: Lunar and Planetary Science Conference, 9th, Houston, Tex., 1978, Proceedings, p. 3351–3378.

Moore, H.J., and Hodges, C.A., 1980, Some martian volcanic craters with small edifices [abs.], *in* Holt, H.E., and Kosters, E.C., compilers, Reports of Planetary Geology Program—1980: U.S. National Aeronautics and Space Administration Technical Memorandum 82385, p. 266–268.

Moore, J.G., 1967, Base surge in recent volcanic eruptions: Bulletin Volcanologique, v. 30, p. 337–363.

Moore, J.G., and Fiske, R.S., 1969, Volcanic substructure inferred from dredge samples and ocean-bottom photographs, Hawaii: Geological Society of America Bulletin, v. 80, no. 7, p. 1191–1202.

Morris, E.C., 1981, Structure of Olympus Mons and its basal scarp [abs.], *in* International Colloquium on Mars, 3d, Pasadena, Calif., 1981, Papers: Houston, Tex., Lunar and Planetary Institute Contribution 441, p. 161–162.

———1982, The aureole deposits of the martian volcano Olympus Mons: Journal of Geophysical Research, v. 87, no. B2, p. 1164–1178.

Morris, E.C., and Dwornik, S.E., 1978, Geologic map of the Amazonis quadrangle of Mars: U.S. Geological Survey Miscellaneous Investigations Series Map I–1049, scale 1:5,000,000.

Morris, E.C., and Tanaka, K.L., in press, Geologic maps of the Olympus Mons region of Mars: U.S. Geological Survey Miscellaneous Investigations Series Map I–2327.

Mouginis-Mark, P.J., 1981, Late stage summit activity of martian shield volcanoes: Lunar and Planetary Science Conference, 12th, Houston, Tex., 1981, Proceedings, p. 1431–1447.

———1990, Recent water release in the Tharsis region of Mars: Icarus, v. 84, no. 2, p. 362–373.

Mouginis-Mark, P.J., Robinson, M.S., and Zuber, M.T., 1990, Evolution of the Olympus Mons caldera, Mars [abs], *in* Solomon, S.C., Sharpton, V.L., and Zimbelman, J.R., eds., Scientific results of the NASA-sponsored study project on Mars; evolution of volcanism, tectonics, and volatiles: Houston, Tex., Lunar and Planetary Institute, Technical Report 90–06, p. 225–226.

Mouginis-Mark, P.J., Wilson, Lionel, and Head, J.W., 1981, Explosive volcanism on Hecates Tholus, I; surface morphology [abs.], *in* International Colloquium on Mars, 3d, Pasadena, Calif., 1981, Papers: Houston, Tex., Lunar and Planetary Institute Contribution 441, p. 166–168.

———1982a, Explosive volcanism on Hecates Tholus, Mars; investigation of eruption conditions: Journal of Geophysical Research, v. 87, no. B12, p. 9890–9904.

Mouginis-Mark, P.J., Wilson, Lionel, and Head, J.W., Brown, S.H., Hall, J.L., and Sullivan, K.B., 1984, Elysium Planitia, Mars; regional geology, volcanology, and evidence for volcano-ground ice interactions: Earth, Moon, and Planets, v. 30, no. 2, p. 149–173.

Mouginis-Mark, P.J., Wilson, Lionel, and Zimbelman, J.R., 1988, Polygenic eruptions on Alba Patera, Mars: Bulletin of Volcanology, v. 50, no. 6, p. 361–379.

Mouginis-Mark, P.J., Zisk, S.H., and Downs, G.S., 1982b, Ancient and modern slopes in the Tharsis region of Mars: Nature, v. 297, no. 5867, p. 546–550.

Mutch, T.A., Arvidson, R.E., Head, J.W., Jones, K.L., and Saunders, R.S., 1976, The geology of Mars: Princeton, N.J., Princeton University Press, 400 p.

Nash, D.B., Carr, M.H., Gradie, Jonathan, Hunten, D.M., and Yoder, C.F., 1986, Io, *in* Burns, J.A., and Matthews, M.S., eds., Satellites: Tucson, University of Arizona Press, p. 629–288.

Neukum, Gerhard, and Hiller, K.H., 1981, Martian ages: Journal of Geophysical Research, v. 86, no. B4, p. 3097–3121.

Neukum, Gerhard, Hiller, K.H., Henkel, J., and Bodechtel, Johann, 1978, Mars chronology [abs.], *in* Strom, R.G., and Boyce, J.M., compilers, Reports of Planetary Geology Program, 1977–1978: U.S. National Aeronautics and Space Administration Technical Memorandum 79729, p. 172–174.

Neukum, Gerhard, and Wise, D.U., 1976, Mars; a standard crater curve and possible new time scale: Science, v. 194, no. 4272, p. 1381–1387.

Owen, Tobias, Biemann, Klaus, Rushneck, D.R., Biller, J.E., Howarth, D.W., Lafleur, A.L., 1977, The composition of the atmosphere at the surface of Mars: Journal of Geophysical Research, v. 81, no. 28, p. 4635–4639.

Parker, T.J., Saunders, R.S., and Schneeberger, D.M., 1989, Transitional morphology in West Deuteronilus Mensae, Mars; implications for modification of the lowland/upland boundary: Icarus, v. 82, no. 1, p. 111–145.

Peale, S.J., Cassen, P.M., and Reynolds, R.T., 1979, Melting of Io by tidal dissipation: Science, v. 203, no. 4383, p. 892–894.

Pepin, R.O., 1985, Volatile inventory of Mars [abs.], *in* Carr, M.H., James, Philip, Leovy, Conway, Pepin, R.O., and Pollack, J.B., eds., MECA workshop on the evolution of the martian atmosphere, Houston, Tex., Lunar and Planetary Institute Technical Report 86–07, p. 20–21.

Peterson, J.E., 1977, Geologic map of the Noachis quadrangle of Mars: U.S. Geological Survey Miscellaneous Investigations Series Map I–910, scale 1:4,336,000.

———1978, Volcanism in the Noachis-Hellas region of Mars, 2: Lunar and Planetary Science Conference, 9th, Houston, Tex., 1978, Proceedings, p. 3411–3432.

Phillips, R.J., and Bills, B.G., 1979, Mars: Crust and upper mantle structure [abs.], *in* International Colloquium on Mars, 2d, Pasadena, Calif., 1979, Papers: U.S. National Aeronautics and Space Administration Conference Publication 2072, p. 65–67.

Phillips, R.J., Sleep, N.H., Banerdt, W.B., and Saunders, R.S., 1981, Tharsis; ten years later [abs.], *in* International Colloquium on Mars, 3d, Pasadena, Calif., 1981, Papers: Houston, Tex., Lunar and Planetary Institute Contribution 441, p. 191–193.

Pike, R.J., 1978, Volcanoes on the inner planets; some preliminary comparisons of gross topography: Lunar and Planetary Science Conference, 9th, Houston, Tex., 1978, Proceedings, p. 3239–3273.

Pike, R.J. and Clow, G.D., 1981a, Martian volcanoes in a classification of central edifices [abs.], *in* International Colloquium on Mars, 3d, Pasadena, Calif., 1981, Papers: Houston, Tex., Lunar and Planetary Institute Contribution 441, p. 199–201.

———1981b, Revised classification of terrestrial volcanoes and catalog of topographic dimensions, with new results on edifice volume: U.S. Geological Survey Open-File Report 81–1038, 40 p.

Pike, R.J., Jordan, Raymond, and Schafer, F.J., 1980, Quantitative morphology of volcanoes; recent results for Earth and Mars [abs.], *in*

Wirth, P., Greeley, Ronald, and D'Alli, R.E., compilers, Reports of Planetary Geology Program, 1979–1980: U.S. National Aeronautics and Space Administration Technical Memorandum 81776, p. 192–194.

Plescia, J.B., 1981, The Tempe volcanic province of Mars and comparisons with the Snake River Plains of Idaho: Icarus, v. 45, no. 3, p. 586–601.

———1990, Recent flood lavas in the Elysium region of Mars: Icarus, v. 88, no. 2, p. 465–490.

Plescia, J.B., and Saunders, R.S., 1979, The chronology of martian volcanoes: Lunar Planetary Science Conference, 10th, Houston, Tex., 1979, Proceedings, p. 2841–2859.

———1982, Tectonic history of the Tharsis region, Mars: Journal of Geophysical Research, v. 87, no. B12, p. 9775–9791.

Pollack, J.B., and Black, D.C., 1979, Implications of the gas compositional measurements of Pioneer Venus for the origin of planetary atmospheres: Science, v. 205, no. 4401, p. 56–59.

Pollack, J.B., Kasting, J.F., Richardson, S.M., and Poliakoff, K., 1987, The case for a wet, warm climate on early Mars: Icarus, v. 71, no. 2, p. 203–224.

Potter, D.B., 1976, Geologic map of the Hellas quadrangle of Mars: U.S. Geological Survey Miscellaneous Investigations Series Map I–941, scale 1:4,336,000.

Reimers, C.E., and Komar, P.D., 1979, Evidence for explosive volcanic density currents on certain martian volcanoes: Icarus, v. 39, no. 1, p. 88–110.

Richards, A.F., 1959, Geology of the Islas Revillagigedo, Mexico, 1. Birth and development of Volcan Barcena, Isla San Benedicto (1): Bulletin Volcanologique, ser. 2, v. 22, p. 73–123.

Robinson, M.S., 1990, Precise topographic measurements of Apollinaris and Tyrrhena paterae, Mars, [abs.], *in* Solomon, S.C., Sharpton, V.L., and Zimbelman, J.R., eds., Scientific results of the NASA-sponsored study project on Mars; evolution of volcanism, tectonics, and volatiles: Houston, Tex., Lunar and Planetary Institute Technical Report 90–06, p. 251–252.

Rossbacher, L.A., and Judson, Sheldon, 1981, Ground ice on Mars; inventory, distribution, and resulting landforms: Icarus, v. 45, no. 1, p. 39–59.

Roth, L.E., Downs, G.S., Saunders, R.S., and Schubert, Gerald, 1980, Radar altimetry of South Tharsis, Mars: Icarus, v. 42, no. 3, p. 287–316.

Saunders, R.S., Arvidson, R.E., Head, J.W., III, Schaber, G.G., Stofan, E.R., and Soloman, S.C., 1991, An overview of Venus geology: Science, v. 252, no. 5003, p. 249–252.

Saunders, R.S., Roth, L.E., Downs, G.S., and Schubert, Gerald, 1980, Early volcanic-tectonic province: Coprates region of Mars [abs.], *in* Wirth, P., Greeley, Ronald, and D'Alli, R.E., compilers, Reports of Planetary Geology Program, 1979–1980: U.S. National Aeronautics and Space Administration Technical Memorandum 81776, p. 74–75.

Schaber, G.G., 1982, Syrtis Major; a low relief volcanic shield: Journal of Geophysical Research, v. 87, no. B12, p. 9852–9866.

Schaber, G.G., Horstman, K.C., and Dial, A.L., 1978, Lava flow materials in the Tharsis region of Mars: Lunar and Planetary Science Conference, 9th, Houston, Tex., 1978, Proceedings, p. 3433–3458.

Schaber, G.G., Scott, D.H., and Greeley, Ronald, 1989, Geologic map of the Ruwa Patera quadrangle of Io (Ji2): U.S. Geological Survey Miscellaneous Investigations Series Map I–1980, scale 1:5,000,000.

Schaber, G.G., Tanaka, K.L., and Harmon, J.K., 1981, Syrtis Major revisited; a highland volcanic planum, not a planitia [abs.], *in* International Colloquium on Mars, 3d, Pasadena, Calif., 1981, Papers: Houston, Tex., Lunar and Planetary Institute Contribution 441, p. 223–225.

Schaefer, M.W., 1990, Geochemical evolution of the northern plains of Mars; early hydrosphere, carbonate development, and present morphology: Journal of Geophysical Research, v. 95, no. B9, p. 14291–14300.

Schneeberger, D.M., and Pieri, D.C., 1991, Geomorphology and stratigraphy of Alba Patera, Mars: Journal of Geophysical Research, v. 96, no. B2, p. 1907–1930.

Schultz, P.H., 1984, Impact basin control of volcanic and tectonic provinces on Mars [abs.], *in* Lunar and Planetary Science XV: Lunar and Planetary Science Conference, 15th, Houston, Tex., 1984, Abstracts of Papers, pt. 2, p. 728–729.

———1985, Polar wandering on Mars: Scientific American, v. 253, no. 6, p. 94–102.

Schultz, P.H., and Frey, H.V., 1990, A new survey of multiring impact basins on Mars: Journal of Geophysical Research, v. 95, no. B9, p. 14175–14189.

Schultz, P.H., and Glicken, H., 1979, Impact crater and basin control of igneous processes on Mars: Journal of Geophysical Research, v. 84, no. B14, p. 8033–8047.

Scott, D.H., 1981, Map showing lava flows in the southeast part of the Phoenicis Lacus quadrangle of Mars: U.S. Geological Survey Miscellaneous Investigations Series Map I–1274, scale 1:2,000,000.

———1982, Volcanoes and volcanic provinces; martian western hemisphere: Journal of Geophysical Research, v. 87, no. B12, p. 9839–9851.

Scott, D.H., and Allingham, J.W., 1976, Geologic map of the Elysium quandrangle of Mars: U.S. Geological Survey Miscellaneous Investigations Series Map I–935, scale 1:5,000,000.

Scott, D.H., and Carr, M.H., 1978, Geologic map of Mars: U.S. Geological Survey Miscellaneous Investigations Series Map I–1083, scale 1:25,000,000.

Scott, D.H., Morris, E.C., and West, M.N., 1978, Geologic map of the Aeolis quadrangle of Mars: U.S. Geological Survey Miscellaneous Investigations Series Map I–1111, scale 1:5,000,000.

Scott, D.H., Schaber, G.G., and Dial, A.L., 1981a, Map showing lava flows in the southwest part of the Phoenicis Lacus quadrangle of Mars: U.S. Geological Survey Miscellaneous Investigations Series Map I–1275, scale 1:2,000,000.

Scott, D.H., Schaber, G.G., Horstman, K.C., Dial, A.L., and Tanaka, K.L.,1981b, Map showing lava flows in the northwest part of the Phoenicis Lacus quadrangle of Mars: U.S. Geological Survey Miscellaneous Investigations Series Map I–1272, scale 1:2,000,000.

———1981c, Map showing lava flows in the northwest part of the Tharsis quadrangle of Mars: U.S. Geological Survey Miscellaneous Investigation Series Map I–1266, 1:2,000,000.

———1981d, Map showing lava flows in the southwest part of the Tharsis quadrangle of Mars: U.S. Geological Survey Miscellaneous Investigations Series Map I–1268, scale 1:2,000,000.

Scott, D.H., Schaber, G.G., and Tanaka, K.L., 1981e, Map showing lava flows in the southeast part of the Tharsis quadrangle of Mars: U.S. Geological Survey Miscellaneous Investigations Series Map I–1269, scale 1:2,000,000.

Scott, D.H., and Tanaka, K.L., 1980, Mars Tharsis region; volcano-stratigraphic events in the stratigraphic record: Lunar and Planetary Science Conference, 11th, Houston, Tex., 1980, Proceedings, p. 2403–2421.

———1981a, Map showing lava flows in the northeast part of the Amazonis quadrangle of Mars: U.S. Geological Survey Miscellaneous Investigations Series Map I–1279, scale scale 1:2,000,000.

———1981b, Map showing lava flows in the northeast part of the Phaethontis quadrangle of Mars: U.S. Geological Survey Miscellaneous Investigations Series Map I–1281, scale 1:2,000,000.

———1981c, Map showing lava flows in the northeast part of the Phoenicis Lacus quadrangle of Mars: U.S. Geological Survey Miscellaneous Investigations Series Map I–1277, scale 1:2,000,000.

———1981d, Map showing lava flows in the southeast part of the Amazonis quadrangle of Mars: U.S. Geological Survey Miscellaneous Investigations Series Map I–1280, scale 1:2,000,000.

———1981e, Map showing lava flows in the northwest part of the Thaumasia quadrangle of Mars: U.S. Geological Survey Miscellaneous Investigations Series Map I–1273, scale 1:2,000,000.

———1981f, Mars: A large highland volcanic province revealed by Viking images: Lunar and Planetary Science Conference, 12th, Houston, Tex., 1981, Proceedings, p. 1449–1458.

———1982, Ignimbrites of Amazonis Planitia region of Mars: Journal of Geophysical Research, v. 87, no. B2, p. 1179–1190.

———1986, Geologic map of the western equatorial region of Mars: U.S. Geological Survey Miscellaneous Investigations Series Map I–1802–A, scale 1:15,000,000.

Scott, D.H., Tanaka, K.L., and Schaber, G.G., 1981f, Map showing lava flows in the southeast part of the Diacria quadrangle of Mars: U.S. Geological Survey Miscellaneous Investigations Series Map I–1276, scale 1:2,000,000.

———1981g, Map showing lava flows in the southwest part of the Arcadia quadrangle of Mars: U.S. Geological Survey Miscellaneous Geologic Investigations Series Map I–1278, scale 1:2,000,000.

Shoemaker, E.M., and Blasius, K.R., 1974, Geology and geomorphology of martian shield volcanoes: final report to U.S. National Aeronautics and Space Administration for Grant NGR05–002–302, 205 p.

Shoemaker, E.M., Roach, C.H., and Byers, F.M., Jr., 1962, Diatremes and uranium deposits in the Hopi Buttes, Arizona, *in* Petrologic studies (Buddington volume): Boulder, Colo., Geological Society of America, p. 327–355.

Simkin, Tom, and Howard, K.A., 1970, Caldera collapse in the Galápagos Islands, 1968: Science, v. 169, no. 3944, p. 429–437.

Simpson, R.A., Tyler, G.L., Harmon, J.K., and Peterfreund, A.R., 1982, Radar measurements of small-scale surface texture; Syrtis Major: Icarus, v. 49, no. 2, p. 258–283.

Sjogren, W.L., 1979, Mars gravity; high-resolution results from Viking Orbiter 2: Science, v. 203, no. 4384, p. 1006–1010.

Smith, B.A., Soderblom, L.A., Banfield, D., Barnet, C.F., Basilevsky, A.T., Beebe, R.F., Bollinger, K., Boyce, J.M., Brahic, André, Briggs, G.A., Brown, R.H., Chyba, C.F., Collins, S.A., Colvin, T.R., Cook, A.F., II, Crisp, D., Croft, S.K., Cruikshank, D., Cuzzi, J.N., Danielson, G.E., Davies, M.E., De Jong, E., Dones, L., Godfrey, D.A., Goguen, Jay, Grenier, I., Haemmerle, V.R., Hammel, H., Hansen, C.J., Helfenstein, C.P., Howell, C., Hunt, G.E., Ingersoll, A.P., Johnson, T.V., Kargel, J., Kirk, R., Kuehn, D.I., Limaye, S., Masursky, H., McEwen, A.S., Morrison, David, Owen, T., Owen, W., Pollack, J.B., Porco, C.C., Rages, K., Rogers, P., Rudy, D.J., Sagan, Carl, Schwartz, J., Shoemaker, E.M., Showalter, M., Sicardy, B., Simonelli, D.P., Spencer, J.R., Sromovsky, L.A., Stoker, C.R., Strom, R.G., Suomi, V.E., Synott, S.P., Terrile, R.J., Thomas, P.C., Thompson, W.R., Verbiscer, A., and Veverka, Joseph, 1989, Voyager 2 at Neptune; imaging science results: Science, v. 246, no. 4936, p. 1422–1449.

Smith, R.L., and Bailey, R.A., 1968, Resurgent cauldrons, *in* Coats, R.R., Hay, R.L., and Anderson, C.A., eds., Studies in volcanology (Williams volume): Geological Society of America Memoir 116, p. 613–662.

Soderblom, L.A., 1977, Historical variations in the density and distribution of impacting debris in the inner solar system; evidence from planetary imaging, *in* Roddy, D.J., Pepin, R.O., and Merrill, R.B., eds., Impact and explosion cratering: New York, Pergamon, p. 629–633.

Soderblom, L.A., Condit, C.D., West, R.A., Herman, B.M., and Kreidler, T.J., 1974, Martian planet-wide crater distributions; implications for geologic history and surface processes: Icarus, v. 22, no. 3, p. 239–263.

Solomon, S.C. and Head, J.W., 1982, Evolution of the Tharsis Province of Mars; the importance of heterogeneous lithospheric thickness and volcanic construction: Journal of Geophysical Research, v. 87, no. B12, p. 9755–9774.

———1990, Heterogeneities in the thickness of the elastic lithosphere of Mars; constraints on heat flow and internal dynamics: Journal of Geophysical Research, v. 95, no. B7, p. 11073–11083.

Sparks, R.S.J., Francis, P.W., Hamer, R.D., Pankhurst, R.J., O'Callaghan, L.O., Thorpe, R.S., and Page, R., 1985, Ignimbrites of the Cerro Galán Caldera, NW Argentina: Journal of Volcanology and Geothermal Research, v. 24, no. 3–4, p. 205–248.

Squyres, S.W., Wilhelms, D.E., and Moosman, A.C., 1987, Large-scale volcano-ground ice interactions on Mars: Icarus, v. 70, no. 3, p. 385–408.

Strobell, M.E., and Masursky, Harold, 1990, Planetary nomenclature, *in* Planetary mapping, Greeley, Ronald, and Batson, R.M., eds.: New York, Cambridge University Press, p. 96–140.

Sutton, R.L., 1974, The geology of Hopi Buttes, Arizona, *in* Area studies and field guides, pt. 2 *of* Geology of northern Arizona, with notes on archaeology and paleoclimate: Geological Society of America, Rocky Mountain Section Annual Meeting, 27th, Flagstaff, Ariz., Guidebook, p. 647–671.

Tanaka, K.L., 1981, Structure of Olympus Mons aureoles and perimeter escarpment [abs.], *in* International Colloquium on Mars, 3d, Pasadena, Calif., 1981, Papers: Houston, Tex., Lunar and Planetary Institute, p. 261–263.

———1985, Ice-lubricated gravity spreading of the Olympus Mons aureole deposits: Icarus, v. 62, no. 2, p. 191–206.

———1986, The stratigraphy of Mars: Journal of Geophysical Research, v. 91, no. B13, p. E139–E158.

Tanaka, K.L., Isbell, N.K., Scott, D.H., Greeley, Ronald, and Guest, J.E., 1988, The resurfacing history of Mars; a synthesis of digitized, Viking-based geology: Lunar and Planetary Science Conference, 18th, Houston, Tex., 1988, Proceedings, p. 665–678.

Tanaka, K.L., and Scott, D.H., 1987, Geologic map of the polar regions of Mars: U.S. Geological Survey Miscellaneous Investigations Series Map I–1802–C, scale 1:9,203,425.

Theilig, Eilene, and Greeley, Ronald, 1986, Lava flows on Mars; analysis of small surface features and comparisons with terrestrial analogs: Journal of Geophysical Research, v. 91, no. B13, p. E193–E206.

Thorarinsson, Sigurdur, 1953, The crater groups in Iceland: Bulletin Volcanologique, ser. 2, v. 14, p. 3–44.

Thorarinsson, Sigurdur, Saemundsson, Kristján, and Williams, R.S., Jr., 1973, ERTS–1 image of Vatnajökull; analysis of glaciological, structural, and volcanic features: Jökull, v. 23, p. 7–17.

Tilling, R.I., Heliker, Christina, and Wright, T.L., 1987, Eruptions of Hawaiian volcanoes; past, present, and future: Denver, Colo., U.S. Geological Survey, 54 p.

Toon, O.B., Pollack, J.B., Ward, W., Burns, J.A., and Bilski, Kenneth, 1980, The astronomical theory of climate change on Mars: Icarus, v. 44, no. 3, p. 552–607.

U.S. Geological Survey, 1976, Topographic map of Mars: Miscellaneous Investigations Series Map I–961, scale 1:25,000,000.

———1979, Controlled photomosaic of the Phoenicis Lacus northest quadrangle of Mars: Miscellaneous Investigations Series Map I–1206 (MC–17NE), scale 1:2,000,000.

———1980a, Controlled photomosaic of the Tharsis northeast quadrangle of Mars: Miscellaneous Investigations Series Map I–1258 (MC–9NE), scale 1:2,000,000.

———1980b, Controlled photomosaic of the Tharsis southeast quadrangle of Mars: Miscellaneous Investigations Series Map I–1260 (MC–9SE), scale 1:2,000,000.

———1981a, Controlled photomosaic of the Cebrenia south-central quadrangle of Mars: Miscellaneous Investigations Series Map I–1398 (MC–7 S–C), scale 1:2,000,000.

———1981b, Controlled photomosaic of the Cebrenia southeast quadrangle of Mars: Miscellaneous Investigations Series Map I–1399, scale 1:2,000,000.

———1981c, Topographic contour map of Olympus Mons of Mars: Special Topographic Map MIM 19/134 T, scale 1:1,000,000.

———1984, Controlled photomosaic of the Elysium northwest quadrangle of Mars: Miscellaneous Investigations Series Map I–1581 (MC–15NW), scale 1:2,000,000.

———1989, Topographic maps of the western, eastern equatorial and polar regions of Mars: Miscellaneous Investigations Series Map I–2030, scale 1:15,000,000, 3 sheets.

———1991, Topographic maps of the polar, western, and eastern regions of Mars: Miscellaneous Investigations Series Map I–2160, scale 1:15,000,000, 3 sheets.

U.S. National Aeronautics and Space Administration, 1978, Standard techniques for presentation and analysis of crater size-frequency data: Technical Memorandum 79730, 20 p.

Van Bemmelen, R.W., and Rutten, M.G., 1955, Tablemountains of northern Iceland (and related geologic notes): Leiden, Netherlands, E.J. Brill, 217 p.

Walker, G.P.L., 1973, Lengths of lava flows: Royal Society of London Philosophical Transactions, ser. A, v. 274, p. 107–118.

Ward, A.W., and Spudis, P.D., 1984, Tectonic environments of Martian flood lavas [abs.], in *Lunar* and Planetary Science XV: Lunar and Planetary Science Conference, 15th, Houston, Tex., 1984, Abstracts of Paper, pt. 2, p. 886–887.

Wilhelms, D.E., 1973, Comparison of Martian and lunar multiringed circular basins: Journal of Geophysical Research, v. 78, no. 20, p. 4084–4095.

Williams, Howell, and McBirney, A.R., 1979, Volcanology: San Francisco, Freeman, Cooper and Co., 397 p.

Williams, R.S., 1978, Geomorphic processes in Iceland and on Mars; a comparative appraisal from orbital images [abs.]: Geological Society of America Abstracts with Programs, v. 1, no. 7, p. 517.

Wilson, Lionel, and Head, J.W., 1983, A comparison of volcanic eruption processes on Earth, Moon, Mars, Io and Venus: Nature, v. 302, no. 5910, p. 663–669.

Wilson, Lionel, and Mouginis-Mark, P.J., 1987, Volcanic input to the atmosphere from Alba Patera on Mars: Nature, v. 330, no. 6146, p. 354–357.

Wilson, Lionel, Mouginis-Mark, P.J., and Head, J.W., 1981, Explosive volcanism on Hecates Tholus. II; estimates of eruption characteristics [abs.], *in* International Colloquium on Mars, 3d, Pasadena, Calif., 1981, Papers: Houston, Tex., Lunar and Planetary Institute Contribution 441, p. 281–283.

Wilson, Lionel, Parfitt, E.A., and Head, J.W., 1991, The relationship between the height of a volcano and the depth to its magma source zone; some popular misconceptions [abs.], *in* Lunar and Planetary Science XXII: Lunar and Planetary Science Conference, 22d, Houston, Tex., 1991, Abstracts of Papers, pt. 3, p. 1517–1518.

Wise, D.U., 1979, Geologic map of the Arcadia quadrangle of Mars: U.S. Geological Survey Miscellaneous Investigations Series Map I–1154, scale 1:4,336,000.

Wood, C.A., 1976, Morphological evolution of shield volcanoes on Mars and Earth [abs.]: Eos (American Geophysical Union Transactions), v. 57, no. 4, p. 344.

———1979, Monogenetic volcanoes of the terrestrial planets: Lunar Planetary Science Conference, 10th, Houston, Tex., 1979, Proceedings, p. 2815–2840.

———1984a, Calderas; a planetary perspective: Journal of Geophysical Research, v. 89, no. B10, p. 8391–8406.

———1984b, Why Martian lava flows are so long [abs.], *in* Lunar and Planetary Science XV: Lunar and Planetary Science Conference, 15th, Houston, Tex., 1984, Abstracts of Papers, pt. 2, p. 929–930.

Wood, J.A., and Ashwal, L.D., 1981, SNC meteorites; igneous rocks from Mars?: Lunar and Planetary Science Conference, 12th, Houston, Tex., 1981, Proceedings, v. 12B, p. 1359–1375.

Wu, S.S.C., Garcia, P.A., Jordan, Raymond, Schafer, F.J., and Skiff, B.A., 1984, Topography of the shield volcano, Olympus Mons on Mars: Nature, v. 309, no. 5967, p. 432–435.

Yung, Y.L., and McElroy, M.B., 1979, Fixation of nitrogen in the prebiotic atmosphere: Science, v. 203, no. 4384, p. 1002–1004.

Zimbelman, J.R., 1985, Estimates of rheologic properties for flows on the martian volcano Ascraeus Mons: Journal of Geophysical Research, v. 90, supp., p. D157–D162.

Zimbelman, J.R. and McAllister, R., 1985, Surface morphology on the Martian volcano Ascraeus Mons [abs.], *in* Lunar and Planetary Science XVI: Lunar and Planetary Science Conference, 16th, Houston, Tex., 1985, Abstracts of Papers, pt. 2, p. 936–937.

Zimbelman, J.R., and Fink, J.H., 1989, Estimates of rheologic properties for flows on the martian volcano Olympus Mons [abs.], *in* Lunar and Planetary Science XX: Lunar and Planetary Science Conference, 20th, Houston, Tex., 1989, Abstracts of Papers, pt. 3, p. 1241–1242.

Zisk, S.H., Mouginis-Mark, P.J., Goldspeil, J., Slade, M.A., and Jurgens, R.M., 1991, New radar-derived topography for Tyrrhena Patera, Mars [abs.], *in* Lunar and Planetary Science XXII: Lunar and Planetary Science Conference, 22d, Houston, Tex., Abstracts of Papers, pt. 3, p. 1555–1556.

Zuber, M.T., and Mouginis-Mark, P.J., 1990, Constraints on the depth and geometry of the magma chamber of the Olympus Mons volcano, Mars [abs.], *in* Solomon, S.C., Sharpton, V.L., and Zimbelman, J.R., eds., Scientific results of the NASA-sponsored study project on Mars; evolution of volcanism, tectonics, and volatiles: Houston, Tex., Lunar and Planetary Institute Technical Report 90–06, p. 321–322.

☆ U.S. GOVERNMENT PRINTING OFFICE: 1994–584-925